



University of
Sheffield

Enolase 2 is a key player in prostate cancer bone metastasis

A thesis submitted in fulfilment of the requirements
for the degree of Doctor of Philosophy

by

Yuhan Zhou

May 2024

Division of Clinical Medicine

School of Medicine & Population Health

University of Sheffield

Acknowledgement

I would like to extend my warmest thanks to my primary supervisor, Dr. Ning Wang, for his unwavering guidance and insightful advice throughout all stages of this project. Since I started my master's degree in 2019 by his side, his guidance has profoundly influenced me academically, while also providing immense encouragement and assistance in my everyday life. He has been both a supervisor and a friend. Whether offering meticulous guidance during research challenges or providing care and motivation when facing personal difficulties, his actions have always been a source of warmth and inspiration. Working under his supervision has been an immensely enjoyable and educational experience, during which I have grown both personally and professionally.

I am also deeply grateful to my secondary supervisor, Dr. Gareth Richards, for valuable supervision, advice and guidance on crucial inputs and suggestions on my PhD the project and career development. His encouragement, patience, and enthusiasm made my research career fulfilling and meaningful. My sincere appreciation goes to everyone in our research group, including Hector M. Arredondo, Norain B. Ab Latif, Jiepei He, Jiashuang Fan for their advice, support, and for making my laboratory experience both productive and enjoyable. Special thanks to Feier Zeng, Jiabao Zhou, Yidan Sun and Karan Shah, my colleagues and friends in the department, for their assistance and encouragement during challenging times, guiding me how to be a wonderful scientist while having fun.

Last but certainly not least, I would like to express my deepest gratitude to my parents and my husband, Xingchen Li, for their continuous financial support and endless love throughout my education. I am also profoundly thankful to my friends in China for their encouragement and support, despite the distance and time difference. Their unwavering support has been a tremendous source of strength and motivation for me.

Publications

Published Articles

- **Zhou, Y.**; Zeng, F.; Richards, G.O.; Wang, N. ENO2, a Glycolytic Enzyme, Contributes to Prostate Cancer Metastasis: A Systematic Review of Literature. *Cancers* 2024, 16, 2503. <https://doi.org/10.3390/cancers16142503>
- Hodgson K, Orozco-Moreno M, Goode EA, Fisher M, Garnham R, Beatson R, Turner H, Livermore K, **Zhou Y**, Wilson L, Visser EA, Pijnenborg JF, Eerden N, Moons SJ, Rossing E, Hysenaj G, Krishna R, Peng Z, Nangkana KP, Schmidt EN, Duxfield A, Dennis EP, Heer R, Lawson MA, Macauley M, Elliott DJ, Büll C, Scott E, Boltje TJ, Drake RR, Wang N, Munkley J. Sialic acid blockade inhibits the metastatic spread of prostate cancer to bone. *EBioMedicine*. 2024 Jun; [doi:https://doi.org/10.1016/j.ebiom.2024.105163](https://doi.org/10.1016/j.ebiom.2024.105163).
- Hodgson, K., Orozco-Moreno, M., Scott, E., Garnham, R., Livermore, K., Thomas, H., **Zhou, Y.**, He, J., Bermudez, A., Marques, F., Bastian, K., Hysenaj, G., Goode, E., Heer, R., Pitteri, S., Wang, N., Elliott, D and Munkley, J. The role of GCNT1 mediated O-glycosylation in aggressive prostate cancer. *Sci Rep* 13, 17031 (2023). <https://doi.org/10.1038/s41598-023-43019-8>
- **Zhou Y**, Arredondo HM, Wang N. P2Y Receptors in Bone - Anabolic, Catabolic, or Both? *Front Endocrinol (Lausanne)*. 2022 Jan 7;12:818499. [doi: 10.3389/fendo.2021.818499](https://doi.org/10.3389/fendo.2021.818499).
- He, J.; **Zhou, Y.**; Arredondo Carrera, H.M.; Sprules, A.; Neagu, R.; Zarkesh, S.A.; Eaton, C.; Luo, J.; Gartland, A.; Wang, N. Inhibiting the P2X4 Receptor Suppresses Prostate Cancer Growth In Vitro and In Vivo, Suggesting a Potential Clinical Target. *Cells* 2020, 9, 2511. <https://doi.org/10.3390/cells9112511>

Published Abstract

- **Zhou, Y.**, Richards, G., and Wang, N. Enolase 2 is positively associated with prostate cancer progression. *Molecular Oncology*. Volume 17, Supplement 1, June 2023.

Presentations

- Poster presentation at the “17th Annual University of Sheffield Medical School Research Meeting” (2022). University of Sheffield, United Kingdom. Title: “Enolase 2 is positively associated with prostate cancer progression”. Authors: **Zhou, Y.**, Richards, G., and Wang, N.
- Poster presentation at the “European Calcified Tissue Society PhD Training Course.” (2022). Valbonne, Nice, Italy. Title: “Enolase 2 is positively associated with prostate cancer progression”. Authors: **Zhou, Y.**, Richards, G., and Wang, N.
- Poster presentation at the “12th Annual Mellanby Centre Research Day” (2023). University of Sheffield, United Kingdom. Title: “Enolase 2 is positively associated with prostate cancer progression”. Authors: **Zhou, Y.**, Richards, G., and Wang, N.
- Poster presentation at the “Annual Congress of the European Association for Cancer Research”, 12-15 June 2023, Torino, Italy. Title: “Enolase 2 is positively associated with prostate cancer progression”. Authors: **Zhou, Y.**, Richards, G., and Wang, N.
- Poster presentation at the “Prostate Cancer UK's From Ideas to Innovation”, 17-18 April 2024, London, United Kingdom. Title: “Enolase 2 is a key regulator in prostate cancer progression and bone metastasis”. Authors: **Zhou, Y.**, Fisher, M., Richards, G., and Wang, N.
- Poster presentation at the “Bone Research Society conference for Cancer and Bone Society”, 12-14 July 2024, Sheffield, United Kingdom. Title: “Enolase 2 is a key player in prostate cancer bone metastasis via regulating E2F pathway”. Authors: **Zhou, Y.**, Fisher, M., Orozco-Moreno, M., Zeng, F., Richards, G., and Wang, N.

Awards

- Travel award from the Department of Oncology and Metabolism, University of Sheffield, UK (2023).
- Publication Scholarship from the University of Sheffield, UK. (2024)

List of contents

Acknowledgement	II
Publications	III
List of contents	VI
List of Figures	XII
List of Tables	XV
Appendix Tables and Supplementary Figures	1
List of Abbreviations	3
Abstract	9
Chapter 1: Introduction	11
1.1 Prostate cancer	12
1.1.1 The Genetic Epidemiology and Risk Factors	12
1.1.2 Diagnosis of Prostate Cancer	15
1.1.3 The Pathologic Grade and Clinical Stage of Prostate Cancer	15
1.1.4 Treatments of Prostate Cancer	17
1.1.5 Bone microenvironment and PCa bone metastasis	21
1.1.5.1 Bone microenvironment	21
1.1.5.2 PCa bone metastasis	22
1.1.5.3 Treatment of PCa bone metastasis	26
1.1.6 Metabolic reprogramming in PCa	28
1.2 Enolase 2	31
1.2.1 Characteristics of Enolase	31
1.2.2 Characteristics, structures and distributions of Enolase 2	31
1.2.3 The function of Enolase 2 in glycolysis pathway	32
1.2.4 The function of Enolase 2 in cancer	35
1.3 Project rational	39
1.4 Hypothesis and Aims	41
Chapter 2: Materials and Methods	42
2.1 General Tissue Culture Cell lines and Conditions	43
2.1.1 Cell lines	43
2.1.1.1 Cancer cell-lines	43
2.1.1.2 Prostatic myofibroblast cell line	43

2.1.1.3	Cell line Authentication	43
2.1.2	<i>Tissue Culture Medium</i>	46
2.1.2.1	Standard medium	46
2.1.2.2	Low glucose, glucose-free and pyruvate-free medium	46
2.1.3	<i>Cell Culture Condition</i>	46
2.1.3.1	Cell frozen and thawing	47
2.2	Molecular and Cellular Biology Techniques	47
2.2.1	<i>ENO2 Knockdown (Small interfering RNA (siRNA) knockdown)</i>	47
2.2.1.1	siRNA product information	47
2.2.1.2	Transfection process	50
2.2.2	<i>ENO2 Knockout (CRISPR Cas 9 technology)</i>	51
2.2.2.1	CRISPR Guide RNA (gRNA) plasmid information	51
2.2.2.2	Transfection process	54
2.2.2.3	Screening by Fluorescence-activated cell sorting (FACS)	54
2.2.3	<i>Real-time Quantitative Reverse Transcription Polymerase Chain Reaction (RT-qPCR)</i>	55
2.2.3.1	RNA extraction	55
2.2.3.2	First-strand cDNA synthesis (reverse transcription polymerase chain reaction (RT-PCR))	56
2.2.3.3	TaqMan Real-time quantitative PCR (RT-qPCR)	57
2.2.3.4	Data analysis for RT- qPCR	58
2.2.4	<i>Western Blot</i>	58
2.2.4.1	Preparation of cell lysates	58
2.2.4.2	Protein concentration measurement – (Pierce™ Bicinchoninic acid (BCA) protein assay)	59
2.2.4.3	Gel electrophoresis	59
2.2.4.4	Electrophoretic transfer	60
2.2.4.5	Membrane blocking and antibody incubation	60
2.2.4.6	Visualization	61
2.2.5	<i>Enzyme-linked immunosorbent assay (ELISA)</i>	63
2.2.5.1	Preparation of cell lysates	63
2.2.5.2	Preparation for Standard	63
2.2.5.3	Enzyme-linked immunosorbent assay (ELISA)	63
2.2.6	<i>Genetic Verification</i>	66
2.2.6.1	Primer Design	66
2.2.6.2	Agarose Gel Electrophoresis	68
2.2.6.2.1	Genomic DNA purification	68
2.2.6.2.2	Polymerase chain reaction (PCR)	68
2.2.6.2.3	Gel preparation	71
2.2.6.2.4	Gel electrophoresis	71
2.2.6.2.5	Genomic DNA purification	71
2.2.6.3	Sanger DNA Sequencing	72

2.2.7	Cell Viability Assays (alamarBlue™ Assay)	72
2.2.8	Cell Proliferation Assays (CyQuant® Assay)	75
2.2.9	Cell apoptosis Assays (Caspase 3/7™ Assay)	75
2.2.10	Cell Migration Assays	77
2.2.10.1	Wound-healing Assay	77
2.2.10.2	Boyden Chamber Transwell® Assay	79
2.2.11	Cell Invasion Assays (Trans-well Invasion assay)	80
2.2.12	Metabolism related assays	82
2.2.12.1	Glucose consumption assay	82
2.2.12.2	Lactate production assay	83
2.2.13	RNA-Sequencing (RNA-Seq)	84
2.3	In vivo Studies	87
2.3.1	Ethical statement and Animals	87
2.3.2	Intracardiac Injection of PCa	87
2.3.3	Bioluminescent Imaging (IVIS imaging)	88
2.3.4	Body Weight Measurement	88
2.3.5	Euthenisation and dissection	89
2.3.6	Analysis of Osteolysis	89
2.3.6.1	Micro-Computed Tomography (Micro-CT)	89
2.3.7	Analysis of Prostate cancer - Bone cell Interactions	93
2.3.7.1	Histological studies	93
2.3.7.1.1	Bone sectioning	93
2.3.7.1.2	Haematoxylin & Eosin staining (H&E staining)	93
2.4	Meta-analysis, Retrospective and Bioinformatic studies	93
2.4.1	Systematic Review and Meta-analysis	93
2.4.1.1	Literature source and searches	93
2.4.1.2	Inclusion and exclusion criteria	94
2.4.1.3	Types of intervention and outcome measurement	94
2.4.1.4	Selection of studies	94
2.4.1.5	Data extraction	95
2.4.1.6	Data analysis	95
2.4.1.7	Quality assessment	95
2.4.1.8	Certainty of evidence	96
2.4.2	Retrospective study	96
2.4.3	Bioinformatic Studies	97
2.4.3.1	Kaplan-Meier survival analyses	97
2.4.3.1.1	Gene Expression analysis	97
2.4.3.1.2	Genetic alternation analysis	97
2.5	Statistical Analysis	98

CHAPTER 3: Systematic Review, Meta-analysis, Retrospective Study and Bioinformatics of Association between ENO2 and Prostate Cancer Metastasis

3.1	Introduction	100
3.2	Results of Systematic Review and Meta-analysis	100
3.2.1	Article selection	101
3.2.2	Quality assessment	103
3.2.3	Certainty of evidence	103
3.2.4	Characteristics of included studies	103
3.2.4.1	Clinical studies	106
3.2.4.2	in vitro studies	107
3.2.5	Meta-analysis of outcomes	109
3.2.5.1	Meta-analysis on clinical studies indicates the connection between ENO2 and PCa progression	109
3.2.5.2	Meta-analysis on <i>in vitro</i> studies indicates the relationship between ENO2, androgen deprivation environment and bone metastasis potential	111
3.3	Results of retrospective study for assessment of relationship between ENO2 expression and metastatic PCa patients	113
3.3.1	Increased ENO2 expression was correlated with advanced metastatic PCa	113
3.4	Results of Bioinformatics for assessment of Kaplan-Meier survival curves of ENO2 in PCa patients	115
3.4.1	ENO2 alternation was associated with poor survival rate in Pca patients	115
3.4.2	Increased ENO2 expression was correlated with decreased survival rate in PCa patients	117
3.5	Discussion	119
3.5	Conclusion	124

Chapter 4: ENO2 expression and related glucose metabolism in prostate cancer cell lines

4.1	Introduction	126
4.2	Results	126
4.2.1	ENO2 expression was associated with metastatic potential at transcriptional level	127
4.2.1.1	Confirmation of ENO2 expression associates with metastatic potential at translational level by RT q-PCR	127

4.2.2	<i>ENO2 expression was associated with metastatic potential at translational level</i>	129
4.2.2.1	Confirmation of ENO2 expression was associated with metastatic potential at translational level using ELISA	129
4.2.2.2	Confirmation of ENO2 expression was associated with metastatic potential at translational level using Western Blotting	131
4.2.3	<i>ENO2 expression was associated with environmental glucose and pyruvate at translational level</i>	133
4.2.3.1	Glucose level in cell culture medium affected the Enolase 2 expression in prostatic myofibroblast cells more than in PCa cells	133
4.2.3.2	Enolase 2 expression in PCa cells was affected by the presence of pyruvate in cell culture medium	135
4.2.4	<i>Effects of environmental glucose in human prostatic myofibroblast and PCa cell behaviour in vitro</i>	137
4.2.4.1	Environmental glucose affected cell viability in human prostatic myofibroblast and PCa cells	137
4.2.4.2	Environmental glucose caused cell apoptosis in human PCa cells but not in prostatic myofibroblast cells	139
4.3	Discussion	141
4.4	Conclusion	144
 Chapter 5: Effects of ENO2 Knockdown and Knockout on Prostate Cancer		
	Cell Behavior in vitro	145
5.1	Introduction	146
5.2	Results	146
5.2.1	<i>Effects of ENO2 knockdown on human PCa cell in vitro</i>	146
5.2.1.1	Confirmation of successful knockdown of ENO2 in human PCa cells	146
5.2.1.2	ENO2 knockdown reduced the viability and proliferation, but increased the apoptosis of human PCa cells <i>in vitro</i>	149
5.2.1.3	ENO2 knockdown affected the expression of ENO1 and ENO3 in human PCa cells <i>in vitro</i>	151
5.2.2	Effects of ENO2 genetic knockout on human PCa cell behavior in vitro	153
5.2.2.1	Confirmation of successful knockout of ENO2 in human PCa cells	153
5.2.2.2	ENO2 knockout reduced the cell growth of human PCa cells <i>in vitro</i>	158
5.2.2.3	ENO2 knockout reduced the motility of human PCa cells <i>in vitro</i>	160
5.2.2.4	ENO2 knockout reduced the glycolytic metabolic behavior of human PCa cells <i>in vitro</i>	163
5.3	Discussion	165
5.4	Conclusion	168

Chapter 6: Evaluation of the Role of ENO2 in PCa Bone Metastasis in vivo

	169
6.1 Introduction	170
6.2 Results	171
6.2.1 Genetically inhibition of ENO2 improved the metastatic tumour growth in BALB/c nude mice	171
6.2.2 Genetically inhibition of ENO2 led to reduced tumour incidence in tibia after systemically administered in BALB/c nude mice	174
6.2.3 Genetic inhibition of ENO2 reduced tumour induced bone destruction in long bones of BALB/c nude mice, but does not affect bone morphometry	177
6.3 Discussion	180
6.4 Conclusion	185

Chapter 7: Evaluation of the Role of ENO2 in Prostate Cancer Developments using RNA Sequencing

7.1 Introduction	187
7.2 Results	187
7.2.1 ENO2-KO induces widespread gene dysregulations and altered oncogenic expression pathways in human PCa cells	188
7.2.2 Potential key DEGs played essential roles in regulating tumour-related and metabolic pathways	194
7.2.3 Co-dysregulated DEGs in PC3 and 22Rv1 cells after ENO2-KO	197
7.2.4 Verification of co-dysregulated DEGs using retrospective analysis	200
7.3 Discussion	203
7.4 Conclusion	212

Chapter 8: General Discussion

8.1 Discussion	214
8.2 Future Plan	223
8.2.1 Short term technical plan	223
8.2.2 Long term research plan	226
8.3 General conclusion	227

Appendix Tables

Supplementary Figures

References

List of Figures

Figure 1.1 The number of new cases and death for PCa in men worldwide. _____	14
Figure 1.2 The multi-step process of PCa bone metastasis. _____	25
Figure 1.3 The function of Enolase 2 in aerobic glycolysis in tumour cells. _____	34
Figure 1.4 The comparison of ENO2 gene expression levels between dormant metastasis-initiating cells and fast-growing counterparts by RT-qPCR, Proteomics and RNA-Seq. _____	40
Figure 2.1 The mechanism of siRNA knockdown. _____	49
Figure 2.2 The mechanism of CRISPR Cas 9 knockout. _____	52
Figure 2.3 The map of U6-gRNA plasmid. _____	53
Figure 2.4 The Western Blotting procedure involves several steps. _____	62
Figure 2.5 The ELISA assay procedure involves several steps. _____	65
Table 2.4 Information of designed Primer for ENO2. _____	67
Figure 2.6 The schematic comparison of PCR, RT-PCR and RT- qPCR. _____	70
Figure 2.7 The process of alamarBlue™ reaction. _____	74
Figure 2.8 Cell migration evaluated by the wound-healing assay. _____	78
Figure 2.9 The comparison of Boyden Chamber migration and trans-well invasion assay. _____	81
Figure 2.10 Schematic representation of the landmark and ROI selected for trabecula bone in tibia and femur. _____	92
Figure 3.1 The flow chart of screening process in this systematic review and meta-analysis. _____	102
Figure 3.2 Forest plots included clinical studies showing association between ENO2 and PCa progression. _____	110
Figure 3.3 Forest plots included in vitro study showing the connection among ENO2 and androgen deprivation environment as well as metastatic potentials using LNCaP and C4-2B cell lines. _____	112
Figure 3.4 ENO2 gene expression is upregulated in metastatic PCa compared to primary PCa and benign patient samples. _____	114
Figure 3.5 Kaplan-Meier curves indicates an association between ENO2 alteration and survival. _____	116
Figure 3.6 Kaplan-Meier curve indicates an association between ENO2 overexpression and decreased survival. _____	118

Figure 4.1 22RV1, LNCaP-LN3, WPMY-1, DU145 and PC3 cell lines exhibit elevated levels of ENO2 expression at mRNA level. _____	128
Figure 4.2 22RV1, WPMY-1, DU145, LNCaP and C4-2B4 cell lines exhibit elevated levels of ENO2 expression examined using ELISA. _____	130
Figure 4.3 22RV1 and LNCaP-LN3 are associated with ENO2 higher expression protein level. _____	132
Figure 4.4 Glucose affect the expression of ENO2 of PC3, 22RV1, LNCaP-LN3 and WPMY-1 cell lines. _____	134
Figure 4.5 Pyruvate affect the expression of ENO2 of PC3, 22RV1, LNCaP-LN3 and WPMY-1 cell lines. _____	136
Figure 4.6 Glucose affect the viability of PC3, 22Rv1, LNCaP-LN3 and WPMY-1 cells. _____	138
Figure 4.7 Glucose affects apoptosis of PC3, 22Rv1, LNCaP-LN3 and WPMY-1 cells. _____	140
Figure 5.1 siRNA knockdown reduced the expression of ENO2 at mRNA level in PC3 and 22Rv1 cells. _____	148
Figure 5.2 ENO2 knockdown reduced the viability and proliferation but increased the apoptosis in PC3 and 22Rv1 cell lines. _____	150
Figure 5.3 ENO2 knockdown reduced the expression of ENO1 but increased the expression of ENO3 at mRNA level in 22Rv1 cells, but not in PC3 cells. _____	152
Figure 5.4 CRISPR Cas 9 knockout of ENO2 suppressed the expression of ENO2 at mRNA and protein level in PC3 and 22Rv1 cells. _____	155
Figure 5.5 Chromosome location, gene structure and sequence analysis of ENO2 in PC3 and 22Rv1 cells. _____	156
Figure 5.6 Representative images of their WTs and respective ENO2-KO single clones for PC3 and 22Rv1 cells. _____	157
Figure 5.7 ENO2 knockout reduced the viability and proliferation but did not affect apoptosis in PC3 and 22Rv1 cell lines. _____	159
Figure 5.8 ENO2 knockout reduced the migration in PC3 and 22Rv1 cell lines. _____	161
Figure 5.9 ENO2 knockout reduced the invasion in PC3 and 22Rv1 cell lines. _____	162
Figure 5.10 ENO2 knockout reduced the glucose consumption and lactate production in PC3 and 22Rv1 cell lines. _____	164
Figure 6.1 Outline of experimental setup and body weight measurement. _____	173
Figure 6.2 Sections of H&E stained decalcified left tibia form PC3 ENO2-KO and WT control injected mice. _____	175

Figure 6.3 The incidence of tumour from left tibia in PC3 ENO2-KO and WT control injected mice. _____	176
The data are mean \pm standard deviation (n=8). Chi-square test, **p<0.01. _____	176
Figure 6.4 Representative 3D models of PC3 WT and ENO2-KO cells injected tumour-bearing and non-tumour bearing. _____	178
Figure 6.5 The effects of genetically inhibition of ENO2 on bone morphometry in BALB/c nude mice. _____	179
Figure 7.1 RNA-Seq analysis showed genes that are differentially expressed in PC3 and 22Rv1 cells after ENO2 knockout. _____	190
Figure 7.2 RNA-Seq analysis showed GO pathway enrichment of PC3 and 22Rv1 cells after ENO2 knockout. _____	191
Figure 7.3 GSEA results showed co-enriched hallmarks and pathways with 22Rv1 cells in PC3 cells after ENO2 knockout. _____	195
Figure 7.4 GSEA results showed co-enriched hallmarks and pathways with PC3 cells in 22Rv1 cells after ENO2 knockout. _____	196
Figure 7.5 RNA-Seq analysis showed the commonly regulated DEGs in PC3 and 22Rv1 cells after ENO2 knockout. _____	198
Figure 7.6 RNA-Seq analysis showed the integrations and functional classification of the commonly regulated DEGs in PC3 and 22Rv1 cells after ENO2 knockout. ____	199
Figure 7.7 Retrospective studies indicated that 6 of the co-dysregulated DEGs after ENO2-KO showed correlations with the development of PCa. _____	202
Figure 8.1 The metabolic switches in PCa development. _____	217

List of Tables

Table 1.1 Description of classification based on TNM system, Gleason score and PSA level [30].	16
Table 1.2 The descriptions of PCa treatments.	20
Table 1.3 The description of treatment for PCa bone metastasis.	27
Table 1.4 The functions and mechanisms of ENO2 in various types of cancer.	38
Table 2.1 Characteristics of a panel of prostate cancer and prostatic myofibroblast tissue cell lines.	44
Table 2.2 The information of ENO2 Silencer™ Selected Validated siRNA	48
Table 2.3 The information of ENO2 predesigned CRISPR Guide RNA (gRNA) plasmid DNA (Sigma-Aldrich, 03172210MN)	51
Table 2.5 QC report for the sending samples (provided by Source Genomics).	86
Table 2.6 The settings of Micro-CT applied in mice bone scanning.	91
Table 3.1 Characteristics of the included clinical studies of PCa metastasis and ENO2.	104
Table 3.2 Characteristics of the included in vitro studies of PCa metastasis and ENO2.	105
Table 7.1 The information of top 20 DEGs in PC3 ENO2-KO cells.	192
Table 7.2 The information of top 20 DEGs in 22Rv1 ENO2-KO cells.	193

Appendix Tables and Supplementary Figures

Appendix Table 1. List of search strategies of Web of Science, Ovid MEDLINE® and PubMed.	228
Appendix Table 2. List of exclusive studies	231
Appendix Table 3. List of 7 databases of PCa patient samples in NCBI GEO for retrospective study.	238
Appendix Table 4. Quality assessment for clinical studies using a modified Newcastle-Ottawa scale (NOS).	239
Appendix Table 5. Quality assessment for in vitro studies using the OHAT RoB tool.	240
Appendix Table 6. Certainty of evidence for meta-analysis outcomes using Cochrane guidelines.	241
Appendix Table 7. List of differentially expressed genes in PC3 cells with ENO2 knockout.	244
Appendix Table 8. List of differentially expressed genes in 22Rv1 cells with ENO2 knockout.	263
Supplementary Figure 1. Cell line authentication report for PC3.	272
Supplementary Table 2. Cell line authentication report for 22Rv1.	273
Supplementary Figure 3. Cell line authentication report for WPMY-1.	274
Supplementary Figure 4. Cell line authentication report for DU145 and LNCaP-LN3.	275
Supplementary Figure 5. (A and B) The relative expression of ENO1 and ENO3 were normalized to ENO2 with a $2^{-\Delta\Delta Ct}$ fold change in PC3 and 22Rv1 WT cells. The data are mean \pm standard deviation (n=3). One- way ANOVA with Dunnett multiple comparisons. *p<0.05.	276
Supplementary Figure 6. (A and B) Expression of ENO1 of mock controls at 24, 48 and 72-hour time points were normalized to HPRT1 compared to PC3 and 22Rv1 WT, shown as ΔCt . (C and D) Expression of ENO3 of mock controls at 24, 48 and 72-hour time points were normalized to HPRT1 compared to PC3 and 22Rv1 WT, shown as ΔCt . The data are mean \pm standard deviation (n=3). One- way ANOVA with Dunnett multiple comparisons. **p<0.01 and ***p<0.001.	277
Supplementary Figure 7. The effect for the development of PCa bone metastasis in an intracardiacaly injected PC3 xenograft model. (A and B) The skeletal tumour growth in the control cohort was only examined by IVIS measurement on the back and front sides of the mice on Days 5, 19, and 31 after injection, respectively. (C and D) Tumor burden in control mice decreased within 31 days, measured as log total flux (photons/second). The data are mean \pm standard deviation (n=8).	278

Supplementary Figure 8. The effect of genetically inhibition of ENO2 in immune cells in whole blood. (A) The number total white blood cells from Balb/c mice of two different groups (B) The number total red blood cells from Balb/c mice of two different groups (C) The number platelets from Balb/c mice of two different groups (D) The number lymphocytes from Balb/c mice of two different groups (E) The number granulocytes from Balb/c mice of two different groups. The data are mean \pm standard deviation (n=8). Unpaired t-test. _____ 278

Supplementary Figure 9. GSEA results showed the tumour related enriched hallmarks and pathways in PC3 cells after ENO2 knockout. The p values are represented on the figure. _____ 280

Supplementary Figure 10. GSEA results showed the tumour and metabolic related enriched hallmarks and pathways in 22Rv1 cells after ENO2 knockout. The p values are represented on the figure. _____ 281

Scientific Appendix _____ 282

List of Abbreviations

2PG	2-phosphoglycerate
ABI	Abiraterone
ACO2	Mitochondrial aconitase
ADT	Androgen deprivation therapy
ALDO	Aldolase
ALL	Acute lymphoblastic Leukemia
AR	Androgen receptor
ARPIs	AR pathway inhibitors
AR-V7	AR splice variant 7
ATF4	Activating transcription factor 4
ATP	Adenosine triphosphate
BCa	Breast cancer
BCA	Bicinchoninic acid
BLI	Bioluminescent intensity
BMPs	Bone morphogenetic proteins
BP	Biological process
BPH	benign prostatic hyperplasia
BSA	Bovine Serum Albumin
BV/TV	Trabecular bone volume fraction
ccRCC	Clear cell renal cell carcinoma
CDS	Coding sequence
CHGA	Chromogranin A
CI	Confidence intervals
CMV	Cytomegalovirus
CPM	Count-per-million
CRC	Colorectal cancer

CRISPR	Clustered regularly interspaced short palindromic repeats
CRPC	Castration-resistant prostate cancer
CSS	Charcoal-stripped serum
Ct	Cycle threshold
CTCs	Circulating tumour cells
DAZ	Deleted in azoospermia
DAZAP2	DAZ-Associated Protein 2
DEG	Differential gene expression
DHEA	Dehydroisoandrosterone
DHT	dihydrotestosterone
DHT	Dihydrotestosterone
DHT	dihydrotestosterone
DMSO	Dimethyl sulfoxide
DOC	Docetaxel
DRE	Digital rectal examination
dsDNA	Double-stranded DNA
dsRNA	double-stranded RNA
DTCs	Disseminated tumour cells
EB	Ethidium Bromide
ECM	Extracellular matrix
EDTA	Trypsin-ethylenediaminetetraacetic acid
EGFR	Epidermal growth factor receptor
ELISA	Enzyme-linked immunosorbent assay
EMT	Epithelial mesenchymal transition
ENO1	α -Enolase, Enolase 1
ENO2	γ -Enolase, Enolase 2
ENO3	β -Enolase, Enolase 3

ENZA	Enzalutamide
ET-1	Endothelin 1
FACS	Fluorescence-activated cell sorting
FBS	Fetal bovine serum
FC	Fold Change
FGF	Fibroblast growth-factor
GAPDH	glyceraldehyde phosphate dehydrogenase
GBM	Glioblastoma
GEP-NETs	Gastroenteropancreatic neuroendocrine tumour
GFP	Green fluorescence protein
GLUTs	Glucose transporters
GnRH	Gonadotropin-releasing hormone
GO	Gene Ontology
gRNA	Guide RNA
GSEA	Gene Set Enrichment Analysis
GWAS	Genome wide association studies
H&E	Haematoxylin & Eosin
HIFs	Hypoxia-inducible factor
HKs	Hexokinases
HNSCC	Head and neck squamous cell carcinoma
hOBMT	Human osteoblast-derived mineralized microtissue
hOBMT	osteoblast-derived mineralized microtissue
HRP	Horseradish Peroxidas
I.C.	Intracardiac
IGFs	Insulin-like growth factors
Kan	Kanamycin
LDH	Lactate dehydrogenase

LHRH	Luteinizing hormone-releasing hormone
M-CSF	macrophage colony-stimulating factor
mCRPC	Metastatic castration-resistant prostate cancer
MDS	Multidimensional scaling
MF	Molecular function
Micro-CT	Micro Computed Tomography
MRI	Magnetic resonance imaging
NE	Neuroendocrine
NED	Neuroendocrine differentiation
NEPC	Neuroendocrine prostate cancer
NEtD	Neuroendocrine transdifferentiation
NF-κB	nuclear factor kappa beta
NLS	Nuclear localization sequence
NSE	Neuron-specific enolase
O.D.	Optical density
OPG	osteoprotegerin
OXPHOS	oxidative phosphorylation
P/S	Penicillin-streptomycin
PARPi	PARP inhibitor
PBS	Phosphate-buffered saline
PCa	Prostate cancer
PCR	Polymerase chain reaction
PDH	Pyruvate dehydrogenase
PDK	Pyruvate dehydrogenase kinase
PD-L1	Programmed cell death ligand 1
PEP	Phosphoenolpyruvate
PGI	Phosphoglucose isomerase

PGK	Phosphoglycerate kinase
PGM	Phosphoglycerate mutase
PIL	Procedure Individual License
PK	Pyruvate kinase
PPI	Protein-protein interaction
PPL	Procedure Project License
PSA	Prostate-specific antigen
PSMA-PET	Prostate-specific membrane antigen positron emission tomography
PTHRP	Parathyroid hormone-related protein
pUC ori	pUC origin
PVDF	polyvinylidene
QC	Quality controls
RANK	NF- κ B
RANKL	NF- κ B ligand
Rb	Retinoblastoma
RCT	Randomized controlled trial
RISC	RNA-induced silencing complex
RNAi	RNA interference
ROI	Region of interest
RP	Radical prostatectomy
RT- qPCR	Real-time Quantitative Reverse Transcription Polymerase Chain Reaction
RT-PCR	Reverse Transcription Polymerase Chain Reaction
SCLC	Small cell lung cancer cells
SD	Standard deviations
SEM	Standard error measurements
siRNA	Small interfering RNA
SNPs	Single-nucleotide polymorphisms

SREs	Skeletal-related events
ssRNAseq	Single-cell RNA sequencing
SYP	Synaptophysin
TAE	Tris-Acetate-EDTA
Tb.N	Trabecular number
Tb.Pf	Trabecular bone pattern factor
Tb.Sp	Trabecular separation
Tb.Th	Trabecular thickness
TBS	Tris buffer saline
TCA	Tricarboxylic acid
TCA	Tricarboxylic acid
TGFβ	Transforming growth factor-β
TGS	Tris/Glycine/SDS
TMA	Tissue microarrays
TNM	Tumour-Node-Metastasis
tracrRNA	Trans-activating crispr RNA
TRAP	Tartrate-resistant acid phosphatase
TRUS	Transrectal ultrasound
VOI	Volume of interest
ZIP1	Zinc transporter
ΔCt	Delta Ct

Abstract

Prostate cancer (PCa) is the most frequently diagnosed cancer in men which patients with distant bone metastases have high mortality. ENO2 is an important enzyme in the glycolysis process that most cancer cells rely on and also a widely-used biomarker for various neuroendocrine cancers, but there are no studies to determine whether ENO2 is functionally involved in PCa progression and metastasis. Therefore, we hypothesize that ENO2 positively contributes to PCa bone metastasis.

To test the hypothesis, a systematic review and meta-analysis were initially conducted to examine the association between ENO2 expression and PCa progression. Clinical and *in vitro* studies included suggested that high ENO2 expression is significantly associated with more malignant forms of PCa and is not influenced by different treatments. Retrospective and bioinformatic studies further identified higher ENO2 expression in both PCa metastases and benign prostate tissue, more importantly correlates with reduced survival rates. This finding was supported by *in vitro* examining the expression of ENO2 in various PCa and benign prostate tissue cells and data suggested that, the expression of ENO2 was upregulated not only in highly metastatic PCa cell lines but also in benign prostate tissue cells. This is possible due to the unique feature of glucose metabolism in prostate and PCa, demonstrated by the data that glucose supplement influenced ENO2 expression and cellular behaviors in both PCa and benign prostate tissue cells but in a different manner.

To further elucidate the functional contribution of ENO2 to PCa progression, PCa cell lines, 22Rv1 and PC3, were selected for transient knock down and genetic knock out studies. Knockdown of ENO2 by siRNA reduced cell viability and proliferation but increased apoptosis compared to mock-transfected controls at 48 hours post-transfection. Successful knockout of ENO2 in two clones in both PC3 and 22Rv1 cells was verified at both mRNA and protein levels. Genetic knockout of ENO2 significantly

reduced viability, proliferation, migration, and invasion, but had no impact on apoptosis. In a murine xenograft model systemically injected with human PC3 cells, knocking out the ENO2 gene reduced the occurrence of bone metastases, decreased tumour burden, and protected bone from tumour induced destructions. Further bulk RNA sequencing on PC3 and 22Rv1 knockout cells and subsequent bioinformatic analysis suggested that ENO2 is not only a key component of glycolysis but also promotes the progression of PCa by regulating key pathways such as the E2F pathway.

In conclusion, ENO2 functionally contributes to PCa bone metastasis and offers the potential as a pharmaceutical target for developing ENO2 oriented treatments in fighting this deadly disease.

Chapter 1: Introduction

1.1 Prostate cancer

The prostate is a walnut-shaped gland located beneath the urinary bladder and in front of the rectum [1]. It is primarily responsible for the secretion of prostate fluid, which plays a crucial role for semen liquefaction, the clotting cycle, and promoting sperm motility [2]. Structurally, the prostate gland comprises three different types of cells, including basal, luminal epithelial, and neuroendocrine cells, all of which play distinct roles in its normal function [3].

Prostate cancer (PCa) has ranked as the second most commonly diagnosed cancer and stands as the fifth highest cause of mortality globally among men [4, 5], which highlights the clinical need for effective screening, early diagnosis and treatment strategies. Importantly, more than 95% of PCa cases are adenocarcinomas, which arise from the epithelial cells of the gland [6, 7]. Most cases of localized PCa tend to exhibit a slow-growing, indolent nature [8]. However, once it exhibits aggressive behaviour, it can metastasize beyond the prostate gland to other distant organs, predominantly to bone [9].

1.1.1 The Genetic Epidemiology and Risk Factors

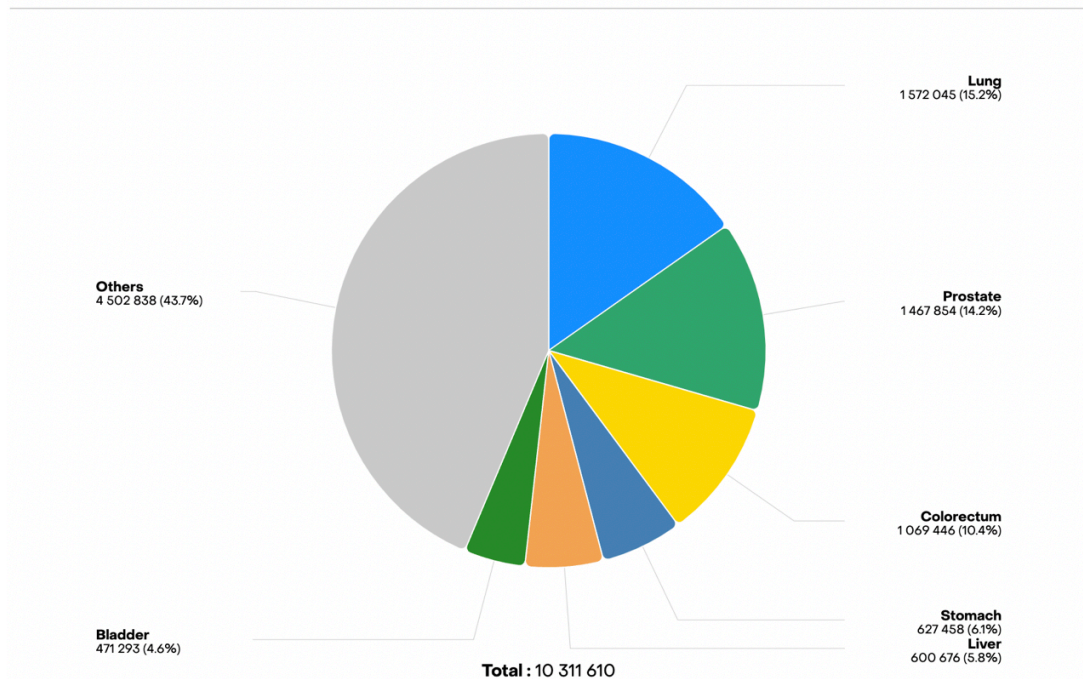
PCa has ranked as the second most commonly diagnosed cancer and stands as the fifth highest cause of mortality globally among men [4, 5]. 14.2% of the total new cases and 7.3% of total cancer-related deaths in men were reported from PCa on a global scale in 2022 (**Figure 1.1**) [5]. The incidence and mortality of PCa are correlated with age, with the average age at diagnosis being approximately 66 years worldwide [4].

Acknowledged risk factors for PCa on a global scale include advanced age, ethnicity, and family history [4]. PCa is commonly regarded as a cancer prevalent among older individuals, with the median age of presentation being 68 years [10]. Notably, the incidence of PCa is notably elevated among individuals of African descent. Reports indicated that the incidence of PCa in African-American men is 64% higher than that of white men, with a mortality rate 2.3 times higher [11, 12]. Interestingly, genome-wide

association studies (GWAS) have verified 76 single-nucleotide polymorphisms (SNPs) which are mainly in regions clinically relevant to the risk of familial clustering PCa [13]. For example, a PCa-related SNP located on chromosome 19, within the regions housing *KLK2* and *KLK3*, has been demonstrated to influence the expression of prostate-specific antigen (PSA) [14]. Furthermore, genetic linkage studies have revealed several genes associated with risk of familial clustering of PCa, such as *HPC1*, *HPC2*, *MSR1*, *BRAC1* and *BRAC2* [4]. For instance, mutations in *HPC1* and *HPC2*, situated on chromosome 1 and 17 respectively, are believed to be genetically linked to PCa and contribute to the regulation of PCa progression. These mutations are implicated in diminishing antiviral activity and enhancing the expression of the TGF- β signaling pathway, thereby influencing PCa development [4, 15]. *MSR1*, located on chromosome 8, has also been found to be associated with the development of PCa [16]. Additionally, men harbouring mutations in *BRCA1* and *BRCA2* genes tend to exhibit a clinically aggressive phenotype of PCa, especially in the case of *BRCA2* mutations, which are linked to an increased risk of developing PCa [4, 17]. The relative risk of PCa in men with germline *BRCA2* mutations is approximately five times that of men without *BRCA2* mutations [13]. Furthermore, the X chromosome including the gene encoding the androgen receptor (AR) has been implicated in PCa inheritance due to deletions within specific regions [18]. Besides, factors such as dietary habits, obesity, inflammation and hyperglycaemia have also demonstrated positive correlations with the incidence of PCa [4, 19, 20].

A

Absolute numbers, Incidence, Males, in 2022
Continents



B

Absolute numbers, Mortality, Males, in 2022
Continents

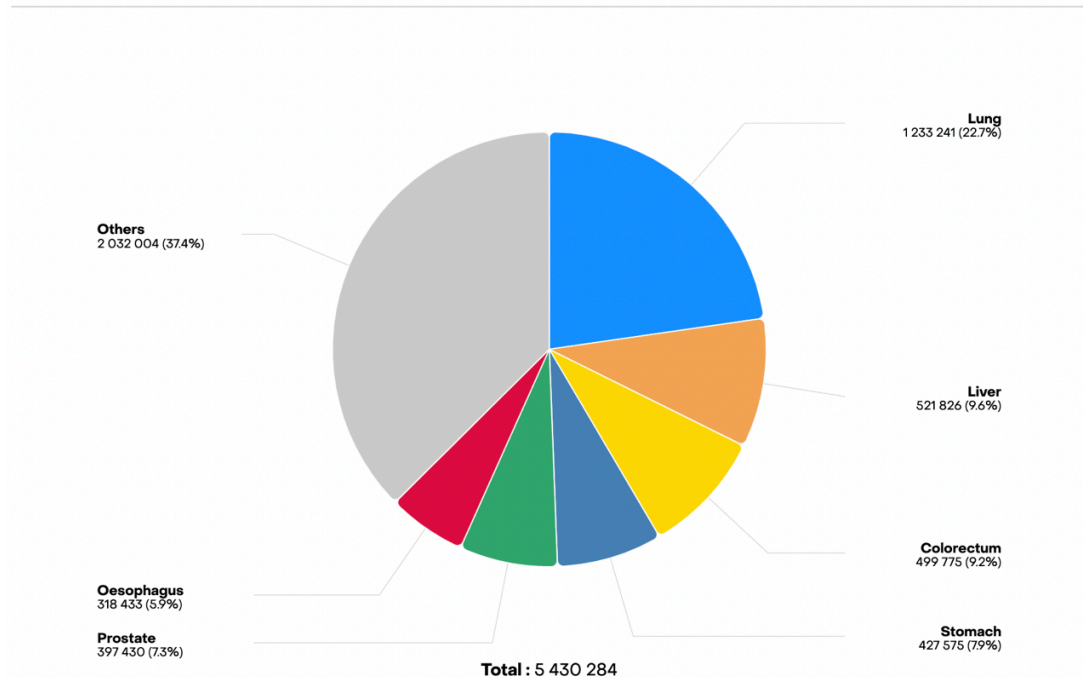


Figure 1.1 The number of new cases and death for PCa in men worldwide.

Source: <https://gco.iarc.fr/today/en/dataviz/pie>.

1.1.2 Diagnosis of Prostate Cancer

Traditionally, PCa diagnosis has involved a combination of digital rectal examination (DRE), PSA blood test, biopsy and imaging [21, 22]. The DRE is applied by feeling inside the rectum to assess the size and abnormalities of the prostate gland [22]. PSA, which is a glycoprotein secreted by prostate epithelial cells, has been widely used as a guiding biomarker for the initial diagnosis and monitoring of progression for PCa [22, 23]. Prostate tumour cells typically result in a significant elevation of approximately 105-fold in circulating levels of PSA [24]. Notably, although PSA serum levels are influenced by the development of tumour, increased PSA levels have also been detected in benign prostatic hyperplasia (BPH) and prostatic inflammatory conditions [25]. Besides, biopsy, by using a needle to collect the tissue samples from the prostate and analysing under microscopes, is the most reliable approach to diagnose PCa [22]. Additionally, an application of magnetic resonance imaging (MRI), transrectal ultrasound (TRUS) and prostate-specific membrane antigen positron emission tomography (PSMA-PET) are not only beneficial in determining the diagnosis and treatment of PCa but can also be used to determine the extent of metastasis [22].

1.1.3 The Pathologic Grade and Clinical Stage of Prostate Cancer

PCa would be classified using the Gleason grading system, which assigns a score based on the microscopic appearance of tumour cells, by adding the first half of the score based on the primary (scored 1 to 5) and the second half based on the secondary grades (scored 1 to 5) [26, 27]. The Gleason grades could predict risk and reflect prognosis in a way as follows: Gleason score ≤ 6 (group I, low risk.); Gleason score = 7 (group II or group III, well-differentiated histology); Gleason score = 8 to 10 (group IV or group V, poor differentiation and the worst prognosis) [28, 29]. In addition, the clinical stages of PCa would be defined by Tumour-Node-Metastasis (TNM) system, which can be used to assess the range of the primary tumour (T), the presence or absence of tumour in regional lymph node (N) and distant metastases (M) [29, 30] (**Table 1.1**).

Table 1.1 Description of classification based on TNM system, Gleason score and PSA level [30].

Group	T	N	M	Gleason Score	PSA level (ng/ml)
I	T1	N0	M0	< 10	≤ 6
	T2	N0	M0	< 10	≤ 6
	T1 or T2	N0	M0	/	/
IIA	T1	N0	M0	< 20	7
	T1	N0	M0	10 - 20	≤ 6
	T2	N0	M0	< 20	≤ 7
	T2	N0	M0	< 20	≤ 7
	T2	N0	M0	/	/
IIB	T2	N0	M0	Any	Any
	T1 or T2	N0	M0	≥ 20	Any
	T1 or T2	N0	M0	Any	≥ 8
III	T3	N0	M0	Any	Any
IV	T4	N0	M0	Any	Any
	Any T	N1	M0	Any	Any
	Any T	Any N	M1	Any	Any

T1: clinically invisible tumour; T2: tumour is limited inside the prostate gland; T3: tumour spreads outside the prostate capsule; T4: tumour invades adjacent tissues beyond the seminal vesicle; N0: tumour has not spread to nearby lymph nodes; N1: tumour has spread to nearby lymph nodes; M0: tumour has not metastasis to distant lymph nodes or organs; M1: tumour has metastasis to distant lymph nodes or organs [30].

1.1.4 Treatments of Prostate Cancer

PCa, which is recognized as an androgen sensitive condition and rely on AR signalling, is categorized into different subtypes according to pathological features and morphological alterations [31]. The predominant subtype is acinar adenocarcinoma, accounting for over 95% of cases [6, 7]. Beyond acinar adenocarcinoma, there are several other less frequent but clinically significant subtypes, including:

- Mucinous adenocarcinoma, accounting for about 0.3 % of all cases, which is characterized by the production of mucin [31].
- Ductal adenocarcinoma, a rare but aggressive form that arises from the prostatic ducts [32].
- Neuroendocrine prostate cancer (NEPC), which often arises after chronic androgen depletion (ADT therapy), exhibits more malignant and aggressive behavior [33].
- Signet ring cell carcinoma, an extremely rare subtype, known for its unique cellular appearance and are widely infiltrative [31].

Different treatment approaches for these subtypes are adopted based on their stages, aggressiveness, hormonal sensitivity, and the presence of specific molecular alterations (**Table 1.2**).

In the early stages of PCa (localized PCa), tumour cells are typically classified as indolent or aggressive based on clinical and pathological factors, including Gleason score and PSA level [34]. A safe approach which is active surveillance, including PSA blood tests, DREs or biopsies at the frequency advised by doctors, is applied to avoid unnecessary interventions for men with low-risk PCa [35]. However, it is advisable to adopt a strategy of "watchful waiting" instead of active surveillance for older men or those with a limited life expectancy. This approach involves fewer tests until any signs of PCa progression become evident [36].

Although the development can be effectively inhibited through surgery (radical prostatectomy) and radiotherapy in the early stage, recurrence is still observed in up to 35% of cases, leading to a progression of distant metastasis [34, 37]. PCa usually remain hormone sensitive during the initial stages of recurrence. Thus, androgen deprivation therapy (ADT) is further employed to effectively suppress tumour growth by blocking the androgen levels [38]. Traditionally, ADT was developed as the predominant treatment for advanced PCa, achieving castrate levels of testosterone through surgical castration or repeated long-acting injections with luteinizing hormone-releasing hormone (LHRH) agonists or gonadotropin-releasing hormone (GnRH) antagonists, either alone or in combination with chemotherapy [39-42].

However, PCa would progress to castration-resistant prostate cancer (CRPC) stage with poor-prognosis in response to ADT [43]. Currently, multiple mechanisms contributing to the resistance against AR-based therapies have been discovered. Interestingly, in CRPC patients, circulating adrenal androgens or intratumoural cholesterol would act as precursors for conversion, initiating intratumoural steroidogenesis, leading to the synthesis of dihydrotestosterone (DHT) and ultimately resulting in serum DHT levels comparable to those observed in patients without ADT therapy [43, 44]. Additionally, AR gene amplification, resulting in protein overexpression, would stand as the most common genetic alteration in patients with CRPC [45]. Furthermore, AR gene mutations, which can not only be activated by adrenal androgens or other steroid hormones, but also convert AR antagonists used for treatment into potential agonists, are also frequently observed in CRPC patients [43]. Consequently, elevated expression of AR would exhibit in CRPC patients since AR signaling is reactivated through the binding of DHT [43]. Hence, persistent AR signaling maintained a primary contributor to the development of CRPC. Notably, next-generation AR pathway inhibitors (ARPIs), containing abiraterone (ABI) and enzalutamide (ENZA), have been developed to address the treatment of CRPC by

effectively blocking the AR axis [46]. Specifically, ABI would inhibit CYP17A1, which is expressed in adrenal, testicular and prostatic tumour tissues, thereby inhibiting androgen biosynthesis [22]. While ENZA would inhibit AR signaling directly by preventing the translocation of the AR from the cytoplasm to the nucleus, thereby blocking AR binding to chromosomal DNA [47]. A promising targeted therapy, known as a PARP inhibitor (PARPi), is being developed to treat DNA repair-deficient PCa [48]. PARPi operates through synthetic lethality, a mechanism that disrupts the DNA damage response in cancer cells [48]. This approach is particularly beneficial for managing metastatic CRPC (mCRPC), especially in cases with *BRCA1/2* mutations, which impair the cell's ability to repair DNA, making them more susceptible to this form of treatment [48, 49]. In addition, immunotherapies, including checkpoint inhibitors, cytokines, and therapeutic cancer vaccines have been developed for the treatment of advanced mCRPC and have shown positive results [50]. Importantly, combination therapy, which combines ADT with chemotherapy or immunotherapy, is a strategy being developed for the treatment of advanced CRPC and mCRPC [22].

Chronic androgen depletion could cause NE differentiation of tumour cells, ultimately leading to the development of AR-negative NEPC in a subset of patients, exhibiting more malignant and aggressive in behavior [33, 51]. Currently, PCa cells experience lineage plasticity, adopting NE with the expression of neuronal markers like ENO2, synaptophysin (SYP) and chromogranin A (CHGA) [33]. NEPC does not typically respond well to ADT and requires platinum-based chemotherapy [52].

Table 1.2 The descriptions of PCa treatments.

Tumour stage	Treatment	Description
Localized or locally advanced PCA	Active surveillance	A safe approach to avoid unnecessary interventions for men with low-risk PCa. Regular PSA blood tests, DREs or biopsies at the frequency advised by doctors [35].
	Watchful waiting	For older men or those with a limited life expectancy [36].
	Radical prostatectomy (RP)	Remove the prostate gland along with the surrounding vesicles and neighboring tissues [37].
	Radiotherapy	For patients with locally advanced disease who are not suitable for surgery [34].
Hormone sensitive recurrent PCa	Hormone therapy (ADT)	Achieving through surgical castration or the application of LHRH agonists or GnRH antagonists as a means of blocking testosterone production [42, 53].
	Chemotherapy	Docetaxel (DOC) is the most commonly used chemotherapy and can be used combine with ADT [54].
CRPC	ARPIs	Abiraterone and enzalutamide, have been developed to address the treatment of CRPC by effectively blocking the AR axis [46].
	Chemotherapy	Cabazitaxel, which is a novel taxane, is employed in the treatment of patients with mCRPC who have no longer responded to hormone and DOC therapies [55].
mCRPC	PARPi (optional)	A promising targeted therapy being developed to treat DNA repair-deficient mCRPC, especially in cases with <i>BRCA1/2</i> mutations [48, 49].
	Immunotherapy	Including checkpoint inhibitors, cytokines, and therapeutic cancer vaccines have been developed for the treatment of advanced mCRPC and have shown positive results [50].

1.1.5 Bone microenvironment and PCa bone metastasis

1.1.5.1 Bone microenvironment

Bones are constantly changing known as bone remodelling throughout a lifespan. Bone remodelling serves to maintain the structural integrity of the skeletal system while also playing a crucial role in metabolic processes by regulating the balance of calcium and phosphorus in the body [56]. It involves the removal of old or damaged bone tissue followed by the deposition of new bone material [56]. Bone serves as a dynamic framework, comprises two main types: cortical and trabecular bone [57]. Cortical bone forms the outer layer of skeleton responsible for bearing the weight load and offering protective abilities [58]. Trabecular bone features a substantial porous matrix situated within the inner regions of bone ends [59]. Despite both cortical and trabecular bone being metabolically active, trabecular bone experiences remodelling higher compared to cortical bone [57].

Three primary cell types facilitate bone remodelling, including osteoblasts, osteoclasts, and osteocytes. Osteoblasts, which derived from mesenchymal stem cells, comprise 4-6% of the total bone cell population. Their primary roles include synthesizing and mineralizing new bone matrix and facilitating the formation of osteoclasts [57]. Osteoclasts are multinucleated cells originating from mononuclear cells found in the bone marrow, play a crucial role in resorbing existing bone matrix and represent approximately 1-4% of the total bone cell population [57, 60]. Additionally, osteocytes, constituting 90–95% of all bone cells, play an essential role not only in sensing mechanical forces, but also for transmitting signals to osteoblasts and osteoclasts to regulate bone deposition or resorption in response [57, 61].

Osteoblasts generate abundant amounts of receptor activator of nuclear factor kappa beta (NF- κ B) ligand (RANKL), which then interacts with RANK receptors on monocytes, triggering the development of mature osteoclasts. Furthermore, macrophage colony-stimulating factor (M-CSF) can also stimulate the maturation of osteoclasts. The

mature multinucleated osteoclasts are generated by fusing of multiple monocytes in the presence of both M-CSF and RANKL [57, 62]. Osteoclasts exhibit a distinctive morphology which develops a ruffled border along their cell membrane that intimately interacts with the bone matrix surface. It amplifies the membrane's surface area, promoting the secretion of bone-degrading enzymes like tartrate-resistant acid phosphatase (TRAP) [57, 63]. The bone-resorbing function of osteoclasts triggers the secretion of growth factors, including transforming growth factor-beta (TGF- β), insulin-like growth factors (IGFs) and bone morphogenetic proteins (BMPs). Subsequently, these factors play an essential role in fostering osteoblast maturation and activity, thereby promoting bone formation [57, 64].

1.1.5.2 PCa bone metastasis

Bone metastases are frequently observed as the predominant site of colonization in distant metastases from PCa, with approximately 70% of individuals diagnosed with advanced PCa presenting incurable bone metastases [9]. The prognosis for patients diagnosed with PCa without bone metastases suggested a five-year survival rate of around 56% [65]. However, the five-year survival rate reduced to only 3% for patients with bone metastasis post-diagnosis. Additionally, the five-year survival rate for PCa patients with bone metastases induced skeletal-related events (SREs), including pathological fractures, hypercalcemia, bone pain and spinal compression, is even less than 1%, thus indicating a poor prognosis [65, 66]. Therefore, it is important to understand the biological process of PCa bone metastasis.

Tumour cells originating from the prostate have a tendency to preferentially migrate into bone via the blood vessels, exhibiting bone tropism and resulting in the formation of secondary skeletal metastases [67]. The process of metastasis involves a series of well-defined steps known as the metastatic cascade. The metastasis initiates with the proliferation of primary intraprostatic tumour cells and spreads through achieving the epithelial mesenchymal transition (EMT). EMT is a process that malignant tumour cells

originating from epithelial tissue dissolve the epithelial cell-cell junctions and transit to mesenchymal-like phenotype. The invasive properties are subsequently obtained by degrading extracellular matrix (ECM) proteins, concomitantly suppressing the expression of epithelial-related genes and activating the expression of mesenchymal-related genes [68, 69]. These changes facilitate detachment from the primary tumour, invasion of the extracellular matrix, and eventual dissemination to distant organs such as the bone. Currently, the reduction of E-cadherin and elevation of N-cadherin, Twist, Snail, Slug, vimentin, fibronectin have been considered as markers for verifying cellular EMT *in vitro* [70, 71]. Only a small proportion of mesenchymal malignant cells that escape from the primary site manage to survive in the circulation and are able to adhere to the vascular endothelium, allowing them to extravasate into the bone marrow environment and initiate colonization [72]. Once reached into the bone, disseminated tumour cells (DTCs) could have the potential to enter a dormant state, residing in the G0 phase of the cell cycle, that may maintain inside the bone marrow thereby evading conventional treatments [73, 74]. Dormant cells can persist for years before reactivating, often triggered by changes in the microenvironment, such as inflammatory signals, hormonal changes, or mechanical stress [75, 76]. Reactivation results in the recovery of mitotic activity and cell division, ultimately leading to the overt bone metastases [73, 75].

The bone tropism of PCa metastasis could be explained by “seed and soil” theory, which indicating that metastases would only develop if the "seed" and "soil" were compatible, created by Paget date back to 1889 [77]. Bone provides the specific microenvironment or niches, containing growth factors, chemokines and cytokines to provide homing signals, conducive to the growth of PCa tumour cells, thereby promoting the preferential colonization [78, 79]. In contrast to other cancer types that generate bone metastases, PCa predominantly produce osteoblastic lesions in bones, characterized by the formation of mechanically fragile woven bone, resulting in

osteosclerotic metastases [80]. Parathyroid hormone-related protein (PTHrP), BMPs, endothelin 1 (ET-1), Wnt ligand, IGFs and fibroblast growth-factor (FGF), would be secreted by PCa tumour cells to stimulate the activation of osteoblasts or promote the differentiation of precursor cells into osteoblasts [69, 81]. Subsequently, activated osteoblasts secrete receptor activator of RANKL, which binds to receptor activator of RANK present on osteoclasts, resulting in activation of osteoclast-mediated bone resorption. It further releases other growth factors stored in bone, e.g. TGF β , that promotes tumour growth, forming a vicious cycle with a mixed osteolytic/osteosclerotic lesions [69, 82]. Normally, the activity of osteoclast is inhibited by osteoprotegerin (OPG) produced by osteoblasts, which binds to RANKL and disrupts the downstream pathway of RANK. However, during the bone metastasis period, the balance between OPG and RANKL will be disrupted, continuing the vicious cycle during bone metastasis [69, 83] (**Figure 1.2**).

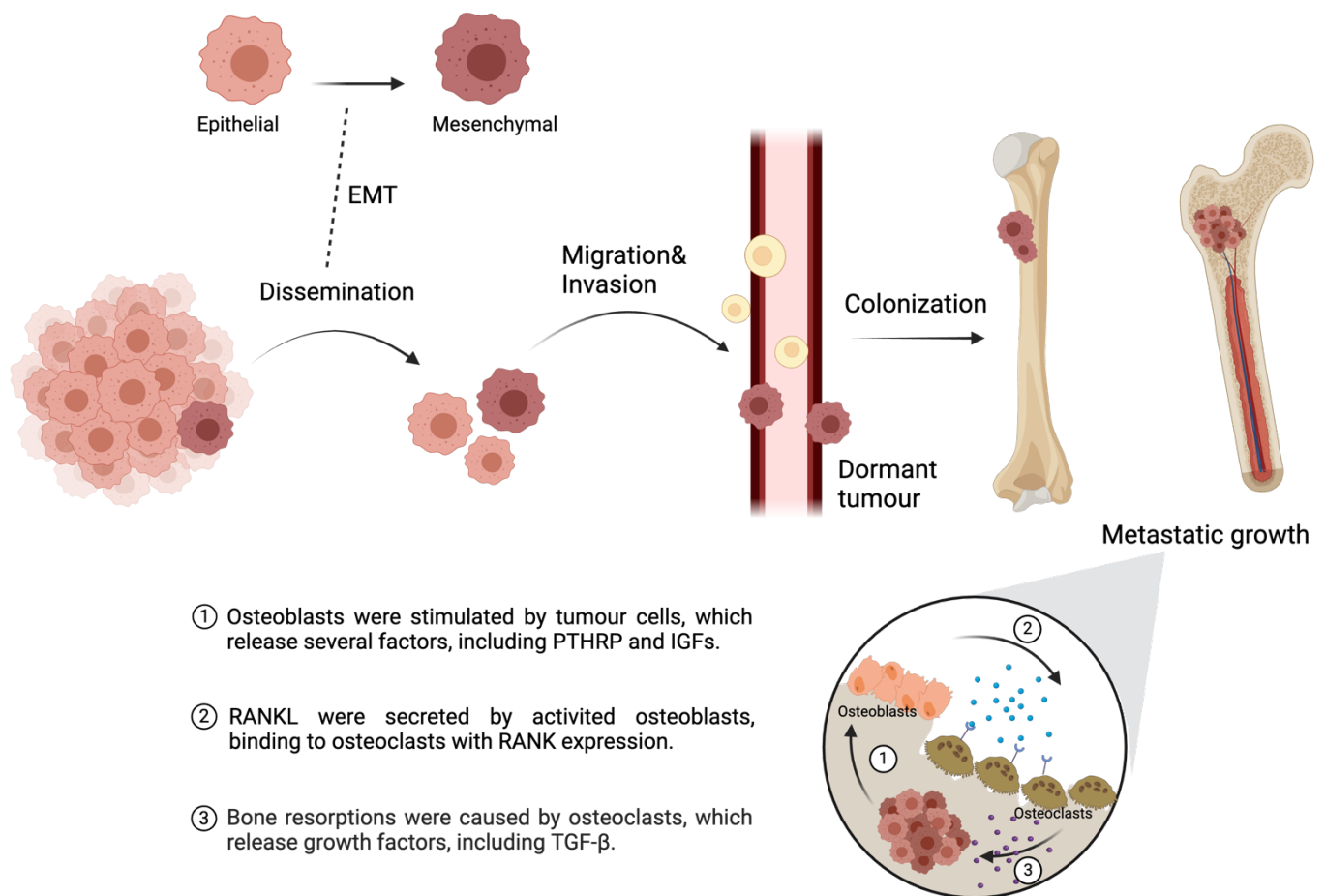


Figure 1.2 The multi-step process of PCa bone metastasis.

A small population of PCa cells with migratory ability detach from the primary site and disseminate. Through EMT, epithelial-derived tumour cells acquire mesenchymal characteristics, lose their connection with the basement membrane and enhance their migratory and invasive abilities. Once invade into the circulation, circulating tumour cells (CTCs) must survive and adhere to the vascular endothelium before extravasating into bone marrow for metastatic colonization. Colonized tumour cells secrete various factors that activate osteoblasts. Activated osteoblasts in turn secrete RANKL, which binds to its receptor, RANK, expressed on osteoclasts, leading to osteoclast activation. Activated osteoclasts then initiate bone resorption, releasing growth factors that further support tumour growth, causing the vicious cycle of bone metastasis (Created in Biorender).

1.1.5.3 Treatment of PCa bone metastasis

Present therapies for bone metastasis in PCa primarily focus on palliative care, which tends to disrupt the vicious cycle and subsequently manage the bone metastasis [36]. Bisphosphonates are commonly used drugs for advanced PCa with bone metastasis. They are pyrophosphates compounds that possess an affinity for hydroxyapatite, allowing them to adhere to bone mineral. They exert their effects by being absorbed by osteoclasts during bone resorption, which function by inhibiting osteoclast activity, thereby preserving bone resorption and facilitating bone formation by osteoblasts, ultimately reducing the risk of fractures [84, 85]. Additionally, radium-223, an alpha-emitting radionuclide with properties mimicking calcium, adheres to newly formed bone and triggers DNA double-strand breaks. It has received approval for treating bone pain in patients with bone metastasis [86]. Moreover, denosumab, which is an immunoglobulin belonging to the IgG subclass 2, can interfere with the binding of RANKL to its receptor RANK, thereby inhibiting the development osteoclasts [84, 87] (**Table 1.2**). However, there are no cure for bone metastasis therefore new effective treatments are urgently needed.

Table 1.3 The description of treatment for PCa bone metastasis.

Tumour stage	Treatment	Description
PCa with bone metastasis	Bisphosphonates	Bisphosphonates function by inhibiting osteoclast activity, thereby preserving bone resorption and facilitating bone formation by osteoblasts, ultimately reducing the risk of fractures [85].
	Radium-223 dichloride	An alpha-emitting radionuclide with properties mimicking calcium, adheres to newly formed bone and triggers DNA double-strand breaks [86].
	Denosumab	A monoclonal antibody inhibits RANKL which expressed on the surface of osteoblasts and PCa cells, thereby preventing the formation of osteoclasts [87].

1.1.6 Metabolic reprogramming in PCa

Alterations in metabolism in PCa cells are considered to be a marker of malignant transformation [88]. Metabolic reprogramming in PCa tumour cells have been found to involved in regulating the resistance during treatment [89]. Healthy prostate epithelial cells typically exhibit citrate-based metabolism, characterized by a relatively inefficient energy metabolic pattern by using glucose to synthesize citrate [88]. Large amounts of zinc are accumulated in prostate acinar epithelial cells, uniquely blocking the activity of mitochondrial aconitase (ACO2) which catalyzes citrate oxidation, thus protecting the entry of citrate into the TCA cycle [90, 91]. Therefore, citrate synthesized from aspartic acid and glucose is secreted as an important component of prostatic fluid as the final product of glucose metabolism [88, 89, 92]. During the initial stages of prostate tumour formation, tumour cells benefit from adequate oxygen and nutrients and oxygen owing to their close contact to the vasculature [89]. Despite glucose being the primary source of cells, early-stage PCa displays minimal or almost no glucose uptake, exhibiting a metabolic pattern characterized by increased oxidative phosphorylation (OXPHOS), which is highly efficient process that produce more adenosine triphosphate (ATP) compared to glycolysis [89, 93, 94]. Furthermore, there was evidence indicating that lipogenesis, especially fatty acid synthesis, is an early occurrence in prostate tumorigenesis and is linked with development of disease [91].

Unlike normal prostatic tissue and primary PCa cells, advanced tumour cells increase their uptake of glucose and produce lactate through aerobic glycolysis, to generate energy to survive and proliferate. This metabolic adaption was discovered and known as Warburg effect [95, 96]. Tumour-affected areas often exist within a hypoxic microenvironment, which is generated by insufficient vascularization, due to the rapid proliferation of tumour cells [97]. Even in a hypoxic environment, tumour cells still tend to use aerobic glycolysis for metabolism. In contrast to OXPHOS, aerobic glycolysis offers a more rapidly ATP production rate, which adequately meets the energy demands of rapidly dividing tumour cells [93, 98]. The elevated glucose uptake serves

as the anabolic carbon source required for malignant proliferation of tumour cells [95]. Tumour cells require not only energy but also metabolic intermediates for biosynthesizing macromolecules crucial for their growth. Numerous intermediates are generated by glycolysis that can be used for the biosynthesis of essential macromolecules, including lipids, nucleic acids and proteins, supporting the accelerated proliferation of cancer cells [93, 99]. Moreover, the efficient uptake and processing of glucose promote the activation of several non-mitochondrial pathways, including the pentose phosphate pathway, which generates ribose for nucleotide synthesis and NADPH for reductive biosynthesis, and the hexosamine pathway, which is responsible for protein glycosylation and glycerol synthesis. This provides evidence that Warburg effect indirectly fosters anabolic processes [89]. In addition, the production and release of abundant lactic acid into the extracellular space generate an acidic microenvironment, which not only promotes the invasion and metastasis of cancer cells, but also blocks the growth of surrounding normal cells and suppresses the activity of immune cells [93, 100].

Genetic alterations are one of the essential factors to affect metabolism in tumour cells in PCa [89]. It is common for cancer cells to experience amplification and/or mutations in genes associated with growth factor signalling pathways. For example, the activation of PI3K/AKT pathway, consequently reprogramming cellular metabolism through elevating the activity of nutrient transporters and metabolic enzymes, maintaining the anabolic requirements malignant tumour cells [101]. Besides, the glycolysis related genetic alterations regulation have been found to involved in the coordination of other metabolic pathways. For instance, the epidermal growth factor receptor (EGFR) signaling have been found to induce a glycolytic blockade, resulting in the accumulation of glycolytic metabolites within tumour cells and elevated levels of lactate in the extracellular environment [102]. However, EGFR oncogenic variant EGFRvIII would cohesively regulate intratumorally cholesterol levels and fatty acid synthesis [89,

103-105]. In addition, due to the limited supplies of nutrients and oxygen in tumour cells, cellular metabolism has to be modified to adapt to stress from the microenvironment, ultimately shapes the metabolic reprogramming in PCa cells. Hypoxia-inducible factor (HIFs) and activating transcription factor 4 (ATF4) are recognized as transcription factors crucial for tumour cells to adjust to nutrient availability [89]. Under conditions of limited nutrients, HIF1- α and ATF4 stimulate the upregulation of glucose and amino acid transporters, enabling cancer cells to effectively acquire diverse nutrients [106]. Additionally, HIF1- α orchestrates the expression of glycolysis-related enzymes, promoting continual ATP production [107].

1.2 Enolase 2

1.2.1 *Characteristics of Enolase*

Enolase is a key glycolytic metalloenzyme, participates in the penultimate step of glycolysis for synthesizing pyruvate in catalyzing the conversion of 2-phosphoglycerate (2PG) into phosphoenolpyruvate (PEP) [108]. The active enolases are highly conserved which consist of dimers comprising noncovalently linked α , β , or γ subunits, each encoded by separate genes [108]. There are three of these isoenzymes, including α -Enolase (Enolase 1, ENO1), β -Enolase (Enolase 3, ENO3) and γ -Enolase (Enolase 2, ENO2), are frequently observed in human cells. Among them, ENO1 has become the most widely researched isoform, with its functions and mechanisms in cancer development have been well studied. For instance, homozygous deletion of 1p36 leads to the loss of ENO1 expression in both primary tumours and cell lines in glioblastoma [109]. Furthermore, ENO1 also have been found to promote the destabilization of programmed cell death ligand 1 (PD-L1) in lung cancer cells by enhancing its ubiquitination and subsequent proteasomal degradation, ultimately boosting the anti-tumour immune response [110]. ENO3 is predominantly expressed in muscle tissue and contributes to muscle maturation and regeneration. Elevated expression of ENO3 has been specifically identified in rhabdomyosarcoma tissue, which is the only evidence of association with cancer [111, 112]. ENO2, which is mainly expressed in neurons and neuroendocrine cells, serves as the key to this project [108].

1.2.2 *Characteristics, structures and distributions of Enolase 2*

Enolase 2 (ENO2), also known as γ -enolase or neuron-specific enolase (NSE), is a 433 amino acid long acidic dimeric intracellular enzyme with C-terminal and N-terminal. It is encoded by the *ENO2* gene and predominantly resides in the neurons and neuroendocrine cells, allowing it to be developed as a biomarker for the diagnosis and prognosis of poorly differentiated neuroendocrine tumours [108, 113]. Furthermore,

levels of ENO2 detected in body fluids have been established as biomarkers for predicting the prognosis of neurological conditions such as stroke, intracerebral hemorrhage and brain injury, due to the release of intracellular ENO2 into the bloodstream or cerebrospinal fluid when neurons sustain damage [108, 114]. It is also expressed but in lower quantities within tissues or cells beyond the nervous and neuroendocrine systems, including platelets, erythrocytes, uterus, breast tissue, and prostate [112, 115]. Although ENO2 is mainly located in the cytoplasm and functions to enhance glycolysis, its presence has also been detected in the nucleus, cell membrane, and extracellular space, suggesting its involvement in various cellular processes except glycolysis [108]. Specifically, the PDZ-binding motif located at the C-terminal end of ENO2 enables it to exert significant influence over subcellular distribution [116, 117]. For instance, various experiments confirmed that ENO2 binds to γ 1-syntrophin through its C-terminal PDZ domain and promoted its translocation from the cytoplasm to the cell membrane [108, 117]. Additionally, ENO2 was observed to bind to the plasma membrane and may even be present on the cell surface in neurons, glial cells and astrocytes, potentially promoted by the hydrophobic segment within its N-terminal region [112, 118].

1.2.3 The function of Enolase 2 in glycolysis pathway

Cancer hallmarks, including sustaining proliferative signalling, evading growth suppressors, resisting cell death, enabling replicative immortality, inducing or accessing vasculature, activating invasion and metastasis, reprogramming cellular metabolism and avoiding immune destruction, are considered to be a group of functional abilities acquired by human cells as transition from a normal state into a state of abnormal tumour growth [119, 120]. Currently, deregulating cellular metabolism and avoiding immune destruction have also been classified as emerging markers [119]. As one of the fundamental hallmarks of cancer malignant development, cellular metabolic reprogramming, particularly the increased glycolysis in tumour cells,

cannot be ignored [121]. Compared to normal tissue cells, tumour cells exhibit a remarkable increase in glucose uptake. It is attributed to an adaptation mechanism known as the Warburg Effect, which suggests that tumour cells rely on increased glucose uptake and lactate production through aerobic glycolysis to generate energy for survival and proliferation, regardless of oxygen availability [95, 112]. Despite being energetically inefficient for ATP production, aerobic glycolysis is markedly accelerated in tumour cells to meet the increased glucose metabolic demands necessary for proliferation, particularly in hypoxic environments [122]. As the essential enzyme in the penultimate step of glycolysis, ENO2 is undoubtedly involved in tumour-related aerobic glycolysis, catalyzing the transformation of 2PG into PEP, synthesizing pyruvate and eventually converted to lactic acid [108].

During aerobic glycolysis in solid tumours, glucose is initially transported into cells via glucose transporters (GLUTs) [123]. Upregulation of GLUTs have been identified to be mediated by Ras, c-Myc and HIF-1, ensuring the accelerated glucose flux across the cell membrane [124, 125]. Subsequently, glucose is phosphorylated, catalyzed, and metabolized into glyceraldehyde-3-phosphate by hexokinases (HKs), phosphoglucose isomerase (PGI) and aldolase (ALDO) [125]. Glyceraldehyde-3-phosphate is then converted to 2PG by glyceraldehyde phosphate dehydrogenase (GAPDH), phosphoglycerate kinase (PGK), and phosphoglycerate mutase (PGM). This process involves not only redox reactions but also the generation of ATP. Notably, ENO2 is involved in the conversion of 2PG to PEP. Downstream signals activate pyruvate kinase (PK) and lactate dehydrogenase (LDH), promoting the conversion of phosphoenolpyruvate to pyruvate and ultimately to lactate, leading to a net gain of two molecules of ATP each molecule of glucose [125]. Interestingly, tumour cells could enhance glycolysis by triggering pyruvate dehydrogenase kinase (PDK) activity, which in turn deactivates pyruvate dehydrogenase (PDH), obstructing the conversion of pyruvate into acetyl-CoA within the mitochondrial matrix [125] (**Figure 1.3**).

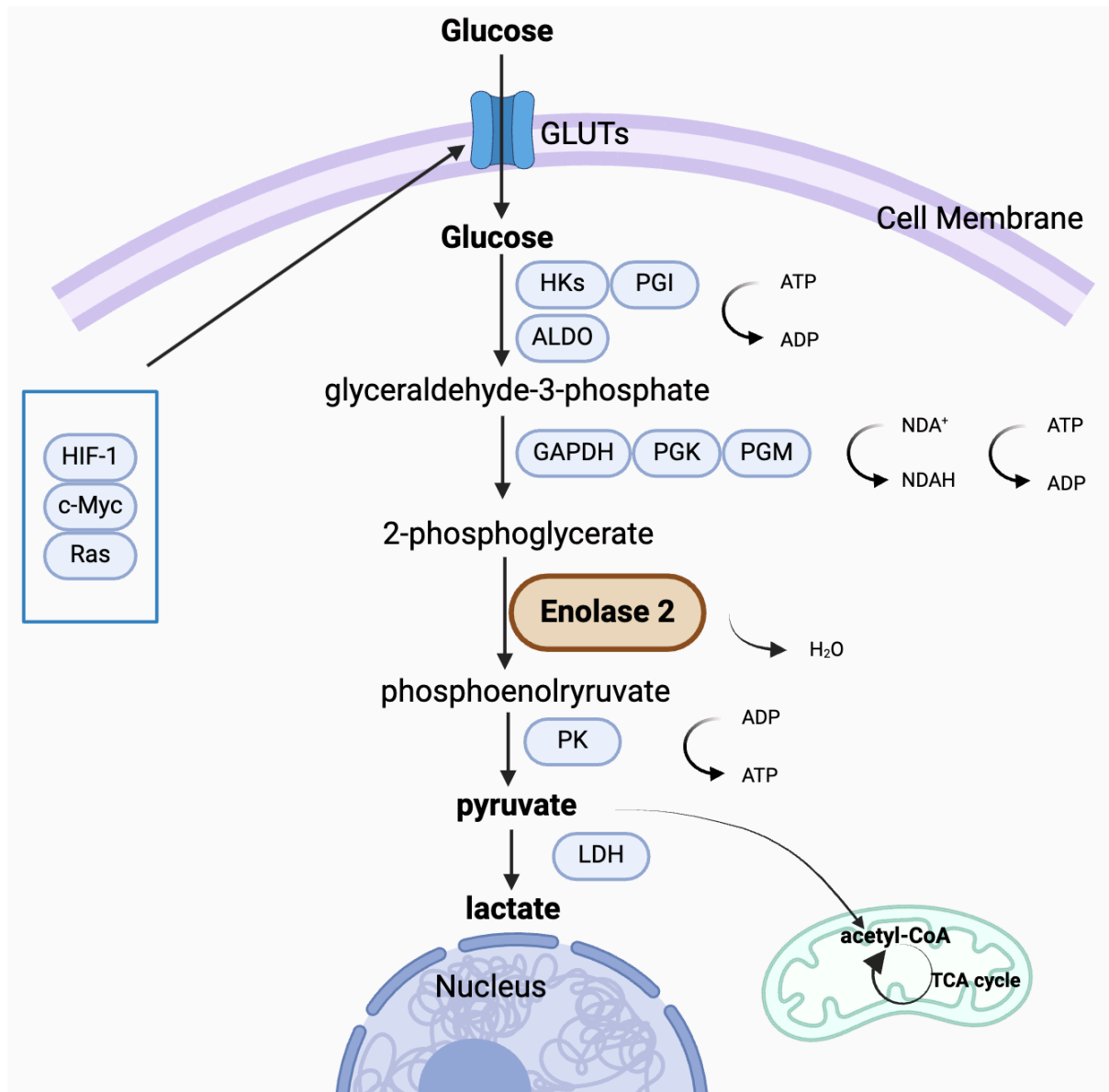


Figure 1.3 The function of Enolase 2 in aerobic glycolysis in tumour cells.

Downstream enzyme Enolase 2 mediated 2-phosphoglycerate eventually converting from glucose into pyruvate, ultimately into lactate, via a series of catalytic reactions in the aerobic glycolytic pathway (created using Biorender).

1.2.4 The function of Enolase 2 in cancer

As a widely recognized biomarker for detecting neuroendocrine cancer, ENO2 exhibits high expression levels in neuroendocrine tumour tissues, serving as a reliable indicator for identifying neuroendocrine differentiation across different cancer types [108, 126]. Notably, ENO2 predominantly resides in the cytoplasm of neuroendocrine cells, distinct from its presence in neurons [108]. For example, NSE levels serve as predictive markers for disease prognosis and treatment responsiveness in individuals with gastroenteropancreatic neuroendocrine tumour (GEP-NETs). Research indicated that elevated NSE expression (>21 ng/mL) correlated with diminished overall survival rates among patients diagnosed with high-grade GEP-NETs [127]. Moreover, this association also exhibited in cases of poorly differentiated GEP-NETs that ENO2 levels were indicative of poorer median overall survival rates [128].

ENO2 has been also recognized as a serum marker for tumours originating from nervous system, such as glioblastoma (GBM) [108]. Studies have demonstrated that knocking down ENO2 using siRNA effectively inhibited the migration of GBM cells and enhanced their susceptibility to hypoxia, chemotherapy and radiotherapy [129]. Subsequently, following the implantation of ENO2-KD GBM cells into the right frontal cortex of NOD/SCID mice, an intracranial GBM xenograft model was successfully established. The outcomes revealed a significant extension in the survival of mice by 7.2% upon ENO2 knockdown [130]. Interestingly, although ENO1 was the predominant isoform, both ENO1 and ENO2 were found to be expressed in GBM cells. When a homozygous deletion affected ENO1 along with the chromosome 1p36 tumour suppressor locus, it triggered the upregulation of ENO2 expression as a compensatory mechanism. Consequently, the targeted knockdown of ENO2 significantly suppressed the viability of ENO1-deleted GBM cells but having almost no impact on cells with intact *ENO1* gene, thereby providing ENO2 as a promising target for therapeutic strategies [108, 109].

ENO2 has been also observed in distinct nonneuronal and non-neuroendocrine type of cancers. A recent study indicated that ENO2 triggered the activation of the BMP2/Smad/ID1 signaling pathway through its interaction with NBL1, thereby gaining of stem cell-like properties in small cell lung cancer cells (SCLC) [131]. Besides, through knockdown and overexpression experiments targeting ENO2, the research demonstrated its role in driving the metastasis of colorectal cancer (CRC) cells by activating the YAP1-induced EMT process, but was independent of glycolysis regulation [132]. Moreover, further studies revealed that BRAF V600E-mutated CRC cells displayed greater reliance on ENO2, thereby regulating the proliferation, migration and drug resistance in CRC cells by activating PI3K/Akt and MAPK pathway [133]. Furthermore, a recent study confirmed that silencing ENO2 notably reduced the expression levels of EMT markers, including N-cadherin and the vimentin, in clear cell renal cell carcinoma (ccRCC) [134]. In addition, ENO2 had been found to interact with PKM2, prevented PKM2 ubiquitin-mediated proteasomal degradation and regulated PKM2-driven CCND1-mediated cell cycle progression, proliferation, and glycolysis in head and neck squamous cell carcinoma (HNSCC) [135]. ENO2 had been identified as a regulator of several glycolytic associated genes, mediating Akt activity to modulate cell proliferation and glycolysis *in vitro*, and promote tumour occurrence *in vivo* in acute lymphoblastic leukemia (ALL) [136]. Current functional and mechanistical studies of ENO2 in various cancer types are summarized.

Importantly, ENO2 has been identified as strongly associated with NEPC. Examination of public datasets revealed a continual increase in ENO2 expression beginning three weeks post-castration may be regulated by IL-8 and FOXA1, with significant upregulation observed in relapsed cases and NEPC cells [51, 108]. Additionally, validation through a NEPC xenograft mouse model discovered a dramatically upregulation of ENO2 compared to adenocarcinoma xenografts, indicating the

potential role of ENO2 in driving NEPC progression [51, 108] (**Table 1.3**). However, no functional studies had been identified the connection between ENO2 and PCa development, especially bone metastasis.

Table 1.4 The functions and mechanisms of ENO2 in various types of cancer.

Type of Cancer		Clinical significance or Biological functions	Molecular mechanism	Reference
Neuroendocrine cancer	GEP-NETs	Predictive marker for prognosis and treatment responsiveness.	/	[108, 127, 128]
	NEPC	Neuroendocrine differentiation.	Regulated by IL-8 and FOXA1	[51, 108]
Nervous system cancer	GBM	Regulate the migration of GBM cells and enhanced their susceptibility to hypoxia, chemotherapy and radiotherapy <i>in vitro</i> . Associated with survival rate <i>in vivo</i> .	Compensate with ENO1.	[108, 109, 129, 130]
SCLC		Promote the tumour growth and stem cell-like properties in small cell lung cancer cells <i>in vitro</i> and <i>in vivo</i> .	Activate the BMP2/Smad/ID1 signaling pathway through its interaction with NBL1.	[131]
CRC		Drive the metastasis activating. Regulated proliferation, migration and drug resistance in BRAF V600E-mutated CRC cells.	Activate the YAP1-induced EMT process. Activate PI3K/Akt and MAPK pathway.	[132, 133]
ccRCC		Regulate migration and invasion <i>in vitro</i> .	Associated with EMT process.	[137]
HNSCC		Regulate cell cycle progression and proliferation <i>in vitro</i> . Induce remission after ENO2 blocking <i>in vivo</i> .	Active PKM2-driven glycolysis.	[135]
ALL		Regulate cell proliferation and glycolysis <i>in vitro</i> . Promote tumour occurrence <i>in vivo</i> .	Mediate Akt activity.	[136]

1.3 Project rational

PCa bone metastasis still remains a crucial clinical challenge associated with elevated mortality rates. This project focuses on this specific type of metastasis due to the high clinical relevance of bone involvement in advanced PCa cases, where skeletal metastasis significantly impairs patient outcomes and quality of life [138, 139]. The bone microenvironment provides a unique niche that fosters tumour cell dormancy and eventual reactivation, contributing to poor prognosis in PCa patients [73, 74].

ENO2, a well-established tumour marker, have been found to be highly expressed in various malignancies at both mRNA and protein levels. Furthermore, as a critical enzyme in the aerobic glycolysis pathway, ENO2 mediates increased pyruvate synthesis from glucose in tumour cells, providing the energy necessary to drive aggressive progression, including metastasis [108]. The overexpression of ENO2 in various malignancies has been consistently reported, positioning it as a promising target for therapeutic interventions aimed at curbing metastatic progression.

In the preliminary q RT-PCR, proteomics and RNA-Seq data (**Figure 1.4**), PC3 cells, which serve as a model for PCa bone metastasis, were used to assess the role of ENO2 in bone metastasis initiation. The experimental approach included comparing the transcriptional and translational levels of ENO2 in dormant metastasis-initiating cells, compared to their fast-growing counterparts. The findings revealed a notable upregulation of ENO2 in the dormant cell population, suggesting its potential involvement in maintaining dormancy or promoting survival within the metastatic niche.

Taken together, the existing evidence suggests that ENO2 may play a functional role in PCa bone metastasis progression (i.e. dormancy) and could serve as a potential target for therapeutic intervention.

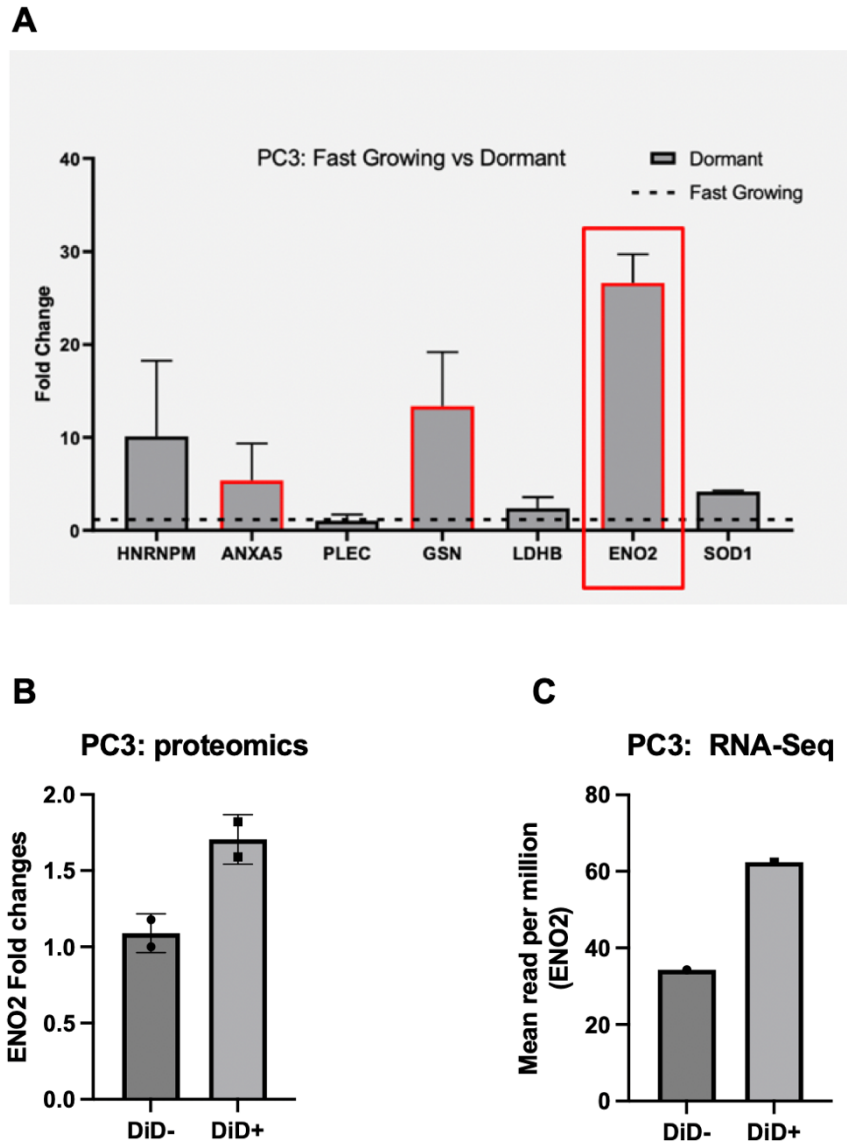


Figure 1.4 The comparison of ENO2 gene expression levels between dormant metastasis-initiating cells and fast-growing counterparts by RT-qPCR, Proteomics and RNA-Seq.

(A) The relative expression of genes in PC3 cell line, with a $2^{-\Delta\Delta C_t}$ fold change. **(B)** The relative expression of ENO2 in DiD- and DiD+ PC3 cells with average expression. LogFC ≥ 0.58 (1.5-fold change), $-\log_{10}$ (P value) < 0.05 . **(C)** The expression of ENO2 in DiD- and DiD+ PC3 cells with mean read per million. LogFC ≥ 0.58 (1.5-fold change), $-\log_{10}$ (P value) < 0.05 . The data are mean \pm standard deviation (n=3 biological repeats with 3 technical repeats for Figure A, n=2 biological repeats with 3 technical repeats for Figure B, n=1 biological repeat with 3 technical repeats for Figure C). Unpaired t-test and multiple One-way ANOVA (unpublished data).

1.4 Hypothesis and Aims

The main hypothesis in this project is: **Enolase 2 positively contributes to PCa malignant development, including bone metastasis.**

This hypothesis will be examined by:

1. Conducting a systematic review and meta-analysis in order to provide comprehensive insights into the current evidences, including *in vitro*, *in vivo* and clinical patients, supporting the correlation between Enolase 2 and PCa metastasis (**Chapter 3**).
2. Exploring the expression of Enolase 2 in PCa (**Chapter 4**):
 - a) Investigating the expression of ENO2 in a panel of PCa cell lines at transcriptional and translational level.
 - b) Investigating the expression of ENO2 under different environmental glucose and pyruvate supplement in a panel of PCa cell lines at translational level.
 - c) Investigating glucose-induced cellular behaviour in PCa cells *in vitro*.
3. Evaluating the effects of genetically inhibition of Enolase 2 in PCa cells *in vitro* (**Chapter 5**):
 - a) Investigating the changes of cell growth, including viability, proliferation and apoptosis, under transient knockdown ENO2 expression using siRNA transfection.
 - b) Investigating cellular consequences *in vitro*, including viability, proliferation, apoptosis, migration and invasion, due to ENO2 knockout created through CRISPR/Cas 9 editing.
 - c) Investigating the metabolic changes in ENO2 knockout PCa cells, including glucose consumption and lactate production.
4. Assessing the effects ENO2 knockout in the development of PCa bone metastasis in xenografts (**Chapter 6**).
5. Conducting RNA-Seq and bioinformatic analysis using stable ENO2-knockout clones to explore ENO2 regulated potential DEGs, mechanisms, processes and functions (**Chapter 7**).

Chapter 2: Materials and **Methods**

2.1 General Tissue Culture Cell lines and Conditions

2.1.1 Cell lines

2.1.1.1 Cancer cell-lines

As indicated in **Table 2.1**, various human PCa cell lines, including PC3, DU145, 22RV1, LNCaP, LNCaP-LN3, C4-2, and C4-2B4, mouse PCa cell lines, including RM1 and TRANMP-C1, were purchased from American Type Culture Collection (ATCC; Rockville, MD, USA). Mouse PCa cell line TRAMP-C2 was obtained from University of Newcastle, Dr Jennifer Munkley.

2.1.1.2 Prostatic myofibroblast cell line

As indicated in **Table 2.1**, human prostatic stromal myofibroblast cell line WPMY-1 (AR+ and PSA+) was purchased from ATCC.

2.1.1.3 Cell line Authentication

Genomic DNA was purified from PCa cell lines using Wizard® Genomic DNA Purification System (Promega, No. A2360). Before sending for sequencing, the quantity of DNA in each sample was assessed using a spectrometry Nanodrop ND100 spectrometer (Thermo Fisher Scientific, Paisley, UK) to ensure a minimum concentration of 10 ng/μL. Each DNA sample was dispatched to NorthGene (Newcastle, UK) and Eurofins (Ebersburg, Germany) for STR analysis. A DNA profile was generated and subsequently compared to a profile within the DSMZ Database.

Table 2.1 Characteristics of a panel of PCa and prostatic myofibroblast tissue cell lines.

	<i>Type of cells</i>	<i>AR expression</i>	<i>PSA expression</i>	<i>Sensitive of AR</i>	<i>Metastasis potential</i>	<i>Note</i>
PC3	Human PCa cells	-	-	Androgen-independent	High	A cell line derived from bone metastasis originating in a 62-year-old Caucasian male with grade IV PCa [140].
DU145	Human PCa cells	+	-	Androgen-independent	High	An epithelial cell line that was obtained from the brain metastasis of a 69-year-old Caucasian male diagnosed with PCa [141].
22Rv1	Human PCa cells	+	+	Androgen-dependent	High	A human PCa epithelial cell line originated from an androgen-dependent CWR22 xenograft that underwent successive propagation in mice [142].
LNCaP	Human PCa cells	+	+	Androgen-dependent	Low	A cell line exhibiting epithelioid morphology was isolated from the left supraclavicular lymph node metastasis of a 50-year-old Caucasian male [143].
LNCaP-LN3	Human PCa cells	+	+	Androgen-independent	High	A cell line with more metastatic potential originally initiated from human PCa LNCaP cell [144].

C4-2	Human PCa cells	+	+	Androgen-dependent	Moderate	A cell line exhibiting epithelial-like morphology was isolated from a subcutaneous xenograft tumour of a castrated mouse, originally derived from human PCa LNCaP cells [145].
C4-2B4	Human PCa cells	+	+	Androgen-independent	Moderate	A cell line originally derived from human PCa LNCaP cells with bone metastatic potential [145].
RM1	Mouse PCa cells	+	/	Androgen-independent	High	A cell line displaying fibroblast-like characteristics was isolated from the prostate of a 17-day-old mouse [146].
TRAMP-C1	Mouse PCa cells	+	/	Androgen-independent		An epithelial cell line was derived in 1966 from the prostate of an adult male transgenic mouse afflicted with adenocarcinoma [147].
TRAMP-C2	Mouse PCa cells	+	/	Androgen-independent	High	An epithelial cell line was derived in 1996 from the prostate of an adult male transgenic mouse with afflicted with adenocarcinoma [147].
WPMY-1	Human prostatic myofibroblast tissue cells	+	+	/	/	A myofibroblast cell line was obtained from the stromal tissue from a white, 54-year-old, male donor in 1992 [148].

2.1.2 Tissue Culture Medium

2.1.2.1 Standard medium

Human PCa PC3, LNCaP, DU145, C4-2B4, mouse PCa RM1 and human prostatic myofibroblast WPMY-1 cell lines were cultured in DMEM + GlutaMAX supplemented + pyruvate (Gibco, 31966-021) with 10% fetal bovine serum (FBS) (Sigma, BCBT9410), 100 U/mL penicillin with 100 ug/mL streptomycin (1% P/S) (Gibco, 15140-122) (standard DMEM). Human PCa 22Rv1, LNCaP-LN3, C4-2 were cultured in RPMI + GlutaMAX supplemented (Gibco, 61870-010) with 10% FBS and 1% P/S (standard RPMI). Mouse PCa TRAMP-C1 was cultured in DMEM + GlutaMAX supplemented + pyruvate with 10% FBS, 0.005 mg/mL bovine insulin (Sigma-Aldrich, I05516-5ML) and 10 nM dehydroisoandrosterone (DHEA) (Sigma-Aldrich, D-063-1ML). Mouse PCa TRAMP-C2 was cultured in DMEM + GlutaMAX supplemented + pyruvate with 5% FBS, 5% Nu-Serum (Corning, 355104) 0.005 mg/mL bovine insulin and 10 nM DHEA.

2.1.2.2 Low glucose, glucose-free and pyruvate-free medium

Low glucose DMEM medium was made by using DMEM, low glucose, pyruvate (Gibco, 31885-023) with 10% FBS and 1% penicillin-streptomycin (P/S). Glucose-free RPMI was made by using RPMI 1640, no-glucose (Gibco, 11879-020) with 10% FBS and 1% Pen-Strep. Pyruvate-free DMEM was made by using DMEM, high glucose, no pyruvate (Gibco, 61965-026) with 10% FBS and 1% P/S.

2.1.3 Cell Culture Condition

Cell culture procedures were conducted within a Class II laminar flow cabinet. Both the cabinet and all equipment were sterilized using 70% (v/v) Industrial Methylated Spirits in advance to use. Additionally, all solutions intended for cellular applications were pre-warmed to 37°C. The cells were maintained in an environment enriched with 5% CO₂ and 95% humidity, at a constant temperature of 37°C. Cell confluency was assessed at magnifications of 10x or 20x using an Olympus CK2 microscope. The cells were cultured in either T25 or T75 flasks and passaged every 48-96 hours at specific ratios: 1:20 for RM1, 1:10 for PC3, DU145, 22RV1, LNCaP, TRAMP-C1, TRAMP-C2 and 1:5

for LNCaP-LN3, C4-2, C4-2B4. The department's technicians perform routine mycoplasma testing monthly using the Geneflow EZ-PCR Mycoplasma Detection Kit by agarose gel electrophoresis.

To perform cell passaging, the monolayer was washed with room temperature phosphate-buffered saline (PBS) (Gibco, 2430585) at least two times and then detached using Trypsin-ethylenediaminetetraacetic acid (EDTA) (Gibco, 25200072) for a minimum of 5 minutes. Standard medium was subsequently added in a 10:1 ratio of trypsin to neutralize the proteolytic activity. The cell suspension was then transferred to a fresh sterile 15 mL tube and centrifuged at approximately 1000 rpm for 5 minutes. After centrifugation, the supernatant was removed, and the cells were resuspended in 1 mL of standard medium. A portion of the suspension was seeded into a new T25 or T75 flask containing 5-mL or 11-mL standard medium, respectively. The remaining cells were counted and used for experimental purposes.

2.1.3.1 Cell frozen and thawing

For cell frozen, the cell pellet obtained during harvesting was stored in a cryogenic vial with a 1:10 solution of dimethyl sulfoxide (DMSO) (Thermo Fisher Scientific, 67-68-5) and FBS. This vial was placed in a Cell Freezing Container containing isopropanol (Thermo Fisher Scientific, P/7500/17) and stored at -80°C. To thaw the cells, the frozen contents of the cryogenic vials were thawed in a 37°C water bath, and the defrosted cell suspension was mixed with up to 5 mL of standard medium in a new T25 or T75 flask.

2.2 Molecular and Cellular Biology Techniques

2.2.1 *ENO2 Knockdown (Small interfering RNA (siRNA) knockdown)*

2.2.1.1 siRNA product information

RNA interference (RNAi) can be initiated by introducing short double-stranded RNA (dsRNA) fragments, referred as siRNAs, into the RNA-induced silencing complex (RISC) [149, 150]. In mammalian cells, siRNAs were generated through the

endonucleolytic processing of exogenously introduced long, double-stranded RNA by the enzyme Dicer [150, 151] (**Figure 2.1**).

To knockdown of ENO2 expression in human PCa PC3 and 22Rv1 cells, the ENO2 Silencer™ Selected Validated siRNA (Thermo Fisher Scientific, 4390842) and Silencer™ Negative Control #1 siRNA (Thermo Fisher Scientific, 4390843) were purchased. The information was presented in **Table 2.2**.

Prior to use, the tubes were centrifuged briefly to ensure the dried content was at the bottom. The provided 5 nmol of siRNA and control siRNA were resuspended in 1.75 mL of the nuclease-free water for a final concentration of 2.86 μ M, stored at -20 °C.

Table 2.2 The information of ENO2 Silencer™ Selected Validated siRNA

	<i>Sense</i>	<i>Antisense</i>
Sequence (5' -> 3')	GGUGCAGAGGUCUACCAUAtt	UAUGGUAGACCUCUGCACCTa
Length	21	21
Percent G/C	48%	48%
Molecular Weight	6800	6600
Molar Extinction Coefficient	211200	204100
Annealed Molecular Weight	13400 (40 ug/OD was used to calculate concentration)	

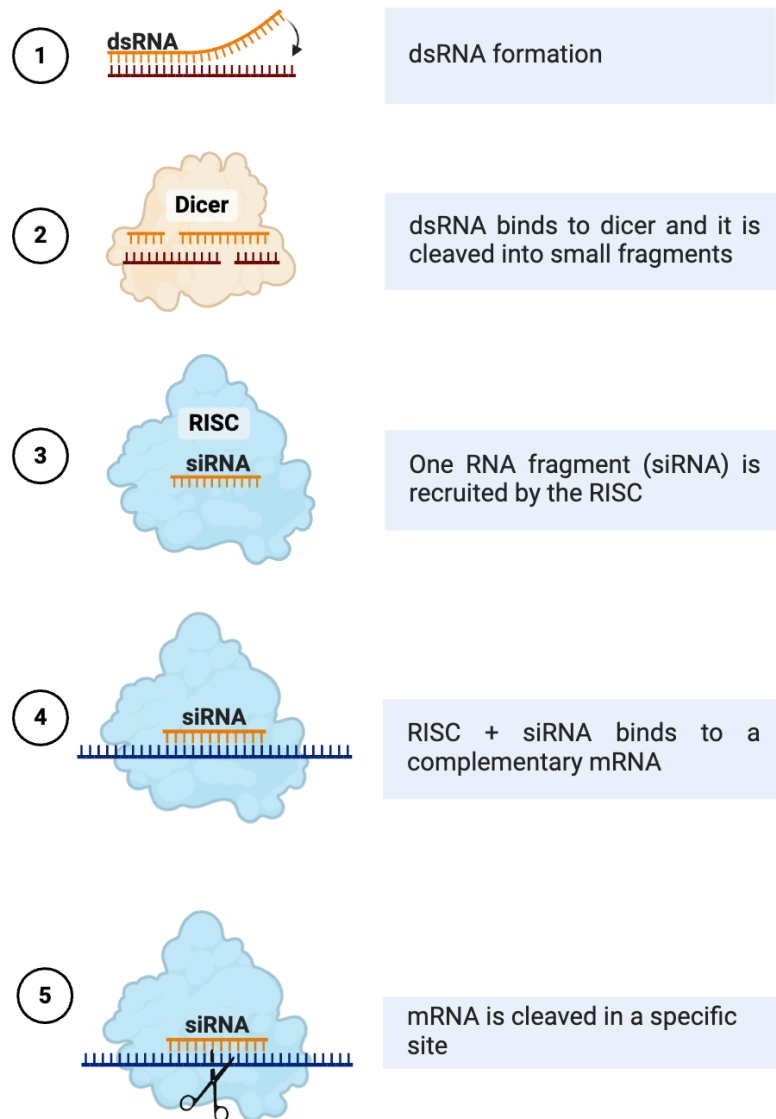


Figure 2.1 The mechanism of siRNA knockdown.

Upon introduction into the cell, the dsRNA fragment is cleaved by an endoribonuclease known as Dicer, producing siRNA. Once siRNA enters the cell it gets incorporated into other proteins to form the RISC. Subsequently, the siRNA associates with proteins to assemble the RISC. A preferential selection of the less thermodynamically stable strand occurs due to base pairing at the 5' end, allowing it to persist within the RISC complex. The siRNA within RISC then guides the cell, scanning for and binding to complementary mRNA sequences, initiating mRNA cleavage. The cleaved mRNA is recognized as abnormal by cells, leading to degradation and impeding its translation into amino acids and proteins, ultimately leading to gene silencing (created using Biorender).

2.2.1.2 Transfection process

The PC3 and 22Rv1 cells were plated at a density of 5×10^4 cells each well in 24-well plates in 400 μ L of growth medium without antibiotics the day prior to transfection. Cells were cultured to achieve a confluence of approximately 70% by the time of transfection in order to ensure optimal transfection efficiency. For each transfection sample, siRNA-LipofectamineTM 3000 complexes were prepared as follows:

- a. 50 pmol of siRNA (equivalent to 17.5 μ L of a 2.86 μ M siRNA stock solution) or an equivalent volume of negative control were diluted in 50 μ L of Opti-MEM[®] I Reduced Serum Medium (Thermo Fisher Scientific, 31985062). The mixture was gently mixed to ensure homogeneity.
- b. 1 μ L of LipofectamineTM 3000 (Thermo Fisher Scientific, L3000008) was diluted in 50 μ L of Opti-MEM[®] I Reduced Serum Medium. The resulting solution was mixed gently and allowed to incubate at room temperature for 15 minutes.
- c. Following the 15-minute incubation, the diluted siRNA or negative control and LipofectamineTM 3000 solutions were combined, respectively. The mixture was further incubated for an additional 15 minutes at room temperature to promote the formation of complexes after gentle mixing.

Approximately 100 μ L of the siRNA-LipofectamineTM 3000 complexes or an equivalent volume of negative control-LipofectamineTM3000 Complex were added to each well containing PC3 or 22Rv1 cells as well as the growth medium. Mixing was conducted gently by rocking the culture plate back and forth. The cells were subsequently incubated at 37°C within a humidified CO₂ incubator. The growth medium could be replaced after 4-6 hours without affecting transfection efficiency. The range of incubation time from 24 to 72 hours to guarantee specific experimental requirements. Successful KDs were examined using qRT-PCR as detailed below in **section 2.2.3**.

2.2.2 ENO2 Knockout (CRISPR Cas 9 technology)

2.2.2.1 CRISPR Guide RNA (gRNA) plasmid information

The RNA-guided Cas9 endonuclease derived from the microbial clustered regularly interspaced short palindromic repeats (CRISPR) adaptive immune system, can be employed for effective genome editing in eukaryotic cells by specifying nucleotide targeting sequence within its gRNA [152]. Predesigned gRNA sequences were bind to DNA and guided Cas9 to the designated region of the genome which guaranteed the Cas9 endonuclease cleave at the precise point in the genome, allowing for the targeted removal of DNA segments [153, 154] (**Figure 2.2**).

To generate ENO2 knockout expression PC3 and 22Rv1 cells, the predesigned CRISPR gRNA plasmid DNA was purchased from Sigma-Aldrich (Sigma-Aldrich, 03172210MN) (**Table 2.3**) (**Figure 2.3**).

Table 2.3 The information of ENO2 predesigned CRISPR Guide RNA (gRNA) plasmid DNA (Sigma-Aldrich, 03172210MN)

Clone ID	HSPD0000012611
Restriction Digest	PASS
gRNA (5'-3')	GCCTCATAGATGCCCGTAG
PAM	TGG
Refseq/Exon	NM_001975/3
Chromosome	12
Final concentration	20 ng/ul
Final volume	50ul

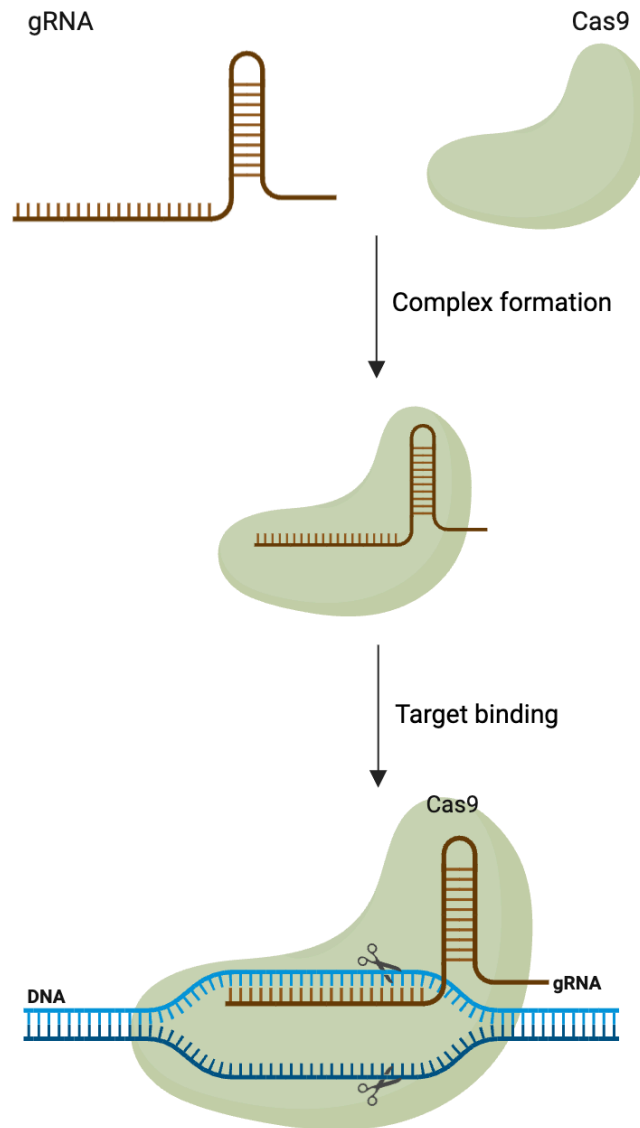


Figure 2.2 The mechanism of CRISPR Cas 9 knockout.

The gRNA, which is composed of approximately 20 nucleotides, forms a complex with the Cas9 protein, causing Cas9 to bind to the target site on the target DNA. Cas9 protein cleaves target DNA through its nuclease activity, generating DNA double-strand breaks (created using Biorender).

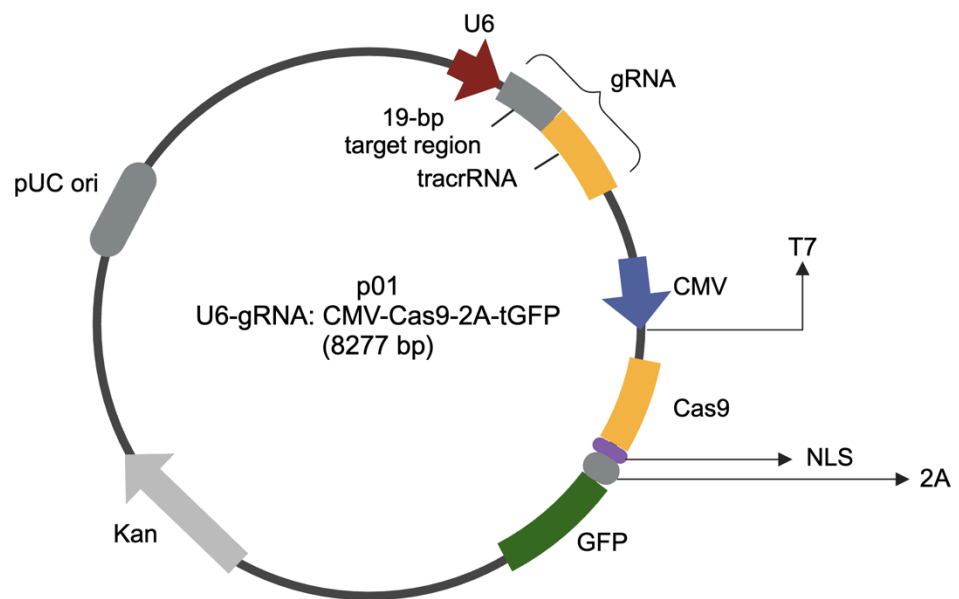


Figure 2.3 The map of U6-gRNA plasmid.

U6-gRNA plasmid consists of U6 promoter, gRNA including target region and trans-activating crisper RNA (tracrRNA), human cytomegalovirus (CMV) promoter, T7 promoter sequence, Cas 9 endonuclease, nuclear localization sequence (NLS), 2A peptide, reporter gene green fluorescence protein (GFP), drug selection kanamycin (Kan) gene and pUC origin (pUC ori) of replication (created using Biorender).

2.2.2.2 Transfection process

The PC3 and 22Rv1 cells were plated at a density of 5×10^4 cells each well in 24-well plate in 400 μL of growth medium without antibiotics the day prior to transfection. Cells were cultured to achieve a confluence of approximately 70% by the time of transfection in order to ensure optimal transfection efficiency. For each transfection sample, the CRISPR gRNA plasmid-Lipofectamine™ 3000 complexes were prepared as follows:

- a. 23.23 μL (5 μg) of CRISPR plasmid DNA or an equivalent volume of PBS control were diluted in 125 μL of Opti-MEM® I Reduced Serum Medium (Thermo Fisher Scientific, 31985062) and 5 μL of P3000 (Thermo Fisher Scientific, L3000008). The mixture was gently mixed to ensure homogeneity.
- b. 7.5 μL of Lipofectamine™ 3000 (Thermo Fisher Scientific, L3000008) was diluted in 125 μL of Opti-MEM® I Reduced Serum Medium. The resulting solution was mixed gently and allowed to incubate at room temperature for 15 minutes.
- c. Following the 15-minute incubation, the diluted CRISPR plasmid DNA or PBS control and Lipofectamine™ 3000 solutions were combined, respectively. The mixture was further incubated for an additional 15 minutes at room temperature to promote the formation of complexes after gentle mixing.

Approximately 286 μL of the CRISPR plasmid DNA -Lipofectamine™ 3000 complexes and an equivalent volume of PBS control-Lipofectamine™ 3000 Complex were added to each well containing PC3 or 22Rv1 cells as well as the growth medium. Mixing was conducted gently by rocking the culture plate back and forth. The cells were subsequently incubated at 37°C within a humidified CO₂ incubator. The growth medium could be replaced after 24 hours without affecting transfection efficiency.

2.2.2.3 Screening by Fluorescence-activated cell sorting (FACS)

FACS was performed 48 hours after transfection facilitated by Ms. Sue Clark using the BD FACSMelody™ Cell Sorter (BD Biosciences). Cells transfected with CRISPR plasmid DNA and PBS control were initially trypsinized, centrifuged, and then collected in FACS tubes respectively. Subsequently, the FACS tubes containing PBS control-

transfected cells were loaded on the machine to determine negative results for the given marker (GFP). Additionally, the FACS tubes containing CRISPR plasmid DNA-transfected cells were loaded on the machine to sort the targeted cell population. The operation of the sorting program on the cytometer and software has been standardized. Only the GFP positive cells could be passed of the sorting process and selected in the 96 well plate as one cell each well. Cells that passed screening were subsequently maintained at 37°C within a humidified CO₂ incubator. Survived single clones were progressively expanded, moving from the 96-well plate to 48-well plate, 6-well plate, T25 flask, and finally a T75 flask. Successful KDs were examined using qRT-PCR, Western blotting and Sanger sequencing as detailed below in **Section 2.2.3**, **Section 2.2.4** and **Section 2.2.6.3**.

2.2.3 Real-time Quantitative Reverse Transcription Polymerase Chain Reaction (RT- qPCR)

2.2.3.1 RNA extraction

Total RNA was purified from PCa and prostatic myofibroblast cell lines using the ReliaPrep™ RNA Cell Miniprep System (Promega, No. z6011). Cells were resuspended in a density of 1x10⁶/mL and isolated by centrifugation at 1000 rpm for 2 minutes. The cell pellets from each sample were washed with ice-cold sterile 1X PBS and isolated by centrifugation at 1000 rpm for 2 minutes.

To shear the DNA, 250 µL of BL+TG Buffer was gently resuspended with the washed cell pellets by mixing 7-10 times. To precipitate RNA, 85 µL of isopropanol was added and mixed by vortexing for 5 seconds. The mixture was then transferred to a fresh minicolumn in a collection tube and centrifuged at 10,000 rpm for 30 seconds at approximately 25 °C. After emptying the collection tubes, 500 µL of RNA Wash Solution was added to each minicolumn and centrifuged at 10,000 rpm for 30 seconds at approximately 25 °C. To purify RNA by removing contaminant DNA, a DNase I incubation mix was prepared by combining 24 µL of Yellow core buffer, 3 µL of MnCl₂ and 3 µL of DNase I for each sample. DNase treatment was then performed by

applying 30 µL of DNase I incubation mix to each membrane of the minicolumn and allowing it to incubate for 15 minutes at room temperature. After 15 minutes, 100 µL of Column Wash Solution with ethanol was added to each minicolumn for further purification, followed by centrifugation at 10,000 rpm for 15 seconds. The samples were subsequently transferred to new collection tubes, and after adding 300 µL of RNA Wash Solution to each, they were centrifuged at 12,000 rpm for 2 minutes. Finally, 30 µL of nuclease-free water was added to each membrane of the minicolumn after unpacking in a fresh elution tube, followed by centrifugation at 10,000 rpm for 1 minute.

Before storing the elution tube containing purified RNA at -80°C, the RNA from each sample was quantified using a spectrometry Nanodrop ND100 spectrometer (Thermo Fisher Scientific, Paisley, UK). RNA quality was monitored by assessing the 260/280 and 260/230 ratios which should be approximately 2 and 1.9, respectively. Images of the cell types prior to RNA extraction were captured at 10X magnification using the EVOS Cell Imaging System (Thermo Fisher Scientific).

2.2.3.2 First-strand cDNA synthesis (*reverse transcription polymerase chain reaction (RT-PCR)*)

The initial step in first-strand cDNA synthesis relied on SuperScript™ III Reverse Transcriptase (Invitrogen, 18080-044). For each 1 µg of RNA, 1 µL of Oligo(dT)20 (50 µM) (Invitrogen, 100023441), 1 µL of dNTP Mix (10 mM) (Invitrogen, 18427-013) and nuclease-free water were combined to achieve a final volume of 13 µL. The RNA solutions were heated to 65°C for 5 minutes, followed by incubation on ice for a minimum of 1 minute. The contents were collected subsequently from the tube through a brief centrifugation. 4 µL of 5X First-strand Buffer (Invitrogen, Y02321), 1 µL of DTT (0.1 M) (Invitrogen, Y00147), 1 µL of SuperScript™ III RT (200 units/µL) (Invitrogen, 56575) and 1 µL of nuclease-free water were added. The mixture was gently pipetted to ensure fully mixing and then incubated in a PCR machine (ProFlex™ PCR system, Pub. No. 4483807) at 50°C for 50 minutes, followed by 70°C for 15 minutes and

maintained at 4°C (**Figure 2.6 B**). The resulting cDNA samples were stored at -20°C until needed.

2.2.3.3 TaqMan Real-time quantitative PCR (RT-qPCR)

RT-qPCR was conducted to evaluate the transcriptional expression of ENO1, ENO2 and ENO3 at the mRNA level. To ensure experiment sterile experiment, all solutions and equipment used in this experiment were exposure in UV irradiation for a minimum of 20 minutes before starting. All primers and cDNA were thawed on ice and briefly vortexed prior to use.

For cDNA, which were generated during the first-strand cDNA synthesis step, a 1:10 dilution involving 1 µL of template cDNA and 10 µL of nuclease-free water was used. Primers for TaqMan Assays, including ENO2 Primer (Thermo Fisher Scientific, Hs00157360_m1), ENO1 Primer (Thermo Fisher, Hs00361415_m1), ENO3 Primer (Thermo Fisher Scientific, Hs01093275_m1) and the Human HPRT1 Endogenous Primer (Thermo Fisher Scientific, Hs02800695_m1) were used at a 1:1 dilution, with 1 µL of primer and 1 µL of nuclease-free water.

Real-time qPCR reactions were set up in triplicates, each containing 1 µL of diluted template cDNA, 1 µL of diluted primers, 5 µL of TaqMan™ Fast Advanced Master Mix (Thermo Fisher Scientific, 4444557), and 3 µL of nuclease-free water. Additionally, an RNA-free water control consisted of triplicate reactions using 1 µL of diluted primers, 5 µL of TaqMan™ Fast Advanced Master Mix, and 4 µL of nuclease-free water. The prepared reaction mixture was loaded into a 384-well PCR plate, sealed with a transparent film and handled with care. The RT-qPCR procedure consisted of an initial cycle at 50°C for 2 minutes, followed by 95°C for 10 minutes, and then 40 cycles at 95°C for 15 seconds (denaturation) and 60°C for 1 minute (annealing) (**Figure 2.6 C**). This entire process was carried out using the QuantStudio 7 Pro Real-Time PCR Systems (Applied Thermo Fisher Scientific, US).

2.2.3.4 Data analysis for RT- qPCR

Data analysis was performed using Design and Analysis software from Thermo Fisher Scientific, which presented the raw data as cycle threshold (Ct) numbers. The Ct value represents the number of amplification cycles at which the fluorescence signal from a sample crosses a predefined threshold situated within the exponential phase. The emitted fluorescent which was generated due to the combination of FAM based reporter and double-stranded DNA (dsDNA), was directly proportional to the quantity of PCR product produced in each amplification cycle. Therefore, a lower Ct value means that fewer amplification cycles are required for fluorescence to reach threshold, indicating a higher concentration of cDNA in the sample.

To assess expression differences between target and housekeeping genes, delta Ct (ΔCt) was firstly calculated to examine the expression difference between target and housekeeping genes:

$$\Delta Ct = \text{Avg. Ct (target gene)} - \text{Avg. Ct (housekeeping gene)}$$

Subsequently, the $2^{-\Delta\Delta Ct}$ method was applied to calculate relative gene expression levels, representing a fold change between different samples based on the $\Delta\Delta Ct$ value:

$$\Delta\Delta Ct = \Delta Ct (\text{sample}) - \Delta Ct (\text{control})$$

The expression level of the housekeeping gene was used for the purpose of normalization. Values from the water control group were used to assess whether the primers are contaminated.

2.2.4 Western Blot

2.2.4.1 Preparation of cell lysates

Cells were seeded in 6-well plate in growth medium at a density of 2×10^5 . When cells grow to approximately 90% confluence, cells were carefully washed with ice-cold PBS at least 3 times. Cells were then incubated with 120 μL of 1X RIPA lysis buffer (**Scientific Appendix**) containing 0.4% (v/v) phosphatase inhibitor (Sigma-Aldrich,

P0044) and 2% (v/v) protease inhibitor (Sigma-Aldrich, P8340) on ice for 5 to 10 minutes. Following the incubation, cells were gently scraped and transferred into Eppendorf tubes. The Eppendorf tubes were subjected to centrifugation at 12,000 rpm for 15 to 20 minutes at 4 °C. The resulting supernatant fraction was carefully transferred into fresh Eppendorf tubes and stored at -20 °C for future use.

2.2.4.2 Protein concentration measurement – (Pierce™ Bicinchoninic acid (BCA) protein assay)

Protein content in cell lysates was quantified using the BCA protein assay following the manufacturer's instructions. As a reference, protein concentrations were determined employing the Pierce™ Bovine Serum Albumin (BSA) standard prediluted set (Thermo Fisher Scientific, No. 23208). 10 µL of each serially diluted BSA standard (ranging from 0 to 2000 µg/mL) was added in duplicate in 96-well plate, comprising eight points: 0 µg/mL, 125 µg/mL, 250 µg/mL, 500 µg/mL, 750 µg/mL, 1000 µg/mL, 1500 µg/mL and 2000 µg/mL. The cell lysate samples which had been diluted 1:4 with distilled water were also applied in duplicate in 96-well plate. A BCA solution (200 µL) was added to all wells in the plate, which was prepared containing copper sulfate (Sigma-Aldrich, C2284) at a 1 in 50 dilution in BCA reagent (Sigma-Aldrich, B9643). Following 25minutes incubation at 37°C, the absorbance at 562 nm was measured using a SpectraMax M5® microplate reader. A standard curve was constructed to determine the total protein content of each lysate using the known BSA concentrations. This allowed for the calculation of the volume of protein extract required to achieve a final protein quantity from 50 to 70 µg.

2.2.4.3 Gel electrophoresis

Prior to loading onto the gel, the quantified protein samples were combined with 4× loading buffer (described in the Scientific Appendix) and subjected to a 5-minute incubation at 95°C. Denatured proteins were resolved through electrophoresis using 12% Criterion™ TGXTM Precast Midi protein gels (Bio-Rad Laboratories, 5671043). These gels were positioned within a vertical electrophoresis chamber and immersed

in 1X Tris/Glycine/SDS (TGS) running buffer. The TGS running buffer was prepared by diluting 10X TGS (Bio-Rad Laboratories, 161-0772) with distilled water in a 1 to 10 ratio. For molecular weight reference, Magic Marker XP Western Protein Standard (Thermo Fisher Scientific, LC5602) was employed. Electrophoresis was conducted at a voltage of 120 V for around 1 hour (**Figure 2.4 A**).

2.2.4.4 Electrophoretic transfer

The proteins were transferred from the gel to a polyvinylidene (PVDF) membrane (Bio-Rad Laboratories, 1704273) following electrophoresis. The membrane was assembled together with filter papers (Bio-Rad Laboratories, 1704273) that had been pre-soaked in transfer buffer. This assembly was placed within the Transblot Turbo® transfer system (Bio-Rad Laboratories). The transfer process was carried out at a constant current of 2.5 A and 21 V for a duration of 7 minutes (**Figure 2.4 B**).

2.2.4.5 Membrane blocking and antibody incubation

The PVDF membranes were ensured saturation of the remaining binding surface and prevents non-specific binding through the blocking step. It was achieved by immersing the membrane in a 5% (w/v) milk blocking solution, consisting of non-fat milk powder in Tris buffer saline solution (TBS) (**Scientific Appendix**), supplemented with 0.1% TWEEN® 20 (Sigma-Aldrich, P9416). The blocking step was carried out for a duration of 1 hour at room temperature with gentle shaking.

Following the blocking step, the membrane was subjected to a series of washing steps, involving three washes with TBST (Tris-buffered saline with 0.1% TWEEN® 20), each lasting for 15 minutes on a shaker set at a moderate speed. Subsequently, the membrane was incubated overnight at 4°C with gentle agitation, with each respective primary antibody. The primary antibodies employed were as follows:

- Enolase-2 (D20H2) Rabbit mAb (Cell Signaling Technology, #8171)
- β -Actin (D6A8) Rabbit mAb (Cell Signaling Technology, #8457)

Following the overnight incubation, the membrane was subjected to three washes with TBST (with 0.1% TWEEN[®] 20), each lasting for 15 minutes on a shaker set at a moderate speed.

Finally, the membrane was incubated with the secondary antibody, specifically peroxidase AffiniPure donkey Anti-Rabbit IgG (H+L) (Jackson ImmunoResearch, 711-035-152). The secondary antibody was applied at a concentration of 1:10,000 in a 5% (w/v) dried non-fat milk solution in TBST for a duration of 1 hour at room temperature with gentle shaking (**Figure 2.4 C**).

2.2.4.6 Visualization

The PVDF membrane was washed three 10-minute with TBST (with 0.1% TWEEN[®] 20). Subsequently, chemiluminescent substrate, Clarity[™] western ECL substrate (Bio-Rad Laboratories, 170-5061) was employed for visualization. This visualization step was conducted using the chemiluminescent detection system on the ChemiDoc[™] Imaging System (Bio-Rad Laboratories) (**Figure 2.4 D**).

Quantification of the bands was carried out using Image Lab 6.0 software (Bio-Rad Laboratories).

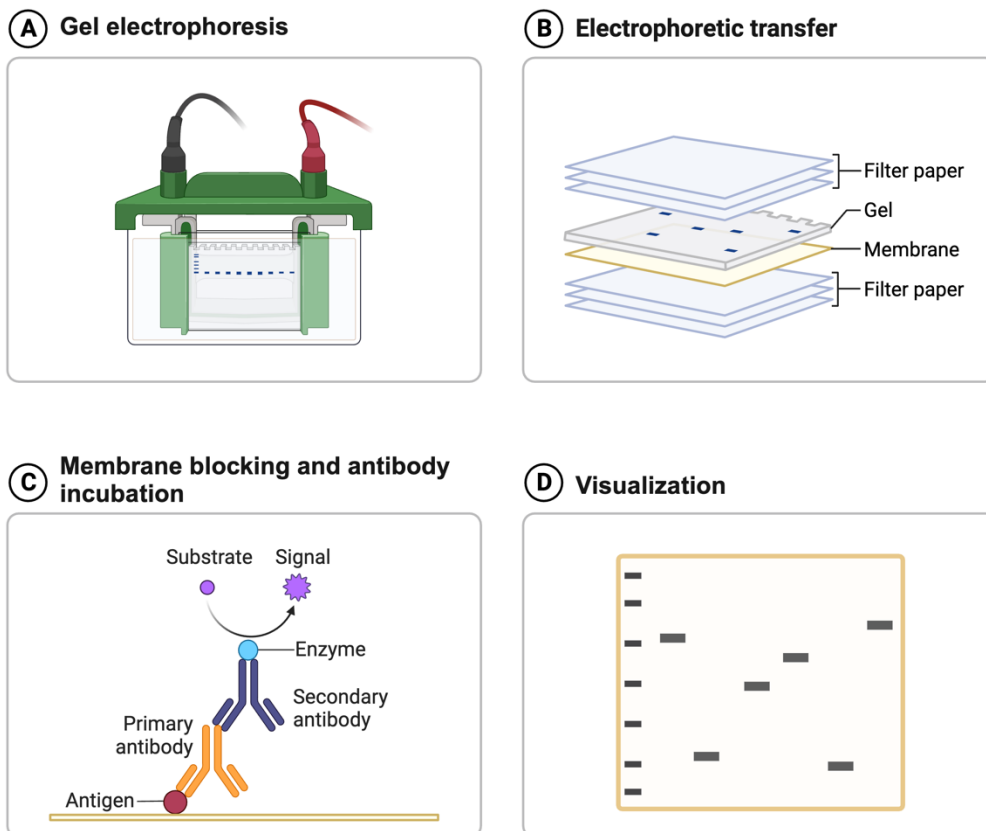


Figure 2.4 The Western Blotting procedure involves several steps.

(A) Heated protein samples were subjected to electrophoresis for around 1 hour at 120 V **(B)** Following electrophoresis, the gel was transferred onto a PVDF membrane, sandwiched between pre-soaked filter papers in transfer buffer **(C)** The PVDF membrane was then blocked with a 5% (w/v) milk blocking solution, washed with TBST and exposed to each primary antibody overnight. Subsequently, the membrane was washed with TBST and incubated with the secondary antibody followed by additional washing steps before visualization **(D)** The visualization was achieved using visualized substrate on the Imaging System (Created using BioRender).

2.2.5 Enzyme-linked immunosorbent assay (ELISA)

2.2.5.1 Preparation of cell lysates

Cells were seeded in 6-well plate in growth medium at a density of 5×10^5 . When cells grow to approximately 90% confluence, cells were carefully washed with ice-cold PBS at least 3 times. Cells were then gently scraped in 1 mL cold PBS, transferred into a 1 mL Eppendorf and centrifuged at 1000 rpm for 5 minutes. The resulting supernatant was discarded, and the cell pellet was resuspended in 200 μ L of PBS before being stored at -20°C . To ensure complete cell lysis, a freeze/thaw cycle was performed at least three times. Before final storage at -20°C , each sample was centrifuged at 12,000 rpm for 10 min at $2-8^{\circ}\text{C}$ to remove any cell debris. The protein concentration of each sample was determined using a spectrometry Nanodrop ND100 spectrometer (Thermo Fisher Scientific, Paisley, UK).

2.2.5.2 Preparation for Standard

The standard preparation followed the kit protocol (Labscoop, No. DL-NSE-Hu), involving the reconstitution of 1 mL of Standard Diluent (40 ng/mL), which was allowed to equilibrate for 10 minutes at room temperature. Subsequently, serial dilutions were conducted in a 96-well plate, resulting in a double dilution series comprising eight points: 40 ng/mL, 20 ng/mL, 10 ng/mL, 5 ng/mL, 2.5 ng/mL, 1.25 ng/mL, 0.625 ng/mL, and a blank with 0 ng/mL. The entire process was completed within 15 minutes of initiating the assay. To determine the concentration of the ENO2-encoded protein NSE, a standard curve was established using known standard concentrations and their corresponding optical density (O.D.) values as references for calculation.

2.2.5.3 Enzyme-linked immunosorbent assay (ELISA)

The ELISA procedure was carried out using the Human Enolase, Neuron Specific (NSE) ELISA Kit (Labscoop, No. DL-NSE-Hu) for multiple PCa cell lines. 100 μ L of standard dilutions, blanks and sample solutions were dispensed into their respective wells. Subsequently, microtiter plates were sealed and incubated at 37°C for 2 hours. Following the 2-hour incubation period, the liquid in each well, containing standards or

samples, was aspirated. And 100 μ L of detection reagent A working solution, containing a biotin-conjugated antibody specific to NSE, was added. The plates were then resealed and incubated at 37°C for 1 hour. After the 1-hour incubation, the solutions were aspirated, and each well was washed by adding 300 μ L of wash solution using a multi-channel pipette. After a brief 1-2-minute incubation, the remaining wash solution was entirely removed from all wells by tapping the plate onto absorbent paper, with this aspiration/wash process being repeated three times. Subsequently, 100 μ L of detection reagent B working solution, containing avidin conjugated to Horseradish Peroxidase (HRP), was applied to each standard and sample well. The aspiration/wash process was repeated five times, as previously described. Following the addition of 90 μ L of TMB substrate solution to each well, the microtiter plates were resealed, shielded from light, and incubated for 15-25 minutes at 37°C. During this incubation period, the plates turned blue. After the incubation, 50 μ L of stop solution was added to each well to stop the reaction, causing the liquid in both standard and sample wells to turn yellow. Before spectrophotometric measurement at a wavelength of 450 nm using a SpectraMax M5® microplate reader (Molecular Devices, California, USA), any residual water drops and fingerprints on the bottom of the plate were removed, and make sure there were no bubbles on the surface of the liquid (**Figure 2.5**).

This experimental procedure was repeated three times for biological replicates and conducted twice for each replicate.

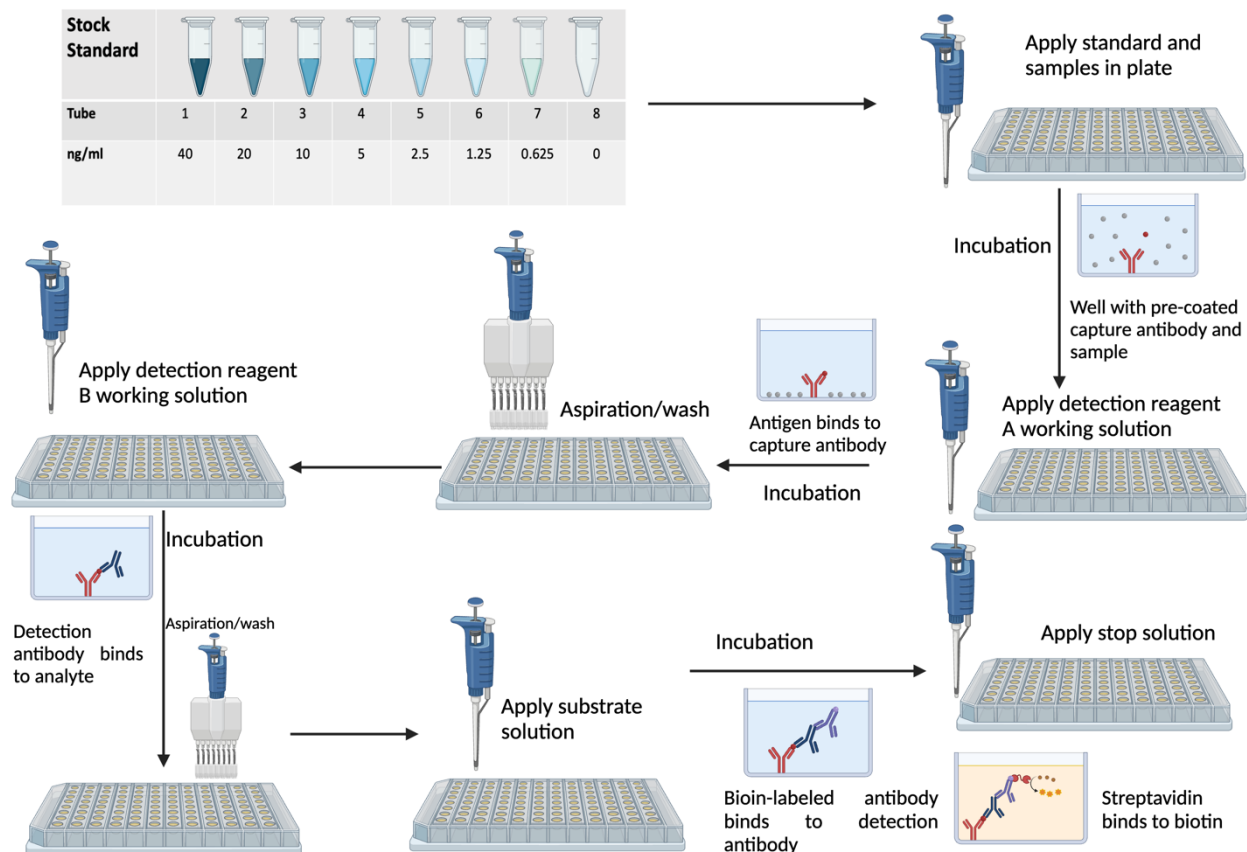


Figure 2.5 The ELISA assay procedure involves several steps.

Following standard preparation, the indirect ELISA was conducted using a dual antibody approach. This method employed an antigen-specific primary antibody (detect reagent A) and a corresponding enzyme-conjugated secondary antibody (detect reagent B). Subsequently, an enzyme substrate (substrate solution) was applied, leading to the formation of precipitates with a blue colour. To quantify the results, a stop solution was applied causing the colour changing to yellow. The measurement was then performed spectrophotometrically at a wavelength of 450 nm (Created using BioRender).

2.2.6 Genetic Verification

2.2.6.1 Primer Design

The design of upstream and downstream primers was accomplished through NCBI primer-BLAST based on the DNA sequence of ENO2 as the reference. The PCR product generated using these primers was intended to contain the gRNA associated with the custom CRISPR. Three pairs of primers were required, with two pairs targeting the coding sequence (CDS), and the third pair spanning the junction of exon and intron, thus not exclusively targeting the CDS.

To facilitate primer design, the ENO2 DNA sequence was entered into the PCR-templated frame available on the NCBI primer-BLAST website. Subsequently, specific ranges for both the forward and reverse primers were selected. The ranges for the CDS-based forward primer extended from 1254 to 1340, while the reverse primer range covered positions 2095 to 2151. Additionally, the non-CDS-based forward primer spanned positions 1321 to 1360, and the reverse primer encompassed positions 2080 to 2110. Once the species "Homo sapiens" was chosen, simply click the "Get primers" button and the website will autonomously generate appropriate primer pairs. The three selected primer pairs were ordered from Thermo Fisher Scientific, and the information is shown in **Table 2.4**.

Table 2.4 Information of designed Primer for *ENO2*.

Primer Name	Sequence (5' -> 3')	Length	Binding Sites	Yield (OD)	Yield (ug)	Yield (nmol)	Vol. for 1uM	Tm (°C)	MW (g/mol)	GC-content	Size of PCR Production
<i>CDS F1</i>	CCACAGTGGAGGTGGATCTCT	21	1306-1326	9.56	270.28	43.89	439	61.4	6158.01	60%	811 bp
<i>CDS R1</i>	GATGTGGTCCACTGCCTTCA	20	2098-2117	9.49	281.81	46.32	463	59.4	6983.94	55%	
<i>CDSF2</i>	CCCACAGTGGAGGTGGATCT	20	1305-1324	8.84	251.64	38.94	389	61.8	6462.2	57%	811 bp
<i>CDS R2</i>	ATGTGGTCCACTGCCTTCAG	20	2097-2116	9.04	268.42	44.12	441	59.4	6083.94	55%	
<i>nonCDS F</i>	AGGTAATGGGTGTGGCATGG	20	1337-1356	7.58	205.53	32.66	327	59.4	6293.11	55%	649 bp
<i>nonCDS R</i>	TAGGGGCATAAGGCTGAGGT	20	1967-1986	7.85	209.97	33.53	335	59.4	6262.1	55%	

2.2.6.2 Agarose Gel Electrophoresis

2.2.6.2.1 *Genomic DNA purification*

Genomic DNA was purified from PCa cell lines using Wizard® Genomic DNA Purification System (Promega, No. A2360). Cells were counted at a ratio of 1×10^6 in 1 mL and isolated by centrifugation at 1000 rpm for 2 minutes. The cell pellets from each sample were washed with ice-cold sterile 1X PBS and isolated by centrifugation at 1000 rpm for 2 minutes.

To lyse cells, 150 μ L of Wizard® SV Lysis Buffer was gently resuspended with the washed cell pellets. Each sample's lysate was then transferred to individual minicolumns which assembled with collection tubes and centrifuged at 10,000 rpm for 3 minutes. For purification of the total DNA, 650 μ L of Column Wash Solution with 95% ethanol was applied to each minicolumn after emptying the collection tubes, followed by centrifugation at 10,000 rpm for 1 minute. This precipitation step was repeated four times.

Following the removal of liquid from each collection tube, each assembly was centrifuged at 10,000 rpm for 1 minute to desiccate the binding matrix. Subsequently, the samples were transferred to new 1.5 mL tubes and incubated at room temperature for 2 minutes after adding 250 μ L of nuclease-free water. After the 2-minute incubation, the samples were centrifuged at 10,000 rpm for 1 minute.

Before storing the tubes containing purified DNA at -20°C , the quantity of DNA in each sample was assessed using a spectrometry Nanodrop ND100 spectrometer (Thermo Fisher Scientific, Paisley, UK).

2.2.6.2.2 *Polymerase chain reaction (PCR)*

For every 1 μ L of DNA or cDNA (less than 250 ng), 12.5 μ L of PCR Master Mix (Promega, M7505), 2.5 μ L of upstream primer, 2.5 μ L of downstream primer and nuclease-free

water were combined to achieve a final volume of 25 μ l. The mixture was gently pipetted to ensure thorough mixing and then incubated in a PCR machine (ProFlex™ PCR system, Pub. No. 4483807) at 95°C for 2 minutes for denaturation. Subsequently, an annealing step was performed at 95°C for 30 seconds, 55°C for 1 minutes and 72°C for 1 minutes. After 35 cycles of annealing step, the extension step was applied at 72°C for 1 minutes and maintained at 4°C (**Figure 2.6 A**). The resulting PCR production can be used immediately or stored at -20°C for future using.

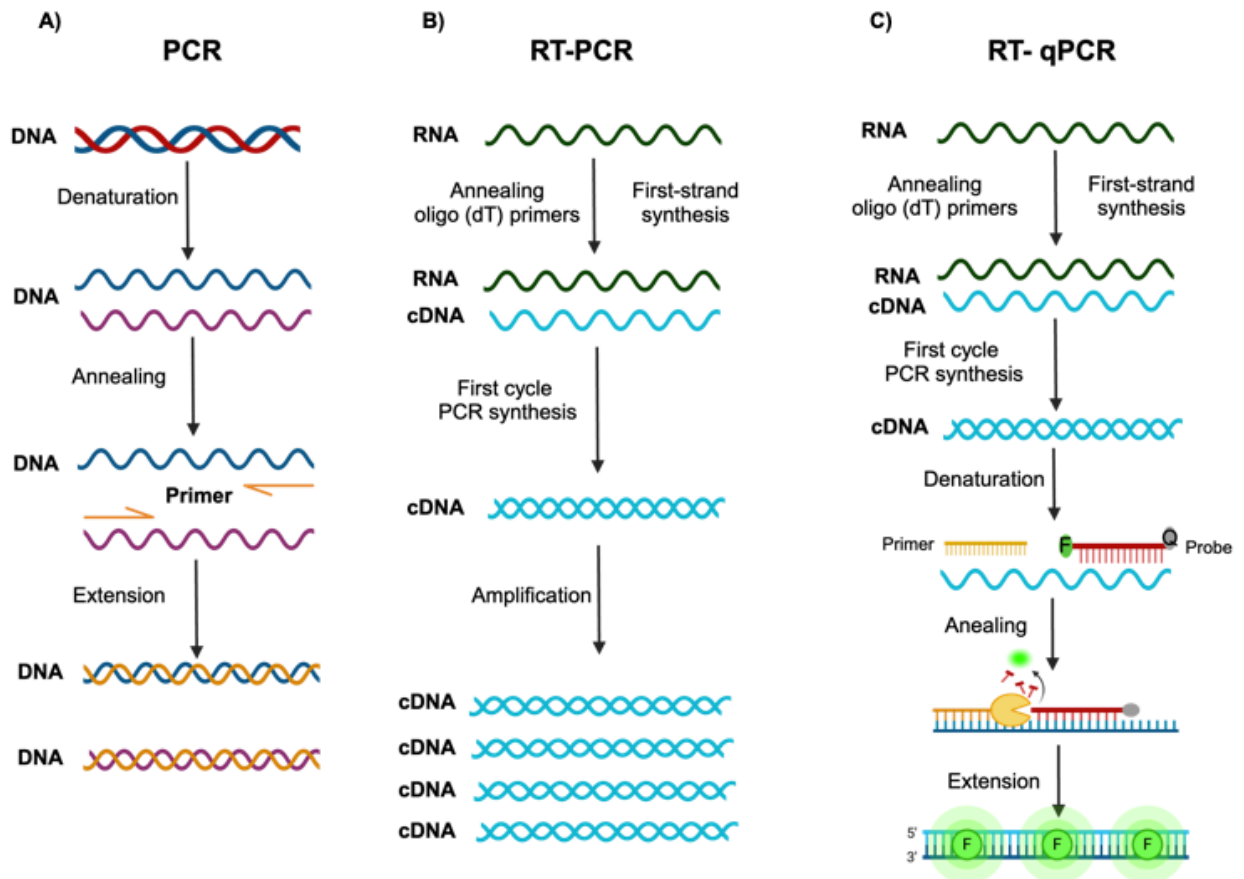


Figure 2.6 The schematic comparison of PCR, RT-PCR and RT- qPCR.

(A) DNA sequences were amplified by PCR **(B)** RNA was extracted and cDNA was generated via RT-PCR using isolated RNA template **(C)** RT- qPCR was conducted basing on the generated cDNA using TaqMan probe including fluorescein (FAM) at 5' end and quencher at 3' end. The increase of fluorescence was positively associated with the amplification of target cDNA (Created using BioRender).

2.2.6.2.3 *Gel preparation*

To prepare 1% agarose gel for gel electrophoresis, 1 g of agarose powder (INVITROGEN, 15510-027) was weighed using a precision balance. To prepare 1X TAE buffer, the weighed agarose powder was combined with 10 mL of 10X Tris-Acetate-EDTA (TAE) buffer (**Scientific Appendix**) and 90 mL of distilled water in a microwave-safe flask. Subsequently, the agarose mixture was melted in microwave for about 1 minute until the agarose is completely dissolved with carefully monitoring the process to avoid overboiling. Once the agarose was completely dissolved, add 10 µL of Ethidium Bromide solution (EB) (Merck, E1385) (0.1% w/v) to the mixture. The hot agarose mixture was poured into a gel casting tray with inserting a comb into the gel to create sample wells. Allow the agarose to cool at room temperature for about 20 minutes to completely solidify.

2.2.6.2.4 *Gel electrophoresis*

Gel electrophoresis was performed using the Bio-Rad Sub-Cell GT Horizontal Electrophoresis Systems. The prepared 1% agarose gel was immersed in 1X TAE buffer. Prior to loading onto the gel, 25 µL PCR products were combined with 6X Blue/Orange Loading Dye (Promega, G1881). For molecular weight reference, PCR Ranger 100 bp DNA Ladder (NORGEN, 11300) was employed. The PCR products and DNA ladder were resolved by electrophoresis at a voltage of 120V for approximately 1 hour after loading. The bands of DNA fragments would be visualized by ChemiDoc™ Imaging System (Bio-Rad Laboratories) under UV. The required bands were carefully excised and placed into fresh Eppendorf tubes for later DNA purification, which involved weighing the samples.

2.2.6.2.5 *Genomic DNA purification*

Genomic DNA purification was performed using the PureLink® PCR Purification Kit (Invitrogen, K3100-01). Before purification, binding buffer (B2) and wash buffer (W1) in the kit were prepared by adding 10 mL isopropanol and 64 mL ethanol, respectively. Subsequently, 4 volumes of B2 was applied to 1 volume of

weighted gels containing DNA binds. After mixing, the samples were accessed into PureLink® Spin Columns in collection tubes and centrifuged at above $10,000 \times g$ for 1 minute. After emptying the collection tubes, 650 μL of W1 was added to each column and centrifuged at above $10,000 \times g$ for 1 minute. After emptying the collection tubes, the columns were re-insert into the collection tubes and centrifuged at maximum speed for 3 minutes. The columns were subsequently transferred to elution tubes. After adding 50 μL Elution Buffer to each, they were incubated 1 minute at room temperature and centrifuged at maximum speed for 2 minutes. Before storing the elution, tube containing purified DNA at -20°C , the DNA from each sample was quantified using a spectrometry Nanodrop ND100 spectrometer (Thermo Fisher Scientific, Paisley, UK).

2.2.6.3 Sanger DNA Sequencing

Before sending for sequencing, the quantity of purified PCR products of each sample was assessed using a spectrometry Nanodrop ND100 spectrometer (Thermo Fisher Scientific, Paisley, UK) to ensure a minimum concentration of 10 $\text{ng}/\mu\text{L}$. Each DNA sample was dispatched to Azenta Life Science for Sanger sequencing. The obtained results were analyzed using SnapGene Software.

2.2.7 Cell Viability Assays (*alamarBlue*[™] Assay)

Cell viability was assessed using the *alamarBlue*[™] Cell Viability Reagent (Invitrogen, DAL1025). This reagent contains Resazurin as active component which is both non-toxic and capable of permeating cells. Resazurin possesses a blue colour and exhibits strong fluorescence within this reagent. It allows for the quantitative measurement of cell vitality by leveraging the reducing power generated during active cell metabolism. Upon entering living cells, the blue hue of Resazurin undergoes a transformation to the pink hue of Resorufin [155, 156]. This change can be detected using a fluorescence or absorbance -based plate reader (**Figure 2.7**).

In order to evaluate the impact on viability of varying environmental glucose concentrations of both PCa and prostatic myofibroblast tissue cells, human PCa cell

lines, including PC3, 22RV1, LNCaP-LN3, as well as prostatic myofibroblast WPMY-1 cells, were seeded in 96-well plates at a density of 3,000 cells per well in 100 μ L of standard, low or glucose-free medium. Fresh medium was changed daily.

To evaluate the effect on viability of knocking out or knocking down ENO2 on PCa cells, PC3 and 22Rv1 WT cell lines, as well as their respective ENO2 knockout and knockdown cell lines, were seeded into 96-well plates at a density of 5,000 cells per well in 100 μ L of standard medium. Fresh medium was changed daily.

At intervals of 24 to 96 hours, 10 μ L of the alamarBlue™ reagent (at a concentration of 10% v/v) was added into each well. Cell viability was assessed using a SpectraMax M5® microplate reader (Molecular Devices, California, USA) with excitation at 560 nm and emission at 590 nm (measuring absorbance at 570 nm) following a 3-hour incubation period, while ensuring protection from light. The experiment was performed in three independent biological replicates.

To eliminate background fluorescence, a baseline absorbance value was subtracted from all measurements. This baseline was obtained from wells containing only the serum-free medium and alamarBlue™ reagent.

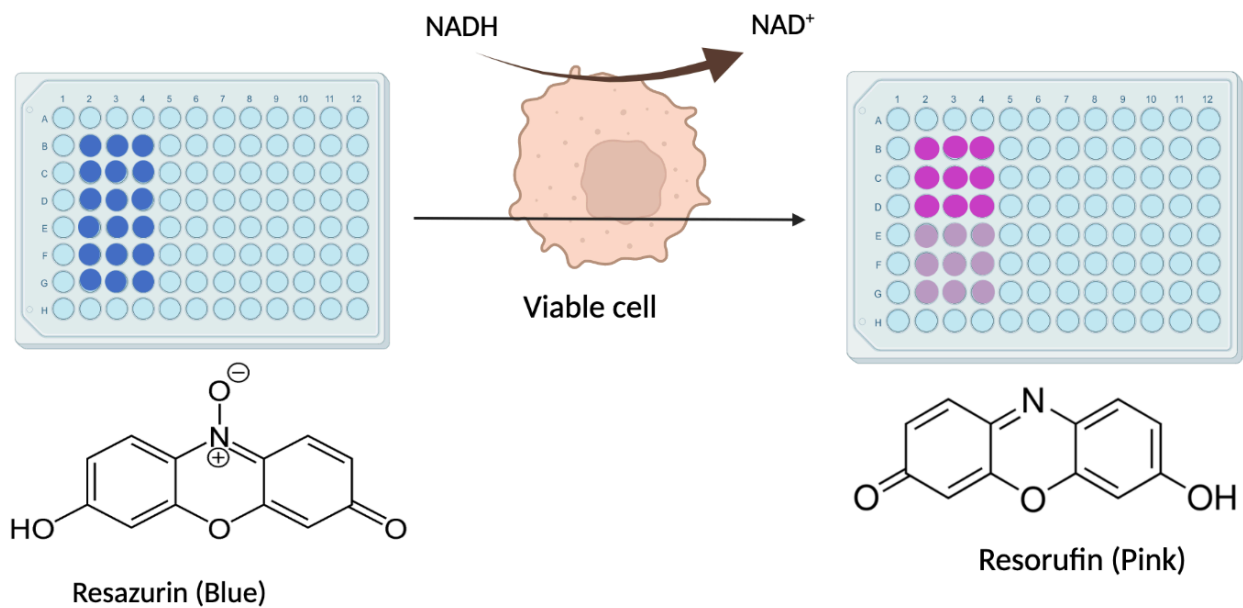


Figure 2.7 The process of alamarBlue™ reaction.

The primary dye in alamarBlue™ reagent is Resazurin, which exhibits low fluorescence. But resazurin would be reduced to Resorufin which is a highly fluorescent compound with a pink coloration when produced by viable cells. The different fluorescence signals serve as indicators of the capability of cells to maintain viability (Created using BioRender).

2.2.8 Cell Proliferation Assays (CyQuant® Assay)

Cell proliferation assay was evaluated using the CyQUANT® NF Cell Proliferation Assay (Invitrogen, C35006). It is an efficient and precise approach to assess cell proliferation by quantifying cellular DNA content, which achieves DNA binding by coupling a dye to a plasma membrane permeabilizing agent, independent of cell metabolic activity [157]. When the reagent composition including probes and suppressors were introduced into cells, the probes effectively stains all cells, whereas the suppressors selectively targets dead cells or cells with compromised membrane integrity. The suppressor effectively blocks the functions of probes at these specific locations, ensuring that only healthy and intact cells are detected by the assay [157]. To evaluate the effect on proliferation of knocking out or knocking down ENO2 on PCa cells, PC3 and 22Rv1 WT cell lines, as well as their respective ENO2 knockout and knockdown cell lines, were seeded into 96-well plates at a density of 5,000 cells per well in 100 μ L of standard medium. Fresh medium was changed daily.

The 1X dye binding solution was prepared by combining 22 μ L of CyQUANT® NF dye reagent with 11 mL of 1X HBSS buffer, which was generated by diluting 2.2 mL of 5X HBSS buffer with 8.8 mL of deionized water. At intervals of 24 to 96 hours, the previous medium was aspirated and 100 μ L of 1X dye binding solution (at a concentration of 100% v/v) was added into each well. Cell viability was assessed using a SpectraMax M5® microplate reader (Molecular Devices, California, USA) with excitation at 480 nm and emission at 520 nm following a 1-hour incubation period, while ensuring protection from light. The experiment was performed in three independent biological replicates. To eliminate background fluorescence, a baseline absorbance value was subtracted from all measurements. This baseline was obtained from wells containing only the 50 μ L of 1X dye binding solution.

2.2.9 Cell apoptosis Assays (Caspase 3/7™ Assay)

Cell apoptosis assay was evaluated using the Cell Meter™ Caspase 3/7 Activity Apoptosis Assay Kit (AAT Bioquest, 22796). It is designed to measure apoptosis by

quantifying the activation of Caspase 3, which act as a dependable indicator for cellular apoptosis [158]. Caspase 3 displays a specific affinity for cleaving substrates bearing the peptide sequence Asp-Glu-Val-Asp (DEVD), which serves as a fluorogenic indicator included in this kit. A strong fluorescence has been generated by Caspase 3 by cleavage of peptides enabling detection with either an absorbance or fluorescence-based plate reader [159].

In order to evaluate the impact on apoptosis of varying environmental glucose concentrations of both PCa and prostatic myofibroblast tissue cells, human PCa cell lines, including PC3, 22RV1, LNCaP-LN3, as well as prostatic myofibroblast WPMY-1 cells, were seeded in 96-well plates at a density of 20,000 cells per well in 100 μ L of standard, low or glucose-free medium. Fresh medium was changed daily.

To evaluate the effect on viability of knocking out or knocking down ENO2 on PCa cells, PC3 and 22Rv1 WT cell lines, as well as their respective ENO2 knockout and knockdown cell lines, were seeded into 96-well plates at a density of 10,000 cells per well in 100 μ L of standard medium. Fresh medium was changed daily.

At intervals of 24 to 96 hours, the previous medium was aspirated and 100 μ L Caspase 3/7 substrate working solution (at a concentration of 100% v/v) was added into each well. Cell viability was assessed using a SpectraMax M5® microplate reader (Molecular Devices, California, USA) with excitation at 490 nm and emission at 525 nm (measuring absorbance at 515 nm) following a 1-hour incubation period, while ensuring protection from light. The experiment was performed in three independent biological replicates.

To eliminate background fluorescence, a baseline absorbance value was subtracted from all measurements. This baseline was obtained from wells containing only the 100 μ L Caspase 3/7 substrate working solution.

2.2.10 Cell Migration Assays

2.2.10.1 Wound-healing Assay

The wound healing assay was used to measure 2D migration of PC3 WT and PC3 ENO2-KO cells. The directed cell migration is easily to detect by wound healing assay to test the regulations of cell-ECM and cell-cell interactions [160]. However, cells do not only migrate into the gap but also undergo proliferation. Therefore, mitomycin C, which is able to achieve covalent cross-links between DNA strands, was used to inhibit DNA synthesis and replication, thus preventing cell proliferation and allowing efficient migration [161].

PC3 WT and PC3 ENO2-KO cells were seeded as a density of 2×10^5 in 24-well plate with standard DMEM. Following a 1-night incubation period, the confluent cell monolayer was exposed to 5 $\mu\text{g/mL}$ of mitomycin-C (Sigma-Aldrich, M0503) for 3 hours to suppress proliferation. Subsequently, a vertical scratch was applied into the monolayer using a 10 μL pipette tip into each well and the cells were washed 7-8 times with serum-free medium to eliminate any detached cells and debris. 1% FBS DMEM were added to the cells and the plate was then transferred to a humidified microscope maintained at 37 °C with 5% CO₂. Migration progress was monitored over a 20-hour period using the Olympus scanR time-lapse imaging system, with sequential images captured at 30-minute intervals (**Figure 2.8**). The percentage of wound closure was subsequently calculated using T scratch software after completion of the wound-healing assay. The experiment was performed in three independent biological replicates.

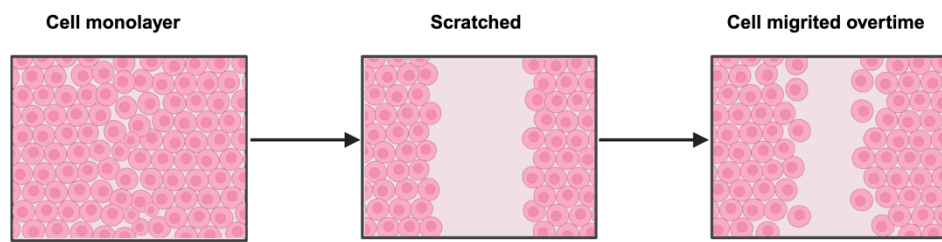


Figure 2.8 Cell migration evaluated by the wound-healing assay.

Cells were seeded as a monolayer. The vertical wound was generated by scratching the middle of the well. Cells were migrated overtime and gradually healed the wound (Created using BioRender).

2.2.10.2 Boyden Chamber Transwell® Assay

The Boyden Chamber transwell assay was used to measure 3D migration of 22Rv1 WT and 22Rv1 ENO2-KO cells. It quantitatively analyses the directed movement and migration response of cells which are attracted by the higher concentration of FBS as a chemoattractant below the chamber and migrate through the pores on the membrane [162].

22Rv1 WT and 22Rv1 ENO2-KO cells were exposed to 5 µg/mL of mitomycin-C (Sigma-Aldrich, M0503) for 3 hours to suppress proliferation. Then the cells were trypsinized and suspended in serum-free medium at a density of 4.5×10^5 cells/mL. Subsequently, 200 µL of the cell suspension was placed onto the Corning® Costar® Transwell® cell culture insert (6.5 mm Transwell® with 8.0 µm Pore Polycarbonate Membrane Insert, Sterile, Corning, No. 3422). 500 µL of 5% FBS DMEM was employed to the 24-well plate, followed by the placement of the transwell insert. The plates with inserts were then incubated at 37 °C with 5% CO₂ for 72 hours.

After the 72-hour incubation, the medium and non-invasive cells were removed from the interior of the insert using a damp cotton swab. The cells on the insert were fixed in 100% ethanol for 5 minutes and then stained with a modified Gill II hematoxylin solution (Sigma-Aldrich, Catalog No. 105175) and eosin Y solution (Sigma-Aldrich, Catalog No. HT110280), commonly known as H&E staining. The inserts were stained with hematoxylin for 5 minutes, washed with tap water, immersed in 1% eosin (w/v) for 1 minute and washed again with tap water. The inserts were excised and mounted on glass slides using Faramount aqueous mounting medium (Agilent, Catalog No. S3025) to prevent air bubbles (**Figure 2.9 A**). Representative images of the insert were captured and cell numbers were counted using a bright-field microscope at 10× magnification with the Osteomeasure7 v4.2.0.1 software.

2.2.11 Cell Invasion Assays (*Trans-well Invasion assay*)

The Transwell invasion assay was employed to assess the cellular ability of respond directionally to a chemoattractant and the invasiveness of basement membrane [163]. PC3 WT, PC3 ENO2-KO, 22Rv1 WT and 22Rv1 ENO2-KO cells were exposed to 5 µg/mL of mitomycin-C (Sigma-Aldrich, M0503) for 3 hours to suppress proliferation. PC3 and PC3 ENO2-KO cells were then trypsinized and suspended in serum-free medium at a density of 2.5×10^5 cells/mL, the 22Rv1 and 22Rv1 ENO2-KO cells were trypsinized and suspended in serum-free medium at a density of 4.5×10^5 cells/mL. Subsequently, the Corning® Costar® Transwell® cell culture insert (6.5 mm Transwell® with an 8.0 µm pore polycarbonate membrane, sterile, Corning, No. 3422) was coated with 20 µl of Phenol Red-Free Corning® Matrigel® Basement membrane matrix (1.5 mg/mL; Corning, No. 356237) and left to incubate at 37°C with 5% CO₂ for 2 hours. Then 200 µL of the cell suspension was placed onto the Corning® Costar® Transwell® cell culture insert. 500 ul of 5% FBS DMEM was employed to the 24-well plate, followed by the placement of the transwell insert. The plates with inserts were then incubated at 37 °C with 5% CO₂ for 72 hours.

After the 72-hour incubation, the medium and non-invasive cells were removed from the interior of the insert using a damp cotton swab. The cells on the insert were fixed in 100% ethanol for 5 minutes and then stained with a modified Gill II hematoxylin solution (Sigma-Aldrich, Catalog No. 105175) and eosin Y solution (Sigma-Aldrich, Catalog No. HT110280), commonly known as H&E staining. The inserts were stained with hematoxylin for 5 minutes, washed with tap water, immersed in 1% eosin (w/v) for 1 minute and washed again with tap water. The inserts were excised and mounted on glass slides using Faramount aqueous mounting medium (Agilent, Catalog No. S3025) to prevent air bubbles (**Figure 2.9 B**). Representative images of the insert were captured and cell numbers were counted using a bright-field microscope at 10× magnification with the Osteomeasure7 v4.2.0.1 software.

A)

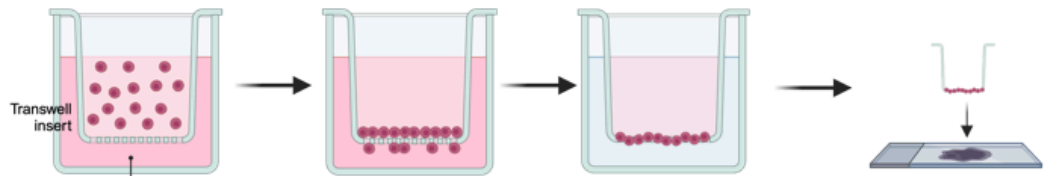
Boyden Chamber Migration assay

Load cell suspension in serum-free medium to the upper chamber of transwell

Cells gradually migrate to bottom of transwell membrane overtime

Remove undetached cells, fix and stain the transwell insert

Excise and mount the insert on glass slides using mounting medium on glass slide



B)

Trans-well Invasion assay

Medium with chemoattractant (FCS)

Transwell insert
Coated with matrigel
Medium with chemoattractant (FCS)

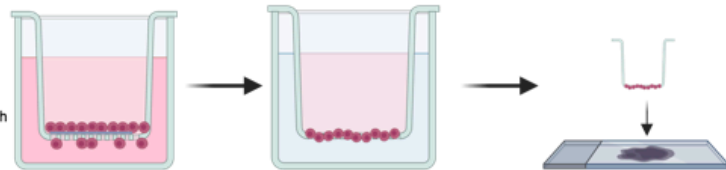


Figure 2.9 The comparison of Boyden Chamber migration and trans-well invasion assay.

Cells were seeded in serum-free medium and placed onto transwell inserts, with or without matrigel coating, positioned in wells containing standard medium to establish a chemoattractant gradient. Following a 72-hour incubation period, transwell membranes were stained with H&E and mounted on glass slides for subsequent visualization and analysis (Created using BioRender).

2.2.12 Metabolism related assays

2.2.12.1 Glucose consumption assay

Glucose consumption assay was employed using Glucose Assay Kit (Abcam, ab102517). Glucose would be specifically oxidized in this assay to form a product that reacts with the dye to produce a colour whose intensity is proportional to the glucose concentration.

To evaluate the effect on glucose uptake of knocking out ENO2 on PCa cells, PC3 and 22Rv1 WT cell lines, as well as their respective ENO2 knockout cell lines, were seeded into 6-well plates at a density of 1 million cells each well in 1 mL of standard medium. The culture mediums were collected as test samples after overnight incubation.

As a reference, glucose concentrations were determined by using the diluted 1 nmol/ul standard (adding 10 μ L of the glucose standard to 990 μ L of glucose assay buffer). Subsequently, 0, 2, 4, 6, 8 and 10 μ L of standards were added into a series of wells of a 96 well plate. The volume of all wells was adjusted to 50 μ L with glucose assay buffer to generate 0, 2, 4, 6, 8 and 10 nmol/well of glucose standard. The 49 μ L of glucose assay buffer and 1 μ L of test samples were added in triplicates in 96-well plate. The glucose reaction mix (50 μ L) was added to all wells in the plate, which was prepared containing 46 μ L of glucose assay buffer, 2 μ L of glucose enzyme mix and 2 μ L of glucose substrate mix. Following 30 minutes incubation at room temperature, the absorbance at 450 nm was measured using a SpectraMax M5® microplate reader. Notably, samples with signals greater than the highest standard should be additional diluted 1:2 in assay buffer before reanalyzing.

To eliminate background fluorescence, the zero-glucose standard value was subtracted from all measurements. Subsequently, a standard curve was constructed to determine the total glucose concentration of each sample using the known glucose concentrations. This allowed for the calculation of the amount of glucose required to

achieve a final quantity from 0 to 10 nmol. Glucose consumption of the test samples can then be calculated:

$$\text{Glucose consumption (mM)} = 25 \text{ (mM) (Glucose concentration in 1ul standard medium)} - \frac{\text{sample amount calculated from standard curve (nmol)}}{\text{sample volume added in in the well (ul)}} \times 2 \text{ (dilution factor)}$$

The calculated outcome represents the concentration of glucose consumed per million cells.

2.2.12.2 Lactate production assay

Lactate production assay was employed using L-Lactate Assay Kit (Abcam, ab 65331). To evaluate the effect on lactate production of knocking out ENO2 on PCa cells, PC3 and 22Rv1 WT cell lines, as well as their respective ENO2 knockout cell lines, were trypsinized and calculated at a density of 200,000 cells each in 200ul of iced PBS. The culture mediums were collected as test samples after one-night incubation. After centrifugation at maximum speed for 5 min at 4°C, the supernatant was collected and kept on ice.

As a reference, lactate concentrations were determined by using the diluted 1 nmol/ul standard (adding 10 µL of the glucose standard to 990 µL of glucose assay buffer). Subsequently, 0, 2, 4, 6, 8 and 10 µL of standards were added into a series of wells of a 96 well plate. The volume of all wells was adjusted to 50 µL with lactate assay buffer to generate 0, 2, 4, 6, 8 and 10 nmol/well of standard. The 49 ul of lactate assay buffer and 1 ul of test samples had been added applied in triplicate in 96-well plate. The lactate reaction mix (50 µL) was added to all wells in the plate, which was prepared containing 46 ul of lactate assay buffer, 2ul of lactate enzyme mix and 2 ul of lactate substrate mix. In addition, the background controls were set up in triplicate containing 1 ul of iced PBS, 97 ul of lactate assay buffer and 2ul of lactate enzyme mix to verify whether the presence of NADH/NADPH in test samples which would create

background in this assay. Following 30 minutes incubation at room temperature, the absorbance at 450 nm was measured using a SpectraMax M5® microplate reader.

To eliminate background fluorescence, the zero-lactate standard value was subtracted from all measurements. If the sample background controls were not significant, it was not subtracted from the sample readings. Subsequently, a standard curve was constructed to determine the total lactate concentration of each sample using the known lactate concentrations. This allowed for the calculation of the amount of lactate required to achieve a final quantity from 0 to 10 nmol. Lactate production of the test samples can then be calculated:

$$\text{Lactate production (mM)} = \frac{\text{sample amount calculated from standard curve (nmol)}}{\text{sample volume added in the well (ul)}}$$

The calculated outcome represents the concentration of lactic acid produced per 200,000 cells. For assessing lactate production each million cells, the derived result should be multiplied by a factor of 5.

2.2.13 RNA-Sequencing (RNA-Seq)

RNA samples were extracted following the step from **Chapter 2.2.3.1** from PC3 WT and ENO2-KO, 22Rv1 WT and ENO2-KO cells with 3 biological repeats of WT cells, 2 single clones from KO cells. Before sending for sequencing, the quantity of RNA in each sample was assessed using a spectrometry Nanodrop ND100 spectrometer (Thermo Fisher Scientific, Paisley, UK) to ensure the A260/280 values around 2. Sample was dispatched to Source Genomics for sequencing. All samples had passed the quality controls (QC) (**Table 2.5**). All data were downloaded and then analyzed in Galaxy version 23.1 (<https://usegalaxy.eu/>). QC were conducted with FastQC version 0.12.1 (<http://www.bioinformatics.babraham.ac.uk/projects/fastqc/>) and the reads were trimmed with Cutadapt [164]. Subsequently, HISAT2 and featureCounts were employed to map the trimmed reads to the human hg38 reference genome and

quantification [165, 166]. Differential gene expression (DEG) analysis, generation of multidimensional scaling (MDS) plots and heatmaps were performed by limma-voom (minimum 0.5 of the filtering on count-per-million (CPM), 0.58 of minimum Log2 Fold Change (FC), FDR< 0.05) [167]. The visualization of the results were achieved through ggplot2 by creating volcano plots (0.58 of Log2 FC threshold to colour) [168]. Gene Ontology (GO) analysis was conducted using goseq to generate bubble plots with biological process (BP) and molecular function (MF) (FDR<0.05) [169]. Gene Set Enrichment Analysis (GSEA) was conducted using the fgsea [170]. Venn diagram were created with Bioinformatics & Evolutionary Genomics (<https://bioinformatics.psb.ugent.be/webtools/Venn/>). The protein-protein interaction (PPI) network figure of commonly up- or down-regulated genes was generated from the Search Tool for Interacting Genes/Proteins (STRING) (<https://string-db.org/>), the minimum required interaction score as medium confidence (0.4) [171]. The functional classification was viewed by creating a pie chart by PANTHER (<https://www.pantherdb.org/>) [172]. The functional relationship was observed by performing DAVID Functional Annotation Bioinformatics Analysis (<https://david.ncifcrf.gov/>) [173].

Table 2.5 QC report for the sending samples (provided by Source Genomics).

External ID	Conc. (ng/μl)	Size (average bp)	nM
PC3 WT n=1	10.84	360.00	45.18
PC3 WT n=2	8.46	353.00	35.95
PC3 WT n=3	7.93	355.00	33.49
PC3 ENO2-KO #1	7.81	356.00	32.90
PC3 ENO2-KO #2	7.33	365.00	30.12
22Rv1 n=1	5.07	343.00	22.18
22Rv1 n=2	4.32	333.00	19.47
22Rv1 n=3	6.50	361.00	27.00
22Rv1 ENO2-KO #4	8.98	366.00	36.81
22Rv1 ENO2-KO #8	5.47	348.00	23.58

2.3 *In vivo* Studies

2.3.1 *Ethical statement and Animals*

All experimental procedures and protocols received approval from the Animal Welfare and Ethical Review Body of The University of Sheffield, UK and in accordance with the UK Animals (Scientific Procedures) Act 1986 standards. All the scientific experiments were conducted under the Procedure Project License (PPL) PP3267943 and Procedure Individual License (PIL) I83129335.

In this project, BALB/c nude mice were sourced from Charles River Laboratories, Inc. in Wilmington, Massachusetts, USA. The BALB/c nude mouse strain is characterized by athymia, ultimately causing them immunocompromised and deficient in T cells, therefore suitable for applying in PC3 related PCa xenograft models. The mice were kept in RB-3 sterile cages maintained under optimal laboratory mouse conditions, including a temperature range from 19 to 23°C, relative humidity between 45-55%, and a 12-hour light/dark cycle with light intensity between 350-400 lux. They were provided with unrestricted access to Teklad Global 18% Protein Rodent Diet (Envigo, Huntingdon, UK) and water to ensure their dietary needs were met. The overall health and well-being of the mice were overseen by the dedicated staff members of the "Biological Services" team at the University of Sheffield, UK, who performed routine healthcare procedures for the mice.

2.3.2 *Intracardiac Injection of PCa*

A pre-clinical model of PCa was established by intracardiac (I.C.) injection of either PC3 WT Luc or PC3 ENO2-KO #1 cells into 6 to 7-week-old BALB/c nude mice (injection was conducted by Dr Ning Wang). The study cohort comprised a total of 16 mice, segregated into two distinct groups: the experimental group, consisting of 8 mice receiving injections of PC3 ENO2-KO #1 cells, and the control group, which received injections of PC3 WT Luc cells.

After the mouse was anesthetized by 2-5% isoflurane inhalation, each mouse was positioned in a supine posture with its head gently elevated and maintained in 1-2% isoflurane. An insulin syringe, containing 100 μ l of prepared cell suspension comprising a total of 1×10^5 PC3 WT Luc or PC3 ENO2-KO #1 cells in PBS, was inserted horizontally into the left ventricle of the mouse. During the injection process, as the plunger was gradually retracted, the presence of bright red blood within the syringe indicated precise needle placement. Subsequently, the mixture of red blood and the cell suspension was gently reinjected into the left ventricle of the mouse. Following the procedure, mice were carefully placed in a veterinary incubator set at a controlled temperature of 25°C to ensure complete postoperative recovery.

2.3.3 Bioluminescent Imaging (IVIS imaging)

Prior to the imaging procedure, the IVIS system was initialized to stabilize the lens temperature, and the exposure time was configured to "Auto." The mice were anesthetized by inhalation of a gas mixture comprising 2-5 % isoflurane, and 30% O₂. Subsequently, every set of three to five mice received a subcutaneous injection of 100 μ L of D-Luciferin (Invitrogen, L2916) solution at a concentration of 40 mg/mL. The mice were then placed in dorsal and supine positions within the IVIS chamber while maintaining continuous inhalation of 1-2% isoflurane. After a seven-minute interval following the D-Luciferin injection, the bioluminescent imaging of these three to five mice was conducted using the IVIS system. Following the IVIS imaging, the mice were returned to their chambers to regain consciousness. During the analysis of the IVIS data, a maximum threshold for bioluminescent intensity (BLI) was set at 5×10^5 photons. Moreover, the minimum BLI threshold was adjusted for each experimental model to facilitate the visualization of bioluminescent signals emanating from the tumours.

2.3.4 Body Weight Measurement

The body weight of mice was measured twice a week before the Luciferase signal appeared in control group in the IVIS imaging. The mice's body weight was measured three times each week following the onset of the Luciferase signal in control group.

The weight loss rate of mice was calculated using the following equation:

$$\text{Weight loss rate (\%)} = \frac{\text{Body weight (Day n)} - \text{Body weight (Day 0)}}{\text{Body weight (Day 0)}} \times 100$$

2.3.5 Euthenisation and dissection

The mice were kept in deep anesthesia via the inhalation of a gas mixture composed of 2% isoflurane along with 30% O₂. Each mouse was positioned on its back on a warm surface and continued to receive isoflurane anesthesia. The bleeding process in this project was completed by Mr Matthew Fisher. After bleeding, the mouse was promptly humanely euthanized based on Schedule 1, specifically through cervical dislocation.

Following dissection, tibias and femurs were immersed in a 10% w/v Formalin solution and fixed at room temperature for 1 week. After fixation, the tibias and femurs were subsequently placed in 70% ethanol for micro-CT scanning. Livers, kidneys, spleens and lungs were immersed in a 10% w/v Formalin solution and fixed at room temperature for 2 days. After fixation, the organs were subsequently placed in 70% ethanol for histology studies.

The 40 µl obtained blood sample was mixed with 20 µl of EDTA in a separate tube to quantify whole blood cells. The remaining blood was centrifuged at 10,000g for 20 minutes to separate the serum. Subsequently, the serum was transferred to fresh Eppendorf tubes and stored at -80°C.

2.3.6 Analysis of Osteolysis

2.3.6.1 Micro-Computed Tomography (Micro-CT)

A non-destructive imaging tool, Micro Computed Tomography (Micro-CT), is used to generate high-resolution 3D representation and of the object and subsequent quantitative analysis, directing X-ray beams into a target sample [174]. The Micro-CT system consist of three key elements: an X-ray source, a turntable and the X-ray

detector. After the sample was positioned on the turntable and turning on the X-ray, numerous 2D images were captured as the samples rotates around its axis under the introducing of X-ray beams, preventing any overlap of internal and external structures and ensuring a comprehensive scan. Following the reconstruction of the initial 2D pictures to cross-sectional images, the selected region of interest (ROI) was analyzed and modelled to 3D images [162].

The Skyscan 1272 scanner (Bruker, Billerica, Massachusetts, USA) was employed to conduct left femur and tibia structure analysis. The scanner was set to a 0.5 mm aluminum filter, producing images at a resolution of 2016 x 1344 pixels, with each pixel measuring 4.3 μm in size. The left femur and tibia were wrapped in transparent cling film inside the tube to avoid movement during scanning the head of the femur and tibia. A total of 272 2D images were captured continuously until a 180-degree rotation at intervals of approximately 0.66 degrees. These images were subsequently subjected to reconstruction using the NRecon software. The settings of Micro-CT settings are detailed in **Table 2.6**.

A key reference point was determined by moving through the slices from the metaphysis towards the knee growth plate, which was established as the initial occurrence of a bridging connection within the low-density growth plate chondrocyte seam for each sample. Within this volume of interest (VOI), a ROI shape was delineated to differentiate trabecular bone from cortical bone (**Figure 2.10**). The analyzed bone parameters included the following:

- Trabecular bone volume fraction (BV/TV)
- Trabecular thickness (Tb.Th)
- Trabecular number (Tb.N)
- Trabecular separation (Tb.Sp)
- Trabecular bone pattern factor (Tb.Pf)

These parameters were examined to assess various aspects of bone structure and density.

Table 2.6 The settings of Micro-CT applied in mice bone scanning.

Bone Sample	Location	Scan resolution	Rotation	NRecon threshold	CTan threshold	ROI off set (mm)	ROI height (mm)
<i>Tibia</i>	Trabecula	4.3 um	180°	0-0.14	90-255	0.198	0.998
	Cortical tissue					0.499	
<i>Femur</i>	Trabecula	4.3 um	180°	0-0.14	90-255	0.198	0.998
	Cortical tissue					0.499	

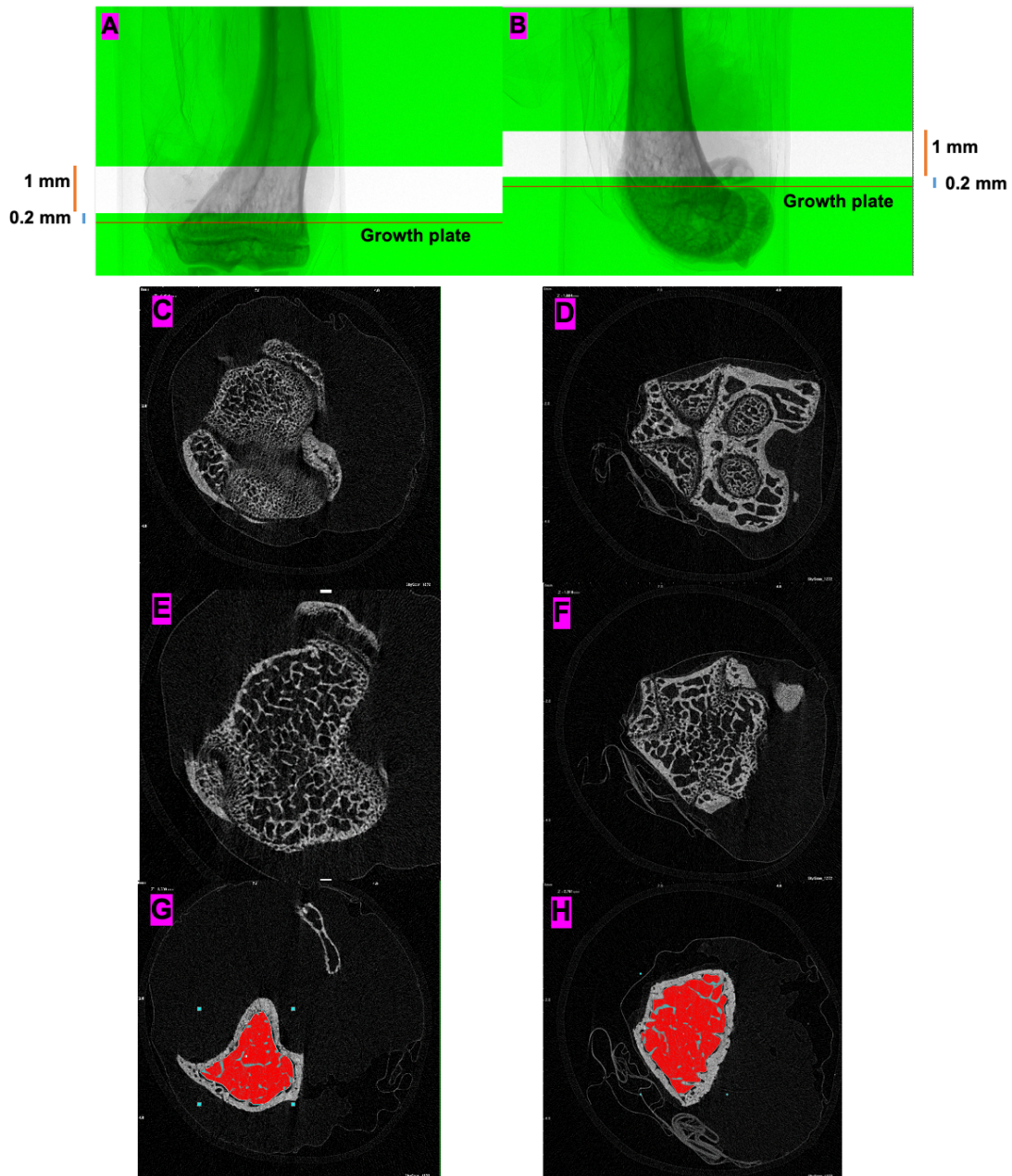


Figure 2.10 Schematic representation of the landmark and ROI selected for trabecula bone in tibia and femur.

(A and B) The BV/TV was calculated as a region of 1mm in thickness, starting at 0.2mm from the lowest part of the growth plate from tibia and femur, respectively **(C and D)** Two and four condyles were the firstly appeared landmarks of bridging connections of the tibia and femur, respectively **(E and F)** The low-density growth plate chondrocyte seams were the secondary appeared landmarks of the tibia and femur, respectively **(G and H)** The ROI of trabecular bone in tibia and femur, coloured in red, respectively.

2.3.7 Analysis of Prostate cancer - Bone cell Interactions

2.3.7.1 Histological studies

2.3.7.1.1 Bone sectioning

Bone sections from the left tibia were stained into coloured bone tissue to identify osteocytes, in order to investigate cellular events. The bone sections were prepared by Ms. Orla Gallagher (skelet.AL, University of Sheffield).

2.3.7.1.2 Haematoxylin & Eosin staining (H&E staining)

H&E staining was effectively used for visualization of tumour size by staining nuclei and cytoplasm, was conducted by Ms. Orla Gallagher (skelet.AL, University of Sheffield) [175]. Representative images were captured using a bright-field microscope at 4× and 10× magnification with the Osteomeasure7 v4.2.0.1 software. Image analysis was performed using ImageJ to quantify tumour burden areas. The tumour burden areas of mice tibia were calculated using the following equation:

$$\text{Tumour burden areas (\%)} = \frac{\text{Tumour area}}{\text{Bone marrow area}} \times 100$$

2.4 Meta-analysis, Retrospective and Bioinformatic studies

2.4.1 Systematic Review and Meta-analysis

2.4.1.1 Literature source and searches

This meta-analysis was conducted following the Preferred Reporting Items for Systematic Reviews and Meta-analyses (PRISMA) statement [173]. A protocol was conducted in accordance with the purpose-driven hypothesis. Keyword searches related to "prostate cancer," "ENO2," and "metastasis" were carried out using Web of Science, Medline, and PubMed on May 12th, 2021, and updated on Nov 8th, 2023. The developed search strategies for Web of Science, Medline and PubMed are shown in **Appendix Table 1**. Relevant articles were individually screened based on search strategy terms. Duplications were automatically removed using EndNote 20.6 (Clarivate Analytics, 2023).

2.4.1.2 Inclusion and exclusion criteria

The selection criteria for this systematic review comprised both inclusion and exclusion criteria. Human studies that reported ENO2 expression and PCa progression as well as patient survival were included. Study used *in vitro* models to test the association between ENO2 and PCa metastatic potentials was also included. Reviews and case reports articles were excluded. Studies that did not specifically address PCa and lacked clear data were excluded. Additionally, studies that were published in non-English language were also excluded. A list of the excluded studies can be found in **Appendix Table 2**.

2.4.1.3 Types of intervention and outcome measurement

Inclusion criteria encompassed both *in vitro* and studies exploring the impact of ENO2 on PCa metastasis using cell models and patient data. Eligible outcomes included analyses of CTCs enrichment, co-cultured results assessed via RT q-PCR, measurement of clinical biomarkers using B·R·A·H·M·S KRYPTOR Analyzers, RNA-seq data obtained through bioinformatic analysis and Kaplan Meier survival curves.

2.4.1.4 Selection of studies

After removing of duplications, an initial screening process was employed which involved screening the titles, abstracts and keywords for a comprehensive list of keywords. Subsequently, the full texts of the articles were screened secondarily based on origin of countries, languages, type of articles, basic data and research findings. Further screening of the full texts was carried out to identify eligible studies with figures containing relevant data. For the purpose of conducting the qualitative systematic review, a total of 6 articles were acquired. For the purpose of conducting the quantitative synthesis meta-analysis, a total of 4 studies addressing the specific criteria detailed were acquired.

2.4.1.5 Data extraction

Information obtained from each individual study included the name of authors, publication year, experimental design, sample size and outcome measures. Mean values, standard deviations (SD) and standard error measurements (SEM) were extracted from relevant graphs using the online tool WebPlotDigitizer software (<https://apps.automeris.io/wpd/>). In cases where studies reported mean \pm SEM, SD was calculated using the following formula: $SEM = SD/\sqrt{N}$.

2.4.1.6 Data analysis

The meta-analysis was conducted when at least 2 studies with similar designs were identified. Forest plots were generated using Review Manager 5.4, providing a visual representation of effect size and their corresponding 95% confidence intervals (CI). Mean differences were either extracted or calculated with 95% CI, if a sufficient number of experiments provided the necessary data[176].

Statistical heterogeneity in each study was assessed using Cochrane's Q statistic, τ^2 , and the I^2 statistic to identify the outcome variations. The degree of heterogeneity was determined by I^2 , with cutoffs at 25%, 50% or 75% indicating low, moderate or high heterogeneity, respectively. Random-effect models were employed for initial calculations when the I^2 ratio exceeded 50% [177]. Conversely, a fixed-effect model was used for initial calculations when the I^2 ratio was below 50%. If studies reported mean \pm SEM, the SD was computed using the formula showed in Section 2.4.1.5. If studies presented results in different units, the standardized mean difference (Std. mean difference) was used as the effect measure.

2.4.1.7 Quality assessment

Risk of bias assessment of all eligible clinical and in vitro studies were assessed using The Newcastle-Ottawa Scale (NOS) and OHAT (Office of Health Assessment and Translation) risk of bias rating tool respectively [178, 179]. The following criteria were used for the NOS risk of bias rating: representativeness of the exposed cohort,

selection of the non-exposed cohort, ascertainment of exposure, demonstration that outcome of interest was not present at start of study, comparability of cohorts on the basis of the design or analysis, assessment of outcome, was follow-up long enough for outcomes to occur and adequacy of follow up of cohorts [178]. The following criteria were used for OHAT risk of bias rating: randomization, allocation concealment, identical experimental conditions, blinding of researchers, complete outcome data, exposure characterization, outcome assessment, outcome reporting, and other potential threats [179]. Studies with NOS scores of at least six was considered high-quality, with higher scores indicating superior literature quality.

2.4.1.8 Certainty of evidence

The certainty of evidence from eligible human and *in vitro* studies was evaluated using the Grading of Recommendations Assessment, Development, and Evaluation (GRADE) approach [180].

2.4.2 Retrospective study

To investigate the potential association between diverse stages of PCa and the expression of ENO2, a retrospective study was carried out using patient samples from the Gene Expression Omnibus (NCBI, <https://www.ncbi.nlm.nih.gov/geo/>). A comprehensive search using the keyword "prostate cancer" performed a total of 71 relevant databases in Homo sapiens. Only 7 of these databases specifically focused on tumour samples, and their accession numbers are detailed in **Appendix Table 3**. Among these 7 datasets, distinct transcriptional levels in patient samples representing benign prostatic tissue, primary PCa, and metastatic PCa were observed in only 2 datasets: GDS1439 (n=19 in total, including n=6 benign, n=7 primary, and n=6 metastasis) and GDS3289 (n=85 in total, including n=33 benign, n=32 primary, and n=20 metastasis). The transcriptional levels of the enriched genes after RNA-Seq were performed only in GDS3289.

2.4.3 Bioinformatic Studies

2.4.3.1 Kaplan-Meier survival analyses

2.4.3.1.1 Gene Expression analysis

To explore the correlation between ENO2 expression levels and the survival rates of disease-free PCa patients, Kaplan-Meier survival curve was initially generated using the GEPIA online database (<http://gepia.cancer-pku.cn/>) (performed on April 2021) [181, 182]. This analysis was based on The Cancer Genome Atlas Prostate Adenocarcinoma (TCGA-PRAD), employing quartile group cutoffs.

2.4.3.1.2 Genetic alternation analysis

To investigate the association between ENO2 genetic alternation and the survival rates of both overall and disease-free PCa patients, Kaplan-Meier survival curve was subsequently generated using the cBioPortal online tool (<https://www.cbioportal.org/>) (performed on April 2021) [183-185]. The approach involved merging selected databases according to gene-altered types: for ENO2 amplification analysis (n=128 in total, including n=4 with gene alteration and n=124 unaltered), databases Prostate Adenocarcinoma (Fred Hutchinson CRC, Nat Med 2016) and Metastatic Prostate Adenocarcinoma (SU2C/PCF Dream Team, PNAS 2019) were combined.

For the combined study of both ENO2 deep deletion and mutation (n=826 in total, including n=9 with gene alteration and n=991 unaltered), databases Prostate Adenocarcinoma (TCGA, Cell 2015), Prostate Adenocarcinoma (TCGA, Firehose Legacy), Metastatic Prostate Cancer (SU2C/PCF Dream Team, Cell 2015), Prostate Adenocarcinoma (MSK Cancer Cell 2010), Prostate Adenocarcinoma (TCGA, PanCancer Atlas) and Prostate Adenocarcinoma (MSK/DFCI, Nature Genetics 2018) were integrated.

Respective figures were generated according to the specific gene-altered types identified in each analysis.

2.5 Statistical Analysis

All calculations in this thesis were performed using GraphPad Prism 10. All data are expressed as the mean \pm SD. Apart from the transcriptional validation performed on 22Rv1 (figure 5.4B), all other wet-lab *in vitro* experiments were conducted in triplicate at both the biological and technical levels. Unpaired T test (parametric) was used to evaluate the significance for two individual groups from a single experiment. To evaluate normality, assess the p-value obtained from the Shapiro-Wilk test and Kolmogorov-Smirnov test. If $p > 0.05$, the data is likely normally distributed, meaning fail to reject the null hypothesis of normality [186]. One-way analysis of variance (one-way ANOVA) was used to assess the significance with more than two columns in a single experiment, backed up by a multiple comparison test with each group. Simple linear regression was used to determine the significance between two quantitative variables in a single experiment. The results are considered to not statistically significant if the p-value below 0.05.

CHAPTER 3: Systematic

Review, Meta-analysis,

Retrospective Study and

Bioinformatics of Association

between ENO2 and Prostate

Cancer Metastasis

3.1 Introduction

Patients with localized PCa would experience RP or ADT for the initial treatment [187]. Once the disease was no longer sensitive to ADT and progresses to CRPC, DOC chemotherapy would be performed as the standard first-line treatment. Currently, two next-generation ARPI, ABI and ENZA have been widely used for the progressed mCRPC [188]. However, persistent androgen depletion can lead to the emergence of new ARPI resistance mechanisms, which may contribute to disease progression in different pathways, including but not limited to NEPC [51, 189]. Thus, there is a crucial requirement to review new targets focusing on key mechanisms involved in the regulation of metastatic potentials of PCa cells. ENO2 was reported to associated with the metastasis of multiple cancer, including colorectal, pancreatic and renal cell [132, 134, 190]. However, the involvements of ENO2 in the metastatic mechanisms of PCa remains uncertain, despite being a widely recognized marker for neuroendocrine tumour detection. Our preliminary study indicated that ENO2 was increased at the mRNA level in PCa dormant metastasis initiating cells compared with fast-growing cells. The NSE protein encoded by *ENO2* has been identified as a tumour marker for neuroendocrine PCa, which is often accompanied by distant metastasis with an extremely poor prognosis [113]. Therefore, it is essential to study whether increased ENO2 expression level is participated in the advanced progression of PCa, especially in conjunction with androgens leading to metastasis.

In this chapter, a systematic review and meta-analysis were initially established to examine the relationship between ENO2 and PCa metastasis across available *in vitro* and clinical studies. With the evidence obtaining from meta-analysis, a retrospective study and Kaplan-Meier curves were subsequently generated to compare the association between ENO2 and the advanced development of PCa using public clinical datasets and online databases.

3.2 Results of Systematic Review and Meta-analysis

3.2.1 Article selection

The search strategy employed in this study is detailed in **Appendix Table 1**. An initial search was conducted on May 12th, 2021, using Web of Science, Medline and PubMed on May 12th, 2021, and updated on Nov 8th, 2023. A total of 350 articles were identified using the search strategy, including a total of 14 articles have been updated in past two years. I have identified 88 papers in “Medline”, 176 papers in “Web of Science” and 86 papers in “PubMed”. A detailed schematic representation of the search strategy and outcomes are shown in Figure 3.1. Among this study, 151 papers were removed due to duplication using EndNote. Additionally, 2 non-English papers were eliminated, 27 non-researched papers were excluded, and 86 papers were removed based on the evaluation of their abstracts, titles, and keywords. After a thorough full-text screening, another 79 records were excluded. The remaining included English-language articles (n=5) were categorized into human clinical and in vitro studies. No in vivo studies were identified during this search. 4 studies, comprising 3 clinical studies and 1 in vitro study, were selected in this meta-analysis. The only 1 article used in the systematic review but not included in the meta-analysis were excluded due to incomplete data (**Figure 3.1**).

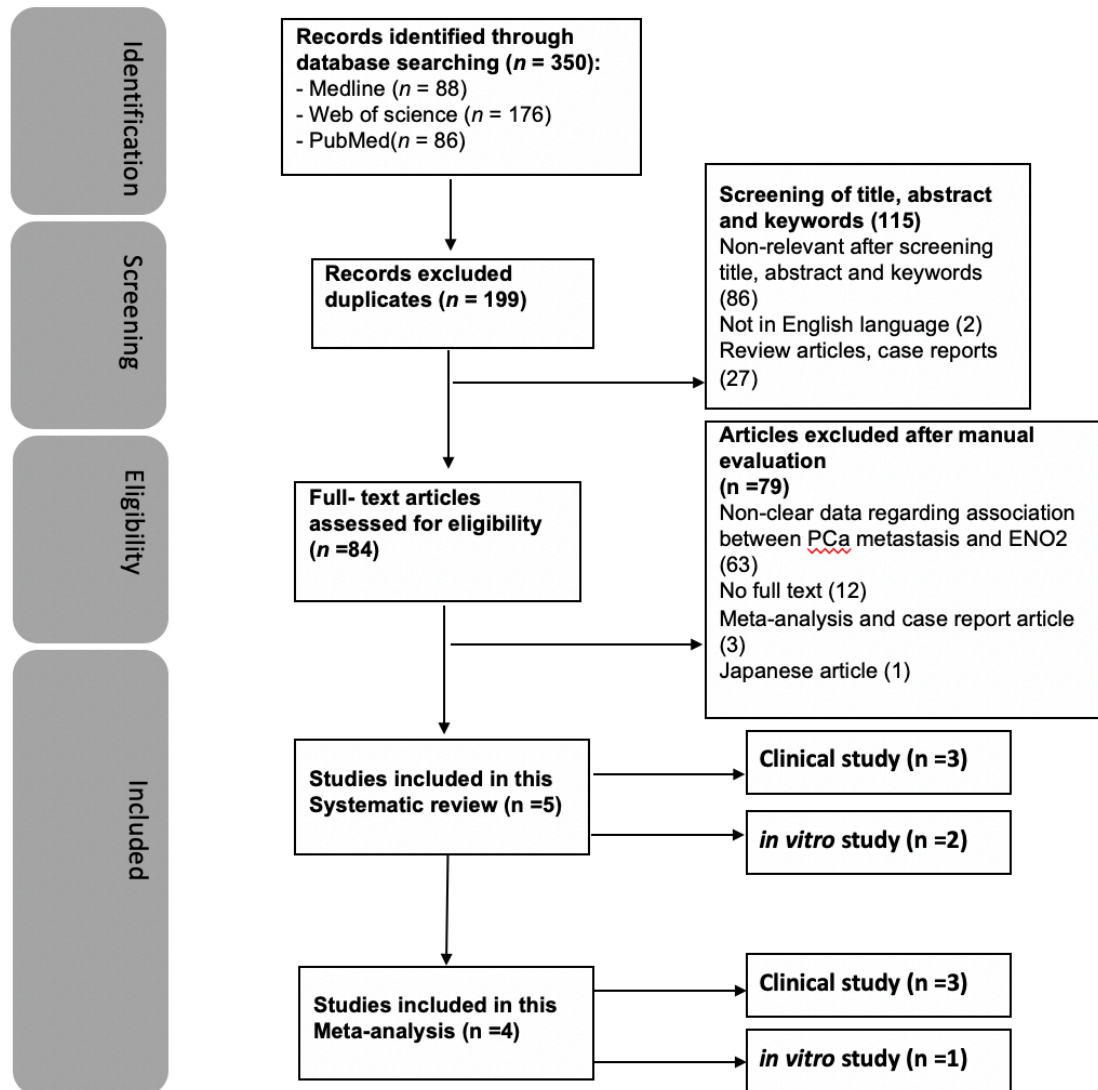


Figure 3.1 The flow chart of screening process in this systematic review and meta-analysis.

3.2.2 Quality assessment

All of the included clinical studies were scored as high quality and passed the Quality assessment, as shown in **Appendix Table 4**. Subsequently, all of the *in vitro* studies were scored as 'probably high risk' at the criteria 'blinding of researchers' in **Appendix Table 5**. But it wasn't a significant issue because it is relatively uncommon for researchers to employ blinding during *in vitro* experiments [191]. Besides, all of the *in vitro* studies were scored 'probably low risk' for 'complete outcome data' criterion. Out of the 2 included *in vitro* studies, 1 was considered 'probably high risk' for the detection criterion (exposure characterization and outcome assessment) and 'definitely high risk' for the statistical methods criterion [192]. Therefore, this article was excluded based on the poor quality and was not selected for the subsequent meta-analysis.

3.2.3 Certainty of evidence

The overall quality of the body of evidence for the clinical and *in vitro* studies was judged as follows:

- 1) Very low for clinical ENO2 expression (mRNA and protein level by RNA-Seq, q RT-PCR and serum biomarker analysis).
- 2) Very low for *in vitro* ENO2 expression (mRNA level by q RT-PCR).

For clinical and *in vitro* studies, the overall quality of outcomes was judged very low due to non-randomized controlled trial (RCT) (starts as low quality) and imprecision (small sample size) (**Appendix Table 6**).

3.2.4 Characteristics of included studies

Table 3.1 and **Table 3.2** summarized the characteristics of 3 clinical and 2 *in vitro* studies, respectively. No *in vivo* studies have been identified after performing search strategy. All studies were published from 2017 to 2021. From 5 individual studies with available data, 3 came from Germany, 1 came from USA and 1 came from Australia.

Table 3.1 Characteristics of the included clinical studies of PCa metastasis and ENO2.

<i>Author</i>	<i>Year</i>	<i>Region</i>	<i>Study Type</i>	<i>No. of patients evaluated</i>	<i>Median age (years)</i>	<i>The comparison details</i>
<i>Kim et al. [51]</i>	2017	USA	Bioinformatics (RNA-seq)	n=86	/	The influence of ENO2 expression in patients with primary, CRPC or NEPC in a clinical setting.
<i>Kessel et al. [193]</i>	2020	Germany	Cohort Study (CTCs enrichment and RT qPCR)	n=19	68.8	The impact of ENO2 expression in blood samples obtained from either healthy individuals or mCRPC patients.
<i>Szarvas et al. [194]</i>	2021	Germany	Cohort study (serum biomarker analysis)	n=1095	66 (RP group) 71 (DOC group) 73 (ABI/ENZA group)	The effects of serum ENO2 protein level in patients who received RP or received DOC or ABI/ENZA treatment in a clinical setting.

Table 3.2 Characteristics of the included *in vitro* studies of PCa metastasis and ENO2.

Author	Year	Region	Assay Type	Cell line	Culture conditions	The comparison details
Bock et al. [195]	2019	Australia	RT-qPCR	PC3	Monoculture medium: RPMI1640 + L-glutamine, 5%FBS+1%P/S	The impact of ENO2 expression <i>in vitro</i> in PCa cell lines, which were either mono- or co-cultured with human osteoblast-derived mineralized microtissue (hOBMT) in a medium with or without dihydrotestosterone (DHT).
				LNCaP		
				C4-2B	Co-culture medium: RPMI1640, 10%FBS (containing 0.6 nmol/L DHT) +1%P/S (PCa-Norm) RPMI1640, 10%CSS+1%P/S (PCa-AD)	
					RPMI1640, 10%FBS (containing 10 nmol/L DHT) +1%P/S (PCa-DHT)	
Bery et al. [192]	2020	Germany	RT-qPCR	PC3	RPMI 1640, 5% FBS +1% P/S	Expression levels of ENO2 in PCa cell lines of different types and origins.
				22Rv1	RPMI 1640, 10% FBS +1% P/S	
				NCI-H660	RPMI1640, 0,005mg/ml insulin + 0.01 mg/ml Transferrin +30nM Sodium selenite +10nM β -estradiol +2 mM 5% FBS +1% P/S	

3.2.4.1 Clinical studies

The included data from three clinical studies that assessed the association between ENO2 expression, either in blood samples or downloaded from online datasets, and PCa malignant progression.

Kim et al., performed a bioinformatic study which was carried out to validate their *in vitro* results by examining the ENO2 expression level through PCa gene expression profiling datasets using cBioportal [51, 196, 197]. ENO2 tended to be strongly expressed in NEPC patients relative to both primary and CRPC patients. ENO2 expression was extremely up-regulated in NEPC (n=7) than primary (n=30) (p=0.003). Concordantly, ENO2 expression was significantly increased in NEPC (n=15) than CRPC (n=34) (p=0.002). Altogether, these data suggest that ENO2 may contribute to the aggressive development of PCa. However, whether ENO2 contributes to the initiation and aggressive development of PCa cannot be concluded, as the original paper lacks a comparison between primary PCa and healthy controls, as well as between CRPC and primary PCa [51].

Kessel et al., conducted a cohort study to examine the ENO2 expression by isolating CTCs from 19 patients which had bone metastases (89%), lymph node metastases (68%) and visceral metastases (21%) with an average age of 68.8 years [193]. 10 of the blood samples from healthy donors were also collected to compare ENO2 expression levels with those of CRPC patients. ENO2 was dramatically upregulated in mCRPC patients compared with healthy individuals (P<0.00005). The fact that all patients underwent distant metastases implies a connection between the malignant progression of PCa and ENO2 high expression. However, the study has certain deficiencies due to the lack of comparison of ENO2 expression between patients with CRPC and primary PCa, as well as among healthy individuals and patients with primary PCa.

Szaevas et al., performed a cohort study to identify the serum ENO2 protein level from 395 PCa patients [194]. A total of 157 of hormone-sensitive patients with RP, 95 of mCRPC patients with DOC chemotherapy and 143 of mCRPC patients who underwent ABI/ENZA chemotherapy were comprised the three cohort in this study. Notably, the expression level of ENO2 in the mCRPC DOC group was significantly higher than that in the RP cohort ($p=0.001$). Concordantly, the expression level of ENO2 in the ABI/ENZA group was also significantly evaluated compared to RP group ($p=0.046$). More importantly, ENO2 expression was significantly higher in patients with mCRPC than in hormone-naïve patients before treatment started. Taken together, this study indicated that the expression of ENO2 is upregulated in CRPC, especially the aggressive metastatic CRPC. This provided critical evidence by comparing ENO2 expression between primary PCa and CRPC, and filled the gap left by both Kim's and Kessel's research [194]. A univariate analysis in this paper also showed that the prognostic value of ENO2 is significant in ABI/ENZA-treated mCRPC patients, whereas it is not significant in DOC-treated mCRPC or PR-treated primary PCa patients, indicating the association between ENO2 level and PCa aggressiveness under the androgen-deprived condition.

3.2.4.2 *in vitro* studies

The two selected *in vitro* studies both examined ENO2 expression as a neuroendocrine transdifferentiation (NEtD) marker at transcriptional level by performing qRT-PCR assay using PCa cell lines.

One of the studies [195] conducted a human osteoblast-derived microtissues models (hOBMT) which was co-cultured with distinct types of PCa cells to simulate the bone metastatic microenvironment. In addition, PCa cells were cultured in two different medium, either adequate or deficient in androgens in this model. 10% FBS in normal RPMI medium was replaced with 10% charcoal-stripped serum (CSS) to simulate an androgen-deprived environment (PCa-AD). Subsequently, 10 nmol/L DHT was applied to the PCa-AD medium as the PCa-DHT medium to simulate a living environment with

sufficient androgens. Notably, ENO2 expression was relatively higher in the androgen-deficient environment compared to the adequate environment in all groups. This is consistent with the aforementioned clinical studies showing that the expression of ENO2 is significantly upregulated in the androgen-deficient environment (CRPC) compared to the androgen-adequate environment (hormone-naive primary PCa or healthy individual). Intriguingly, regardless of whether in the PCa-AD or in the PCa-DHT medium, the relative expression of ENO2 in the osteotropic C4-2B cells co-cultured with hOBMT was upregulated compared to C4-2B cells cultured alone, while this was not observed in the non-bone tropic LNCaP cells, suggesting a possible association between ENO2 expression and the bone tropism of PCa cells. This is particularly important, as PCa predominantly metastasizes to bone.

Another study [192] examined the expression levels of ENO2 in each of three different PCa cell lines: NCI-H660, 22RV1, and PC3. The human PCa epithelial 22Rv1 cell line used in this study, was derived from an androgen-dependent CWR22 xenograft and was collected from a patient with skeletal metastasis [142, 198]. The human PCa epithelial androgen-independent PC3 cell line which was also derived from bone metastasis, was also used in this study [140]. Additionally, as the only epithelial neuroendocrine cancer cell line in this study, NCI-H660 was identified as an extrapulmonary small cell carcinoma isolated from prostate gland [199]. Notably, it was discovered that the expression level of ENO2 in 22RV1, the only androgen-dependent cell line with bone metastasis potential, was higher than traditional neuroendocrine androgen-independent NCI-660 cells [200]. Interestingly, the expression level of ENO2 in 22Rv1 cells, which are also PCa cells of non-neuroendocrine origin, is approximately 3 times higher than that in androgen-independent PC3 cells. Additionally, ENO2 expression in PC3 was the lowest among the three cell lines, approximately half that of NCI-H660 cells. However, owing to the absence of statistical analysis in the original article, whether ENO2 expression is associated with bone metastasis potential or AR status of the PCa cells is up for further investigation [192]. Despite the limited statistical power, this study shows all three PCa cell lines, no matter the metastatic or

neuroendocrine status, exhibit detectable ENO2 expression. Additionally, ENO2 expression is not consistently higher in NEPC.

3.2.5 Meta-analysis of outcomes

3.2.5.1 Meta-analysis on clinical studies indicates the connection between ENO2 and PCa progression

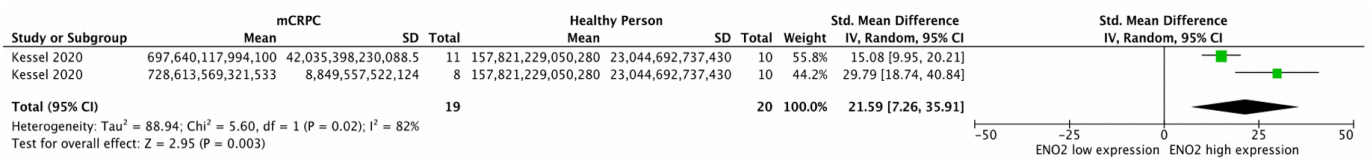
This meta-analysis identified recent clinical studies examining ENO2 expression levels in the progression of PCa, especially in cases involving distant metastases. Three human studies were included in this meta-analysis involving a total of 677 patients, with CTCs enrichment measurement through RT-qPCR, bioinformatics and biomarkers measurement, respectively.

Kessel et al. [193] conducted a study revealing a correlation between ENO2 and metastatic mCRPC. High ENO2 expression was significantly associated with mCRPC patients, both with and without the AR splice variant 7 (AR-V7) (Std. Mean Difference = 21.59, 95% CI 7.26, 35.91, **Figure 3.2 A**).

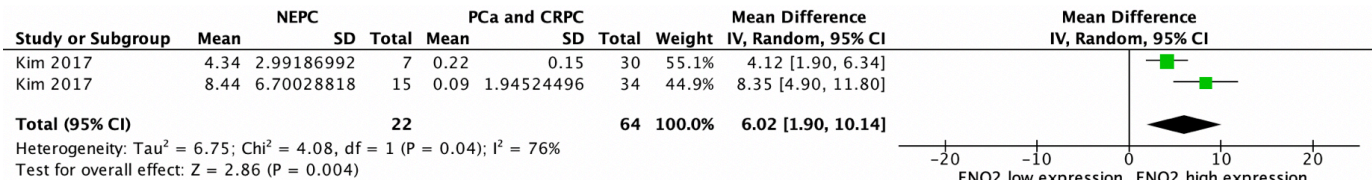
Kim et al. [51] conducted a study covering different subtypes of PCa, suggesting an association between ENO2 and late-stage PCa. The forest plot indicated that ENO2 tends to be expressed in the more aggressive types of PCa (Mean Difference = 6.02, 95% CI 1.90, 10.14, **Figure 3.2 B**).

Szarvas et al. [194] conducted a study of serum ENO2 levels in PCa patients receiving various clinical treatments. The forest plot demonstrated no statistically significant difference ($p=0.20$) in ENO2 expression among different treatments, including radical prostatectomy, DOC, and ABI/ENZA (Mean Difference = 3.42, 95% CI 1.86, 8.71, **Figure 3.2 C**).

A



B



C

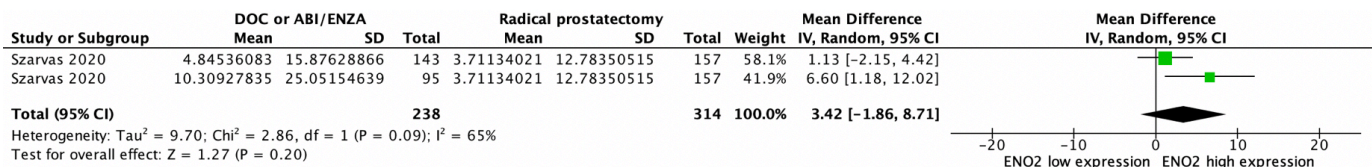


Figure 3.2 Forest plots included clinical studies showing association between ENO2 and PCa progression.

The number of samples, weight, analysis model and heterogeneity (presented as I^2) of each study are detailed in the individual plot. The forest plots were generated using Review Manager 5.4, presenting associations with 95% confidence intervals (CIs) and calculated as mean differences or Std. mean differences +/- standard deviation **(A)** The forest plot illustrates the correlation between ENO2 expression and CRPC patients with metastasis. A single study, comprising 39 samples, resulted in an I^2 of 82% and $p=0.003$ **(B)** The forest plot illustrates the association between ENO2 expression and NEPC patients. A single study, with a total of 86 samples, resulted in an I^2 of 76%, and $p=0.004$ **(C)** The forest plot demonstrates the lack of association between ENO2-encoded protein expression and various PCa treatments. A single study, encompassing 552 samples, showed an I^2 of 65% and $p=0.2$.

3.2.5.2 Meta-analysis on *in vitro* studies indicates the relationship between ENO2, androgen deprivation environment and bone metastasis potential

Meta-analysis derived from an *in vitro* study reveals a correlation between ENO2 expression and the potential for bone metastasis in PCa. The study involved two cell lines, LNCaP and C4-2B, cultured in different environments, either alone or co-cultured with hOBMT. The cultured medium, designed to mimic varying androgen conditions, employed standard RPMI with or without DHT supplementation [195]. Data extracted from this *in vitro* study originated from RT-qPCR experiments with three biological repeats.

High ENO2 expression at the mRNA level is significantly associated with the cultured environment featuring androgen deprivation (Mean Difference = 1.95, 95% CI 0.21, 3.69) (**Figure 3.3 A**). Furthermore, the data generated from C4-2B cell line, which has higher potential of bone metastasis compared to LNCaP, was analysed in another forest plot (**Figure 3.3 B**). This analysis indicates that ENO2 high expression in C4-2B cells correlates with bone metastasis, regardless of whether the cells were exposed to an androgen-deficient environment (Mean Difference = 9.14, 95% CI 6.90, 11.39). The heterogeneity in this forest plot is 0%, even when applying the fixed effect model.

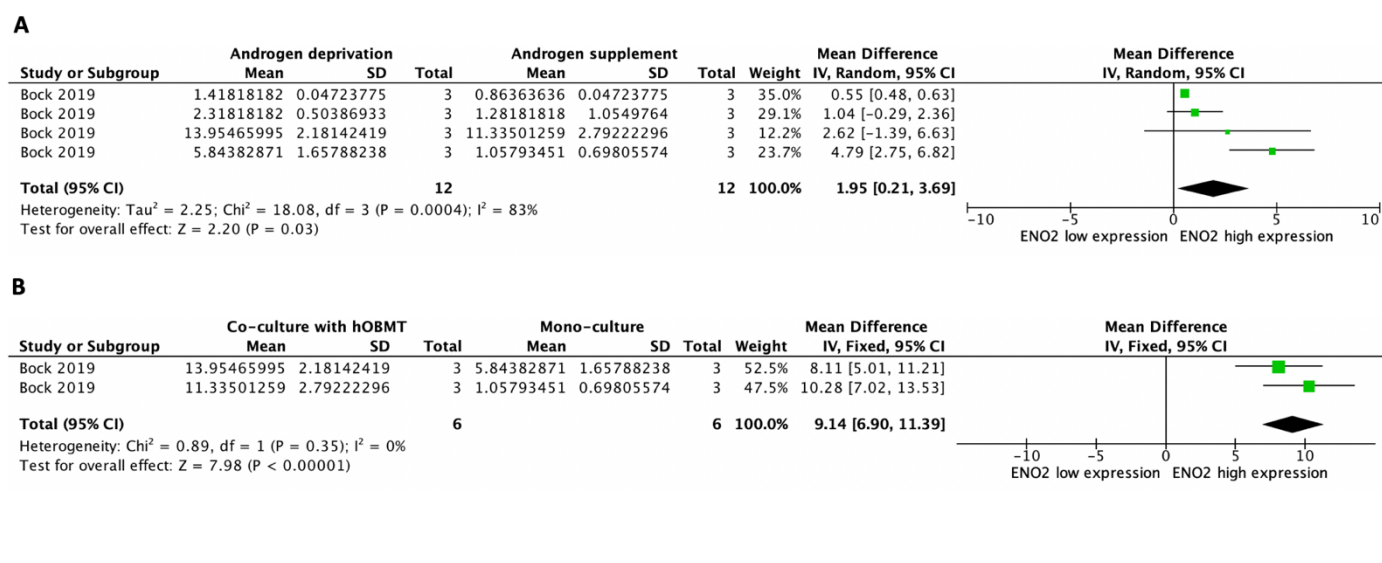


Figure 3.3 Forest plots included in vitro study showing the connection among ENO2 and androgen deprivation environment as well as metastatic potentials using LNCaP and C4-2B cell lines.

The number of samples, weight, analysis model and heterogeneity (presented as I^2) of each study are detailed in the individual plot. The forest plots were generated using Review Manager 5.4, presenting associations with 95% confidence intervals (CIs) and calculated as mean differences or Std. mean differences \pm standard deviation. **(A)** The forest plot illustrates the association of ENO2 expression with androgen deprivation. A single study, encompassing 24 samples, resulted in an I^2 of 83%, and $p=0.03$. **(B)** Forest plot shows the association of ENO2 expression and bone metastasis potential. A single study, with a total number of 12 samples, $I^2=0\%$, $p<0.00001$.

3.3 Results of retrospective study for assessment of relationship between ENO2 expression and metastatic PCa patients

3.3.1 *Increased ENO2 expression was correlated with advanced metastatic PCa*

Bioinformatic analysis was employed to investigate ENO2 expression across three patient cohorts representing benign, primary and metastatic stages of PCa. Two datasets (GDS1439 and GDS3289) were applied in this retrospective study [201, 202]. It was observed that ENO2 exhibited a significant up-regulation in metastatic PCa compared to primary PCa at the transcriptomic level (GDS1439, primary PCa 271.9 ± 117.0 vs. metastatic PCa 2723.0 ± 2636 ; $P = 0.0227$) (GDS3289, localized PCa -0.1276 ± 0.2499 vs. metastatic PCa 0.4067 ± 0.5307 ; $P < 0.0001$) (**Figure 3.4 A and 3.4 B**). Notably, the expression level of ENO2 in metastatic PCa was also found to be higher than that in benign prostate tissue (GDS3289, benign prostate tissue 0.1239 ± 0.3509 vs. metastatic PCa 0.4067 ± 0.5307 ; $P = 0.0229$). Besides, the expression level of ENO2 in benign prostate tissue was also higher than that in localized PCa (GDS3289, benign prostate tissue 0.1239 ± 0.3509 vs. localized PCa -0.1276 ± 0.2499 ; $P = 0.0204$) (**Figure 3.4 B**).

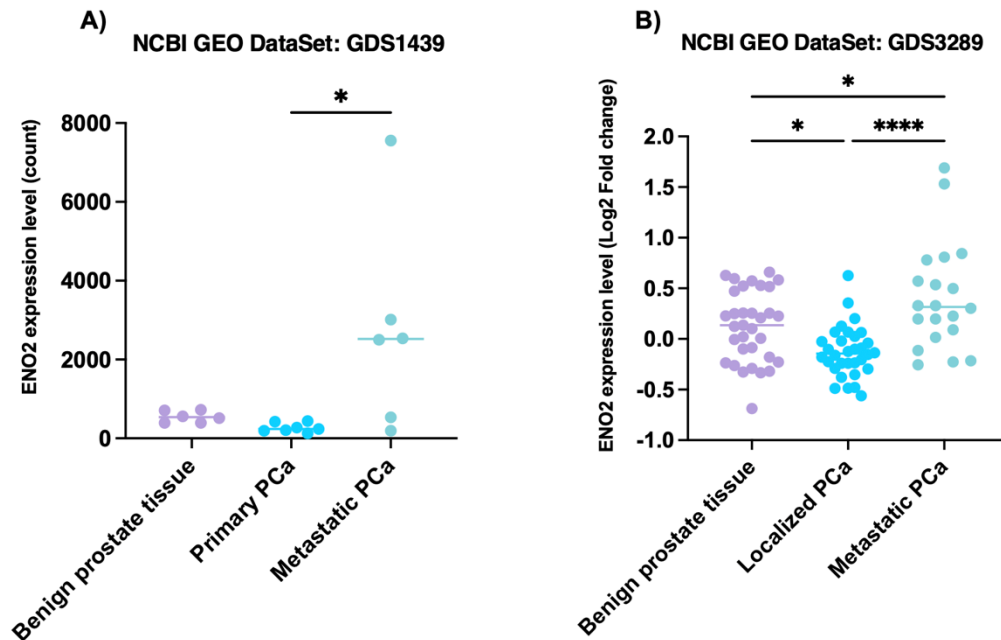


Figure 3.4 ENO2 gene expression is upregulated in metastatic PCa compared to primary PCa and benign patient samples.

An analysis using Gene Expression Omnibus databases with accession number GDS1439 and GDS3289. **(A)** Quantitative comparison of ENO2 gene expression among benign prostate tissue (n=6), primary PCa (n=7), and metastatic PCa (n=6) patient samples. Expression values are presented as count. **(B)** Quantitative comparison of ENO2 gene expression among benign prostate tissue (n=33), primary pPCa (n=32), and metastatic PCa (n=20) patient samples. Expression values are presented as log2 fold change. Each dot represents individual patient sample. p-values were determined using ordinary One-way ANOVA with multiple comparisons. *p<0.05, ****p<0.0001.

3.4 Results of Bioinformatics for assessment of Kaplan-Meier survival curves of ENO2 in PCa patients

Kaplan-Meier curves were generated using the online databases GEPIA and cBioPortal to compare ENO2 expression levels and gene alteration status, respectively.

3.4.1 *ENO2 alternation was associated with poor survival rate in Pca patients*

The connection among alteration of ENO2 gene and survival rate was evaluated in PCa patients by producing Kaplan-Meier survival curve using cBioPortal. Although the log rank test p value is bigger than 0.05 (log rank test p value=0.4090), median overall survival for PCa patients with ENO2 amplification was only 12 months compared with 28 months for patients without gene amplification (altered group, n= 4; unaltered group, n=124) (**Figure 3.5 A**). Furthermore, ENO2 gene deletions and mutations were found to be related with reduced survival in PCa patients, with a median disease-free survival of only 32 months (log rank test p value=0.002259; altered group, n=9; unaltered group, n=991) (**Figure 3.5 B**). Due to the limited cohort size, the relationship between ENO2 expression and survival rate of PCa patients was further examined using GEPIA.

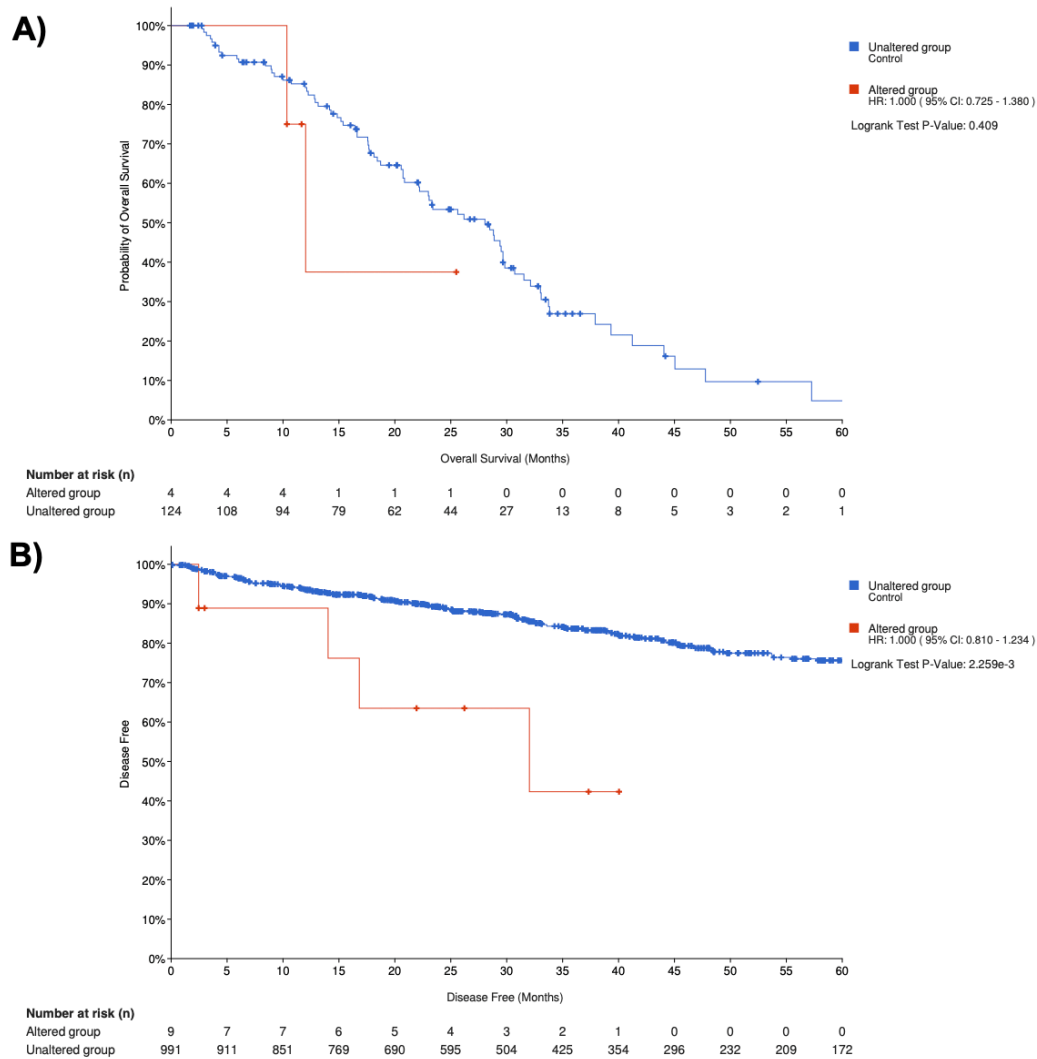


Figure 3.5 Kaplan-Meier curves indicates an association between ENO2 alteration and survival.

Curves were generated and downloaded from cBioPortal. **(A)** Kaplan-Meier overall survival curve in PCa patients with altered ENO2 amplification (Fred Hutchinson CRC, Nat Med 2016, SU2C/PCF Dream Team, PNAS 2019) (n=4) and without gene alteration (n=124) **(B)** Kaplan-Meier disease-free survival curve in PCa patients with ENO2 deep deletion and mutation (TCGA, Cell 2015, TCGA, Firehose Legacy, SU2C/PCF Dream Team, Cell 2015, MSK Cancer Cell 2010, TCGA, PanCancer Atlas, MSK/DFCI, Nature Genetics 2018) (n=9) and without gene alteration (n=991). P value was calculated using the online tool for the log-rank test.

3.4.2 Increased ENO2 expression was correlated with decreased survival rate in PCa patients

The association among overexpression of ENO2 and survival rate was evaluated in PCa patients by producing Kaplan-Meier survival curve using GEPIA. Although lacking statistical significance ($p=0.15$), evident from the data that compared to the around 60% survival rate at 100-months for individuals with low ENO2 expression. The survival rate of individuals with high ENO2 expression is low, with the survival rate at 100-months is only approximately 40% (high ENO2 expression, $n=123$; low ENO2 expression, $n=122$) (**Figure 3.6**).

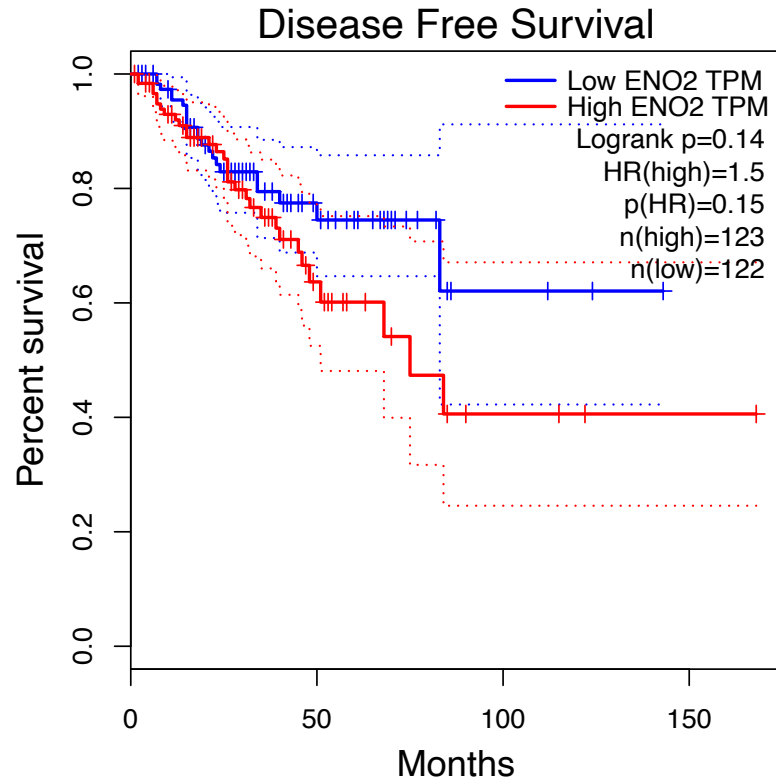


Figure 3.6 Kaplan-Meier curve indicates an association between ENO2 overexpression and decreased survival.

Curve was generated and downloaded from GEPIA. Kaplan-Meier disease-free survival curve in PCa patients with high (n=123) and low (n=122) ENO2 expression level from TCGA PCa samples. Cut-off was performed quartile. P-values were calculated from the online tool of log-rank test.

3.5 Discussion

Metastasis is the leading cause of death in men diagnosed with advanced PCa. Although there are multiple treatments including surgery and chemotherapy to inhibit the progression of PCa, subsequent acquired resistance to these treatments still cannot prevent malignant progression, especially the development of metastasis [188]. This systematic review, meta-analysis and bioinformatics validation were conducted to evaluate the effects of ENO2 on PCa malignant progression, and to assess the connection among ENO2 expression and ADT status. Five studies included in the qualitative systematic review focused specifically on PCa-related methods and outcomes, including different cell culture systems and patient study. The 3 clinical and 1 *in vitro* selected paper from qualitative synthesis with independent experimental designs were analyzed individually by quantitative meta-analysis. Retrospective study and bioinformatics were subsequently established to verify the association between ENO2 expression/alteration and metastatic PCa development/survival.

The initial step in the meta-analysis involved using a clinical study by Kessel et al., which recognized ENO2 as a prevalent neuroendocrine differentiation (NED) marker significantly up-regulated in mCRPC patients. The mCRPC patient cohort, comprising both AR-V7neg and AR-V7pos individuals, was integrated together for comparison with a control group of healthy individuals. This combination was justified by the original article's findings which indicating that ENO2 exhibited up-regulation at the mRNA level independently of AR-V7 expression. AR-V7 is a splice variant of AR mRNA typically expressing its protein after ADT [193, 203]. It suggested that alterations in the AR gene may not influence ENO2 expression. However, whether such alterations impact the ENO2-mediated metabolic response and tumour metastatic progression remains unexplored. Furthermore, the selected patient cohort exclusively comprised individuals with CRPC and metastases in bones (89%), lymph nodes (68%), and viscera (21%). It suggested a potential role for ENO2 in promoting PCa metastasis, providing additional supporting evidence for ongoing research into the role of ENO2 in PCa metastasis.

Subsequently, according to Kim's investigation, the meta-analysis had established a correlation between elevated ENO2 expression and the progression from localized PCa to NEPC. It was expected given that ENO2 encoded protein has become a widely used biomarker for detecting NEPC [113]. Notably, ENO2 exhibited up-regulation in the CRPC cohort in contrast to patients with primary PCa [51]. Additionally, although the meta-analysis subjectively grouped primary PCa and CRPC for comparison with NEPC, the original paper still indicated a gradually rising trend in ENO2 expression with the advanced progression of PCa.

Based on the results I conducted meta-analysis of Szarvas's study, there is no significant difference in the translational expression of ENO2 among various ADT methods in mCRPC patients. Prostatectomy is a traditional approach to treating patients with low-risk PCa [187]. However, in case of CRPC patients maintain reliant on AR signaling, the standard ADT strategies are commonly applied and combined with next-generation antiandrogens (e.g., ABI/ENZA) or DOC chemotherapy [188, 204, 205]. Resistance develop in some instances following ADT, resulting in the emergence of NEPC with a more aggressive behavior [189, 194]. Intriguingly, my meta-analysis findings suggest that the expression of ENO2 remained unaffected by the physical removal of the prostate or by chemotherapy inhibiting androgen signaling. It implied that the expression of ENO2 is independent of androgen. Moreover, data from the original article indicated that the expression level of ENO2 remains relatively stable, whether employing chemotherapy with DOC to induce mitotic arrest or performing next-generation antiandrogens to target the AR [194, 206, 207]. Consequently, the evidence derived from the meta-analysis suggested that various ADT treatments targeting free circulating androgens do not impact the high expression of ENO2 in patients.

Bery's study included in the quantitative systematic review revealed elevated expression levels of ENO2 in androgen-sensitive cell lines compared with androgen-independent cell lines, although both exhibited higher bone metastasis potential. In

contrast, the meta-analysis conducted from Bock's study strongly suggested that an androgen-deprived environment induces an up-regulation of ENO2 at the mRNA level. The inconsistency in findings with results from clinical studies may be attributed to variations in the assessment of different ENO2 gene products (mRNA or protein) by the diverse testing methods. Furthermore, when charcoal-stripped FBS was employed instead of regular FCS to reduce androgen levels in the serum, it also eliminated levels of other nutrients and hormones. Therefore, the increase in ENO2 levels may be a consequence of this removal, rather than attributable to the absence of androgens [208]. Moreover, the *in vitro* expression of ENO2 might not be subject to the comprehensive influence of multiple metabolic processes throughout the entire body, potentially contributing to the opposing results compared to the study by Szarvas. Additionally, it could be influenced by the diverse ages and racial backgrounds within a single patient cohort. Further results from the original article revealed a significant up-regulation of ENO2 expression in C4-2B cells, which have been known for its higher potential for bone metastasis compared to the parental LNCaP cells [209]. It was obtained through co-culturing osteoblasts with LNCaP and C4-2B cells in a designed osteoblastic model, investigating potential cellular changes under conditions of *in vitro* androgen deprivation. Combining the results of the meta-analysis, it supported that PCa cell lines with a greater potential for bone metastasis are more likely to adapt to insufficient androgen, displaying characteristics of NED. To specifically explore the impact of ENO2 in bone metastasis, the data from C4-2B were categorized into two groups, mono- and co-culture, without considering the hormone status. Although high ENO2 expression was found to be associated with the potential for bone metastasis, an I^2 value of zero indicated no heterogeneity and therefore causing the result inconclusive. Overall, the correlation between ENO2 and the potential for bone metastasis in PCa, as identified in the meta-analysis, provided supporting evidence for our hypothesis. To further elucidate the specific effects of androgen status on ENO2 expression, dry-lab experiments including single-cell RNA sequencing (ssRNAseq) would be suggested to identify the specific cell types within the tumour microenvironment contribute to ENO2 expression. In addition, tissue microarrays

(TMA) could be employed to validate these findings across a broader cohort of benign, localized, and metastatic PCa samples.

The outcomes obtained from a retrospective study had initially provided support for the role of ENO2 in PCa metastasis. The observed downregulation of ENO2 in localized PCa patient cohorts and its upregulation in metastatic PCa patients suggested a potential correlation among ENO2 expression and the metastatic potential of PCa, rather than its involvement in tumorigenesis. Besides, the results indicate a U-shaped correlation between disease stage and ENO2 expression, i.e. higher ENO2 expression in the benign stage and metastatic PCa stage while lower ENO2 expression in primary PCa. This is probably due to the unique glucose metabolic feature of prostate epithelial and PCa cells, in term of their dependency on ENO2 regulated glycolysis. In general, the proliferation of tumour cells mainly depends on aerobic glycolysis which called Warburg effect. Despite being an inefficient method for ATP production, tumour cells exhibit enhanced glucose uptake and lactate production to sustain metabolism. Conversely, normal non-tumorigenic cells primarily dependent on mitochondrial oxidative phosphorylation to metabolize glucose and generate pyruvate for energy production [89, 210]. However, this is not the case in PCa. It is known that citrate, synthesized from aspartic acid and glucose, would be secreted as a crucial component of prostatic fluid [89]. However, large amounts of zinc accumulated in prostatic acinar epithelial cells would specifically inhibit citrate oxidation generating the disruption of tricarboxylic acid (TCA) cycle. Therefore, citrate-producing prostate epithelial cells may employ alternative metabolic pathways to guarantee standard energy demands [89] and evidence suggested that citrate-producing prostate cells rely on high levels of aerobic glycolysis [211]. During the early stages of primary PCa, there was a decrease in zinc and citrate levels, which triggered the activation of TCA cycle and a subsequent reduction in glycolysis. Following the disease advances, glycolysis became predominant again to maintain metabolism, resulting in the upregulation of ENO2 [212, 213]. However, it is important to acknowledge the inherent limitations of bulk RNA

analysis. For example, stromal cells such as fibroblasts may also express ENO2 and contribute to the total RNA pool.

Furthermore, results from GEPIA indicated that upregulation of ENO2 expression is associated with reduced survival rates in PCa patients. However, results from the cBioPortal datasets revealed that ENO2 gene alterations, whether deeply deleted or mutated, significantly decreased disease-free survival in PCa patients. Although it was inconsistent with the outcomes from GEPIA, the results are considered inconclusive because of their limited statistical power, with only 9 of the deletion and mutation, 4 of the amplification individuals available for analysis. Studies have found that ENO2 gene deletion and mutation are associated with decreased survival in PCa patients (**Figure 3.5 B**). In addition to exploring ENO2 deletions or mutations, future studies should investigate the role of ENO2 amplification or copy number gain, as increased dosage of the ENO2 gene could contribute to its heightened activity in advanced metastatic PCa. Besides, the Kaplan-Meier analysis should ideally provide a breakdown of PCa stages, with a particular focus on Stage II/III patients who are at higher risk of developing metastatic disease, which would be helpful for the understanding of role of ENO2 in disease progression. Due to the limitations of the functionality of these two websites, subdivision of disease stages is not currently possible.

There are still several other limitations exist in this study. Firstly, meta-analysis is susceptible to potential confounding factors present in the original studies, introducing bias [214, 215]. The lack of homogeneity in selected patient populations and the variability in expression detection methods may impact the reliability of the meta-analysis results. Additionally, the low number of relevant articles included in the meta-analysis and the small sample size in each individual article also limit with exposing the outcomes to low confidence and are not representative. For instance, both Kim and Kessel's studies separately included only 7 NEPC patients and 8 CRPC patients. Furthermore, the three clinical studies included differed in experimental design and limited of individual information led to separate analyses, resulting in weaker evidence

compared to a synthesis of the studies. Besides, although all included studies were based on the expression of ENO2 in patients with malignant types of PCa or in cell lines with varying metastasis potential, the focus was not directly related to bone metastasis. In addition, since the number of studies included in this summary is limited, a funnel plot, which are frequently conducted in meta-analysis as a visual tool for identifying potential publication bias, was not generated [216]. For subsequent bioinformatics verification, in addition to the small sample size of individual groups, technical limitations were integral considerations throughout the experimental process. For instance, the subjective selection of databases may lead to the missing of available data. Additionally, certain less-relevant individual data within the selected database, such as gene-deletion data in the gene amplification dataset used in this survival study through cBioPortal, cannot be manually excluded.

3.5 Conclusion

In summary, ENO2 expression is associated with PCa progression but not to androgen status. However, there are no functional studies that have identified the molecular mechanism of ENO2 in promoting PCa metastasis. Therefore, further validation and investigation of targeting ENO2 in advanced PCa development, especially in regulating bone metastasis, is innovative and clinical needed.

Chapter 4: ENO2 expression and related glucose metabolism in prostate cancer cell lines

4.1 Introduction

The *ENO2* encoded protein NSE, has become a prominent biomarker for diagnosing NEPC [113]. Numerous studies have illustrated the association of *ENO2* with the PI3K/Akt and MAPK/ERK signaling pathways, which play crucial roles in migration and apoptosis [217, 218]. In addition, as a downstream regulated gene in aerobic glycolysis, *ENO2* played the crucial role in mediating 2-phosphoglyceric acid eventually converting from glucose into pyruvate, ultimately contributing to the production of lactate [196]. In contrast to normal cells, tumour cells exhibit increased glucose uptake and elevated lactate production through aerobic glycolysis [95, 112]. Currently, increased glycolysis has been emerged as a feature of advanced PCa [89]. Moreover, disruptions in glycolysis were identified to exert detrimental effects on the skeleton [219]. Despite these findings, the functional contribution of *ENO2* in tumour progression, especially for skeletal metastasis, still remains for exploration. With the evidence of Meta-analysis retrospective studies and bioinformatics, *ENO2* was shown to be related to malignant development of PCa. Therefore, it is critical to obtain further supporting evidence from studies using PCa cell lines *in vitro*.

In this chapter, RT-qPCR analysis was performed to evaluate *ENO2* expression at the transcriptional level using a panel of PCa cell lines with different AR expression levels and metastatic potentials, as well as a prostatic myofibroblast cell line. Subsequently, Western Blotting and ELISA assays were performed to verify the findings from RT-qPCR at the translational level. To investigate whether the glucose metabolism and glycolysis process, particularly glucose and pyruvate, would impact *ENO2* expression, protein levels of *ENO2* were examined using Western Blotting in PCa PC3, 22Rv1, LNCaP-LN3 and prostatic myofibroblast WPMY-1 cells. Furthermore, alamarBlue™ cell viability assay and Caspase 3/7 apoptosis assay were applied in the same panel of cell lines to study the ability of cells maintaining viabilities and resisting apoptosis in an environment with or without glucose supplement.

4.2 Results

4.2.1 ENO2 expression was associated with metastatic potential at transcriptional level

4.2.1.1 Confirmation of ENO2 expression associates with metastatic potential at translational level by RT q-PCR

To evaluate the expression of ENO2 in prostatic myofibroblast cells and various types of PCa cell lines with distinct metastatic potentials, the RT q-PCR analysis was conducted to assess ENO2 expression at the transcriptional level in a cell panel.

Initially, ENO2 expression levels were determined as ΔC_t values normalized to the respective endogenous control (**Figure 4.1 A**). Lower ΔC_t values correspond to higher gene expression, where values below zero indicate target gene expression higher than the housekeeping gene (*HPRT1*). By contrast, values above zero suggest lower expression than the reference. Notably, ENO2 mRNA expression in 22RV1 (-1.68 ± 0.28 ; $P < 0.0001$), LNCaP-LN3 (-1.20 ± 0.26 ; $P < 0.0001$), and WPMY-1 (-1.03 ± 0.27 ; $P < 0.0001$) cells was higher than that of the housekeeping gene *HPRT1*, whereas in DU145 (0.76 ± 0.10 ; $P < 0.0001$), PC3 (1.43 ± 0.17 ; $P < 0.0001$), C4-2B4 (4.774 ± 0.06 ; $P = 0.0006$), LNCaP (5.34 ± 0.59 ; $P = 0.086$), and C4-2 cells, ENO2 expression is lower than *HPRT1*. Subsequently, relative quantification was assessed using the $2^{-\Delta\Delta C_t}$ method with normalization to the lowest expressing cell line (C4-2) (**Figure 4.1 B**). The highest ENO2 expression was observed in 22RV1 (197.4 ± 34.89 ; $P < 0.0001$), approximately 170-fold higher than C4-2. Additionally, LNCaP-LN3 (142.0 ± 22.63 ; $P = 0.0026$) and WPMY-1 (169.2 ± 94.18 ; $P = 0.0005$) exhibited high ENO2 expression, approximately 140- and 130-fold higher than C4-2, respectively. Although not statistically significant, DU145 (36.04 ± 42.21 ; $P = 0.7991$) and PC3 (22.71 ± 1.56 ; $P = 0.9728$) cell lines also exhibit a correlation with ENO2 up-regulation, approximately 40- and 30-fold higher than C4-2, respectively. Notably, there was no significant difference between C4-2B4 (2.24 ± 0.16 ; $P > 0.9999$), LNCaP (0.38 ± 0.52 ; $P > 0.9999$), and C4-2 cells, as their fold changes are nearly zero (**Figure 4.1 B**).

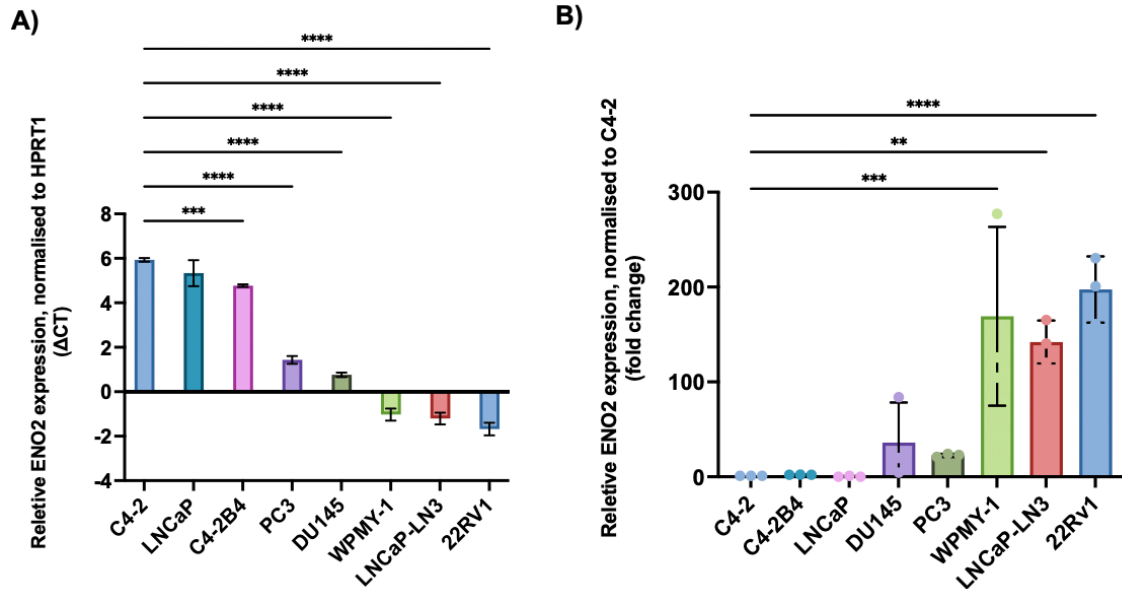


Figure 4.1 22Rv1, LNCaP-LN3, WPMY-1, DU145 and PC3 cell lines exhibit elevated levels of ENO2 expression at mRNA level.

(A) The expression of ENO2 in each cell line was normalized to HPRT1 and presented as ΔC_t values. **(B)** The relative expression of ENO2 in each cell line was normalized to C4-2, which displayed the lowest expression, with a $2^{-\Delta\Delta C_t}$ fold change. The data are mean \pm standard deviation (n=3 biological repeats with 3 technical repeats). One-way ANOVA with Dunnett multiple comparisons. **p<0.01, ***p<0.001, ****p<0.0001 compared to C4-2.

4.2.2 ENO2 expression was associated with metastatic potential at translational level

4.2.2.1 Confirmation of ENO2 expression was associated with metastatic potential at translational level using ELISA

The presence of mRNA expression of ENO2 across various cell lines have been identified after performing RT-qPCR. Subsequently, the protein NSE, encoded by the ENO2 gene, was assessed using ELISA in cell lysates sourced from both prostatic myofibroblast tissue and PCa cell lines within the same cohort (**Figure 4.2**). Interestingly, the 22RV1 (0.71 ± 0.10 ; $P < 0.0001$) cell line exhibited the highest NSE expression which was consistent with RT-qPCR results. Although some of them did not show significant differences, WPMY-1 (0.69 ± 0.05 ; $P < 0.0001$), DU145 (0.41 ± 0.11 ; $P = 0.0037$), LNCaP (0.44 ± 0.05 ; $P = 0.0016$), and C4-2B4 (0.32 ± 0.11 ; $P = 0.0371$) also demonstrated significantly elevated NSE levels compare to C4-2 (0.09 ± 0.08). Conversely, LNCaP-LN3 (0.19 ± 0.11 ; $P = 0.6262$) and PC3 (0.11 ± 0.10 ; $P = 0.9998$) did not exhibit a clear correlation with NSE up-regulation.

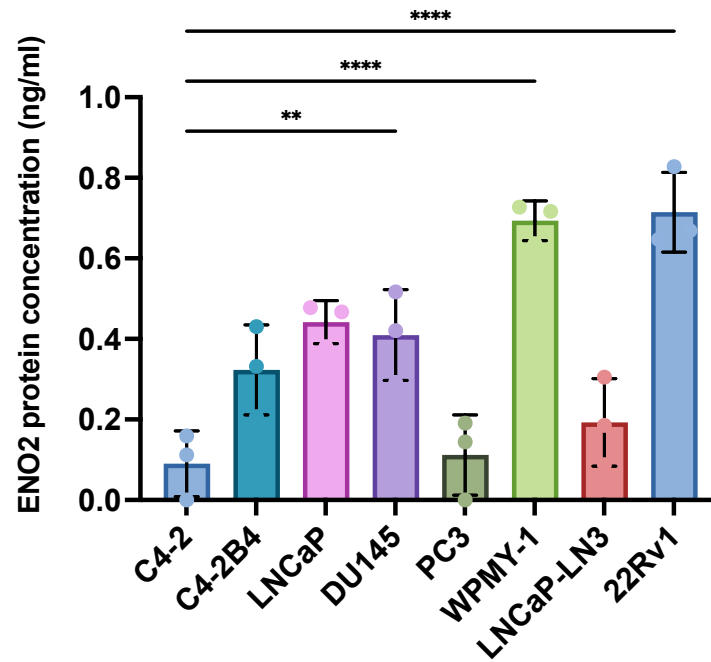


Figure 4.2 22Rv1, WPMY-1, DU145, LNCaP and C4-2B4 cell lines exhibit elevated levels of ENO2 expression examined using ELISA.

NSE expression levels for each cell line were generated based on standards of known concentration. The expression of NSE in each cell line was normalized to C4-2. The data are mean \pm standard deviation (n=3 biological repeats with 3 technical repeats). P-values were determined using ordinary One-way ANOVA with multiple comparisons. **p<0.05, ****p<0.0001 compared to C4-2.

4.2.2.2 Confirmation of ENO2 expression was associated with metastatic potential at translational level using Western Blotting

The expression of ENO2 at protein level was doubly evaluated through Western Blotting using cell lysates obtained from both human and mouse PCa cell lines, along with prostatic myofibroblast tissue cell line, within the same study cohort (**Figure 4.3**). Notably, the 22RV1 cell line (2.93 ± 0.19 ; $P < 0.0001$) consistently maintained the highest relevant ENO2 expression, aligning with previous RT-qPCR and ELISA results (**Figure 4.3 A**). Moreover, LNCaP-LN3 (1.86 ± 1.01 ; $P = 0.0019$) also exhibited elevated ENO2 expression which was consistent with the RT-qPCR results. Although PC3 (0.96 ± 0.15 ; $P = 0.1612$), DU145 (0.81 ± 0.32 ; $P = 0.3073$), and LNCaP (0.59 ± 0.30 ; $P = 0.6581$) cells did not display significant differences, they all maintained a stable ENO2 expression (**Figure 4.3 A**). Additionally, the protein expression of ENO2 in three mouse PCa cells was also examined. Except for TRAMP-C1 (0.11 ± 0.01 ; $P = 0.0069$), which exhibited a modest amount of ENO2 expression, the other two cells (TRAMP-C2, 0.03 ± 0.04 ; $P = 0.8698$ and RM1, 0.02 ± 0.02) showed almost no expression (**Figure 4.3 B**).

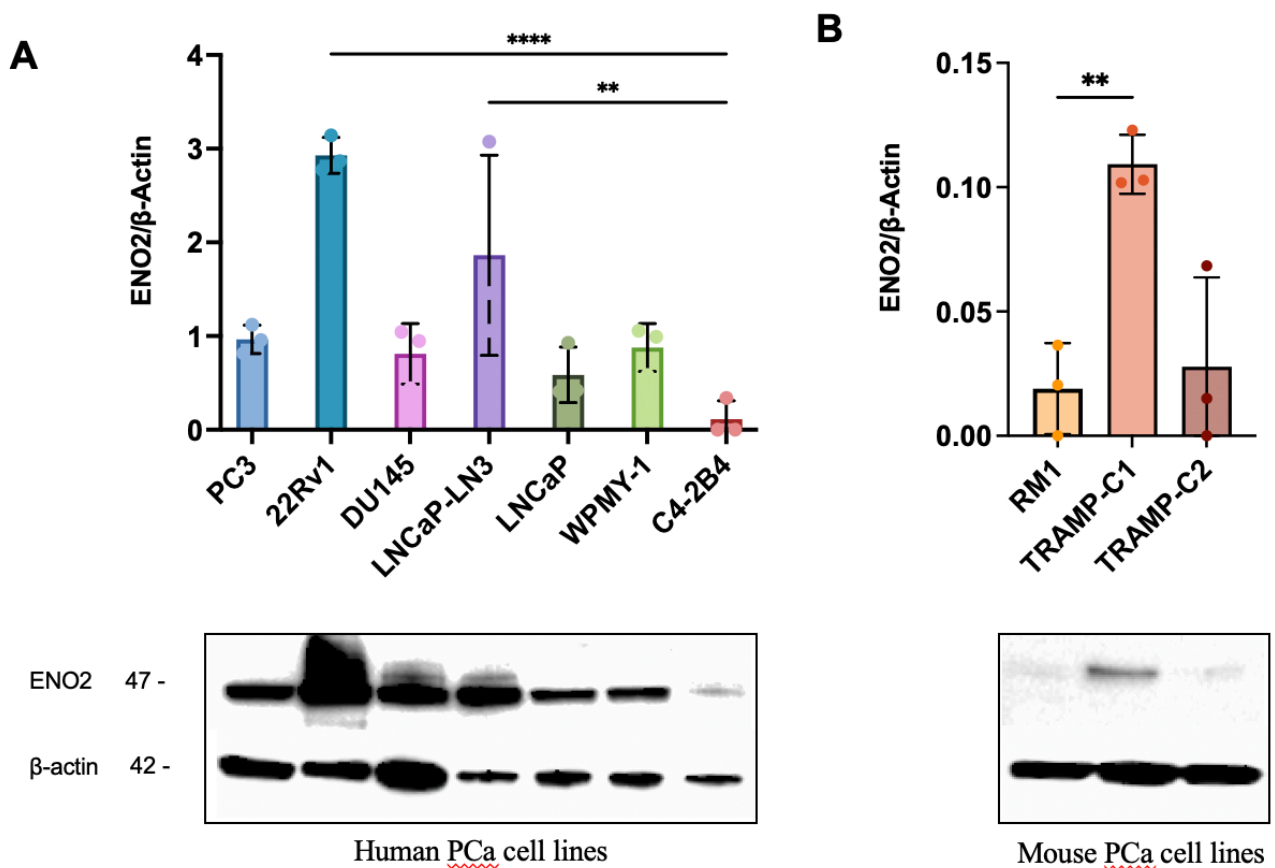


Figure 4.3 22Rv1 and LNCaP-LN3 are associated with ENO2 higher expression protein level.

(A) Relative expression of ENO2 in human prostatic tissue and PCa cell lines was normalized to C4-2B4 with the lowest expression. **(B)** Relative expression of ENO2 of mouse PCa cell lines was normalized to RM1 with the lowest expression. The data are mean \pm standard deviation (n=3 biological repeats with 3 technical repeats). One- way ANOVA with Dunnett multiple comparisons. **p<0.01, ****p<0.0001 compared to C4-2B4 and ****p<0.0001 compared to RM1.

4.2.3 ENO2 expression was associated with environmental glucose and pyruvate at translational level

In order to study whether changes in the concentration of glucose and pyruvate in the microenvironment would affect the expression of ENO2, the protein level of ENO2 were evaluated using Western Blotting through culturing PCa and prostatic myofibroblast cells in standard, glucose-free and pyruvate-free medium.

4.2.3.1 Glucose level in cell culture medium affected the Enolase 2 expression in prostatic myofibroblast cells more than in PCa cells

The expression of ENO2 at protein level at normal and glucose-free environment were evaluated through Western Blotting using cell lysates obtained from human PCa and prostatic myofibroblast cell lines, within the same study cohort (**Figure 4.4**). Although environmental glucose deprivation caused an increased ENO2 expression in PC3 (standard medium, 0.47 ± 0.28 vs glucose-free medium, 0.80 ± 0.16 ; $P= 0.1544$) (**Figure 4.4 A**), 22Rv1 (standard medium, 0.77 ± 0.11 vs glucose-free medium, 0.93 ± 0.19 ; $P= 0.2496$) (**Figure 4.4 B**) and LNCaP-LN3 (standard medium, 0.78 ± 0.28 vs glucose-free medium, 1.00 ± 0.30 ; $P= 0.4068$) (**Figure 4.4 C**), no significant differences had been observed. Interestingly, environmental glucose deprivation causes a significant increase by 157.1% in ENO2 in prostatic myofibroblast cells (standard medium, 0.35 ± 0.06 vs glucose-free medium, 0.91 ± 0.19 ; $P= 0.0089$) (**Figure 4.4 D**).

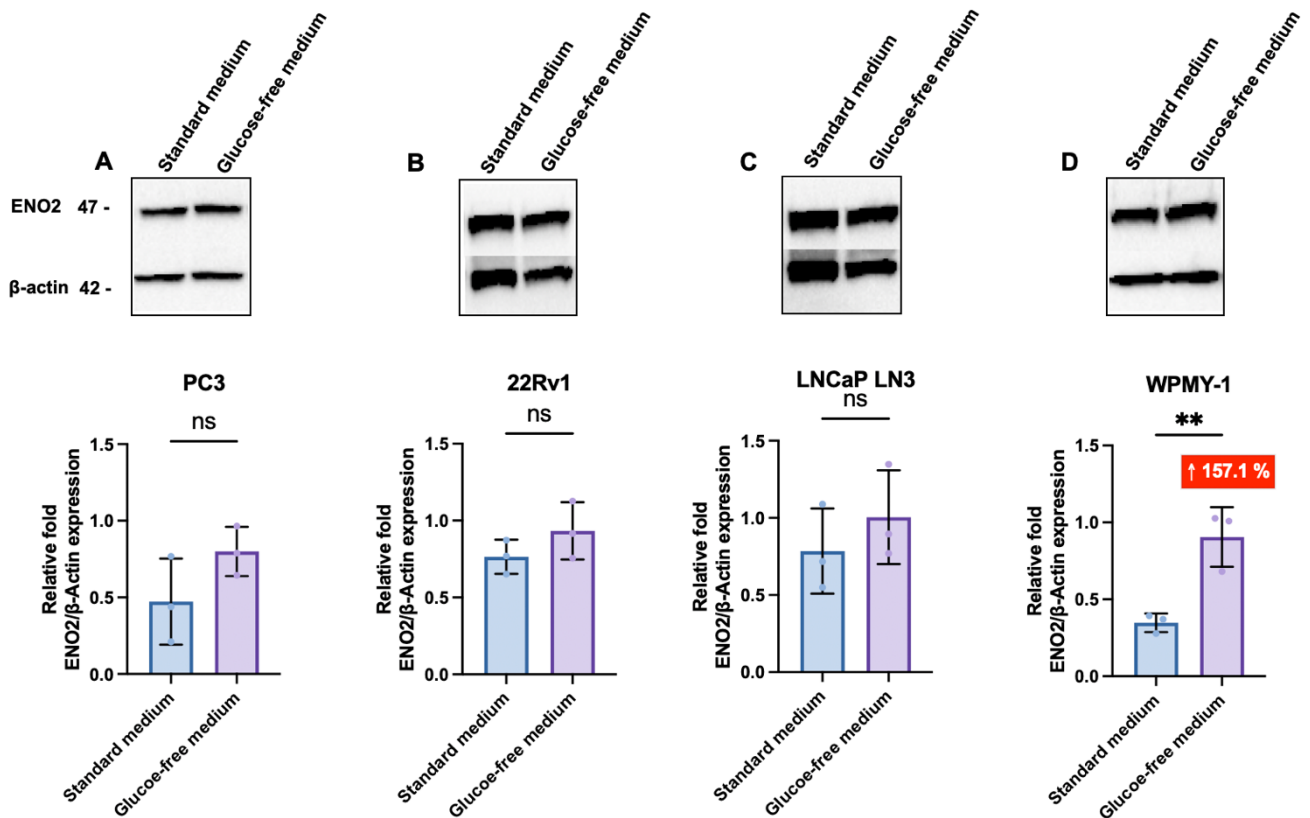


Figure 4.4 Glucose affect the expression of ENO2 of PC3, 22Rv1, LNCaP-LN3 and WPMY-1 cell lines.

(A, B, C and D) Cell lines treated with standard and glucose-free medium within 24 hours, assessed by Western Blotting. Results showed through representative Western blotting images and assessed by relative fold of ENO2/ β -actin expression of each cell lines. The data are mean \pm standard deviation (n=3 biological repeats with 3 technical repeats). Unpaired t-test. **p<0.01, compared to standard medium group, respectively.

4.2.3.2 Enolase 2 expression in PCa cells was affected by the presence of pyruvate in cell culture medium

The expression of ENO2 at protein level at normal and pyruvate-free environment were evaluated through Western Blotting using cell lysates obtained from human PCa and prostatic myofibroblast cell lines, within the same study cohort (**Figure 4.5**). Notably, the protein level of ENO2 in pyruvate-free medium was significantly upregulated by 286.8% in 22Rv1 cells (standard medium, 0.77 ± 0.11 vs pyruvate-free medium, 2.94 ± 1.19 ; $P = 0.0337$) (**Figure 4.5 B**). In addition, the absence of the pyruvate in the environment does not affect the expression of ENO2 in PC3 cells (standard medium, 0.10 ± 0.01 vs pyruvate-free medium, 0.12 ± 0.02 ; $P = 0.1629$) (**Figure 4.5 A**), LNCaP-LN3 (standard medium, 0.78 ± 0.28 vs pyruvate-free medium, 0.79 ± 0.02 ; $P = 0.9856$) (**Figure 4.5 C**) and prostatic myofibroblast WPMY-1 cells (standard medium, 0.21 ± 0.13 vs pyruvate-free medium, 0.20 ± 0.10 ; $P = 0.9350$) (**Figure 4.5 D**).

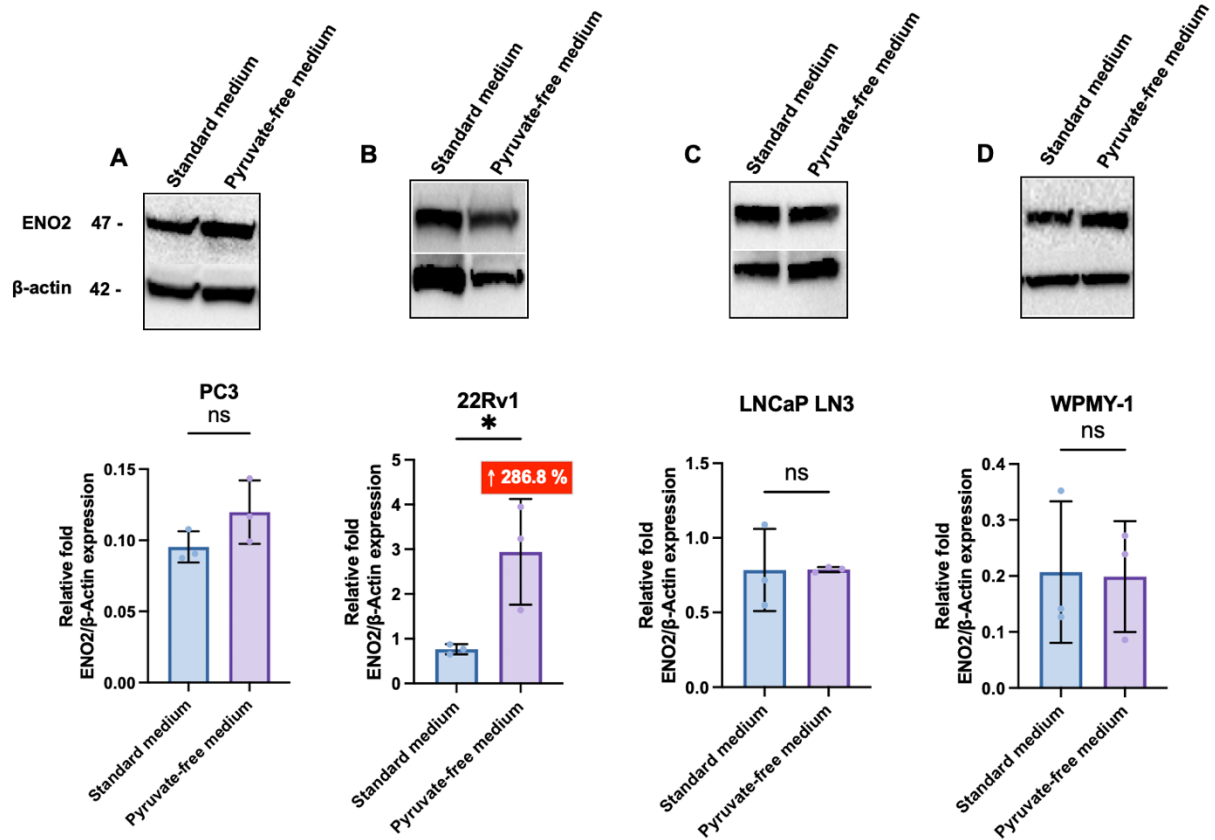


Figure 4.5 Pyruvate affect the expression of ENO2 of PC3, 22Rv1, LNCaP-LN3 and WPMY-1 cell lines.

(A, B, C and D) Cell lines treated with standard and pyruvate-free medium within 24 hours, assessed by Western Blotting. Results showed through representative Western blotting images and assessed by relative fold of ENO2/β-actin expression of each cell lines. The data are mean ± standard deviation (n=3 biological repeats with 3 technical repeats). P- values were obtained from unpaired t-test. *p<0.05, compared to standard medium group, respectively.

4.2.4 Effects of environmental glucose in human prostatic myofibroblast and PCa cell behaviour in vitro

As indicated by Western Blotting results, the protein expression of the ENO2 in both PCa and prostatic myofibroblast cell lines was influenced by the concentration of glucose in their surrounding microenvironment. To confirm these findings, alamarBlue™ cell viability assay and Caspase 3/7 apoptosis assay were employed on PC3, 22RV1, LNCaP-LN3, and WPMY-1 cell lines to assess their ability of cells maintaining activity in an environment lacking adequate glucose supplementation.

4.2.4.1 Environmental glucose affected cell viability in human prostatic myofibroblast and PCa cells

PC3 cells stopped growth from the 48th time-point under the glucose-free conditions. The viability of cells at all four time-points in the standard medium was notably higher than that in the glucose-free medium. Interestingly, the viability of the glucose-free medium-treated group was reduced up to 84.4% at the 96-hour time point in PC3 cells (standard medium, 13604 ± 299.6 vs glucose-free medium, 2126 ± 121.4 ; $P < 0.0001$) (**Figure 4.6 A**). A similar trend was observed in 22Rv1 cells, where although cells continued to survive, the viability at all four time-points in the glucose-free environment was significantly lower than that in the normal environment. The viability of the glucose-free medium-treated group was reduced by 41.2% at the 96-hour time point (standard medium, 3667 ± 64.22 vs glucose-free medium, 2156 ± 39.3 ; $P < 0.0001$) (**Figure 4.6 B**). In addition, as for LNCaP-LN3 cells, cells in the glucose-free medium grew slowly and the significant difference appeared only at 96th hours and decreased by 64.5% (standard medium, 3832 ± 49.68 vs glucose-free medium, 1362 ± 15 ; $P < 0.0001$) (**Figure 4.6 C**). Furthermore, glucose affected the growth of prostatic myofibroblast WPMY-1 cells, which stopped growth from the 48th time-point under the glucose-free conditions. And the viability of the glucose-free medium-treated group was reduced up to 94.3% at the 96-hour time point (standard medium, 9798 ± 348.4 vs glucose-free medium, 53.3 ± 290 ; $P < 0.0001$) (**Figure 4.6 D**).

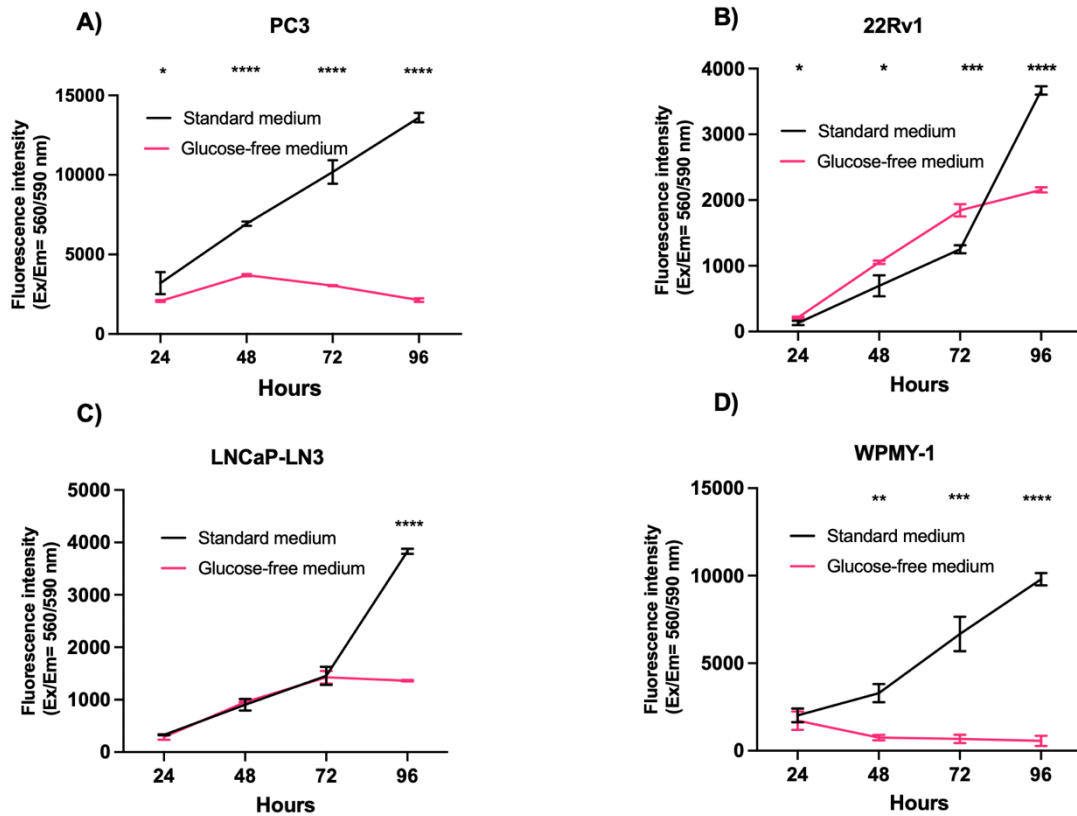


Figure 4.6 Glucose affect the viability of PC3, 22Rv1, LNCaP-LN3 and WPMY-1 cells.

Cell lines treated with standard and glucose-free medium within 96 hours, assessed by alamarBlue™ assay in vitro. The data are mean \pm standard deviation (n=3 biological repeats with 3 technical repeats). Unpaired t-test. *p<0.05, **p<0.01, ***p<0.001, ****p<0.0001 compared to standard medium group at each time point, respectively.

4.2.4.2 Environmental glucose caused cell apoptosis in human PCa cells but not in prostatic myofibroblast cells

Following a 24-hour treatment, a notable elevation in apoptosis was observed in all PCa cultures subjected to low-glucose medium compared to those in the standard medium. The environmental glucose deprivation caused an increased trend in apoptosis in PC3 (standard medium, 36.54 ± 5.70 vs glucose-free medium, 49.64 ± 3.23 ; $P=0.0257$), 22Rv1 (standard medium, 35.28 ± 4.52 vs glucose-free medium, 48.03 ± 4.39 ; $P=0.0246$) and LNCaP-LN3 cell lines (standard medium, 4.48 ± 2.82 vs glucose-free medium, 20.24 ± 0.63 ; $P=0.0007$) by 35.9%, 36.1% and 351.8%, respectively (**Figure 4.7 A, B and C**). Interestingly, there was a markedly decrease by 52.3% in apoptosis evident in WPMY-1 cells following a 24-hour treatment with low-glucose medium (standard medium, 3.80 ± 0.35 vs glucose-free medium, 1.81 ± 0.73 ; $P=0.0132$) (**Figure 4.7 D**).

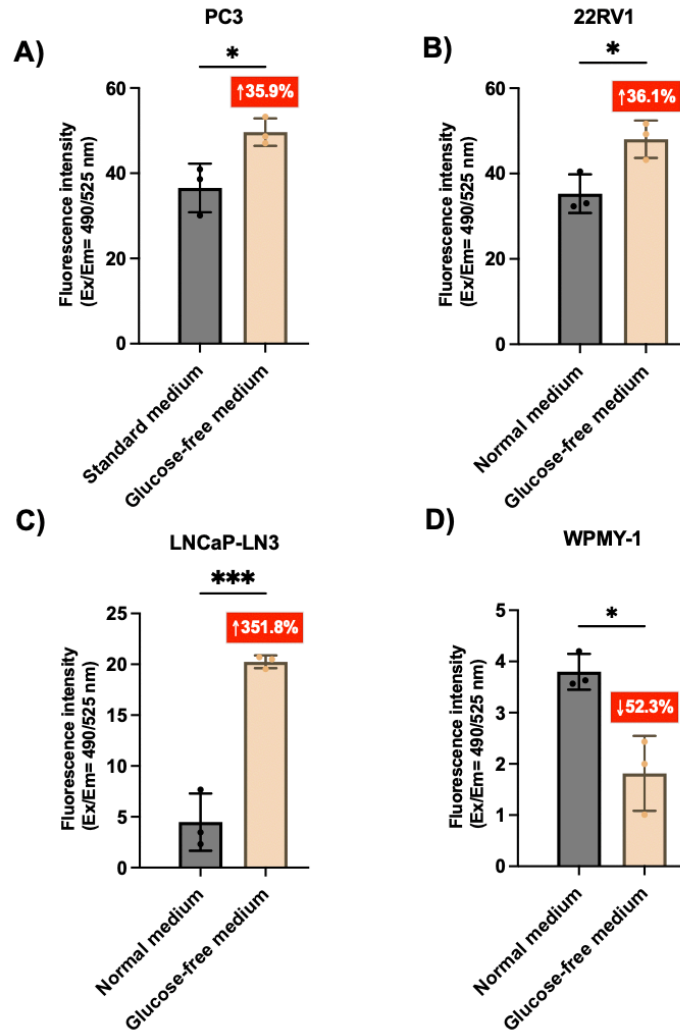


Figure 4.7 Glucose affects apoptosis of PC3, 22Rv1, LNCaP-LN3 and WPMY-1 cells.

Cell lines were treated with standard and glucose-free medium in 24 hours *in vitro*, assessed by Caspase 3/7 Assay. The data are mean \pm standard deviation (n=3 biological repeats with 3 technical repeats). Unpaired t-test. *p<0.05, ***p<0.001 compared to standard medium group, respectively.

4.3 Discussion

Existing evidence have indicated that ENO2 plays an important role in tumour cell migration and apoptosis, mediated by the well-known PI3K/Akt and MAPK/ERK signaling pathways [217, 218]. Additionally, as a key downstream enzyme in aerobic glycolysis, ENO2 involved in glucose conversion. It is known that one of the critical hallmarks of malignancy, including advanced PCa, is the substantial elevation in glucose consumption, representing the modified cellular metabolism known as the Warburg Effect [89, 122]. Therefore, there is no doubt that ENO2 is involved in regulating elevated glycolytic metabolism in tumour cells. Given that the disturbance of glycolysis has been recognized to exert detrimental effects on bone, the exploration of ENO2 as a novel therapeutic strategy requires not only the investigation of ENO2 expression *in vitro* various types of PCa cell lines, but also the examination of ENO2 expression under different metabolic conditions involving glucose and pyruvate modifications [219]. Besides, ENO2 represents a therapeutic approach that requires further investigations on PCa in the modified survival environment that mimic the presence or absence of glucose.

In this chapter, I initially performed q RT-PCR to test the raw expression of ENO2 at mRNA level in a panel of PCa and prostatic myofibroblast cell lines. Subsequently, ELISA and Western Blotting were further used to verify the expression of ENO2 in the same cohort of cell lines at the protein level. Notably, PCa cell lines 22Rv1, LNCaP-LN3 and DU145, exhibiting relatively high metastatic potentials, demonstrated elevated ENO2 expression at the mRNA and protein level. 22Rv1, an androgen-dependent xenograft originating from the bone metastasis PCa cell line CWR22, induced osteolytic lesions and osteoblastic responses [142, 220, 221]. LNCaP-LN3, an aggressive derivative of LNCaP with elevated metastatic potential presented pronounced ENO2 mRNA expression [144, 198]. Interestingly, only the LNCaP-LN3 cell line exhibited the highest metastatic potential among the four cell lines derived from LNCaP (LNCaP, LNCaP-LN3, C4-2 and C4-2B4) from q RT-PCR and Western Blotting assay, displayed the significant increased transcriptional and translational

expression of ENO2, which underline the notion that ENO2 expression connected with PCa metastatic potentials. Interestingly, the other two PCa cell lines (PC3 and DU145) widely employed for *in vivo* investigations of bone metastasis, only exhibited a moderately higher expression of ENO2, compared to other non-bone metastatic cell lines [141, 222, 223]. Additionally, the prostatic myofibroblast cell line WPMY-1 also exhibited a higher expression of ENO2. It is important because the role of ENO2 may extend beyond the cancerous epithelium to influence the stromal compartment, particularly through its expression in myofibroblasts. Fibroblasts have been found to be the second most abundant cell population in the tumour microenvironment [88]. It is known that the interaction between PCa cells and fibroblasts present in the microenvironment further complicates the metabolic situation within the prostate gland [88]. In PCa, cancer-associated fibroblasts are manipulated by cancer cells to support tumour growth and metabolic adaptation. PCa cells degrade cancer-associated fibroblasts to trigger the Warburg effect, where increased glycolysis leads to lactate production. This lactate is used by cancer cells to fuel anabolic and catabolic processes essential for tumour growth. Cancer-associated fibroblasts induce OXPHOS in cancer cells, enhancing their metabolic flexibility and promoting tumour progression. This metabolic crosstalk between PCa cells and CAFs is crucial for sustaining the energy demands of the growing tumour [88]. Therefore, future bone metastasis studies should specifically explore whether ENO2 expression in fibroblasts and myofibroblasts affects metastatic PCa progression. It could be accomplished through co-culture models of bone metastasis-related PCa cells with ENO2-deficient stromal cells to determine how stromal ENO2 influences cancer cell behavior. Additionally, *in vivo* experiments could assess whether stromal ENO2 is required for the formation of bone metastases. These studies could clarify the functional role of stromal ENO2 in the metastatic niche and reveal whether targeting stromal ENO2, in combination with cancer cell-directed therapies, could offer a novel approach to treating metastatic PCa.

Following the examination of the ENO2 expression in prostatic myofibroblast and PCa cells under normal conditions, the Western Blotting was carried out to assess whether the expression of ENO2 in a panel of metastatic PCa cell lines was affected by glucose and pyruvate existence. The expression of ENO2 in prostatic myofibroblast cells have been more impacted by glucose, as environmental glucose deprivation led to a significant increase, whilst non-significant increases were observed in PCa cell lines (**Figure 4.4**). In addition, deprivation of the downstream product pyruvate led to higher expression of ENO2 in 22Rv1 cells (**Figure 4.5 B**). The impact of glucose on cell behavior was evaluated through viability and apoptosis assays. The findings suggested that the viability of PCa and prostatic myofibroblast cells was reliant on glucose (**Figure 4.6 A, B, C and D**). Interestingly, myofibroblast WPMY-1 cells cultured in a glucose-free environment displayed a distinctly opposite apoptosis trend compared to PCa cells where glucose deficiency induced enhanced apoptosis in all PCa cell lines but protected WPMY-1 from apoptosis (**Figure 4.7**). Again, this is possibly the consequence of the unique metabolic phenotype of PCa and their dependency on glucose uptake [213]. The distinct opposite apoptosis trend between WPMY-1 cells and PCa cells could be due to that, under conditions of glucose or pyruvate deprivation, metabolic pathways would tend to be altered, such as the uptake of exogenous lactate or other metabolic methods, to maintain intracellular ATP production. The expression level of ENO2 may be adjusted to improve substrate utilization capacity to adapt to changes in metabolic pathways [89, 224]. Upregulation of ENO2 expression, which represented a response to stress caused by limited nutrients, increases catalytic steps in the glycolytic pathway and maintains energy production. Therefore, all these data suggested a correlation between ENO2 expression and cellular survival as well as resistance to stress. This is consistent with observations from other cancer types. For example, ENO2 has been shown to promote tumour cell proliferation and glycolysis in acute lymphoblastic leukemia, lung, head and neck cancer [135, 136, 225].

There are still several limitations exist in this study. Firstly, there was a U-shaped correlation between the disease stage and ENO2 expression according to the results from retrospective study in **Chapter 3 (Figure 3.4)**, i.e. higher ENO2 expression in the benign stage and metastatic PCa stage while lower ENO2 expression in primary PCa. However, the lack of benign prostatic cell lines during the initial selection of cell lines in this Chapter resulted in a lack of *in vitro* validation of ENO2 expression in normal benign prostatic cells. Besides, the genetic and phenotypic variation can be generated by serial passages over an extended period of time of cell lines [226]. Additionally, the protein levels of NSE in the conditioned medium should be investigated after monitoring changes in cell behavior following glucose deprivation, since it had the potential to be released into the extracellular environment in the event of cell damage or death [227]. Finally, since ENO2 functions as a downstream signaling enzyme, converting 2PG to phosphoenolpyruvate, rather than directly facilitating glucose uptake and catalysis, further experiments need to be designed to elucidate whether this alteration in cellular behavior is influenced by immediate upstream proteins, such as 2PG [228].

4.4 Conclusion

In summary, the results in this chapter suggested the high expression of ENO2 is associated with the metastatic potentials in PCa cell lines. Besides, glucose and pyruvate induced distinct ENO2 expression and cellular changes in tumour and non-tumourigenic cells, especially myofibroblast cells. The data generated in this study strongly suggests that ENO2 is important within the stromal microenvironment, not just in cancer cells. Therefore, it is important to attempt to interpret their data using *in vitro*, *in vivo* or bulk RNA-Seq. It highlights the need for a more comprehensive approach to studying ENO2 in both the tumour and stromal compartments, particularly in the context of bone metastasis. Importantly, this provides a prospective insight into targeting ENO2 at different stages of PCa, particularly metastatic PCa, as a potential therapeutic application.

Chapter 5: Effects of ENO2 Knockdown and Knockout on Prostate Cancer Cell Behavior *in* *vitro*

5.1 Introduction

Although ENO2 has been established as a well-known tumour marker for the detection of neuroendocrine carcinomas. Previous studies have demonstrated that ENO2 promoted proliferation and glycolysis in various cancer types. For instance, silencing ENO2 expression using shRNA resulted in the inhibition of cell proliferation, glycolysis, and glucocorticoid resistance in acute lymphoblastic leukemia cells [136]. In addition, the downregulation of ENO2 was found to block the growth and glucose metabolism of head and neck cancer cells partially through the downregulation of PKM2 [135]. Despite these findings, the functional contribution of ENO2 in PCa malignant progression, especially for skeletal metastasis, still remains for exploration.

In contrast, ENO1, a paralog of ENO2, has demonstrated multifactorial therapeutic potential against PCa [229]. Similar to ENO2, ENO1 serves as a crucial cellular enzyme catalyzing the conversion of 2PG to PEP in the penultimate step of glycolysis [196]. Suppressing ENO1 was observed to diminish the growth of subcutaneous PC3 xenografts and intertumoral angiogenesis *in vivo*. Notably, a decreased osteoclast activation within the bone was evident in the PC3 tibial implant model [229]. Furthermore, ENO3, serving as another paralog of ENO2, has been identified as a promoter of the progression of colorectal cancer when overexpressed, while not demonstrated to play a functional role in PCa [230]. Hence, it is crucial to monitor alterations in the expression levels of ENO1 and ENO3 following the inhibition of ENO2.

In this chapter, the impact of ENO2 inhibition on PCa has been investigated using genetic methods, including siRNA knockdown and CRISPR Cas-9 knockout, to assess its influence on PCa cell behaviors and glycolysis *in vitro*.

5.2 Results

5.2.1 Effects of ENO2 knockdown on human PCa cell *in vitro*

5.2.1.1 Confirmation of successful knockdown of ENO2 in human PCa cells

In **Chapter 4**, the ENO2 expression had been verified that was relatively high in PC3 and highest in 22Rv1. Thus, in this chapter, PC3 and 22Rv1 were selected for ENO2 siRNA knockdown to assess the functional assays.

The ENO2 was transiently knocked down in both PC3 and 22Rv1 cells using ENO2 Silencer™ Selected Validated siRNA and Negative Control #1 siRNA, an empty vector (mock) as control. Mock control group was used instead of WT group to exclude effects caused by the experimental operation itself, such as contamination or off-target effects. Successful knockdown of ENO2 was confirmed via qRT-PCR quantification of mRNA expression in ENO2-deficient and mock controls at 24-hour (Mock, 1.00 ± 0.00 vs siENO2-24h, 0.04 ± 0.03 ; $P < 0.0001$), 48-hour (Mock, 1.00 ± 0.00 vs siENO2-48h, 0.09 ± 0.06 ; $P < 0.0001$), and 72-hour (Mock, 1.00 ± 0.00 vs siENO2-72h, 0.28 ± 0.17 ; $P < 0.0001$) post-transfection. ENO2 expression was significantly inhibited by 95.5% at 24-h, 91.6% at 48-h and 72.1% at 72-h of PC3 cells compared to mock group (**Figure 5.1 A**). In 22Rv1 cells, ENO2 expression was significantly inhibited (92.5%) after 24-hour post transfection compared to mock group (Mock, 1.00 ± 0.00 vs siENO2-24h, 0.08 ± 0.12 ; $P = 0.01$). Although the expression of ENO2 was not significantly suppressed at the other two time points in 22Rv1 (Mock, 1.00 ± 0.00 vs siENO2-48h, 0.48 ± 0.29 ; $P = 0.13$ and Mock, 1.00 ± 0.00 vs siENO2-72h, 0.51 ± 0.47 ; $P = 0.1502$), it still had a downward trend compared to mock group (51.7% at 48-h, 49.3% at 72h) (**Figure 5.1 B**). Notably, the recovery of ENO2 expression after transient transfection were progressive in a time-dependent manner both in PC3 and 22Rv1 cells. For example, the expression level of ENO2 in PC3 recovered from 4.5% at 24-hour to 27.9% at 72-hour, while the expression level of ENO2 in 22Rv1 recovered from 7.5% at 24-hour to 50.7% at 72-hour.

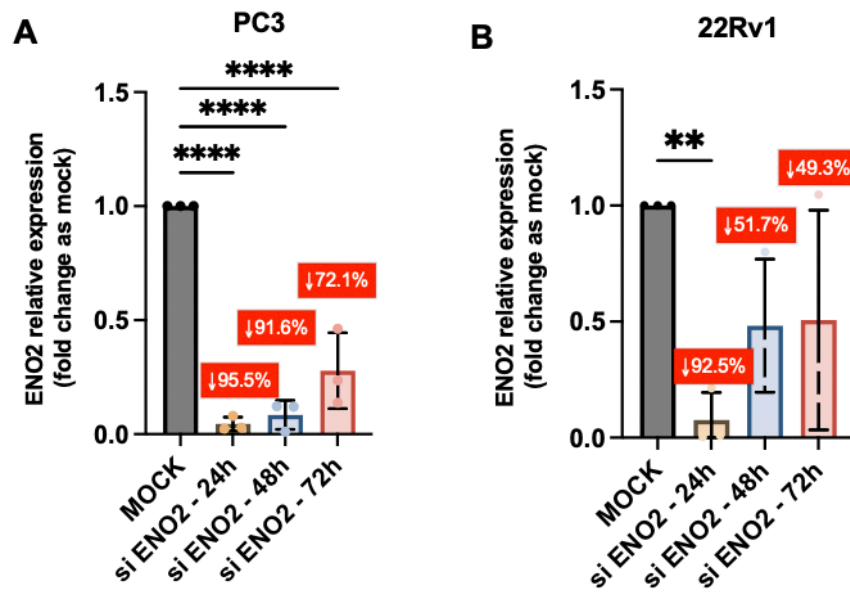


Figure 5.1 siRNA knockdown reduced the expression of ENO2 at mRNA level in PC3 and 22Rv1 cells.

(A and B) Relative expressions of ENO2 siRNA transfection were evaluated at 24-, 48- and 72-hour post-transfection in PC3 and 22Rv1 cell lines and normalized to each mock control as $2^{-\Delta\Delta C_t}$ fold change. The data are mean \pm standard deviation (n=3 biological repeats with 3 technical repeats). One- way ANOVA with Dunnett multiple comparisons. **p<0.01 and ****p<0.0001.

5.2.1.2 ENO2 knockdown reduced the viability and proliferation, but increased the apoptosis of human PCa cells *in vitro*

Subsequently, the viability, proliferation and apoptosis of PC3 and 22Rv1 cells were assessed following 48-hour post-transfection. ENO2 knockdown significantly reduced the viability of both PC3 (5% reduction, Mock, 8497.00 ± 66.25 vs siENO2, 8076.00 ± 139.20 ; $P=0.0091$) and 22Rv1 (23.9% reduction, Mock, 4965.00 ± 489.80 vs siENO2, 3795.00 ± 381.40 ; $P=0.0309$) cells after 48 hours (**Figure 5.2 A and B**). Consistently, ENO2 knockdown also significantly inhibited the proliferation of PC3 cells (30.6% reduction, Mock, 684.90 ± 68.87 vs siENO2, 475.60 ± 21.78 ; $P=0.0074$) (**Figure 5.2 C**). Although the decrease in ENO2 expression also inhibited the proliferation of 22Rv1 cells (36.6% reduction, Mock, 978.50 ± 219.2 vs siENO2, 620.80 ± 87.17 ; $P=0.0584$), no significant difference was observed (**Figure 5.2 D**). Interestingly, ENO2 knockdown dramatically increased the apoptosis of PC3 cells (160.6% upregulation, Mock, 6.25 ± 2.46 vs siENO2, 16.29 ± 4.57 ; $P=0.0286$) (**Figure 5.2 E**). Although the reduction in ENO2 expression also enhanced the apoptosis in 22Rv1 cells (34.9% upregulation, Mock, 47.71 ± 8.55 vs siENO2, 64.36 ± 8.71 ; $P=0.0773$), no significant difference was observed which is consistent the proliferation results (**Figure 5.2 F**). It may be related to the gradual recovery of ENO2 expression at 48 hours after transfection (**Figure 5.1 B**).

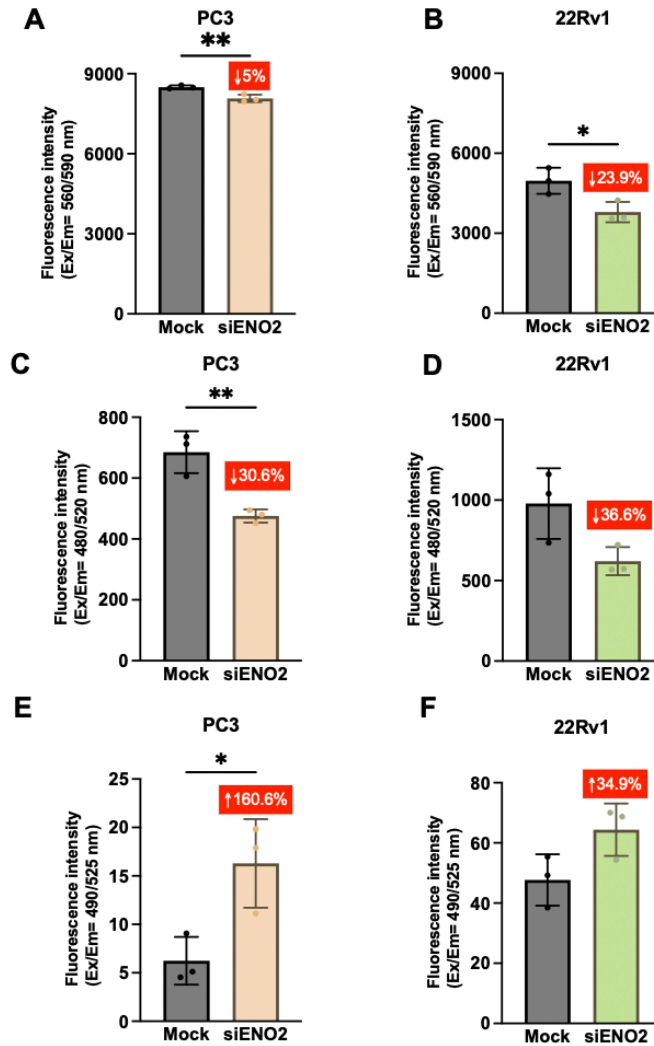


Figure 5.2 ENO2 knockdown reduced the viability and proliferation but increased the apoptosis in PC3 and 22Rv1 cell lines.

(A and B) Cell lines were assessed using AlamarBlue™ cell viability assay. **(C and D)** Cell lines were assessed using CyQuant™ cell proliferation assay **(E and F)** Cell lines were assessed using Caspase 3/7 cell apoptosis assay. Each assay was performed at 48-hour post-transfection. The data are mean ± standard deviation (n=3 biological repeats with 3 technical repeats). Unpaired t-test. *p<0.05, **p<0.01.

5.2.1.3 ENO2 knockdown affected the expression of ENO1 and ENO3 in human PCa cells *in vitro*

In order to evaluate whether a compensatory response occurred following ENO2 inhibition, the expression of its paralogous genes ENO1 and ENO3 after ENO2 was successfully knocked down was also assessed by qRT-PCR. The original expression of ENO1 and ENO3 in PC3 and 22Rv1 WT cells are illustrated as fold change normalized to ENO2 (**Supplementary Figure 5**). After knockout of ENO2 expression, the expression of its paralogous gene ENO1 remained unchanged in PC3 (Mock, 1 ± 0.00 vs siENO2-24h, 0.89 ± 0.33 ; $P=0.8276$ and vs siENO2-48h, 0.77 ± 0.15 ; $P=0.3883$ and vs siENO2-72h, 0.75 ± 0.16 ; $P=0.3370$), but gradually decreased with time in 22Rv1 (Mock, 1 ± 0.00 vs siENO2-24h, 1.05 ± 0.16 ; $P=0.9905$ and vs siENO2-48h, 0.39 ± 0.19 ; $P=0.0413$ and vs siENO2-72h, 0.25 ± 0.43 ; $P=0.0158$) (**Figure 5.3 A and B**). There was also no significant change in ENO3 expression in PC3 (Mock, 1 ± 0.00 vs siENO2-24h, 1.28 ± 0.39 ; $P=0.3797$ and vs siENO2-48h, 1.37 ± 0.14 ; $P=0.2$ and vs siENO2-72h, 1.27 ± 0.22 ; $P=0.4147$) and 22Rv1 cells (Mock, 1 ± 0.00 vs siENO2-24h, 2.79 ± 2.98 ; $P=0.666$ and vs siENO2-72h, 2.64 ± 1.07 ; $P=0.7165$) compared to the mock group, although it was significantly enhanced in 22Rv1 only at the 48-hour time point (Mock, 1 ± 0.00 vs siENO2-48h, 6.86 ± 3.26 ; $P=0.0331$) (**Figure 5.3 C and D**). Furthermore, the expression of ENO1 and ENO3 in the mock group after transfection of the empty vector and the wild type without any transfection was also compared as ΔC_t values (**Supplementary Figure 6**).

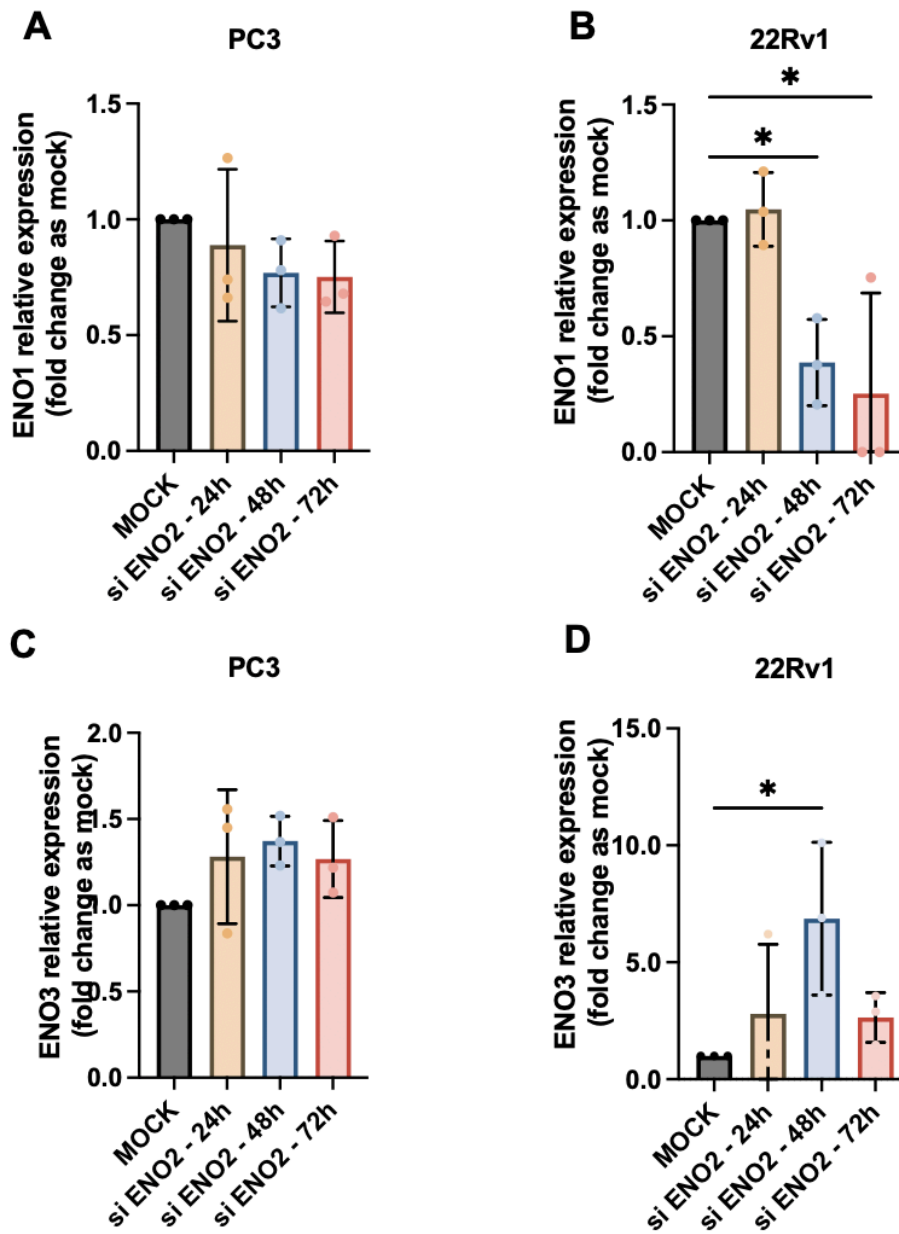


Figure 5.3 ENO2 knockdown reduced the expression of ENO1 but increased the expression of ENO3 at mRNA level in 22Rv1 cells, but not in PC3 cells.

(A and B) Relative expressions of ENO1 after siRNA transfection were evaluated at 24-, 48- and 72-hour post-transfection and normalized to each scrambled control as $2^{-\Delta\Delta C_t}$ fold change. **(C and D)** Relative expressions of ENO3 after siRNA transfection were evaluated at 24-, 48- and 72-hour post-transfection and normalized to each scrambled control as $2^{-\Delta\Delta C_t}$ fold change. The data are mean \pm standard deviation (n=3 biological repeats with 3 technical repeats). One- way ANOVA with Dunnett multiple comparisons. *p<0.05.

5.2.2 Effects of ENO2 genetic knockout on human PCa cell behavior in vitro

5.2.2.1 Confirmation of successful knockout of ENO2 in human PCa cells

In this chapter, PC3 and 22Rv1 were selected for ENO2 genetic inhibition to validate previous siRNA knockdown results and further investigation.

The ENO2 knockouts had been conducted via using the predesigned CRISPR gRNA plasmid DNA which detailed in **Section 2.2.2**. Eleven of distinct ENO2-KO clones from PC3 and 22Rv1 cell lines were comprehensive examined in transcriptional, translational and genomic level. ENO2 expression was significantly suppressed at mRNA level in all KO clones compared to WT group (**Figure 5.4 A and B**). Subsequently, in contrast to the WT group, the ENO2 expression at protein level expression were markedly inhibited in all KO clones, with Western Blotting images revealing almost no detectable bands (**Figure 5.4 C and D**). However, 22Rv1 ENO2-KO #5 and #7 were not tested at the protein level due to failure in protein extraction.

Next, the PCR products obtained using the custom primers introduced in **Section 2.2.6** were subjected to agarose gel electrophoresis in PC3 and 22Rv1 WT and KO clone cells, in order to conduct the sanger sequencing for targeted region. Certain PCR products derived from ENO2-KO clones exhibited a noticeable reduction in size compared to the PCR products from the WT cells, especially in 22Rv1 ENO2-KO #3 to #9 (**Figure 5.4 E and F**). The genomic DNAs were cut and recovered from the electrophoresis gel, and the purified products were sent to Zenta Life Science for Sanger sequencing. Here, the sequence results of only the single clones I selected for subsequent cellular assays (PC3 ENO2-KO #1 and #2, 22Rv1 ENO2-KO #4 and #8) (**Figure 5.5 A and B**). The Sanger sequencing chromatogram illustrates a comparison of WT and ENO2-KO clones in PC3 and 22Rv1 cells, revealing point mutations and frameshift mutations observed in all four clones. The morphology and phenotypes of ENO2 CRISPR-mediated KO cells in both PC3 and 22Rv1 cell lines shows clear differences compared to WT cells (**Figure 5.6**). PC3 WT cells display an elongated, spindle-shaped and more mesenchymal in morphology in culture (**Figure 5.6 A**) [231].

Although both have ENO2 gene deletion, different appearances have been showed in PC3 ENO2-KO #1 and #2 cells. PC3 ENO2-KO #1 cells retain some elongated features (**Figure 5.6 B**), but PC3 ENO2-KO #2 cells appear rounder (**Figure 5.6 C**). In addition, 22Rv1 WT cells have an epithelial-like morphology and are tightly packed in clusters (**Figure 5.6 D**) [142]. 22Rv1 ENO2-KO #4 cells appear more isolated and less clustered compared to WT (**Figure 5.6 E**). 22Rv1 ENO2-KO #8 cells show the most obvious morphological changes, with cells appearing clustered and more tightly packed than WT cells (**Figure 5.6 F**).

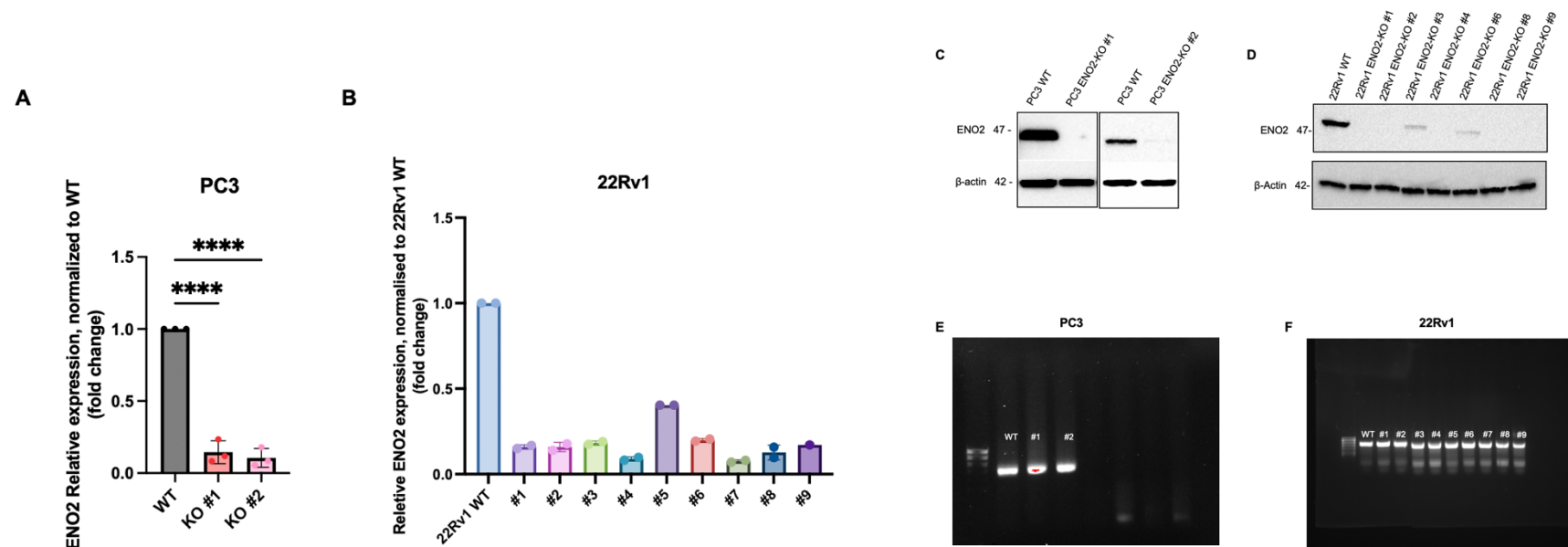


Figure 5.4 CRISPR Cas 9 knockout of ENO2 suppressed the expression of ENO2 at mRNA and protein level in PC3 and 22Rv1 cells.

(A and B) q RT-PCR shows relative mRNA expression of ENO2 after formation of single clones compared to wild types as $2^{-\Delta\Delta C_t}$ fold change in PC3 and 22Rv1 cells. **(C and D)** Western Blotting shows the protein expression of ENO2 after formation of single clones in PC3 and 22Rv1 cells. The data are mean \pm standard deviation. **(E and F)** The PCR products obtained using custom primers were subjected to agarose gel electrophoresis in PC3 and 22Rv1 cells. The data are mean \pm standard deviation (n=3 biological repeats with 3 technical repeats for Figure A, n=2 biological repeats with 3 technical repeats for Figure B). One- way ANOVA with Dunnett multiple comparisons. ****p<0.0001.

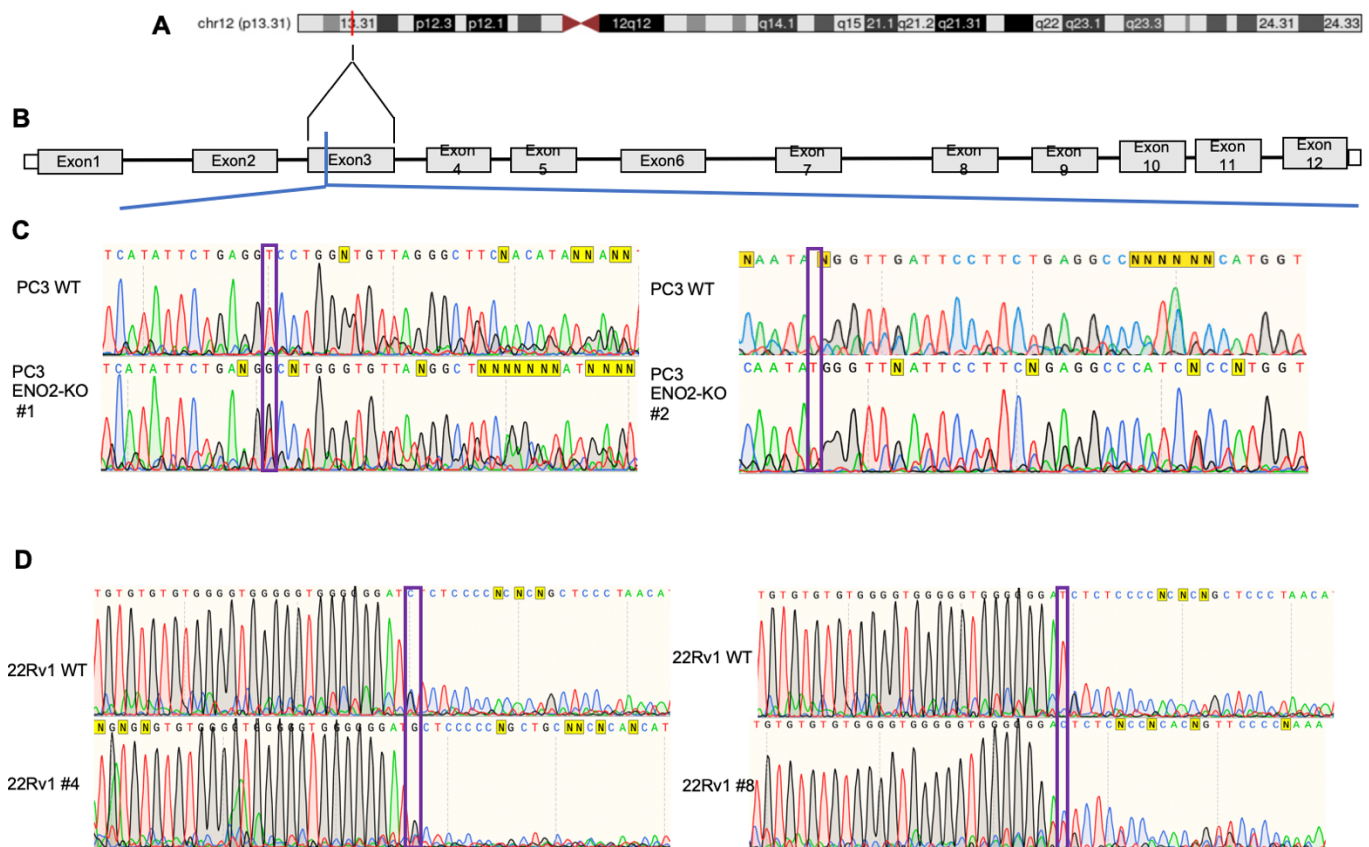


Figure 5.5 Chromosome location, gene structure and sequence analysis of ENO2 in PC3 and 22Rv1 cells.

(A) Chromosome 12 and the location of *ENO2* drawn to scale. **(B)** Genomic DNA map for *ENO2* **(C and D)** Sanger sequencing chromatogram showing comparison of wild type and *ENO2* knockout clones of PC3 and 22Rv1 cells. The location of the mutation is marked on the graph with purple squares.

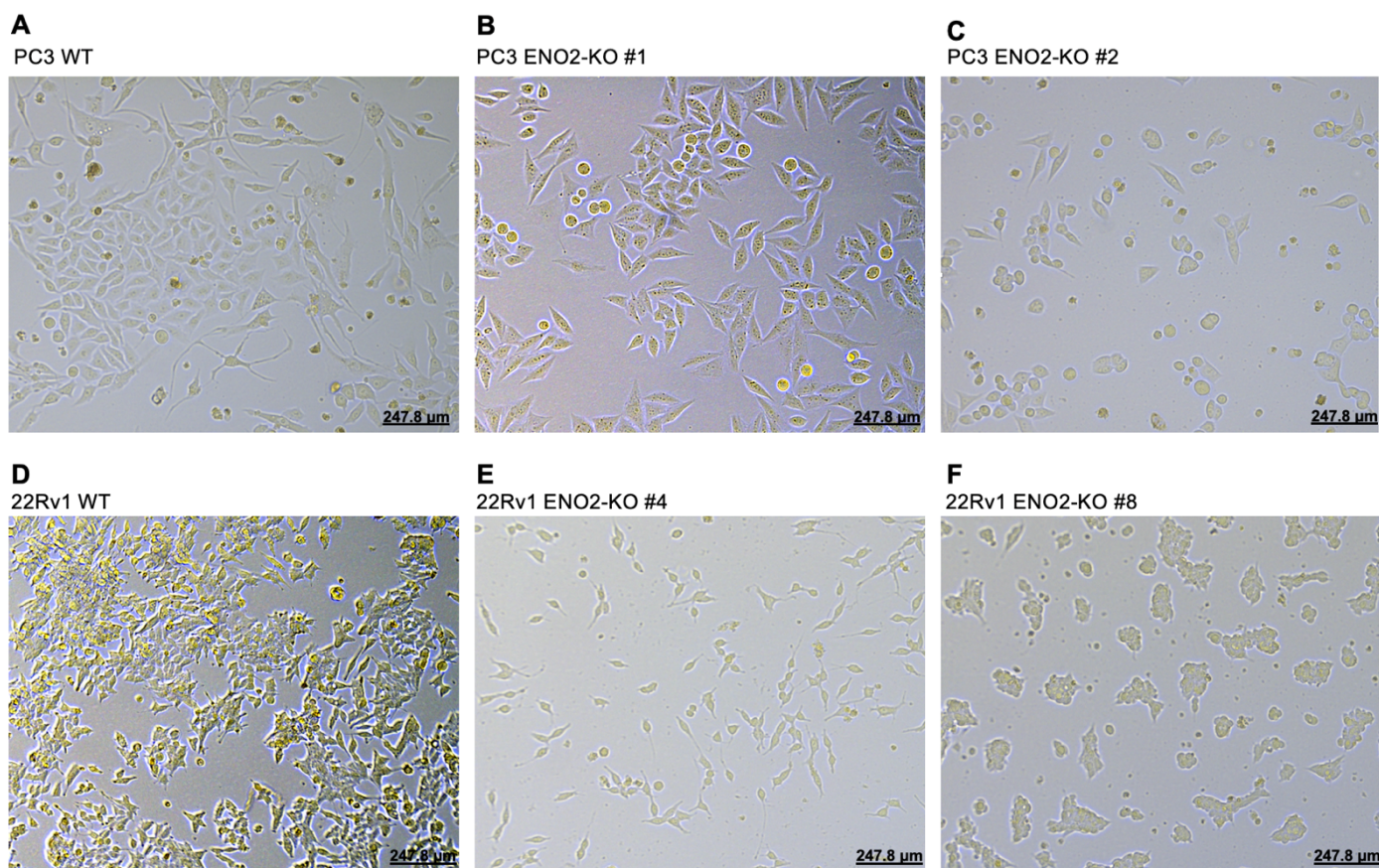


Figure 5.6 Representative images of their WTs and respective ENO2-KO single clones for PC3 and 22Rv1 cells.

The images were captured at the 10x magnifications by Leica DMI8, scale bar= 247.8μm.

5.2.2.2 ENO2 knockout reduced the cell growth of human PCa cells *in vitro*

The viability, proliferation and apoptosis of ENO2-KO PC3 and 22Rv1 cells were assessed following the generation and expansion of single clones. The deletion of ENO2 significantly reduced the viability of both PC3 (38.7% reduction, WT 14819.00 \pm 1208.00 vs KO #1 9020.00 \pm 290.40; P=0.0005 and 39% reduction, WT 14819.00 \pm 1208.00 vs KO #2 9016.00 \pm 1017.00; P=0.0005) and 22Rv1 (63% reduction, WT 5137.00 \pm 196.80 vs KO #4 1899.00 \pm 121.90; P<0.0001 and 31.5% reduction, WT 5137.00 \pm 196.80 vs KO #8 3515.00 \pm 324.80; P=0.0002) (**Figure 5.7 A and B**). Correspondingly, ENO2-KO also markedly inhibited the proliferation of both PC3 (22.6% reduction, WT 2079.00 \pm 186.40 vs KO #1 1616.00 \pm 270.70; P=0.0465 and 27% reduction, WT 2079.00 \pm 186.40 vs KO #2 1510.00 \pm 73.04; P=0.0205) and 22Rv1 (35.7% reduction, WT 3359.00 \pm 69.65 vs KO #4 2165.00 \pm 75.01; P<0.0001 and 5.5% reduction, WT 3359.00 \pm 69.65 vs KO #8 3173.00 \pm 38.32; P=0.0199) cells (**Figure 5.7 C and D**). Notably, loss of ENO2 expression had no impact on the apoptosis of PC3 (WT 33.00 \pm 3.67 vs KO #1 40.41 \pm 2.33; P=0.0814 and WT 33.00 \pm 3.67 vs KO #2 40.49 \pm 4.57; P=0.0783) and 22Rv1 (WT 48.84 \pm 1.70 vs KO #4 48.68 \pm 1.83; P=0.9897 and WT 48.84 \pm 1.70 vs KO #8 51.67 \pm 1.45; P=0.1392) cells (**Figure 5.7 E and F**). Taken together, ENO2 played an important role in the cell growth of PCa.

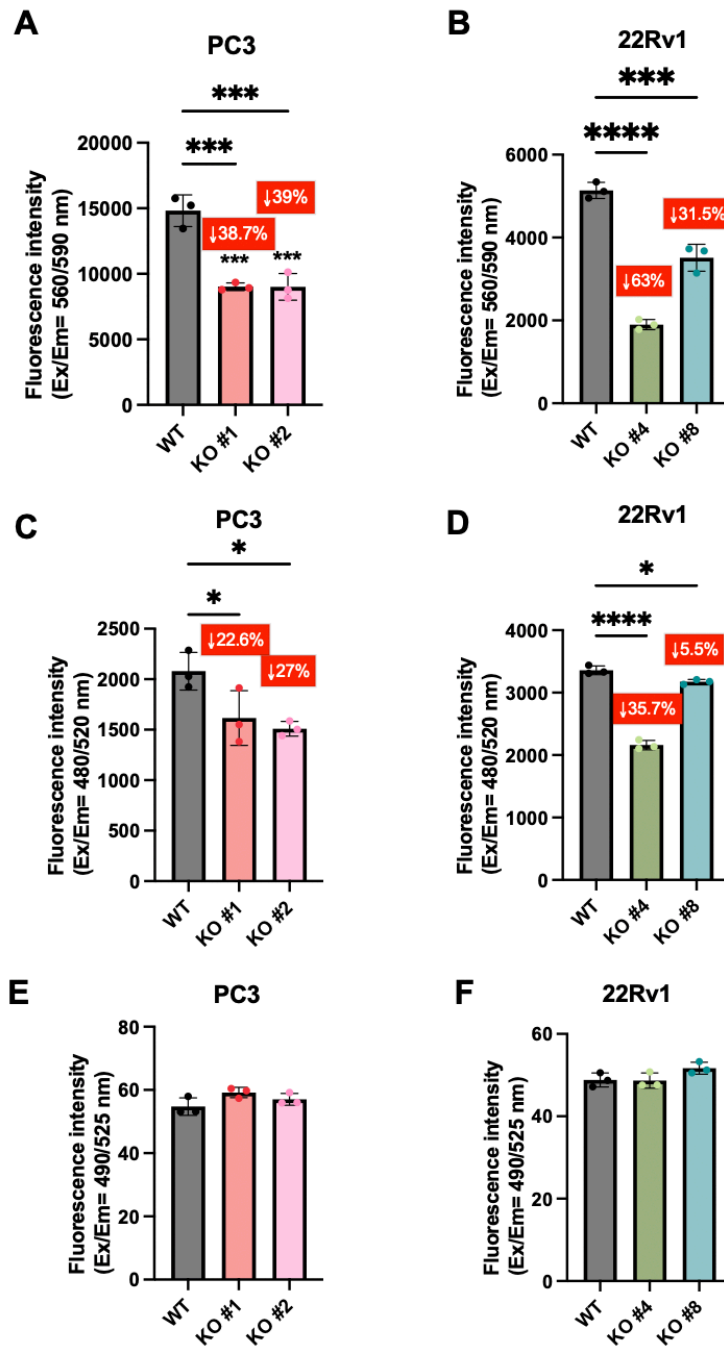


Figure 5.7 ENO2 knockout reduced the viability and proliferation but did not affect apoptosis in PC3 and 22Rv1 cell lines.

(A and B) Cell lines were assessed using AlamarBlue™ cell viability assay. **(C and D)** Cell lines were assessed using CyQuant™ cell proliferation assay. **(E and F)** Cell lines were assessed using Caspase 3/7 cell apoptosis assay. The data are mean ± standard deviation (n=3 biological repeats with 3 technical repeats). One- way ANOVA with Dunnett multiple comparisons. *p<0.05, ***p<0.001 and ****p<0.0001.

5.2.2.3 ENO2 knockout reduced the motility of human PCa cells *in vitro*

The migration and invasion of ENO2-KO PC3 and 22Rv1 cells had been further evaluated after proving that ENO2 affects the growth of PCa cells. The effects of ENO2 absence on the *in vitro* migration of human PC3 cells was assessed by wound healing assay. Knockout of ENO2 significantly reduced the 2D-directed migration of PC3 cells. At 20-hour time point, ENO2 knockout reduced the migration of PC3 #1 and #2 cells by 68.6% and 61.4%, respectively (WT 42.21 ± 8.87 vs KO #1 13.25 ± 6.45 ; $P=0.0029$ and WT 42.21 ± 8.87 vs KO #2 16.30 ± 2.74 ; $P=0.005$) (**Figure 5.8 A and B**). Additionally, the effects of ENO2 absence on the *in vitro* migration of human 22Rv1 cells was assessed by using the Boyden Chamber assay, due to 22Rv1 cells form clusters instead of exhibiting a monolayer growth pattern *in vitro* so that wound healing assay is not appropriate. Knockout of ENO2 markedly downregulated the 3D migration of 22Rv1 ENO2-KO #8 cells (74.4% reduction, WT 100.00 ± 0.00 vs KO #8 25.55 ± 9.17 ; $P<0.0001$). Although there was no significant difference observed among 22Rv1 WT and 22Rv1-KO #4 cells, a trend of reduced migration was also found (13.3% reduction, WT 100.00 ± 0.00 vs KO #4 86.68 ± 6.44 ; $P=0.0779$) (**Figure 5.8 C and D**). Subsequently, the effects of ENO2 absence on the *in vitro* of human PC3 and 22Rv1 cells were assessed by Matrigel coated Transwell® assay. Notably, knocking out of ENO2 reduced the invasion of PC3 (74.5% reduction, WT 100.00 ± 0.00 vs KO #1 25.54 ± 13.15 ; $P=0.0016$ and 68.4% reduction WT 100.00 ± 0.00 vs KO #2 31.59 ± 22.36 ; $P=0.0025$) and 22Rv1 (23.9% reduction, WT 100.00 ± 0.00 vs KO #4 76.06 ± 16.70 ; $P=0.0473$ and 58% reduction, WT 100.00 ± 0.00 vs KO #8 42.04 ± 5.15 ; $P=0.0007$) cells (**Figure 5.9 A, B, C and D**). Taken together, ENO2 played an important role in the motility of PCa.

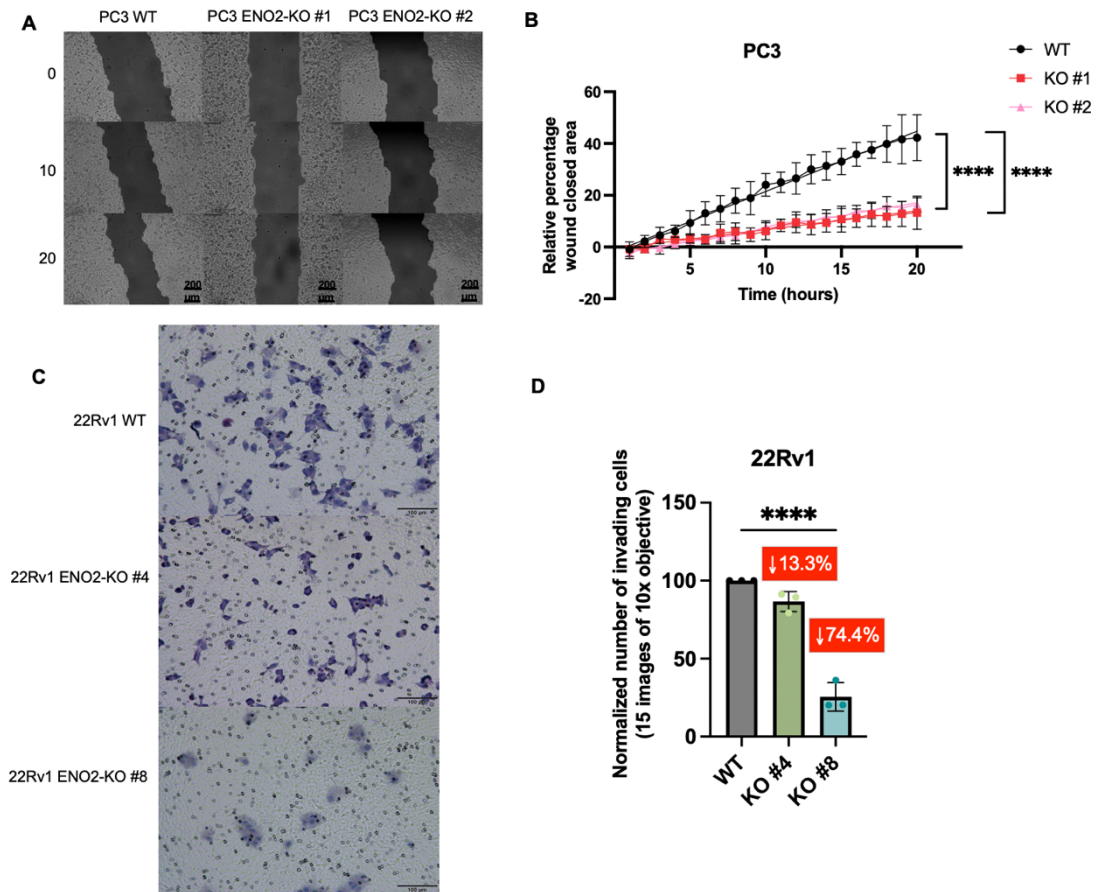


Figure 5.8 ENO2 knockout reduced the migration in PC3 and 22Rv1 cell lines.

(A and B) PC3 wild type and knockout cell lines were assessed by wound healing scratch assay and analysed at every 30 minutes at total 20 hours. Scale bar = 200 μ M

(C and D) 22Rv1 wild type and knockout cell lines were assessed by Transwell assay and analysed at 72 hours after seeding, normalized to control as % WT. Scale bar = 100 μ M. The data are mean \pm standard deviation (n=3 biological repeats with 3 technical repeats). Simple linear regression and one- way ANOVA with Dunnett multiple comparisons. ****p<0.0001.

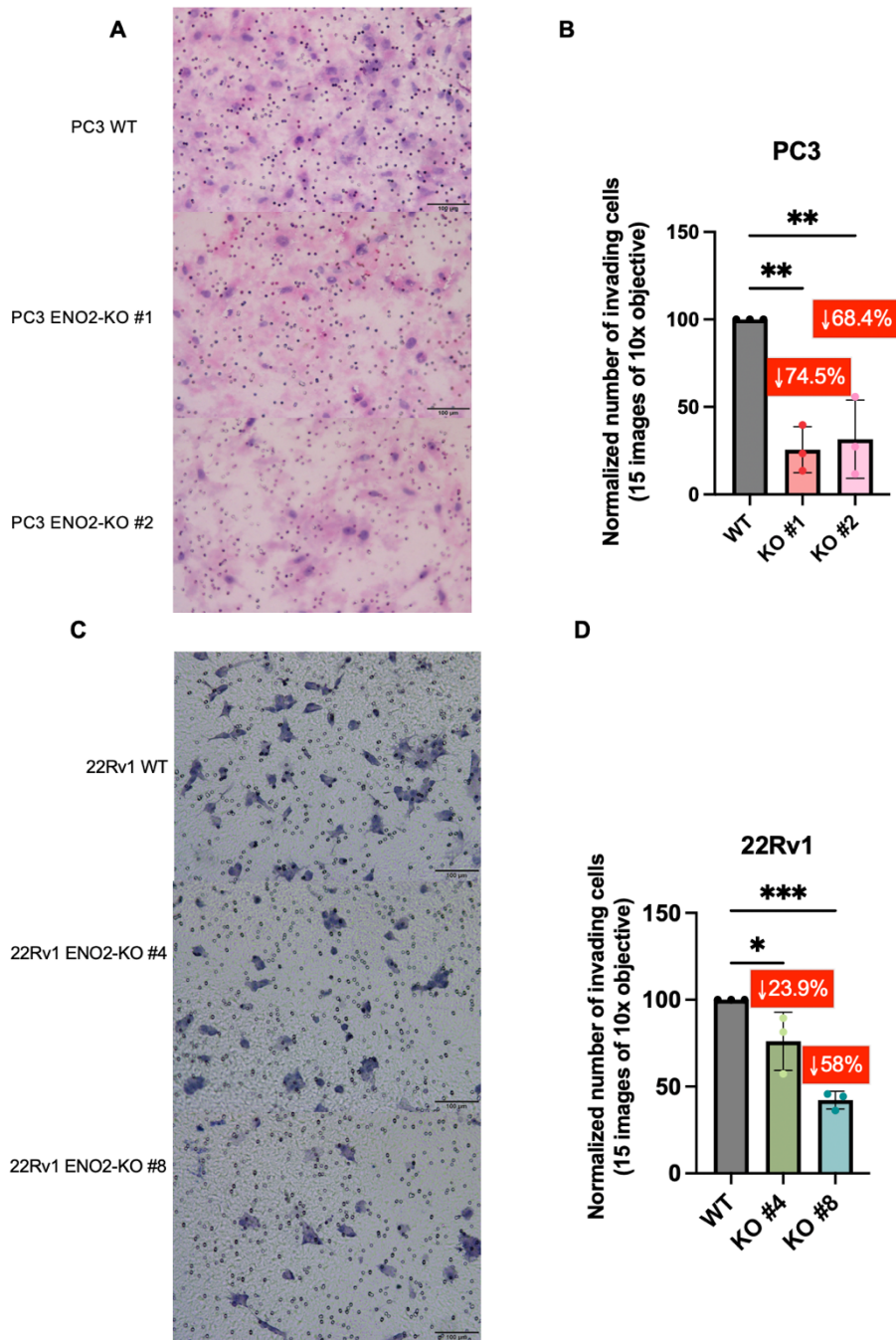


Figure 5.9 ENO2 knockout reduced the invasion in PC3 and 22Rv1 cell lines.

(A and B) PC3 wild type and knockout cell lines were assessed by Transwell assay and analysed at 72 hours after seeding, normalized to control as % WT. Scale bar = 100 μ M. **(C and D)** 22Rv1 wild type and knockout cell lines were assessed by Transwell assay and analysed at 72 hours after seeding, normalized to control as % WT. Scale bar = 100 μ M. The data are mean \pm standard deviation (n=3 biological repeats with 3 technical repeats). One- way ANOVA with Dunnett multiple comparisons. *p<0.05, **p<0.01 and ***p<0.001.

5.2.2.4 ENO2 knockout reduced the glycolytic metabolic behavior of human PCa cells *in vitro*

To determine whether knockout of ENO2 could affect the glycolysis level of PCa cells, the glucose consumption and lactate production assays had been conducted in ENO2-KO PC3 and 22Rv1 cells. Knockout of ENO2 could markedly inhibit the glucose consumption of PC3 (27.9% reduction, WT 12.79 ± 0.14 vs KO #1 9.23 ± 1.55 ; $P=0.005$ and 35.6% reduction, WT 2.79 ± 0.14 vs KO #2 8.24 ± 0.17 ; $P=0.0015$) and 22Rv1 ENO2-KO #8 (42.2% reduction, WT 12.91 ± 1.79 vs KO #8 7.47 ± 1.01 ; $P=0.0026$) cells (**Figure 5.10 A**). Although the ENO2 absence also inhibited the glucose consumption of 22Rv1 ENO2-KO #4, no significant difference was observed (20.9% reduction, WT 12.91 ± 1.79 vs KO #4 10.21 ± 0.30 ; $P=0.0568$) (**Figure 5.10 B**). Correspondingly, ENO2 knockout dramatically downregulated the production of lactate both in PC3 ENO2-KO #2 (38.9% reduction, WT 12.43 ± 0.95 vs KO #2 11.16 ± 1.80 ; $P=0.0067$) and 22Rv1 (40.4% reduction, WT 18.55 ± 3.41 vs KO #4 11.06 ± 2.69 ; $P=0.0453$ and 43.9% reduction, WT 18.55 ± 3.41 vs KO #8 10.41 ± 3.22 ; $P=0.0329$) cells (**Figure 5.10 C and D**). Although the ENO2 absence also inhibited the lactate production of PC3 ENO2-KO #1, no significant difference was observed (10.2% reduction, WT 12.43 ± 0.95 vs KO #1 11.16 ± 1.80 ; $P=0.0568$) (**Figure 5.10 C**). Taken together, these results demonstrated ENO2 may involve in the regulation of glycolytic metabolic behavior.

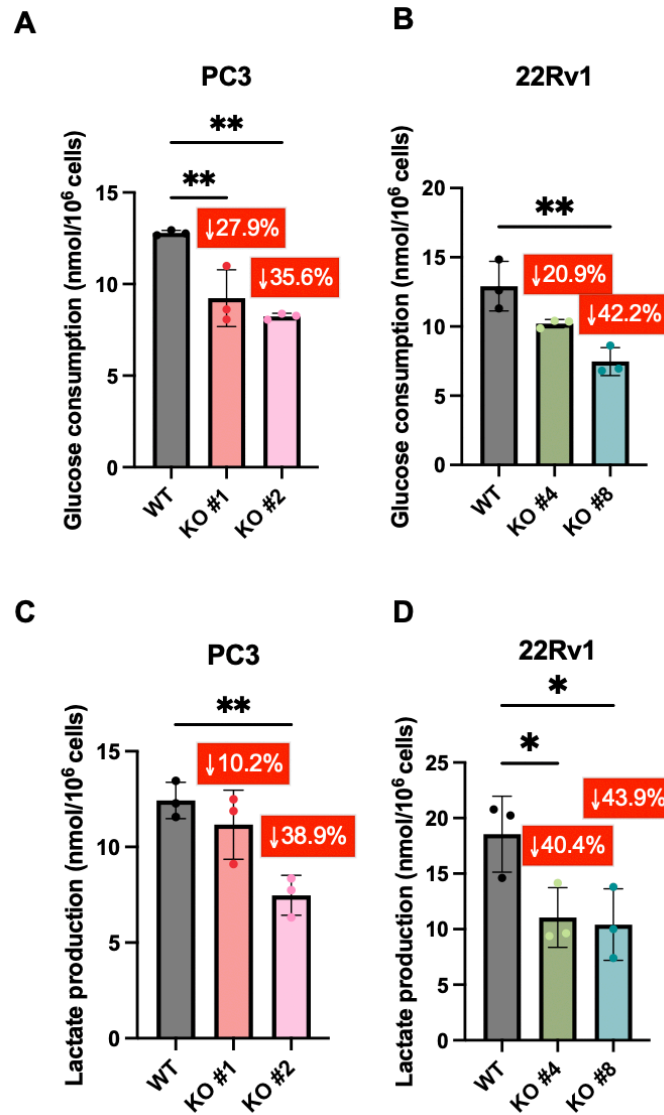


Figure 5.10 ENO2 knockout reduced the glucose consumption and lactate production in PC3 and 22Rv1 cell lines.

(A and B) cell lines were assessed using glucose consumption assay. **(C and D)** Cell lines were assessed using lactate measurement assay. (The data are mean \pm standard deviation (n=3 biological repeats with 3 technical repeats). One- way ANOVA with Dunnett multiple comparisons. *p<0.05 and **p<0.01.

5.3 Discussion

Evidences from **Chapter 3** and **Chapter 4** suggested upregulation of ENO2 was associated with advanced development of PCa in patients and metastasis potential in cell lines *in vitro*. In addition, extracellular glucose and pyruvate affected the expression of ENO2 in PCa tumour cells *in vitro*, which also proved that the elevated glycolysis in PCa depends on the high expression of ENO2. Based on these findings, whether cellular functional involvements, including cell growth, motility and glycolytic metabolic behavior, depends on ENO2 expression have been demonstrated in this chapter.

In this chapter, I initially performed q RT-PCR to verify the effects of ENO2 knockdown in PC3 and 22Rv1 cell lines after siRNA transfection. After efficiently knocking down of ENO2, the viability and proliferation had been reduced but the apoptosis had been increased of human PC3 and 22Rv1 cells *in vitro* (**Figure 5.1 and 5.2**). However, due to the transient nature of the siRNA transfection, the sustained down-regulation of ENO2 expression was not feasible for an extended period. For instance, the recovery of ENO2 expression after transient transfection were progressive in a time-dependent manner both in PC3 and 22Rv1 cells (**Figure 5.1**). Consequently, there was insufficient time to validate whether the reduction in ENO2 has an impact on alterations in PCa cell motility and glycolysis. Therefore, ENO2-KO clones were successfully generated via CRISPR Cas 9 stable transfection for the subsequent studies that explored the effects of ENO2 on the ability of highly metastatic PCa cells with grow, motility and glycolysis. The knockout of ENO2 in PC3 and 22Rv1 was verified at the mRNA, protein and genomic levels, respectively. The PC3 cells in which the ENO2 gene was knocked out, only two clones were expanded, and both have been used for further cellular assays. Furthermore, ENO2 knockout was performed on 22Rv1 cells, resulting in the expansion of 9 single clones in total. However, only clones #4 and #8 were selected for subsequent functional assessments. This selection was based not only on the distinctive morphology observed under the microscope compared to the wild type (**Figure 5.6**) but also on the identification via Sanger sequencing, with similar

frameshift mutations to those found in the PC3 clones (**Figure 5.5**). Consistent with previous siRNA knockdown results, the deletion of ENO2 significantly reduced the viability and proliferation of PCa cells (**Figure 5.7**). Although there were no significant differences, their apoptotic ability also showed an upward trend which were consistent with previous results. Interestingly, ENO2 deprivation markedly reduced the motility and glycolytic capacity of PCa cells, which was manifested in affecting migration and invasion, glucose consumption and pyruvate production (**Figure 5.8, 5.9 and 5.10**). As mentioned previously, silencing ENO2 expression has been found to reduce tumour growth and glycolysis in acute lymphoblastic leukemia cells, head and neck cancer cells which were consistence with my studies [135, 136].

Indeed, the expression of its paralogous genes ENO1 and ENO3 after ENO2 was successfully knocked down was also assessed by qRT-PCR in order to evaluate whether a compensatory response occurred following ENO2 inhibition. Notably, the significant alterations in ENO1 and ENO3 did not occur at 24 hours after transfection when transfection efficiency reached its peak but began to change at 48 hours when transfection efficiency gradually began to be lost and the expression of ENO2 was recovering. Therefore, it remains unclear whether the roles of the paralog genes ENO1 and ENO3 in PCa cells are complementary or redundant following the impairment of ENO2 function before verification within clones that has stably knocked out ENO2. Indeed, functional redundancy of ENO1 has been observed with a high dependence on ENO2. Knocking down ENO2 had been shown to suppressed the growth of glioblastoma cells lacking ENO1 [109]. Although the evidence connecting ENO1 and PCa is limited, the use of anti-ENO1 antibodies to block cell surface ENO1 has proven effective in inhibiting invasion and metastasis in pancreatic and lung cancer [232, 233]. In addition, although ENO3 has been recognized as a promoter of colorectal cancer progression when overexpressed, it was more frequently observed to demonstrate suppressor characteristics in various other types of cancers [108, 230]. The downregulation of ENO3 expression was not only found to be associated with poor prognosis in pancreatic ductal adenocarcinoma patients, it was also found to be

negatively correlated with majority of immune cell types [234, 235]. Significantly, ENO3 has been identified as a tumour suppressor gene in hepatocellular carcinoma. Increased ENO3 expression has been found to block the proliferation and lung metastasis abilities of hepatocellular carcinoma cells by inhibiting the EMT process and Wnt/ β -catenin pathway [236]. Overall, the expression changes of ENO1 and ENO3 after ENO2 deprivation is not conclusive. Further verifying the expression alterations of ENO1 and ENO3 relying on the stable knockout of ENO2 single clones is necessary.

Consistent with previous siRNA knockdown results, the deletion of ENO2 significantly reduced the viability and proliferation but did not impact the apoptosis of PCa cells (**Figure 5.7**). Interestingly, ENO2 deprivation markedly reduced the motility and glycolytic capacity of PCa cells, which was manifested in affecting migration and invasion, glucose consumption and pyruvate production (**Figure 5.7, 5.8 and 5.9**). As mentioned previously, silencing ENO2 expression has been found to reduce tumour growth and glycolysis in acute lymphoblastic leukemia cells, head and neck cancer cells which were consistent with my results [135, 136]. ENO2 was identified to play a role in regulating the process of EMT. A recent study confirmed that silencing ENO2 notably decreased the expression levels of EMT markers, including N-cadherin and the vimentin, in renal cell carcinoma [137]. Through the EMT process, Epithelial cells acquire invasive and metastatic characteristics through the EMT, which is considered key markers of cancer progression [237]. Combined with my results, ENO2 deprivation may significantly reduce the growth and motility of PCa cells *in vitro* by downregulating the EMT process thereby downregulating metastatic ability. Thus, it will be crucial to subsequently verify either the ENO2 deletion causes alterations of the metastatic ability *in vivo* or changes the EMT pathway with RNA-seq.

However, there are still several limitations in this chapter. Firstly, in addition to genetically knocking down and knocking out of ENO2, the pharmacological inhibition should also be considered. Since glioma cells covering the passenger deletion of

ENO1 were found to be highly dependent on ENO2, several inhibitors of ENO2 have been developed to treat ENO1-deficient cancers, including the specific inhibitor POMHEX, novel enolase inhibitor SF2312 and AP-III-a4 [135, 211, 238, 239]. They were mature and safe compounds that has been extensively employed in cancer research both *in vitro* and *in vivo*. However, SF2312 only shows a marginal higher IC50 for ENO2 (42.5 nM) than ENO1 (37.9 nM), which means that inhibiting ENO2 expression will also inhibit ENO1 function [238]. Besides, despite being a broad inhibitor of enolase, AP-III-a4 demonstrated highly selective and specific dose-dependent inhibition of ENO2 without affecting ENO1 expression [135]. Nevertheless, as the therapeutic doses increases, there is a probability of concurrent suppression of ENO1, ENO2, and ENO3 expressions, potentially resulting in additional side effects. As the only commercially available specific inhibitor of ENO2, POMHEX also has not been used in my project. This is because that POMHEX was found to be rapidly hydrolyzed in mouse plasma *ex vivo* with a half-life of only 30 seconds, and the half-life in human blood *ex vivo* was only 9 minutes [239]. Even if POMHEX was applied in primates, complete POMHEX cannot be detected at the lowest time point tested [239]. In addition, the results generated from different assay methods may not be directly comparable. Finally, since it has not been verified using stable ENO2 knockout clones, it remains unclear whether the paralogous genes ENO1 and ENO3 are involved in joint regulation of the malignant development of PCa cells after ENO2 function is impaired.

5.4 Conclusion

In summary, the results from this chapter confirmed that ENO2 plays an essential role in the tumorigenic and metastatic behaviour of human PCa cells. Therefore, the further *in vivo* assays will be carried out to confirm these *in vitro* results to jointly validate the feasibility of targeting ENO2 in PCa bone metastasis.

Chapter 6: Evaluation of the Role of ENO2 in PCa Bone Metastasis *in vivo*

6.1 Introduction

Currently, the first-line treatments such as radical prostatectomy, radiotherapy, chemotherapy, and ADT are commonly employed for PCa [240]. Although these treatments are impactful in the early stages of the disease, they do not address bone metastasis which occur in approximately 70% of patients and are considered incurable [241]. Thus, it is crucial to establish a new therapeutic target for PCa bone metastasis. My previous results have suggested that the expression of ENO2 is not only related to advanced metastatic PCa, but also tends to be highly expressed in PCa bone metastasis and bone metastatic cell lines in **Chapter 3 and 4**. Subsequently, the results from **Chapter 5** confirmed that ENO2 plays an important role contributing to the metastatic behaviour of human PCa cells. Similarly, studies of others have validated the involvement of ENO2 in regulating tumour development through *in vitro* trials across various cancers, including acute lymphoblastic leukemia, head and neck cancer, and lung cancer [135, 136, 225]. Besides, Zha et al. conducted studies in BALB/c nude mice, revealing that the upregulation of ENO2 in lung cancer cells increased distant metastasis and accelerated weight loss of mice [225]. Subsequent *in vitro* qRT-PCR experiments illustrated that ENO2 overexpression fosters the EMT process in lung cancer cells, thereby amplifying distant metastasis [225]. Wang et al. used bioinformatics techniques to confirm that ENO2 emerged as a critical gene activated under mechanical load in bone cells. Knockdown of ENO2 leads to alterations in the expression of key genes regulating osteoclast and osteoblast function [242]. However, there are absence of *in vivo* trials examining the impact of targeting ENO2 on tumour progression, especially bone metastasis.

The human PCa xenograft model provides foundation for research on PCa bone metastasis. PC3 has a high propensity to cause bone metastasis after intracardiac injection and is considered one of the choice for the PCa bone metastasis model [243-245]. The osteolytic or mixed metastatic lesions often develop in the metaphysis under the growth plate in tibia and femur after intracardiac injection of PC3 cells [57, 244]. The metaphysis is located between the epiphysis and diaphysis and is mainly

composed of trabecular bone [57]. Trabecular bone, distinguished by its elevated metabolic activity and abundant blood supply, exhibits more susceptibility to abnormal bone remodeling. This heightened susceptibility facilitates the invasion and colonization of tumour cells, making it an optimal location for investigating bone metastasis [246].

In this chapter, the impact of ENO2 inhibition on PCa bone metastasis has been investigated using PC3 xenograft model. Cohorts of BALB/c nude mice (n=8) were intracardiac injected with PC3 WT Luc or PC3 ENO2-KO cells via the left cardiac ventricle. Regular body weight of mice and IVIS were monitored to observe tumour development. Micro-CT and histology analysis were employed to study bone destruction and tumour establishment in the bone marrow *ex vivo*, respectively.

6.2 Results

6.2.1 Genetically inhibition of ENO2 improved the metastatic tumour growth in BALB/c nude mice

To explore the effects of genetically inhibition of ENO2 on PCa bone metastasis, 6 to 7-week-old male mice were injected with 1×10^5 PC3 WT Luc or PC3 ENO2-KO #1 cells in PBS via the left cardiac ventricle. Mice injected with PC3 WT cells were imaged using the IVIS system on Day 5, Day 12, Day 19, Day 24, Day 27 and Day 31 to monitor the tumour development. Mice injected with PC3 ENO2-KO #1 cells were not monitored by IVIS due to the absence of luciferase signalling in this single clone. The mice's body weight was measured twice weekly until Day 19 post-injection, when the luciferase signals started to appear in the control group in the IVIS imaging. Subsequently, body weight measurements were increased to three times each week to warrant animal welfare. All mice were euthanized at Day 32 when the weight loss rate of the first mouse reached humane endpoint (>20% body weight loss) (**Figure 6.1**). Starting from the 21st day, the relative weight of the mice in the control group continued to decrease due to the tumour progression as shown in IVIS imaging, with a significant difference starting from Day 28 (WT, -1.103 ± 7.954 vs KO #1, $10.73 \pm$

8.748; $P = 0.0306$) and reaching an average of -6% on the 32nd day (euthanasia day) (WT, -5.757 ± 11.54 vs KO #1, 11.34 ± 5.895 ; $P = 0.0058$). In contrast, the relative weight of the mice injected with KO cells increased steadily (**Figure 6.2**).

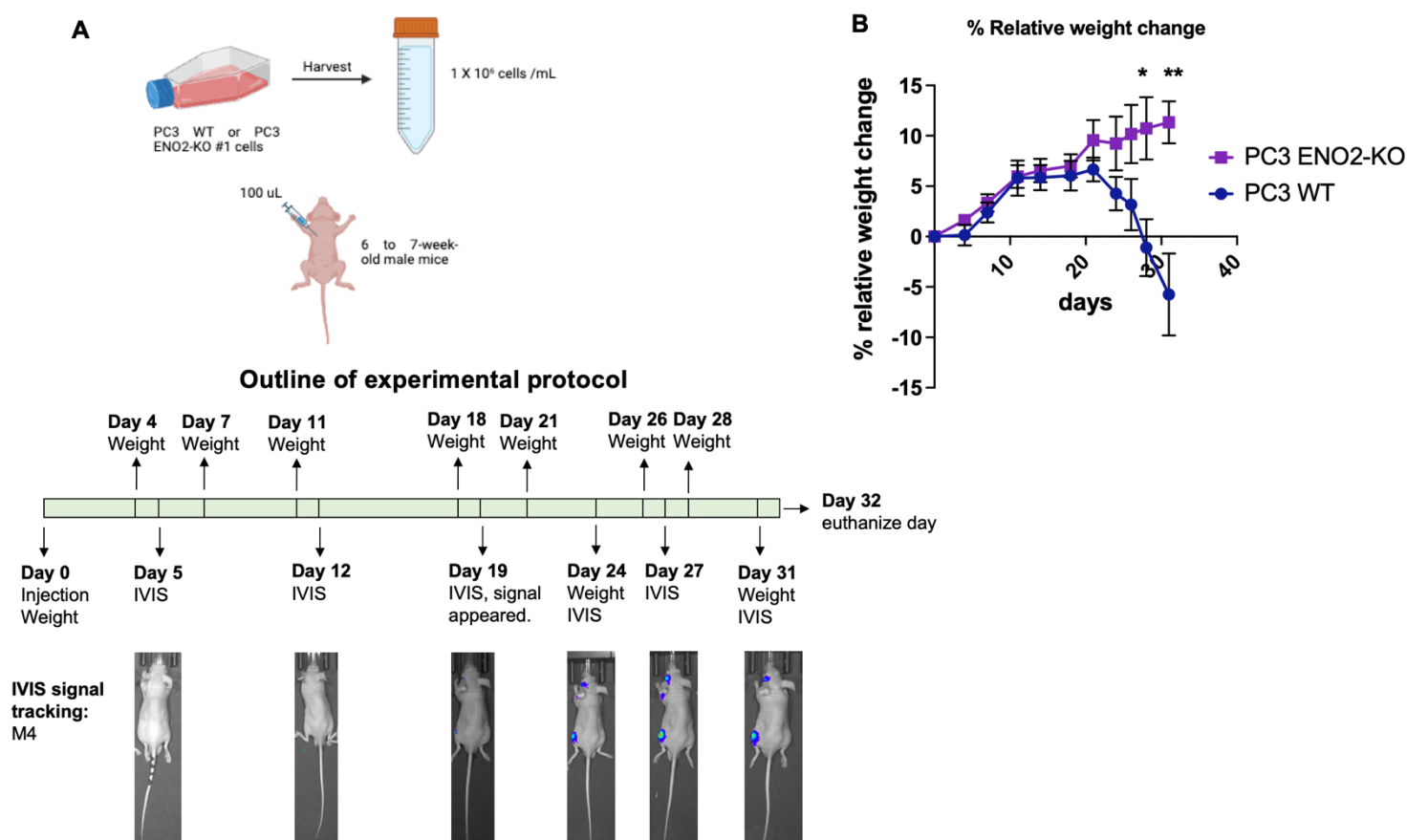


Figure 6.1 Outline of experimental setup and body weight measurement.

(A) Schematic of experimental design. PC3 WT and ENO2-KO #1 cells were harvested and then intracardially injected into 6 to 7-week-old male nude mice at day 0. The body weights of all mice were monitored at Day 0, Day 4, Day 7, Day 11, Day 18, Day 21, Day 24, Day 26, Day 18 and Day 31. Mice injected with PC3 WT cells were monitored by IVIS on Day 5, Day 12, Day 19, Day 24, Day 27 and Day 31 to track tumour development (mouse M4 as the representative). All mice were euthanized at Day 32

(B) The relative body weight changes (%) of the mice. The data are mean \pm standard deviation (n=8). Ordinary One- way ANOVA at each time point. *p<0.05, **p<0.01.

6.2.2 Genetically inhibition of ENO2 led to reduced tumour incidence in tibia after systemically administered in BALB/c nude mice

To investigate the effects of genetically inhibition of ENO2 on tumour metastasis in bone marrow, left tibias mice were dissected free of soft tissues, decalcified, sectioned and then H&E stained. Images were taken a DMRB microscope (Leica, Wetzlar, Germany) at 4x and 20x magnification with the Osteomeasure7 v4.2.0.1 (OsteoMetrics) software.

The incidence of tibia tumour was analyzed according to the histology analyzing results. The skeletal metastasis was identified in 5 of the 8 PC3 WT-injected mice left tibias (62.5%) in the BALB/c nude mice model, whilst there was no skeletal metastasis in the left tibias of mice injected with PC3 ENO2-KO cells (0%) ($P=0.007$) (**Figure 6.2** and **Figure 6.3 A**).

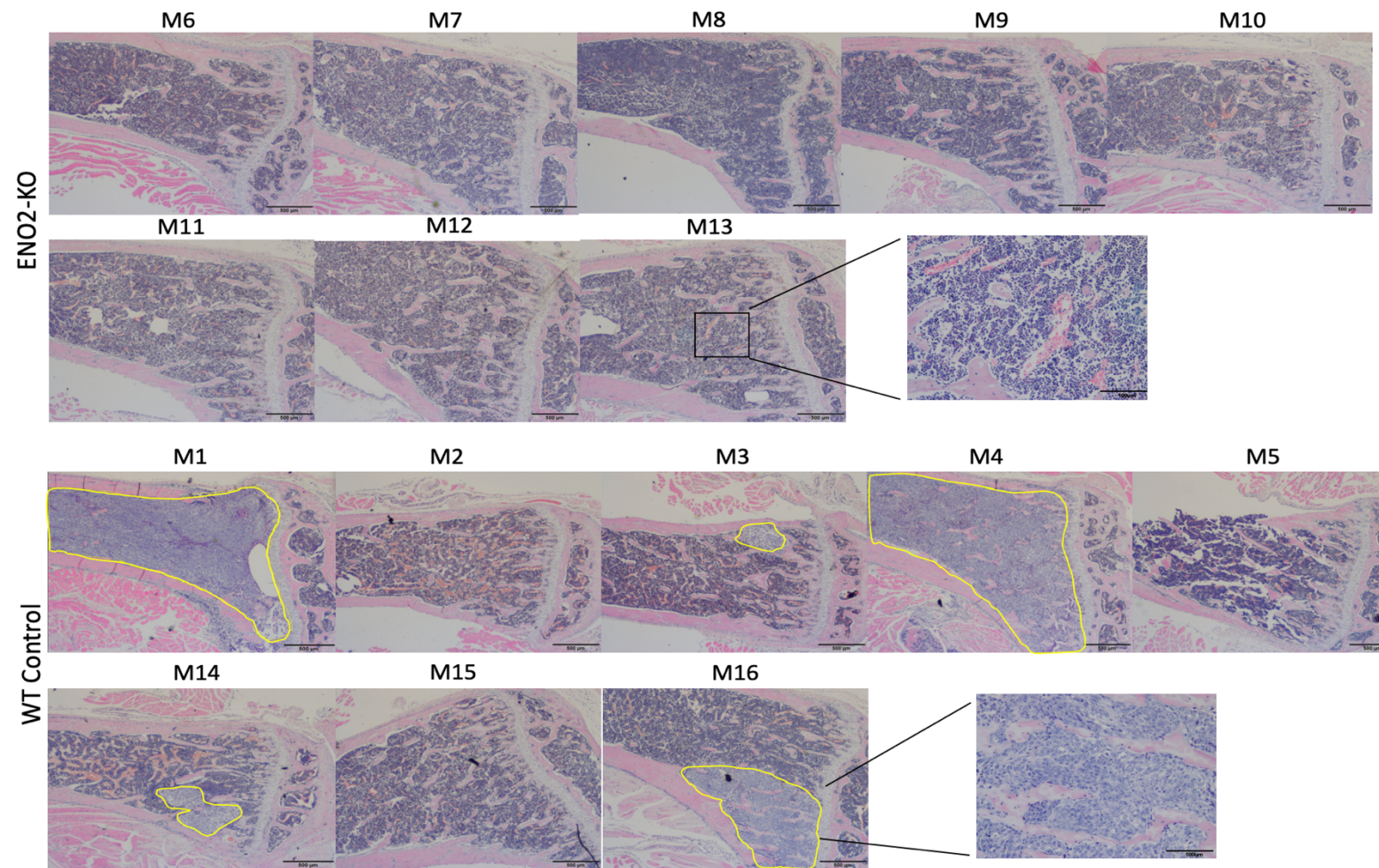


Figure 6.2 Sections of H&E stained decalcified left tibia form PC3 ENO2-KO and WT control injected mice.

The yellow circle represents the tumour area. Scale car =500um in M1 to M16. Scale bare = 100um in zoom in figures.

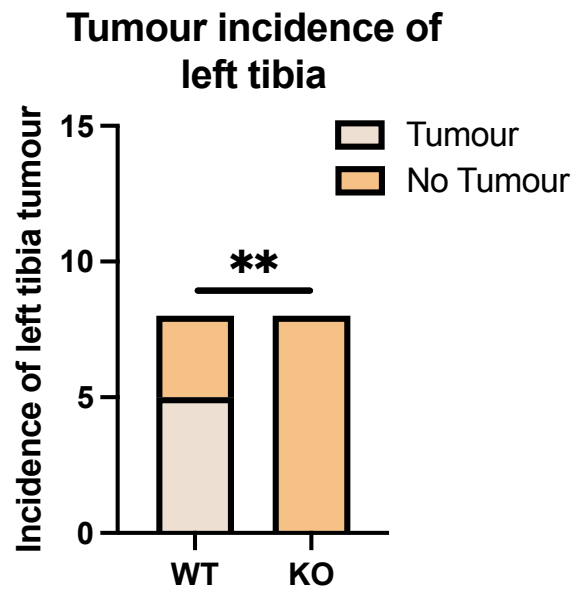


Figure 6.3 The incidence of tumour from left tibia in PC3 ENO2-KO and WT control injected mice.

The data are mean \pm standard deviation (n=8). Chi-square test, **p<0.01.

6.2.3 Genetic inhibition of ENO2 reduced tumour induced bone destruction in long bones of BALB/c nude mice, but does not affect bone morphometry

To understand the tumour induced bone destruction, micro-CT scanning was also used to examine bone morphometry in the metaphyseal region of tibias *ex vivo*.

Consistent with previous H&E staining results, the representative 3D model images confirmed that tumour induced more bone destruction in their tibia and femur in mice injected with PC3 WT cells compared to PC3 ENO2-KO injected mice (**Figure 6.4**). However, no significant differences had been shown after analysis of bone morphometry. Tibia and femur from mice injected with PC3 ENO2-KO cells had almost no increase in bone volume (% BV/TV) compared to the control group (tibia, WT, 7.744 ± 3.044 vs KO #1, 9.009 ± 2.643 ; $P = 0.3896$) (femur, WT, 10.190 ± 4.418 vs KO #1, 11.690 ± 1.918 ; $P = 0.3942$) (**Figure 6.5 A and B**). In addition, tibial and femoral trabecular separation (Tb. Sp) had also almost no reduction in KO groups compared with that in the WT groups (tibia, WT, 0.217 ± 0.149 vs KO #1, 0.158 ± 0.032 ; $P = 0.2871$) (femur, WT, 0.228 ± 0.130 vs KO #1, 0.150 ± 0.027 ; $P = 0.1216$) (**Figure 6.5 C and D**). Similarly, tibial and femoral trabecular number (Tb.N) in KO groups were barely increased compared with that in the WT groups (tibia, WT, 2.722 ± 1.033 vs KO #1, 3.066 ± 0.860 ; $P = 0.4812$) (femur, WT, 3.285 ± 1.500 vs KO #1, 3.838 ± 0.583 ; $P = 0.3471$) (**Figure 6.5 E and F**). Moreover, the trabecular pattern factor (Tb.Pf) of tibia and femur were also unchanged in KO group compared with the WT group (tibia, WT, 53.210 ± 19.060 vs KO #1, 40.810 ± 11.04 ; $P = 0.1337$) (femur, WT, 32.850 ± 16.140 vs KO #1, 27.990 ± 13.550 ; $P = 0.5245$) (**Figure 6.5 G and H**). Consistently, tibia and femur from mice injected with PC3 ENO2-KO cells had almost no changes in trabecular thickness (Tb.Th) compared to the control group (tibia, WT, 0.029 ± 0.003 vs KO #1, 0.029 ± 0.002 ; $P = 0.5397$) (femur, WT, 0.029 ± 0.003 vs KO #1, 0.029 ± 0.002 ; $P = 0.5397$) (**Figure 6.5 I and J**).

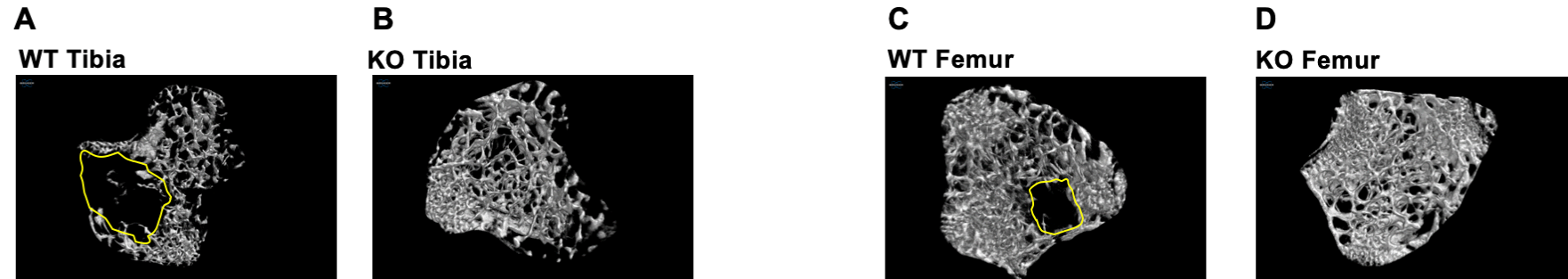


Figure 6.4 Representative 3D models of PC3 WT and ENO2-KO cells injected tumour-bearing and non-tumour bearing.

(A and B) tibia **(C and D)** femur. The Region of Interest (ROI) was selected as a region of 1mm in thickness, starting at 0.2mm from the lowest part of the growth plate from tibia and femur, respectively, with a resolution of 2016 x 1344 pixels, each pixel measuring 4.3 μm in size. 3D models were then built using the CTVol software based on ROIs.

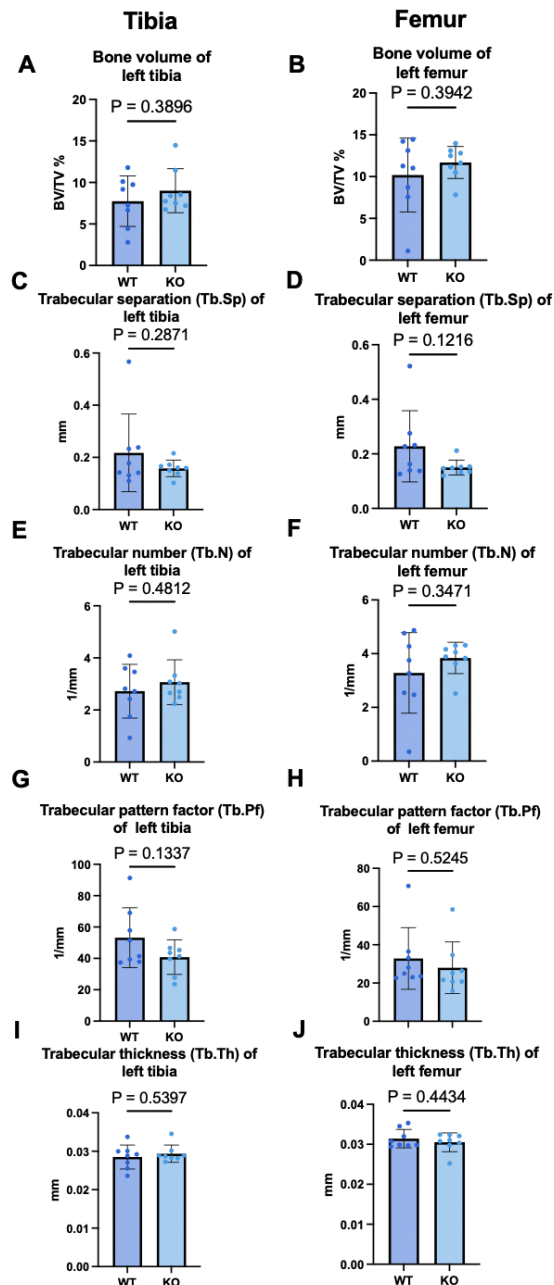


Figure 6.5 The effects of genetically inhibition of ENO2 on bone morphometry in BALB/c nude mice.

(A and B) Bone volume/tissue volume (BV/TV) % of trabecular bone in mice tibia and femur **(C and D)** Trabecular separation (Tb.Sp) in mice tibia and femur **(E and F)** Trabecular number (Tb.N) in mice tibia and femur **(G and H)** Trabecular pattern factor (Tb.Pf) in mice tibia and femur **(I and J)** Trabecular thickness (Tb.Th) in mice tibia and femur. The data are mean \pm standard deviation (n=8). Unpaired t-test.

6.3 Discussion

The evidence in Chapters 3 and 4 not only demonstrates that upregulation of ENO2 is associated with advanced PCa development in patients and metastatic potential in cell lines, but also demonstrates that loss of ENO2 expression decreased cell viability and motility *in vitro*, therefore potentially their metastatic behavior. In this chapter, human PCa PC3 cells with successful knockout of the ENO2 gene were introduced into immunocompromised mice via intracardiac injection into the left ventricle to investigate the effect of ENO2 inhibition on bone metastasis *in vivo*. The regular body weight of mice and IVIS were monitored to observe tumour development. In addition, Micro-CT and histology analysis were employed to study tumour induced bone destruction and tumour engraftment in the bone marrow, respectively.

Firstly, it was found that the relative weight of the control mice steadily decreased after day 21 following timely follow-up monitoring. But the relative weight of the mice in the treatment group increased steadily (**Figure 6.1 B**). The difference in relative weight change trends between the two groups of mice reflected the difference in tumour progression. The primary explanation for the persistent decline in the average body weight of the control mice is the progression and sustained expansion of tumour progression and metastases. In contrast, the continuous development in the average weight of the treatment mice is most likely due to the absence of tumour metastases. Following successful intracardiac injection, the tumour cells migrated through the left atrium and entered systemic circulation, eventually seeding in the bones where they further developed into metastatic lesions [243]. This process of tumour development was demonstrated by monitoring the bioluminescent signals in the control group. For example, luciferase signals in the left leg of the mice exhibited a gradual rise starting from the initial detection of the IVIS signal (day 19), reaching its peak at the final IVIS assessment (day 31). Luciferase signals were consistently observed in the left leg in 6 out of 8 mice throughout the study period (**Appendix Figure 8**). However, due to the absence of luciferase signals in the KO cells, the approach of using IVIS to track tumours and assess tumour size by bioluminescence was only used in the control

group because the PC3 WT cells injected in the control mice had been stably transfected with luciferase gene. To maintain consistency, this luciferase tagged PC3 WT cell line was used in the experiment which the predesigned CRISPR gRNA plasmid DNA was introduced to knock out the ENO2 gene. But the luciferase signal was lost along following the process of selection for single clones of KO cells. One possible explanation is that PC3 Luc WT cells had never been individually cloned, resulting in a mixed population with heterogeneity. Consequently, there may be cells within this population lacking the luciferase gene but have their ENO2 gene successfully CRISPR knocked out and subsequently survive the single clone selection process. Interestingly, these luc-negative cells appear to be more susceptible to CRISPR editing, leading to the occurrence of clones lacking luciferase signals for reasons yet to be fully understood.

In order to study the effect of *ENO2* gene inhibition on bone metastasis in bone marrow, H&E staining of decalcified tibia revealed that no overt tumours were observed in the left tibial bone marrow of 8 mice injected with PC3 ENO2-KO cells. And the skeletal metastases were observed in the bone marrow of the left tibia in five control mice injected with PC3 WT cells (**Figure 6.2 and 6.3**), instead of in 6 out of 8 mice as observed based on luciferase signals (**Appendix Figure 7**). It may be caused that the left tibia of the M5 mouse was accidentally broken during dissection, leading to a leakage of normal marrow and tumour cells from the bone marrow during the fixation and decalcification process. Alternatively, the IVIS signal may not in the tibia but came from the adjacent femur. Nonetheless, the incidence of bone metastases in the tibia of the two groups remained significantly different since no tumours were indeed observed in the tibia bone marrow of mice in the KO group. However, although interesting to investigate, due to the lack of overt tumours in the mice injected with KO cells, the changes in specific bone cells affected by KO tumours, especially osteoblasts and osteoclasts, cannot be examined using histomorphometry (e.g. TRAP staining). Notably, the results in **Chapter 5** are consistent with *in vivo* data that the absence of ENO2 significantly down-regulated the aggressiveness of PC3 cells including viability

and motility. Thus, disrupting ENO2 function may impair their migratory ability of cells, ultimately damage their ability to colonize bone tissue. Alternatively, it is possible that ENO2 KO cells are less viable in the bone microenvironment and therefore do not form metastases. Additionally, it is important to investigate whether ENO2 KO cells can enter the bone but remain dormant rather than form overt metastases. Dormancy is a well-known phenomenon in metastatic cancer, where DTCs can persist in a quiescent state for years before becoming active and proliferating [57, 74]. To distinguish whether the loss of ENO2 function in the metastatic microenvironment causes tumour cell dormancy or decreased viability, *in vitro* assays can be performed to examine the survival and proliferation rates of ENO2-KO clones under conditions that mimic the bone microenvironment, such as hypoxia, insufficient nutrient supply, or exposure to bone stored growth factors (e.g. TGF- β).

In order to investigate the effect of *ENO2* gene inhibition on bone destruction in PCa, micro-CT analysis of left tibia and femur was performed and revealed that changes in bone mass compared with the control group. Almost no change of BV/TV% and Tb.N had been observed in the KO group, confirming that ENO2 KO did not protect against bone destruction induced by WT cells (**Figure 6.5 A, B, E and F**) [162]. Furthermore, no difference in Tb.Th comparing between WT and KO could give the indication that the protection from bone destruction was via avoiding the reduction of the number but the thinning of trabecular (**Figure 6.5 I and J**) [162]. No reduction of Tb.Pf and Tb.Sp in the group injected with KO cells represented the unaffected well-connected trabecular bone tissue and trabecular bone volume, respectively (**Figure 6.5 C, D, G and H**) [247]. Combined with the previous histology, IVIS and micro-CT 3D model images (**Figure 6.3 and 6.4, Appendix Figure 7**), *ENO2* may act as a detrimental gene against PC3 tumour-induced bone destruction. Then combined with previous *in vitro* results (**Chapter 5**), the findings distinctly indicate that the absence of ENO2 leads to a notable reduction or complete absence of PC3 tumour colonization in bone, primarily attributed to compromised motility. The absence of ENO2 may impede the

ability of PCa tumour cells to establish colonies in bone, consequently obstructing the initiation of the RANKL/RANK-mediated vicious cycle within the bone microenvironment, leading to the absence of bone destruction. It is well known that although osteoblastic lesions are present in most patients with bone metastatic PCa, lytic lesion is the predominant lesion types in the PC3 intracardiac injection xenograft model [243, 244]. The vicious cycle was generated within the microenvironment where PCa tumour cells colonized, stimulating the proliferation and differentiation of osteoblasts which would secrete TGF- β and endothelin-1 to combining with RANKL to promote osteoclast activity in bone resorption [57, 248]. RANKL have been considered a key osteoclast factor, which cooperates with M-CSF to control osteoclast formation [78]. Whether ENO2 synergistically participates in RANKL-mediated osteolysis thereby promoting bone remodelling remains unknown. A recent bioinformatic analysis study showed that ENO2 as a biosynthesis of amino acids-related gene, was found to be upregulated in osteogenic differentiation as a DEG [249]. Another bioinformatics analysis confirmed that ENO2 is not only mechanosensitive, but its knockdown leads to changes in the expression of key DEGs that regulate osteoclast and osteoblast function [242]. Thus, it is crucial to conduct whole transcriptome studies to investigate the potential DEGs and pathways related to ENO2 to confirm they combine to regulate the PCa bone metastasis.

In exploring the role of ENO2 in bone metastasis, its function in cancer metabolism emerges as one of crucial factors. ENO2 is a glycolytic enzyme that plays a significant role in metabolism of tumour cells, particularly in highly glycolytic environments such as metastatic sites [108]. ENO2 has been positioned as a key player in the metabolic adaptation of cancer cells during the metastatic process [219]. Although the role of ENO2 in bone metastasis is still unclear, the bone microenvironment is rich in metabolic stressors, making ENO2 a key regulator in cancer cell adaptation to the bone metastatic microenvironment. The presence of GFP+ve cells in bone metastasis models could be used to trace ENO2-expressing or ENO2-KO cells and assess their metabolic behavior within the bone niche [250, 251]. ENO2-positive cells might present

elevated glycolytic activity, enabling cells to survive and proliferate under the hypoxic and insufficient nutrient conditions which observed in metastatic bone sites [89, 252]. The glycolytic advantage could support the metabolic flexibility of PCa cells, thereby maintaining their viability and proliferation in the bone microenvironment [88, 89]. Thus, combined with *in vitro* metabolic assays to measure glycolytic flux, such as the Seahorse assay, metabolic reprogramming in ENO2-KO cells would be examined. Additionally, transcriptomic and proteomic analyses could be used to identify whether other compensatory metabolic pathways are upregulated in the absence of ENO2, suggesting a potential adaptive mechanism to maintain metabolic homeostasis during bone colonization.

There are limitations in this study. First of all, PC3 cells do not express AR and are therefore insensitive to androgens [140]. In contrast, most of the PCa are initially androgen-dependent and only become resistant to castration as the disease progresses. Thus, the PC3 BALB/c mice model does not mimic all scenarios in PCa [253]. In addition, osteolytic lesion is the predominant lesion types in the PC3 intracardiac injection xenograft model. However, osteoblastic disease (30%) and mixed disease (44%) dominate PCa bone metastases, with only a minority of patients having predominantly osteolytic disease (14%) [254]. Another important aspect that cannot be ignored is that the athymic immunodeficient BALB/c strain of mice used in this study lacks adaptive immunity due to their inability to produce T cells [255]. It may result in an inability to better integrate the results into the clinic. Indeed, to determine the effects of ENO2-KO on circulating immune cells in PC3 intracardiac injection xenograft model, blood serum from BALB/c mice have been analyzed using a hematology analyzer (scil Vet abc Plus+, Horiba Medical). The total number of white blood cells, red blood cells, platelets, lymphocytes and granulocyte counts in the two groups showed different trends, although there was no significant difference (**Appendix Figure 8**). However, with these results, we could not draw a conclusion that KO and WT tumours affect the immune system in a similar manner. Moreover, no overt tumours were detected within the bone marrow of eight mice injected with PC3

ENO2-KO cells. In addition to the possible consequence of reduced arrival/seeding of tumour cells in bone marrow due to impaired motility after knocking out ENO2, there are other possibilities that has yet not been explored. Given that the viability and proliferation of PCa cells *in vitro* were significantly reduced in ENO2 KO PCa cells (**Chapter 5**), ENO2 deletion may promote tumour cells to enter a quiescent state, potentially inducing cellular dormancy. To clarify this question, a further *in vivo* experiment, using a combined technique of Vybrant DiD PCa cell staining and multiphoton microscopy, should be adopted to quantify and compare the number of dormant WT and KO PCa arrived in bone marrow [73]. The potential induction of dormancy in PCa cells due to ENO2 knockout. Besides, the cells were injected into the left ventricle of the mouse via intracardiac injection, bypassing the pulmonary circulation and eventually colonized in the bone to achieve the best simulation of the entire dissemination process [256]. However, mis-injection were usually occurred because of the tiny target of the left ventricle. It has been determined through IVIS imaging that mice in the PC3 WT-Luc group did not have such a problem. However, since there was no luciferase signal, the presence of lung tumours caused by mis-injection in mice injected with KO cells can only be determined by opening the chest during dissection. No obvious thoracic tumours were observed through visual inspection.

6.4 Conclusion

In summary, the results from this chapter confirmed that ENO2 indeed plays an essential role and positively contributes to the PCa bone metastasis *in vivo*. Therefore, the further RNA-Seq and bioinformatic analysis will be carried out to determine how ENO2 associates with other factors to regulate PCa development, especially bone metastasis.

Chapter 7: Evaluation of the Role of ENO2 in Prostate Cancer Developments using RNA Sequencing

7.1 Introduction

ENO2 has been developed as a reliable biomarker applying in diagnosis and prognosis of neuroendocrine of poorly differentiated neuroendocrine tumours across various cancer types [113]. Although its primary expression occurs in neuronal and neuroendocrine cells, ENO2 has also been identified in non-neuronal and non-neuroendocrine tissues or cells, including the prostate [115]. In addition, the important enzyme NSE encoded by *ENO2* serves as the penultimate step in the aerobic glycolysis pathway, operating in both normal tissues and malignant tumour cells [257]. Given its significant involvement in anaerobic glycolysis, there is no doubt that the *ENO2* gene plays a crucial role in driving accelerated glycolysis in cancer cells, thereby contributing to tumour progression, including metastasis. Previous bioinformatics, *in vitro* and *in vivo* results confirmed that ENO2 indeed plays an essential role in the PCa malignant development and bone metastasis. Another gene expression profile research using RNA-seq dataset sourced from the TCGA suggested that high ENO2 expression was associated with castration resistance and neuroendocrine progression in PCa, indicating a significant diagnostic utility in distinguishing between benign and malignant disease [258]. However, no studies have demonstrated how loss of ENO2 at the genetic level affects the development of PCa.

In this chapter, whole transcriptome RNA sequencing was conducted at Source Genomics and data analysis was then processed using Galaxy version 23.1 (<https://usegalaxy.eu/>). The analysis was based on PC3 WT and ENO2-KO, 22Rv1 WT and ENO2-KO cells with 3 biological repeats of WT cells, 2 single clones from KO cells, to identify the potential DEGs and the enriched processes, functions and regulated pathways connected with ENO2. Subsequently, the commonly regulated DEGs in the two genetically modified cell lines were explored to determine and cross verify signalings/pathways key to the effects of ENO2 deficiency on diverse types of PCa cells.

7.2 Results

7.2.1 ENO2-KO induces widespread gene dysregulations and altered oncogenic expression pathways in human PCa cells

Firstly, the potential DEGs has been verified by conducting the Differential expression analysis between WT and ENO2-KO clones of PC3 and 22Rv1 cells using limma-voom and ggplot2 [167, 168]. The WT and ENO2-KO clones from PC3 and 22Rv1 cells would be distinguished along the leading logFC dimensions using the MDS plot (**Figure 7.1 A and B**). The distribution distance among point corresponding to each WT and KO samples represented the separation between samples. The total of 13839 and 14790 differential expression counts were screened in PC3 and 22Rv1 ENO2-KO clones after performing RNA-Seq. Subsequently, bioinformatic analyses identified 776 and 342 DEGs when ENO2 was knocked out in PC3 and 22Rv1 cells (adjusted $p < 0.05$, $\text{Log}_2\text{FC} \geq 0.58$) (**Appendix Table 7 and 8**). These include 327 significantly upregulated and 449 downregulated genes in the PC3 ENO2-KO cells, while 72 upregulated and 270 downregulated genes were found to be significantly changed in the 22Rv1 ENO2-KO cells (**Figure 7.1 C and D**). Interestingly, the top-10 DEGs between WT and ENO2-KO were totally different in PC3 and 22Rv1 cells and marked in heatmaps where identified genes show opposite expression tendencies comparing between the WT and KO groups (**Figure 7.1 E and F**). Consistently, no similar DEGs were observed in the ENO2-KO PC3 and 22Rv1 cell lines after expanding the range from top-10 to top-20 (**Table 7.1 and Table 7.2**).

Subsequently, GO enrichment analysis was established to enrich 776 and 342 DEGs in biological processes (BP) and molecular functions (MF) in PC3 and 22RV1 cells after ENO2 knockout [169]. Interestingly, DEGs in PC3 ENO2-KO cells were mainly enriched in cellular behavior regulation and nervous system at the level of BP, including cell motility, adhesion, migration, neurogenesis, neuron projection guidance and nervous system development (**Figure 7.2 A**). In contrast, the DEGs from 22Rv1 ENO2-KO cells were contributed to a variety of metabolic activities, including regulation of hormone levels, hormone metabolic process, organic hydroxy compound metabolic process, alcohol metabolic process and primary alcohol metabolic process

(Figure 7.2 B). At the level of MF, the DEGs from both PC3 and 22Rv1 ENO2-KO cells were enriched in receptor ligand activity, signalling receptor activator activity, signalling receptor activity, molecular transducer activity and signalling receptor regulator activity **(Figure 7.2 C and D).**

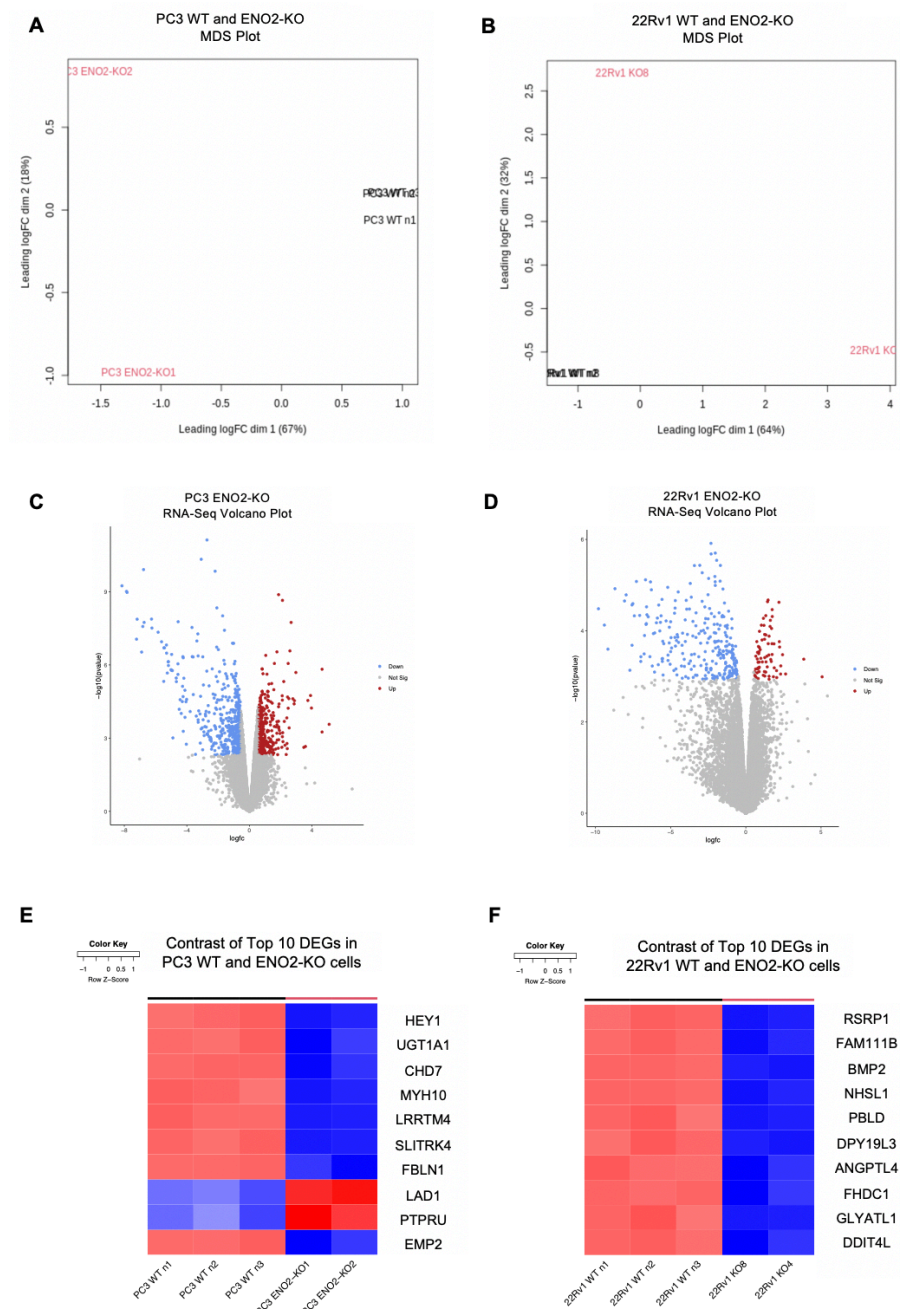


Figure 7.1 RNA-Seq analysis showed genes that are differentially expressed in PC3 and 22Rv1 cells after ENO2 knockout.

(A and B) MDS plots showing separation of WT and ENO2-KO samples of PC3 and 22Rv1 cells **(C and D)** The volcano plots showed that 776 and 342 DEGs were identified in PC3 and 22Rv1 cells after ENO2 knockout, respectively **(E and F)** The heat maps showed top-10 DEGs between WT and ENO2-KO in PC3 and 22Rv1 cells (decreased expression (blue) increased expression (red)). LogFC ≥ 0.58 (1.5-fold change), $-\log_{10}(\text{P value}) < 0.05$.

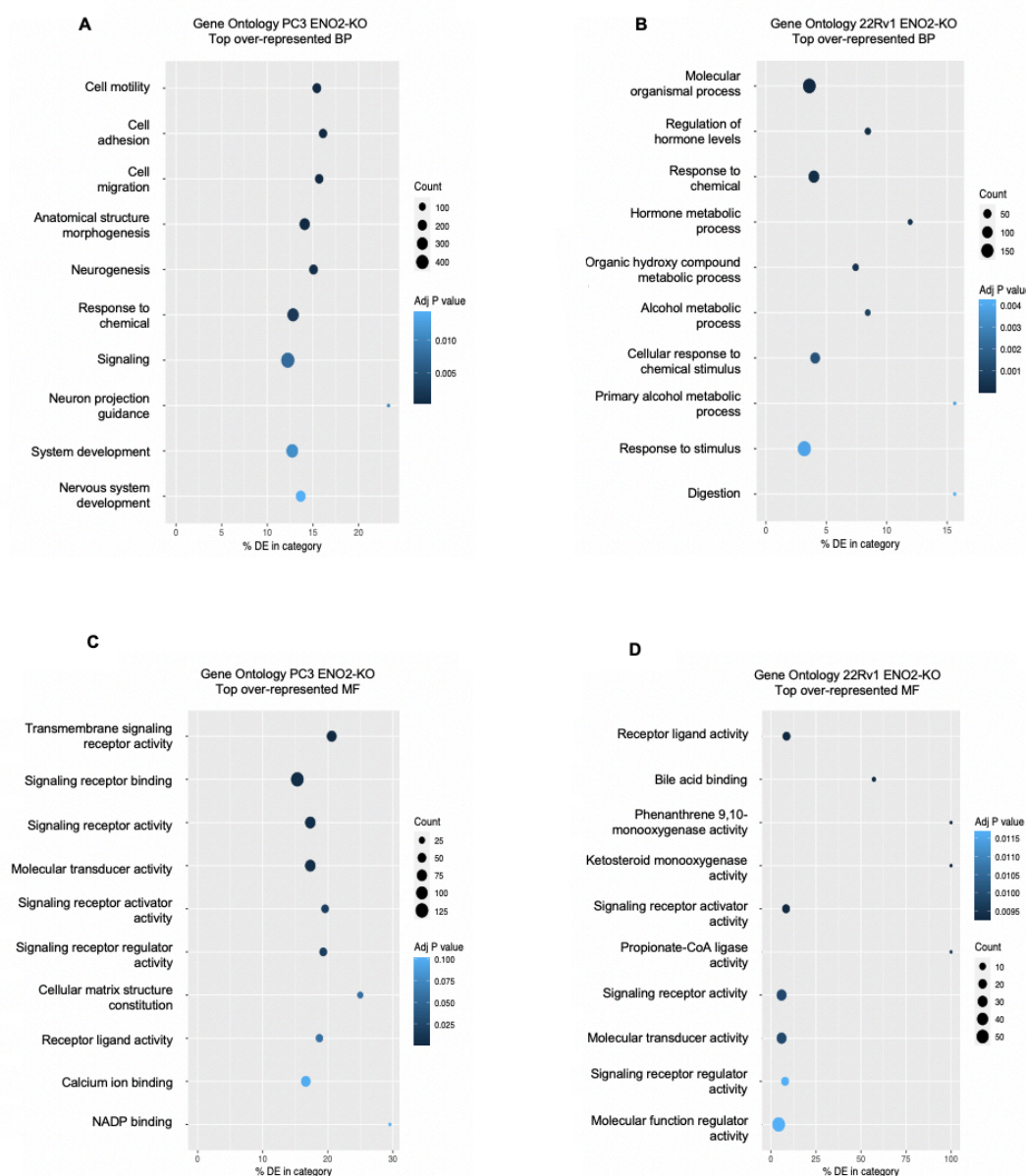


Figure 7.2 RNA-Seq analysis showed GO pathway enrichment of PC3 and 22Rv1 cells after ENO2 knockout.

(A and B) Top-10 significantly enriched GO terms of BP in PC3 and 22Rv1 cells after ENO2 knockout **(C and D)** Top-10 significantly enriched GO terms of MF in PC3 and 22Rv1 cells after ENO2 knockout. The size of the circle corresponds to the number of genes observed in a pathway. $\text{LogFC} \geq 0.58$ (1.5-fold change), $-\log_{10}(\text{P value}) < 0.05$.

Table 7.1 The information of top 20 DEGs in PC3 ENO2-KO cells.

Gene	logFC	AveExpr	P.Value	adj.P.Val
HEY1	-2.7149123	6.05901619	7.55E-12	1.04E-07
UGT1A1	-3.0847778	5.38008432	4.68E-11	3.24E-07
CHD7	-6.7680005	3.08262955	1.23E-10	4.97E-07
MYH10	-2.1954359	5.62893917	1.44E-10	4.97E-07
LRRTM4	-8.1523882	-0.6539521	5.71E-10	1.58E-06
SLITRK4	-7.8610357	-0.8225181	9.66E-10	2.11E-06
FBLN1	-7.8225331	1.36590297	1.07E-09	2.11E-06
LAD1	1.86341496	4.50503478	1.31E-09	2.27E-06
PTPRU	2.11184916	4.48651491	2.25E-09	3.47E-06
EMP2	-2.0844103	4.46081279	4.59E-09	6.35E-06
MCC	-1.7128003	4.7085362	9.74E-09	1.22E-05
TCEA3	-6.2588635	1.04530365	1.32E-08	1.43E-05
LINC00632	-7.1817445	-1.2428711	1.34E-08	1.43E-05
GATA2	-4.5571249	2.24779439	1.69E-08	1.57E-05
PTK7	-6.7355577	1.04400969	1.80E-08	1.57E-05
FNDC10	2.66456426	1.63649237	1.81E-08	1.57E-05
CDR1	-6.8193678	-0.6635401	2.65E-08	2.16E-05
DSP	-3.6737941	2.30759395	2.91E-08	2.24E-05
PRLR	-6.2348156	0.13709543	3.08E-08	2.24E-05
GPC1	-1.5982162	5.51912912	3.80E-08	2.63E-05

Table 7.2 The information of top 20 DEGs in 22Rv1 ENO2-KO cells.

Gene	logFC	AveExpr	P.Value	adj.P.Val
RSRP1	-2.318669	6.567124	1.22E-06	0.007965
FAM111B	-2.033609	8.932656	1.99E-06	0.007965
BMP2	-2.308941	5.366225	2.08E-06	0.007965
NHSL1	-1.940023	5.982227	2.87E-06	0.007965
PBLD	-3.062923	5.210405	3.69E-06	0.007965
DPY19L3	-1.691309	6.956596	3.71E-06	0.007965
ANGPTL4	-3.419021	6.402753	3.74E-06	0.007965
FHDC1	-2.900337	7.188832	5.37E-06	0.008457
GLYATL1	-2.058432	5.603154	6.48E-06	0.008457
DDIT4L	-2.471672	5.332748	7.16E-06	0.008457
DPP4	-6.671243	1.606954	7.66E-06	0.008457
PER2	-1.709323	6.504502	8.20E-06	0.008457
FGL1	-7.275582	0.315468	8.33E-06	0.008457
SMPDL3A	-2.041848	6.086251	8.46E-06	0.008457
KCNK17	-6.338163	1.128516	8.51E-06	0.008457
C1QL4	-3.694145	3.030663	9.19E-06	0.00856
KLK2	-2.03223	5.536553	1.02E-05	0.008939
EDIL3	-5.192836	1.889691	1.12E-05	0.009011
TMLHE	-8.702031	-0.803055	1.20E-05	0.009011
RPS6KA3	-1.521506	6.62971	1.22E-05	0.009011

7.2.2 Potential key DEGs played essential roles in regulating tumour-related and metabolic pathways

To further identify enriched pathways of these DEGs, GSEA was conducted to perform the pathway enrichment analysis by using fgsea [259]. The results revealed that top-20 enriched hallmarks in both PC3 and 22Rv1 cells following ENO2 knockout (**Figure 7.3 A and 7.4 A**). Interestingly, several hallmarks were concurrently enriched in both PC3 and 22Rv1 cells following ENO2 knockout with significant difference ($p < 0.05$). Specifically, the E2F pathway ($P = 0.045$ in PC3 and $P = 0.023$ in 22Rv1) (**Figure 7.3 B and Figure 7.4 B**), adipogenesis ($P = 0.045$ in PC3 and $P = 0.0071$ in 22Rv1) (**Figure 7.3 C and Figure 7.4 C**), G2M checkpoint ($P = 0.045$ in PC3 and $P = 0.023$ in 22Rv1) (**Figure 7.3 D and Figure 7.4 D**), apoptosis ($P = 0.045$ in PC3 and $P = 0.023$ in 22Rv1) (**Figure 7.3 E and Figure 7.4 E**) and coagulation ($P = 0.045$ in PC3 and $P = 0.0071$ in 22Rv1) (**Figure 7.3 F and Figure 7.4 F**) were significantly enriched post-ENO2 knockout in both cell lines. Notably, the levels of adipogenesis (**Figure 7.3 C and Figure 7.4 C**), apoptosis (**Figure 7.3 E and Figure 7.4 E**) and coagulation (**Figure 7.3 F and Figure 7.4 F**) exhibited opposite regulation patterns in PC3 and 22Rv1 cells post-ENO2 knockout. In addition, there were also other co-enriched hallmarks in both PC3 and 22Rv1 cells following ENO2 knockout, including MYC targets, estrogen response and bile acid metabolism, but no significant difference between them ($p > 0.05$). Besides, there were other hallmarks which were enriched in PC3 and 22Rv1 after ENO2 deletion. For example, DNA repair ($P = 0.045$), IL2/STAT5 signalling pathway ($P = 0.045$), P53 signalling pathway ($P = 0.052$), EMT ($P = 0.1$), hypoxia ($P = 0.2$), PI3K/AKT/MTOR signaling pathway ($P = 0.3$) and MYC target v1 ($P = 0.3$) were all up-regulated in PC3 ENO2-KO cells, suggesting a potential correlation between ENO2 and tumour progression in PC3 cells (**Supplementary Figure 9**). Moreover, glycolysis ($P = 0.0071$), KRAS signaling pathway ($P = 0.0071$) and androgen response ($P = 0.0071$) were all down-regulated, but MYC target v2 ($P = 0.094$) was up-regulated in 22Rv1 ENO2-KO cells, indicating the correlation between ENO2 as well as tumour progression and metabolism in 22Rv1 cells (**Supplementary Figure 10**).

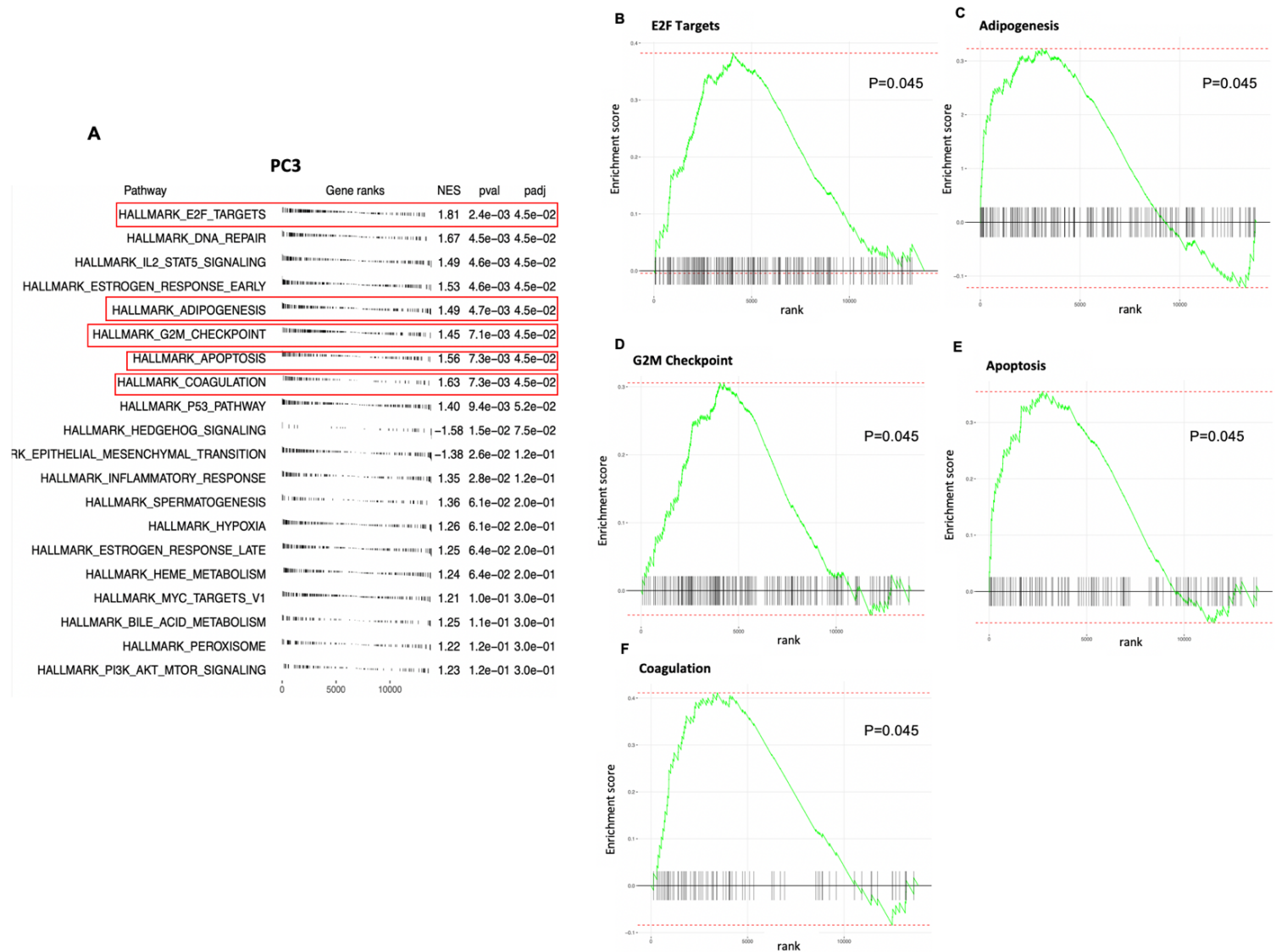


Figure 7.3 GSEA results showed co-enriched hallmarks and pathways with 22Rv1 cells in PC3 cells after ENO2 knockout.

(A) The top-20 enriched hallmarks in PC3 ENO2-KO cells. The separated hallmarks that known as (B) E2F targets, (C) Adipogenesis, (D) G2M checkpoint, (E) Apoptosis and (F) Coagulation are enriched in PC3 cells and co-enriched with 22Rv1 cells after ENO2 knockout with significant difference ($p < 0.05$). The p values are represented on the figure.

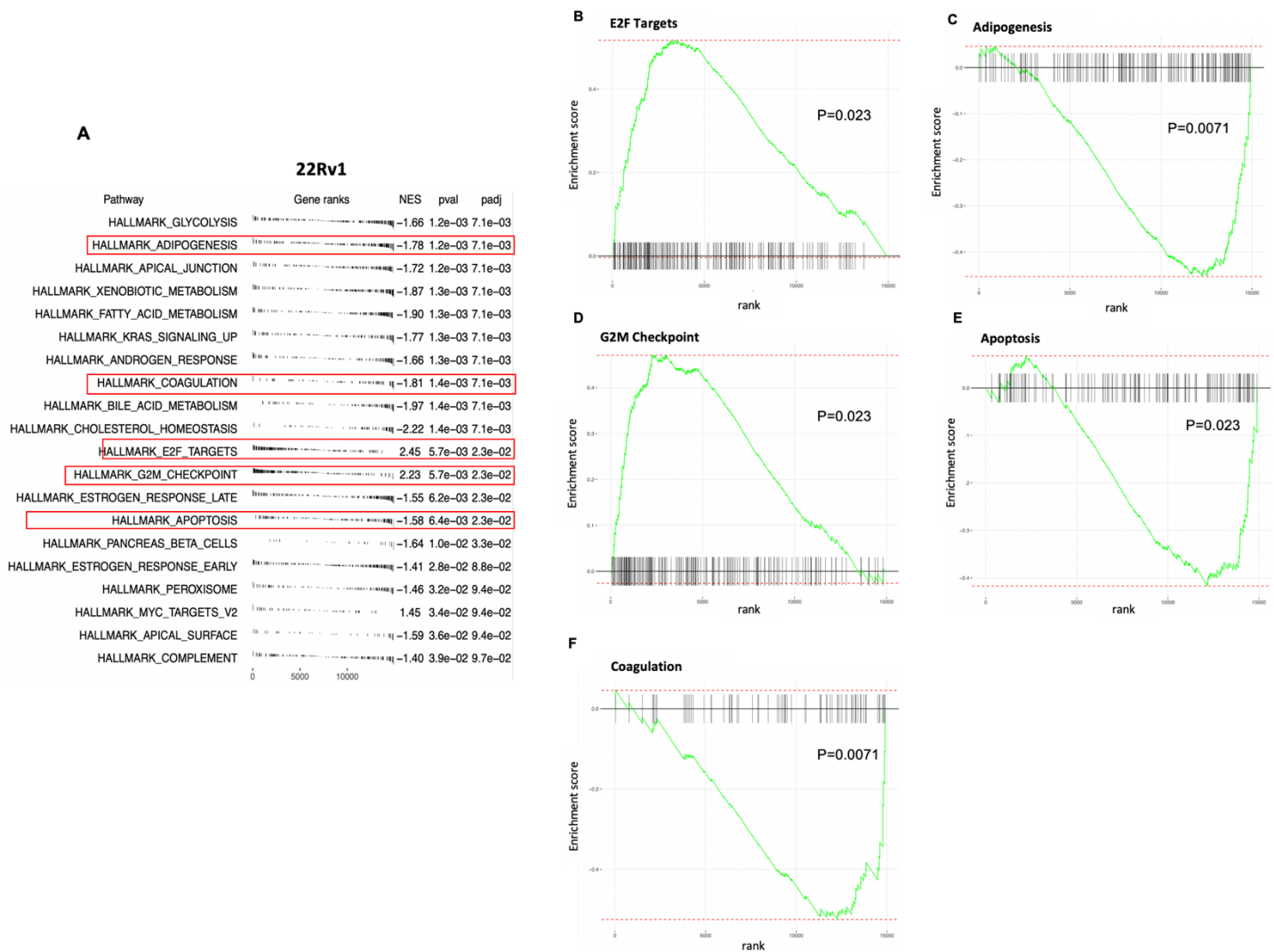


Figure 7.4 GSEA results showed co-enriched hallmarks and pathways with PC3 cells in 22Rv1 cells after ENO2 knockout.

(A) The top-20 enriched hallmarks in 22Rv1 ENO2-KO cells. The separated hallmarks that known as **(B)** E2F targets, **(C)** Adipogenesis, **(D)** G2M checkpoint, **(E)** Apoptosis and **(F)** Coagulation are enriched in 22Rv1 cells and co-enriched with PC3 cells after ENO2 knockout with significant difference ($p < 0.05$). The p values are represented on the figure.

7.2.3 Co-dysregulated DEGs in PC3 and 22Rv1 cells after ENO2-KO

To characterize the commonly up- or down-regulated DEGs in the two genetically modified cell lines, Venn diagram was generated Bioinformatics & Evolutionary Genomics (<https://bioinformatics.psb.ugent.be/webtools/Venn/>). DAZ-Associated Protein 2 (DAZAP2) is the only DEG co-upregulated in PC3 and 22R1 cells after ENO2 depletion (**Figure 7.5 A and C**). Besides, there are 17 DEGs that are jointly down-regulated in PC3 and 22R1 cells after ENO2 knockout (**Figure 7.5 B and D**). Subsequently, STRING database (<https://string-db.org/>) was used to generate a PPI network image to investigate whether there are interactions between these 18 jointly up-regulated or down-regulated DEGs. Except for the interaction between *TRPC3* and *ANK3*, there are almost no reported interactions between the other 16 DEGs (medium confidence (0.4)) (**Figure 7.6 A**). Additionally, PANTHER (<https://www.pantherdb.org/>) was used to generate a pie chart to observe the main molecular functional classification of the 18 DEGs. It indicated that over a quarter of the 18 DEGs were associated with catalytic activity in terms of molecular function, implying a potential link between these genes and metabolic processes. Additionally, these genes exhibited enrichment in various other molecular functions including binding, molecular adaptor activity, molecular function regulator activity, structural molecule activity and transporter activity (**Figure 7.6 B**). Finally, DAVID Functional Annotation Bioinformatics Analysis (<https://david.ncifcrf.gov/>) was performed to explore functional relationship of the 18 DEGs [260]. *CAT* and *ACSS1* were found to be enriched in the glyoxylate and dicarboxylate metabolism pathway according to the KEGG_PATHWAY database. And *RANBP3L* and *ID3* were enriched in the negative regulation of osteoblast differentiation pathway based on GO_PATHWAY analysis. Subsequently, *PER2* and *ID3* exhibited enrichment in the circadian regulation of gene expression pathway according to GO_PATHWAY analysis. *IL1R1* and *AHSG* were enriched in the regulation of inflammatory response pathway based on GO_PATHWAY analysis (**Figure 7.6 C**).

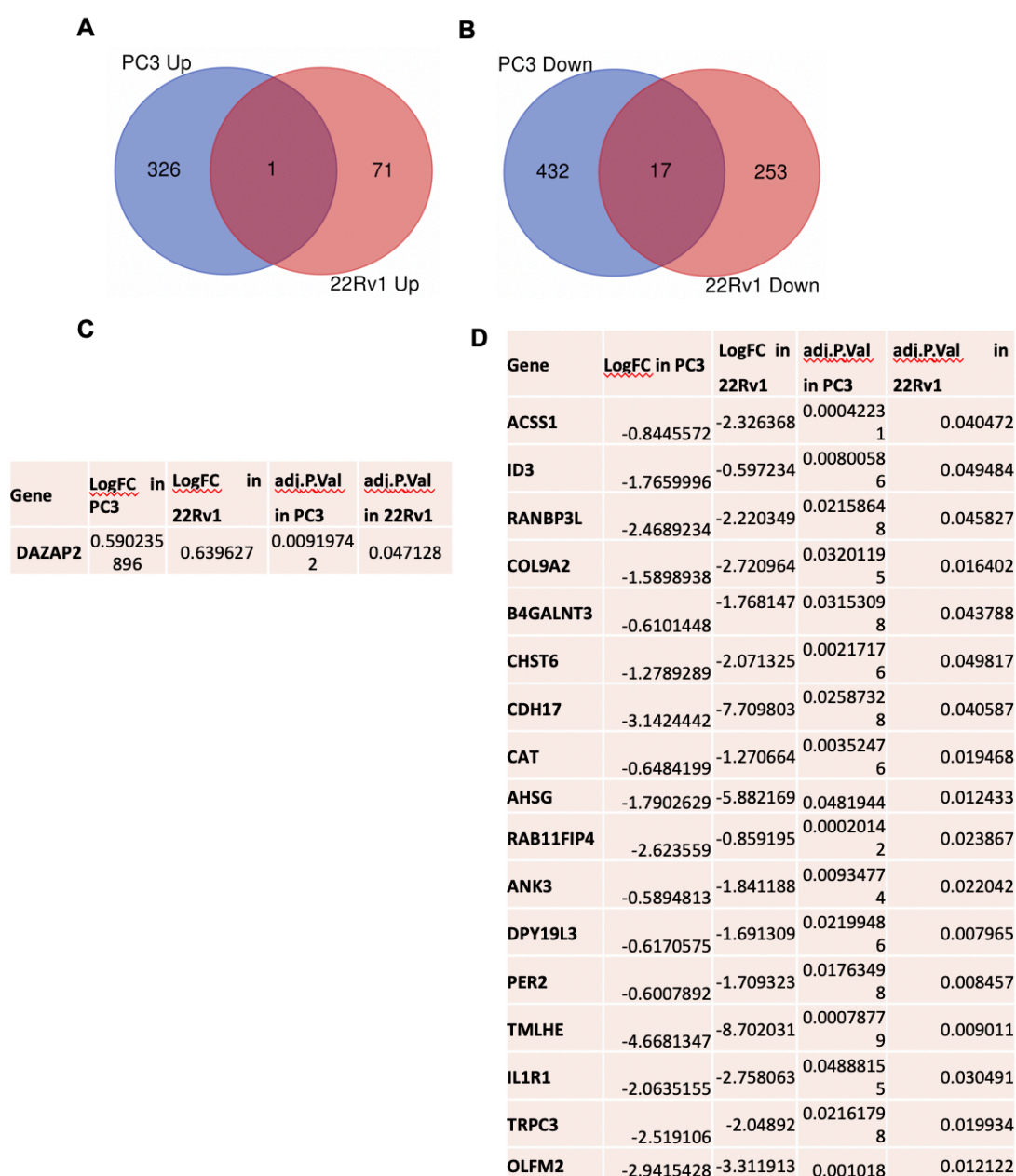


Figure 7.5 RNA-Seq analysis showed the commonly regulated DEGs in PC3 and 22Rv1 cells after ENO2 knockout.

(A and B) Venn diagram presented the DEGs that are commonly up- or down-regulated in PC3 and 22Rv1 cells after ENO2 knockout **(C and D)** Detailed information includes Log FC and p-values of these commonly up- or down-regulated DEGs in PC3 and 22Rv1 cells after ENO2 knockout, respectively.

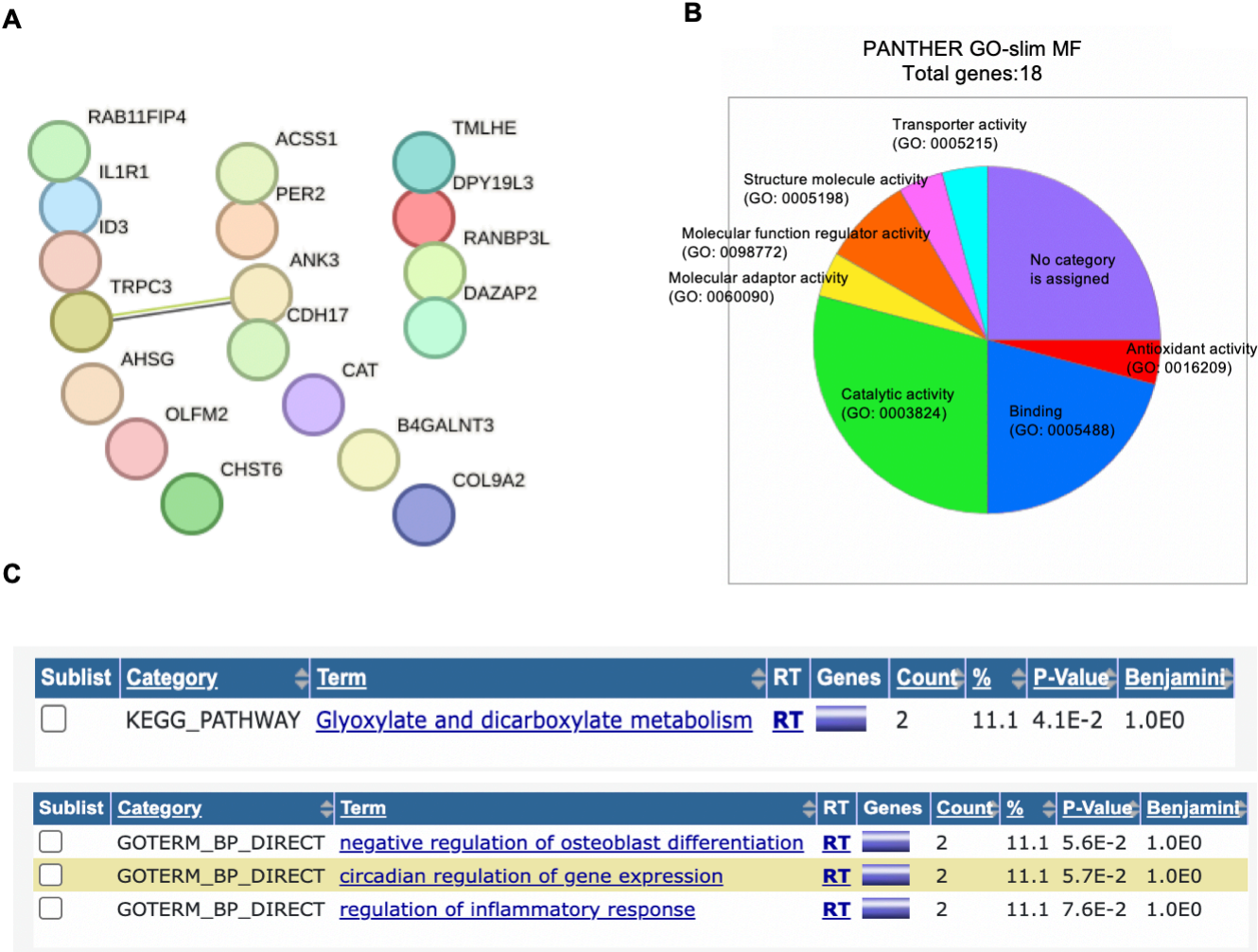


Figure 7.6 RNA-Seq analysis showed the integrations and functional classification of the commonly regulated DEGs in PC3 and 22Rv1 cells after ENO2 knockout.

(A) The PPI network for interactions of the 18 DEGs found in STRING database (0.4 confidence) **(B)** The pie chart for functional classification of the the 18 DEGs found in PANTHER database **(C)** The KEGG and GO enrichment pathways of the 18 DEGs performed by using DAVID Functional Annotation Bioinformatics Analysis.

7.2.4 Verification of co-dysregulated DEGs using retrospective analysis

To validate the total 18 of commonly up- or down-regulated DEGs in the two genetically modified cell lines, retrospective analysis on NCBI GEO dataset (GDS3289) was performed to understand the potential correlation of these genes with PCa progression in clinical samples [201]. The results indicated that six of the DEGs showed significant correlations with the development of PCa. It was observed that the expression of DAZAP2, the only commonly upregulated gene in both PC3 and 22Rv1 cells after ENO2 knockout, is negatively associated with the development of PCa at the transcriptome level (benign prostate tissue 0.2222 ± 0.2460 vs. localized PCa -0.0752 ± 0.2122 , $P= 0.0001$; benign prostate tissue 0.2222 ± 0.2460 vs. metastatic PCa -0.1065 ± 0.3913 , $P= 0.0002$) (**Figure 7.7 A**). In addition, ACSS1, which was down-regulated after ENO2 deprivation, positively associated with the development of PCa at the transcriptome level (benign prostate tissue -0.2504 ± 0.3349 vs. localized PCa 0.0297 ± 0.1617 , $P= 0.0009$; benign prostate tissue -0.2504 ± 0.3349 vs. metastatic PCa 0.1002 ± 0.4009 , $P= 0.0003$) (**Figure 7.7 B**). Interestingly, TMLHE, which was down-regulated after ENO2 deprivation, has a similar expression pattern as ENO2 (**Figure 3.4 B**). It exhibited a significant up-regulation in metastatic PCa compared to primary PCa at the transcriptomic level (localized PCa -0.1349 ± 0.1602 vs. metastatic PCa 0.0226 ± 0.2267 , $P= 0.04$). The expression level of TMLHE in benign prostate tissue was also higher than that in localized and metastatic PCa (benign prostate tissue 0.1722 ± 0.2250 vs. localized PCa -0.1349 ± 0.1602 , $P< 0.0001$; benign prostate tissue 0.1722 ± 0.2250 vs. metastatic PCa 0.0226 ± 0.2267 , $P= 0.0476$) (**Figure 7.7 C**). The expression of CAT had a similar trend as TMLHE but the difference in metastatic PCa vs primary PCa was not significant (benign prostate tissue 0.0858 ± 0.2020 vs. localized PCa -0.0587 ± 0.1632 , $P= 0.0374$) (**Figure 7.7 D**). Furthermore, CDH17, which was down-regulated after ENO2 knockout, exhibited a significant up-regulation in metastatic PCa compared to benign prostate tissue and localized PCa at the transcriptomic level (benign prostate tissue -0.0070 ± 0.1904 vs. metastatic PCa 0.2144 ± 0.3269 , $P= 0.0071$; localized PCa -0.0087 ± 0.1832 vs. metastatic PCa 0.2144 ± 0.3269 , $P= 0.047$) (**Figure 7.7 E**). In contrast to CDH17, AHSG was gradually

downregulated along with the development of PCa at the transcriptome level (benign prostate tissue 0.2407 ± 0.5379 vs. metastatic PCa -0.3412 ± 0.3432 , $P < 0.0001$; localized PCa 0.0575 ± 0.4560 vs. metastatic PCa -0.3412 ± 0.3432 , $P = 0.0116$) (**Figure 7.7 F**).

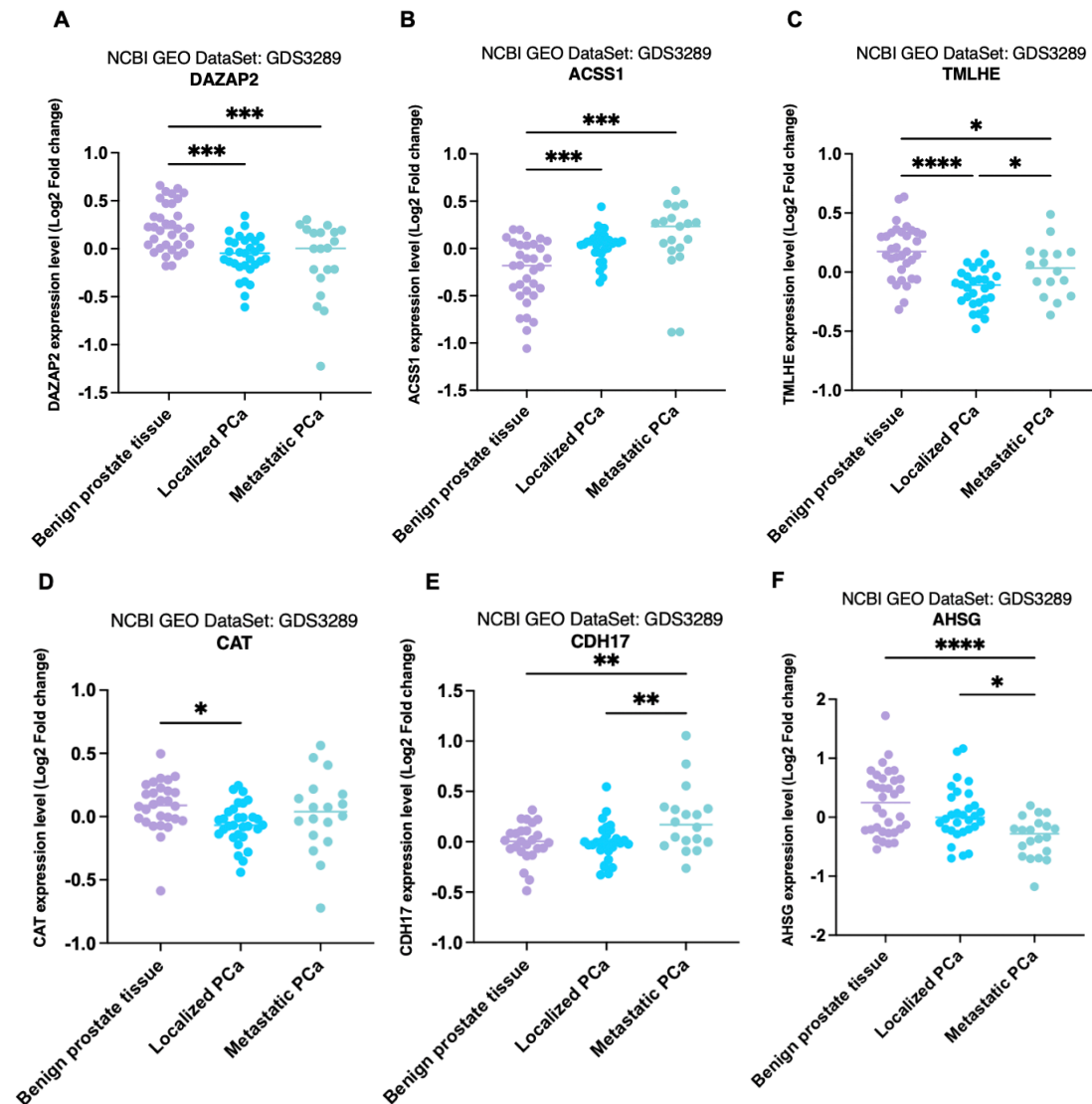


Figure 7.7 Retrospective studies indicated that 6 of the co-dysregulated DEGs after ENO2-KO showed correlations with the development of PCa.

An analysis using Gene Expression Omnibus databases with accession number GDS3289. Gene expression **(A)** DAZAP2, **(B)** ACSS1, **(C)** TMLHE, **(D)** CAT, **(E)** CDH17, and **(F)** AHSG were quantitatively compared among benign prostate tissue (n=34), primary PCa (n=31), and metastatic PCa (n=20) patient samples. Expression values are presented as log2 fold change. Each dot represents individual patient sample. p-values were determined using ordinary One-way ANOVA with multiple comparisons. *p<0.05, **p<0.01, ***p<0.001, ****p<0.0001.

7.3 Discussion

The evidence from previous Chapters not only demonstrates that upregulation of ENO2 is associated with advanced PCa development in patients and metastatic potential in cell lines, but also verified that loss of ENO2 expression reduced its metastatic behavior *in vitro* and the occurrence of bone tumours *in vivo*. Thus, it would be crucial to combine dry laboratory, genetic level experiments with previous wet studies to verify its impact on PCa progression, especially bone metastasis. In this chapter, RNA-Seq analysis was conducted on PC3 and 22Rv1 WT cells and their respective ENO2-KO clones, to identify the potential DEGs and the enriched processes, functions and regulated pathways connected with ENO2. The crucial rationale for selecting PC3 and 22Rv1 cells is based on its well-established role as AR-negative and AR-positive PCa cell line that closely mimics the characteristics of advanced-stage CRPC and primary PCa [261, 262]. The shared DEGs between the two different PCa cell lines will be investigated to explore the impact of ENO2 deficiency on PCa.

Firstly, the WT and ENO2-KO clones from both PC3 and 22Rv1 cells had been clearly distinguished to each other using the MDS plot (**Figure 7.1 A and B**), further verifying that ENO2 has been successfully knocked out at the genetic level. Subsequently, numerous DEGs have been identified (**Figure 7.1 C and D**) and further subdivided into the top 10 in heatmaps (**Figure 7.1 E and F**). Interestingly, the top 10 DEGs between WT and ENO2-KO in PC3 and 22Rv1 cells were completely distinct, presenting opposing expression patterns of each gene between the two groups. After expanding the range of DEGs of the two cell types to the top 20, it was found that the top 20 DEGs between PC3 and 22Rv1 ENO2-KO cells remained distinctly, again suggesting the contrasting expression patterns observed in these two cell lines. Functional predictions from GO enrichment analysis confirmed that the involvement of ENO2 in tumour-related cell behavior and metabolism, as well as neuronal system in

BP, such as cell motility, adhesion, migration, neurogenesis, neuron projection guidance, nervous system development, hormone levels, hormone metabolic process, organic hydroxy compound metabolic process, alcohol metabolic process and primary alcohol metabolic process (**Figure 7.2 A and B**). Consistently, ENO2 played a role in regulating distinct biological processes in these two cell lines. It primarily contributed to the development of nervous system and the modulation of cellular behaviors in PC3 cells. But its main involvement lies were in regulating metabolic processes and hormone levels in 22Rv1 cells.

To further identify the pathways, the pathway enrichment analysis was performed. The results revealed that several hallmarks including E2F targets, adipogenesis, G2M checkpoint, apoptosis and coagulation were concurrently enriched in both PC3 and 22Rv1 cells following ENO2 knockout (**Figure 7.3 and Figure 7.4**). Indeed, E2F is not only known to be involved in cell cycle regulation, but aberrant expression of E2F in tumours was associated with poor prognosis in a variety of cancer types, such as PCa [263, 264]. The G2M checkpoint acts as a regulatory mechanism, inhibiting cells from progressing into mitosis when DNA damage occurs. It allows the cells to repair any DNA damage before proceeding, thereby minimizing the propagation of genetic defects to the daughter cells [265]. Although both the G2M checkpoint and E2F are integral to cell cycle regulation, they function at distinct stages of the cell cycle. The G2M checkpoint operates between the G2 and M phases with ensuring proper DNA integrity before cell division, whereas E2F predominantly governs the G1/S transition, coordinating the initiation of DNA replication [266]. Both are enriched and up-regulated, which may mean that cell division is abnormal in the absence of ENO2. Remarkably, the levels of adipogenesis, apoptosis and coagulation, exhibited opposite regulation patterns in PC3 and 22Rv1 cells post-ENO2 knockout. It may be due to different original properties of the two cell lines, such as their different sensitivity to AR. Indeed, PC3 cell line have been reported to be AR-negative, suggesting its relevance to

advanced PCa, in which PCa cells dedifferentiate to an AR-negative state and transform into CRPC with therapeutic intervention [140, 267]. Conversely, the AR-sensitive state observed in the 22Rv1 cell line appears to mirror an earlier stage of PCa, where the disease maintains AR positivity and therefore remains responsive to the treatment of inhibition of the AR signaling pathway [142, 267]. Consistently, it further explained why PC3 and 22Rv1 cells exhibited distinct top 20 DEGs, BP and MF following ENO2 knockout. Enrichment in the development of the nervous system and the regulation of cell behavior was predominantly observed in AR-negative PC3 ENO2-KO cells (**Figure 7.2 A**). This supports the association between ENO2 and the aggressiveness of advanced metastatic PCa following resistance to AR signaling axis inhibitors. It also implies the potential that the progression from CRPC to NEPC may be linked to ENO2. In contrary, enrichment in the metabolic processes and hormone levels was primarily observed in AR-positive 22Rv1 ENO2-KO cells (**Figure 7.2 B**). This indicate that ENO2 may be linked to elevated hormone expression levels and metabolic pattern shifts in early-stage AR-positive PCa. However, specific details may require mapping to different genes in each pathway.

Furthermore, there were other hallmarks were enriched in PC3 and 22Rv1 after ENO2 deletion (**Supplementary Figure 9 and 10**). For example, p53 signaling pathway exhibited the up-regulated trend in enrichment following ENO2 knockout in PC3 cells, contrary to the down-regulation observed in the previously discussed p53-related DEGs. It may depend on the complex pathway correlations. In addition, the downregulation of the EMT pathway supported exploration of ENO2 regulation of PCa cell metastasis due to the adhesion and migration abilities of the cells, which is consistent with the results of the previous bubble plot (**Figure 7.2 A**) [268]. Moreover, as E2F positive regulatory factors, MYC targets (v1 and v2) were upregulated in both ENO2-deficient PC3 and 22Rv1 cells, again validating the correlation between the E2F pathway and ENO2 [264]. Besides, downregulation of glycolysis validates the

importance of ENO2 loss in metabolism in PCa. And the downregulation of androgen response indicates a transition of 22Rv1 cells from androgen-sensitive to androgen-independent states, indicating the involvement of ENO2 in regulating the malignant progression of PCa that gradually not rely on androgens.

Subsequently, venn diagram was generated in order to characterize the commonly up- or down-regulated DEGs in the two genetically modified cell lines. One commonly upregulated gene and 17 commonly downregulated genes were screened out among hundreds of DEGs (**Figure 7.5**). However, the PPI network analysis reported almost no interaction except *TRPC3* and *ANK3* even after adjusting the confidence level to medium (0.4) (**Figure 7.6 A**). These 18 DEGs were introduced in the PANTHER and DAVID bioinformatic tools and analyzed for their enriched functions on molecular function. These 18 genes were found to be associated with various functions and pathways including binding, molecular adaptor activity, molecular function regulator activity, structural molecule activity, transporter activity, glyoxylate and dicarboxylate metabolism, negative regulation of osteoblast differentiation, circadian regulation of gene expression pathway, and regulation of inflammatory response pathway (**Figure 7.6 B and C**). To understand the functions and elucidate their interrelationships, I then manually searched and studied these genes directly. Intriguingly, *DAZAP2*, *ID3*, *RANBP3L*, *COL9A2*, *CDH17*, *CAT*, *AHSG*, *RAB11FIP4*, *ANK3*, *PER2*, *IL1R1* and *TRPC3* had all been reported to be associated with the p53 pathway [269-280]. For instance, the only co-upregulated DEG, *DAZAP2* was recently found to be a p53-interacting gene, encoding a protein that accumulates in the nucleus binding to p53 in response to DNA damage mediated by chemotherapy [269]. Similarly, *ID3* has become a tumour suppressor gene as a downstream target of p53 pathway to regulate metastasis of lung cancer [270]. Importantly, as a circadian regulated gene, *PER2*, identified as one of the top 20 genes affected in 22Rv1 cells following ENO2 knockout, had been reported to associate with the p53 pathway in human oral squamous cell

tumour. It collaboratively regulated cellular apoptosis, thereby influencing the malignant development of cells [280]. Additionally, I also performed a search process of these genes in a Chip-seq based dataset Harmonizome 3.0 (<https://maayanlab.cloud/Harmonizome/>) and found that all genes except AHSB were related to the E2F pathway [281]. However, there were limited direct research evidences on the correlation of most DEGs with the E2F pathway except for *CDH17*, *CAT*, *RAB11FIP4*, *PER2* and *IL1R1* [282-286]. For example, the enrichment of the *E2F1* in *PER2*-deficient pituitary tumour cells indicates the involvement of *PER2* in regulating cell cycle abnormalities in pituitary adenomas [285]. The variance in search outcomes could be attributed to the distinction in sequencing targets between RNA-seq and Chip-seq methods. In essence, RNA-seq primarily aims to identify quantitative differences in gene expression across mRNA samples at genetic level, whereas the goal of Chip-seq is towards analyze DNA-protein interactions at epigenetic level [287]. In addition, E2F exhibited the up-regulated trend in previous enrichment following *ENO2* knockout (**Figure 7.3 and 7.4**), contrary to the down-regulation observed in the discussed E2F-related DEGs. Currently, there are conflicting findings indicating that E2F possesses both tumour-suppressive and oncogenic roles. For instance, the knockdown of *E2F8* in transformed cells has been shown to decrease viability and impair the ability to form tumours in xenograft models [288]. However, alternative studies performing knockout mice strongly suggest that *E2F8* functions as a tumour suppressor [289]. This difference may depend on changes in the cell cycle or may represent the presence of negative feedback or compensatory mechanisms.

To validate the co-dysregulated DEGs in both cell lines after *ENO2* deletion, a retrospective study was performed using the NCBI GEO dataset (GDS3289) [201]. Initially, *ENO2* exhibited a significant up-regulation in metastatic PCa compared to localized PCa at the transcriptomic level, suggesting a positive correlation with metastatic potentials (**Figure 3.4**). Loss function of *ENO2* led to increased *DAZAP2*

expression and associated with less aggressive PCa, indicating that *DAZAP2* is an anti-tumorigenic gene. Notably, this is consistent with retrospective data where benign prostate tissue expresses higher *DAZAP2* level than PCa and gradually decreased with the development of PCa at the transcriptome level (**Figure 7.7 A**). Importantly, as a Y chromosome-specific gene, deleted in azoospermia (DAZ), which has been shown to interact with *DAZAP2* had been identified to regulate by DNA methylation in PCa [290]. In addition, there was a notable downregulation of *DAZAP2* encoded protein, DAZ-associated protein 2, observed in bone marrow mononuclear cells extracted from multiple myeloma patients [291]. It is worth noting that osteoclasts originate from the mononuclear cells of the hematopoietic bone marrow, thereby indirectly illustrating the potential association between *DAZAP2* and bone microenvironment [292]. In contrast, *ENO2* deprivation associated with less aggressive PCa resulting in reduced *ACSS1* expression at transcriptome levels, suggesting that *ACSS1* is a pro-tumorigenic gene. *ACSS1*, which exhibited decreased expression following *ENO2* deprivation, showed a gradual increase in expression with the progression of PCa at the transcriptomic level (**Figure 7.7 B**). Although there is no direct evidence establishing the connection between *ACSS1* and PCa in published researches, it is noteworthy that another isoform in the same family, *ACSS2*, has been associated with aggressive PCa development [293]. *ACSS2*, has been found to be upregulated in metastatic PCa not only in patients, suggesting that *ACSS* family may hold particular significance in the context of PCa [293]. *TMLHE*, which is downregulated upon *ENO2* deprivation, has a similar expression pattern to *ENO2*, with significant upregulation in metastatic PCa compared with primary PCa at the transcriptome level (**Figure 7.7 C**). Interestingly, *TMLHE* has been identified as a novel gene predicting Gleason score in PCa, with increased expression significantly associated with high-Gleason grades [294]. Consistently, the expression of *CAT* had a similar trend to that of *TMLHE*, but the difference between metastatic PCa and primary PCa was not significant (**Figure 7.7 D**). Research has revealed a reduction in catalase activity encoded by the *CAT* gene

in the plasma of PCa patients compared to healthy individuals [295]. In addition, patients were grouped into groups based on their Gleason score, with catalase activity showing a gradual decline corresponding to higher Gleason scores [295]. Moreover, CDH17, which was downregulated after ENO2 knockout, showed significant upregulation in metastatic PCa compared with localized PCa at the transcriptome level (**Figure 7.7 E**). Currently, available studies had exclusively identified CDH17 as being positively and prominently expressed on the cell membrane of prostate adenocarcinoma cells by immunostaining. However, no expression had been observed in other cellular compartments [296]. Importantly, it has been verified that the CDH17 plays a critical role in mediating BCa bone metastasis. Suppression of CDH17 expression substantially diminished anchorage-independent growth and migration of BCa cells *in vitro*, along with metastasis to the bone marrow *in vivo* [297]. It is worth noting that both CAT and CDH17 have been associated with E2F pathway. For instance, methylation sites within the *CDH17* gene have been identified as predictors for colon cancer recurrence risk. In stage II colon cancer, the MYC/E2F-dependent proliferation signature is notably enriched, indirectly demonstrating the association of CDH7 and E2F [282]. Additionally, E2F1 had been found to attenuate FOXO3-mediated Catalase expression without impacting FOXO3 protein stability, subcellular localization and Akt phosphorylation [283]. Notably regarding AHSG, benign prostate tissue expresses higher DAZAP2 level than PCa and gradually decreased with the development of PCa at the transcriptome level (**Figure 7.7 F**). However, this seems contradict to my RNA-Seq data where the expression of AHSG was downregulated in the less aggressive ENO2 KO PCa cells. Indeed, serum AHSG levels were found to be significantly higher in patients with benign prostatic hyperplasia than in patients with PCa, which is consistent with the retrospective results [298]. *AHSG* encoded protein, fetuin-A, is abundant in bone tissues, with the mineral component of bone (hydroxyapatite), exhibiting a strong binding affinity for fetuin-A [299, 300]. Interestingly, study have reported PCa cells colonizing bone to produce

and release fetuin-A ectopically [301]. Beyond facilitating tumour growth in bone, fetuin-A may suppress new bone formation during remodeling due to elevated calcium and phosphate concentrations within the microenvironment [302]. Given the diminished expression of AHSG in metastatic PCa and its notable downregulation following the loss of ENO2 function, it is reasonable to suggest that AHSG acts downstream of ENO2 and might serve as a compensatory mechanism in response to ENO2 deletion. In conclusion, DAZAP2 and ACSS1 show promise as potential diagnostic markers for PCa. Besides, the E2F-related CDH17 and TMLHE hold potential as predictive or prognostic markers for PCa metastasis. Moreover, ACSS1, CDH17, and TMLHE may present opportunities as potential targets for drug development.

To deeper study potential gene candidates, I expanded scope of study beyond the 18 commonly up/downregulated genes and conducted individual searches for each of the top 10 DEGs in PC3 and 22Rv1 ENO2 cells (**Figure 7.1 E and F**). In particularly, the *LAD1* and *PTPRU* genes are different from other genes in that they are significantly up-regulated in the absence of *ENO2* in PC3 cells. The protein encoded by *LAD1*, known as Ladinin-1, constitutes a crucial component of basement membranes, contributing in ensuring the stability of the connection between epithelial layers and the underlying mesenchyme [303]. The up-regulation of this gene suggests the correlation of ENO2 with the tumour-related EMT pathway, thereby supporting the hypothesis that ENO2 is involved in the advanced development of PCa, especially metastasis. Moreover, the *PTPRU* encoded receptor, protein tyrosine phosphatase receptor U, is recognized for its involvement in regulating numerous cellular processes, such as cell growth and the mitotic cycle [304]. A recent study revealed that *PTPRU* functions as a tumour suppressor gene, inhibiting cancer stemness [305]. A separate investigation had discovered that *PTPRU* participates in mediating the osteogenic differentiation of human mesenchymal stem cells during their quiescent state by

influencing the Wnt/ β -catenin signaling pathway [306]. Hence, the upregulation of PTPRU implies a potential positive feedback loop in disease progression following ENO2 loss, particularly in the context of bone metastasis. Additional genes that were down-regulated in both cell lines following ENO2 knockout, including metabolism-related *UGT1A1*, *ANGPTL4*, *GLYATL1*, and nervous system development-related *LRRTM4*, *SLITRK4*, *FBLN1*, indicating a shift in metabolic profiles and potential implications for neurodevelopmental disorders following ENO2 deletion [307-312]. However, some of these genes have also been reported to be associated with tumour progression, especially metastasis, suggesting the potential of achieving oncogenes. Angiopoietin-like 4, encoded by *ANGPTL4*, plays a direct role in governing lipid metabolism [308]. Besides, *ANGPTL4* deficiency had been shown to suppress metabolic flexibility and impede the progression of EMT-mediated cisplatin chemoresistance in metastatic tumour *in vivo* [313]. The protein Fibulin-1, encoded by *FBLN1*, is a constituent of ECM and had been observed to be elevated in hepatocellular carcinoma tissues, indicating a poor prognosis. It would impede apoptosis and tumour formation *in vivo* through the Notch pathway [312]. Another gene influenced by the Notch pathway is *HEY1*, which facilitates cross talk between the Notch and androgen signaling pathways [314]. EMP2 belongs to the family of epithelial membrane proteins, exhibited the ability to enhance invasion and metastasis in certain tumours like breast cancer. However, it also demonstrated anti-metastatic properties in nasopharyngeal carcinoma [315]. Interestingly, two genes linked to skeletal development exhibited significant down-regulation, indicating their potential association with tumour development. The presence of a de novo heterozygous frameshift mutation in *FAM111B* has been linked to progressive bone dysplasia, resulting in ectopic ossification of the skin and muscle [316]. Notably, it had been demonstrated that the suppression of *FAM111B* led to a reduction in the proliferation and motility of ovarian cancer and Lung adenocarcinoma *in vitro* [317, 318]. While *BMP2*, which encodes a secreted ligand belonging to the TGF- β superfamily of

proteins, is involved in the regulation of bone and osteoblast differentiation [319]. Furthermore, there exists direct evidence indicated that BMP2 stimulated the migration of PCa cells *in vivo* and that inhibiting BMP2 diminishes the formation and progression of osteoblastic lesions triggered by PCa bone metastasis *in vivo* [320, 321]. After expanding the range of DEGs of the two cell types to the top 20, it was found that except for *LAD1* and *PTPRU*, the remaining genes were not only significantly down-regulated, but almost all were related neuronal system, cell behavior and metabolism (**Table 7.1 and 7.2**).

However, it is important to acknowledge the limitations inherent in this chapter, particularly the relatively small sample size (n=3 for WT, n=2 for KO). The limited number of sample size from PC3 and 22Rv1 WT and KO cell lines may weaken the reliability of the results due to the small sample size. Besides, the analysis of a large number of DEGs in the two ENO2-KO cells revealed enrichment primarily in the GO pathway rather than KEGG. It might indicate a potential limitation in capturing other valuable results from the data. In addition, the current analysis does not sufficiently address ENO2 involvement in metastatic progression. To more comprehensively assess the role of ENO2 in metastasis, future experiments should focus on specific metastatic pathways and targets identified through RNA-Seq, followed by validation in relevant *in vitro* and *in vivo* models which are required to bridge the gap in future.

7.4 Conclusion

Taken together, the results from this chapter revealed the potential mechanisms for which ENO2 contributes to PCa development and metastasis by regulating pivotal signalling pathways, such as the E2F pathway.

Chapter 8: General

Discussion

8.1 Discussion

PCa stand as one of the most commons cancers diagnosed in men globally, with an incidence of 1,466,680 new cases and 396,792 deaths in 2022, holding the fourth position in terms of incidence and the eighth in mortality on a global scale [5]. Bone metastases are frequently observed as the predominant site of colonization in distant metastases from PCa, with approximately 70% of patients diagnosed with advanced PCa with uncurable skeletal metastasis [9]. Notably, the one-year survival rate for patients with bone metastatic PCa was estimated to be 47%, with survival reducing to only 3% 5 years post-diagnosis. However, the five-year survival rate for PCa patients with bone metastases induced SREs, including pathological fractures, hypercalcemia, bone pain and spinal compression, was even less than 1%, thus predicting a poor prognosis [65, 66]. Thus, the insufficiency of existing approaches in treating PCa bone metastasis highlight the urgent need for therapeutic strategies specifically targeting skeletal metastases, which may provide patients with more effective therapies aimed at prolonging survival. Despite NSE, encoded by the *ENO2* gene, being identified as a tumour marker for NEPC which often associated with distant skeletal metastases, its functional role and mechanisms in promoting PCa cell bone metastasis remain undiscovered [113]. Hence, it is crucial to explore the involvement of *ENO2* and its mechanisms in regulating the advanced development of PCa, especially bone metastasis.

The evidences from my systematic review and meta-analysis indicate that *ENO2* may become a promising target for elucidating the mechanisms underlying metastasis regulation, providing novel and timely insights (**Chapter 3**). The meta- analysis gave 3 key outcomes in clinical patients: **(1)** Association between *ENO2* and late-stage PCa, indicating *ENO2* tends to be expressed in the more aggressive types of PCa; **(2)** Correction of the AR gene may not influence *ENO2* expression; **(3)** Neither physical therapy nor chemotherapy appears to impact *ENO2* expression in the patient's serum,

identifying that ENO2 expression remains unaffected by current treatments. ADT becomes necessary for patients experiencing recurrent disease and is continued throughout disease progression, despite its tendency to induce resistance at metastatic sites and increase mortality rates [195, 322, 323]. Notably, the systemic inhibition of androgens affects bone health, leading to reduced mineral density, increased rates of remodelling and an elevated risk of fractures during the initial phase of ADT, regardless of whether PCa has advanced to the bones [195, 324]. However, ENO2 expression was not affected either during ADT or by physical therapy and chemotherapy, establishing that ENO2 plays a role independent of AR expression in driving PCa progression, allowing PCa cells to escape ADT treatment. This suggests that ENO2 functions independently of regular mechanism and AR expression in driving PCa progression. However, conflicting results have been observed, confusing on whether ENO2 is androgen-dependent *in vitro*. Nevertheless, regardless of the outcome, high ENO2 expression remains linked to the potential for bone metastasis *in vitro*. Thus, ENO2 will be expected to become a novel target for investigating treatment resistance to ADT and alterations in bone structure post-treatment.

Remarkably, ENO2 exhibits not only elevated expression levels in metastatic PCa but also relatively high expression in benign prostate tissue (**Chapter 3**). The distinctive metabolic pattern of prostate cells might be the primary factor contributing to alterations in ENO2 expression. Normal prostate epithelial cells typically exhibit citrate-based metabolism, characterized by a relatively inefficient energy metabolic pattern by using glucose and aspartic acid to synthesize citrate as an important component of prostatic fluid and the final product of anaerobic glycolysis [88, 89, 212]. Hence, elevated glucose uptake leads to the upregulation of ENO2 in benign prostate tissue of patients and benign cell lines, promoting more efficient citrate synthesis to maintain energy balance. Indeed, there are two metabolic switches appeared in PCa development, including a conversion from anaerobic glycolysis to OXPHOS (benign to

primary cancer) and a transition from OXPHOS to aerobic glycolysis and fatty acid synthesis (primary to advanced cancer) [212]. Zinc transporter (ZIP1) which is a protein in humans encoded by *SLC39A1*, is responsible for the active transportation of zinc into prostate cells [325]. Within the cell, zinc acts as an inhibitor for ACO2, thereby suppressing the synthesis from pyruvate into of citrate for entry into the TCA cycle to generate ATP [211, 212]. However, ZIP1 expression is significantly inhibited in primary PCa, leading to the entry of pyruvate into the TCA cycle, thereby exhibiting increased OXPHOS, which is highly efficient process that produce more ATP compared to glycolysis [89, 93, 212]. Subsequently, aerobic glycolysis is markedly elevated and ZIP1 expression is further inhibited in metastatic PCa, leading to the activated TCA cycle and fatty acid synthesis [89, 212] (**Figure 8.1**).

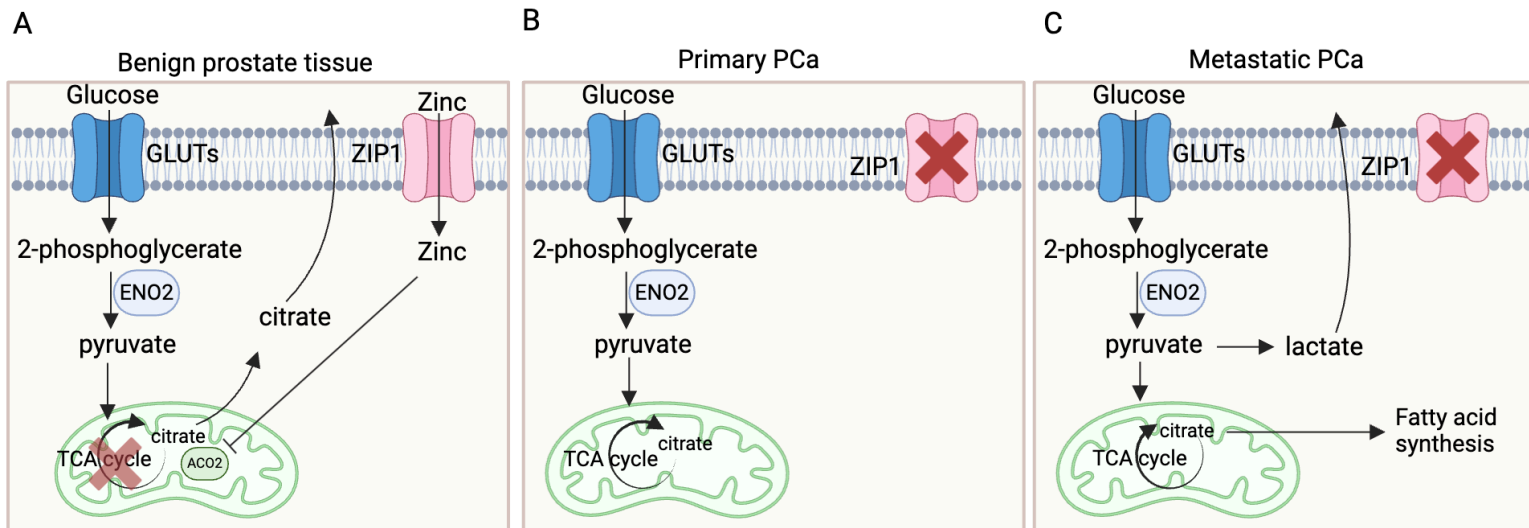


Figure 8.1 The metabolic switches in PCa development.

(A) In benign prostate epithelial cells, zinc enters the cells through ZIP1 and acts as an inhibitor of ACO2, inhibiting the synthesis of citrate from pyruvate entering the TCA cycle. Citrate, synthesized using glucose, becomes an important component of prostatic fluid and the end product of anaerobic glycolysis **(B)** In primary PCa, ZIP1 is significantly inhibited, leading to the entry of pyruvate into the TCA cycle, thereby exhibiting increased OXPHOS **(C)** In metastatic PCa, ZIP1 expression is further inhibited, leading to the aerobic glycolysis is markedly elevated to produce lactate. Part of the pyruvate enters the TCA cycle generating citrate which can be used as a substrate for fatty acid synthesis (Created using BioRender)

In conditions of glucose deprivation in the environment, ENO2 exhibits notable upregulation in myofibroblast cell lines, whilst non-significant increases were observed in PCa cell lines (**Chapter 4**). It could be attributed to the cells sensed a signal of energy deficiency and therefore initiated a stress response to increase energy production. In contrast, despite glucose deprivation, tumour cells are typically highly metabolically active and may maintain their energy requirements through alternative pathways, such as fatty acid oxidation. Thus, the upregulation of ENO2 in tumour cells may not be obvious compared with myofibroblast cell line. Through evaluating the impact of glucose on cellular behaviour, we found that the viability of PCa and myofibroblast prostatic cells was reliant on glucose. However, myofibroblast cell line displayed a distinctly opposite apoptosis trend compared to PCa cells where glucose deficiency induced enhanced apoptosis in all PCa cell lines but protected myofibroblast cell line from apoptosis. Fibroblasts, as key components of the tumour microenvironment, are known to influence cancer cell behaviour, including promoting invasion and metastasis [326]. Accordingly, ENO2-positive fibroblasts regulate the tumour cell microenvironment in a glucose metabolism-dependent manner and may play a key role in promoting the skeletal colonization of PCa cells. Besides, reduced glucose levels may offer potential benefits by impeding the progression of PCa without detrimental effects on other parts of tissues, whereas elevated glucose levels, such as those seen in hyperglycaemia, might foster PCa advancement. Indeed, it is known that elevated levels of glucose in the blood can cause hyperglycaemia in patients and lead to diabetes [327]. Notably, a meta-analysis revealed a correlation between pre-existing diabetes and mortality from PCa, suggesting the PCa-specific and all-cause mortality rates were approximately 29% and 37% higher, respectively, in PCa patients with pre-existing diabetes [328]. The hyperglycaemia circulating in diabetic patients created an environment benefit to Warburg effect and malignant progression of PCa tumour cells [329]. In addition, PCa patients with pre-existing diabetes exhibit higher rates of radiotherapy failure and more severe digestive and urinary complications compared to

those without diabetes, which indicated that diabetes may be related to decreased effectiveness of radiotherapy for PCa [330]. However, a retrospective cohort study presented conflicting results against the previous meta-analysis. An inverse correlation with PCa risk was found in men with long-term diabetes following 28 years of follow-up [331]. It can be explained by the insufficient insulin environment in long-term diabetes resulting in reduced circulating IGF-1 and plasma insulin levels, thereby reducing the risk of PCa [332, 333]. Notably, testosterone deficiency has been shown to contribute to insulin resistance, which is commonly observed in PCa patients with pre-existing diabetes, leading to elevated circulating blood glucose levels and increased risk of death in diabetic PCa patients [334-336]. Therefore, one of the potential adverse prognostic factors that may be encountered in PCa patients receiving long-term ADT is hyperglycemia, which may contribute to the progression of advanced development of tumours.

After screening a panel of human and mice PCa and benign prostate tissue cell lines, PC3 (AR negative) and 22Rv1 (AR positive) cells were selected for further genetically modification and functional assays (**Chapter 5**). As hypothesised, ENO2 was found to significantly impact the growth of PCa cells, including viability and proliferation, demonstrated from data after siRNA knockdown or CRISPR Cas 9 knockdown. There was no obvious alteration in cell apoptosis following the knockout of ENO2, which may suggest that cells may have adapted to the prolonged absence of ENO2 and compensatory mechanisms to protect from apoptotic signals. In addition, ENO2 was discovered to establish a markedly effect on mobility of PCa cells, including migration and invasion, which may be due to the down-regulation of ENO2 affecting factors related to the EMT pathway. A recent study confirmed that suppression of ENO2 markedly reduced the expression levels of EMT markers, including N-cadherin and the vimentin, in renal cell carcinoma [134]. Another recent study demonstrated that ENO2 promotes colorectal cancer metastasis by interacting with lncRNA CYTOR and

activating Yes-associated protein (YAP1)-induced EMT [337]. Taken together, the deprivation of ENO2 can markedly diminish the growth and mobility of PCa cells *in vitro* possibly by suppressing the EMT process, and consequently influence metastatic potential.

Given the effects of ENO2 on cell motility *in vitro*, the *in vivo* model of systematical injection with human PC3 cells was adopted to investigate whether ENO2 knockout affects the occurrence of bone metastasis and associated bone destruction (**Chapter 6**). As hypothesised, genetically inhibition of ENO2 led to reduced tumour incidence and burden in tibia in BALB/c nude mice. The results from H&E staining of decalcified tibia revealed that no overt tumours were observed in the left tibias of total 8 mice injected with PC3 ENO2-KO cells. The outcomes from micro-CT analysis and representative 3D model images confirmed that tibias and femurs from mice injected with PC3 WT cells indeed presented tumour induced bone loss, compared with mice injected with PC3 ENO2-KO cells where bone destructions were prevented due to the absence of overt tumours. As described above, the most possible reason for the absence of tumours in the bone marrow is that ENO2 could directly or indirectly regulate other genes or pathways influencing PCa cells skeletal colonization via affecting EMT. In addition, considering that loss of ENO2 notably decreased the viability and proliferation of PCa cells *in vitro*, it is conceivable that the absence of ENO2 may help tumour cells to enter a quiescent state, potentially leading to dormancy. Throughout the multistep metastatic process, DTCs experience the requisite genetic and epigenetic alterations necessary for progression to subsequent stages [338]. Upon extravasation, dormancy may be occurred which some of the DTCs enter a quiescent state within distant organs to escape the fate being eliminated by regular therapies like chemotherapy [57, 338]. The expansion of dormant DTCs at secondary sites is characterized by inefficiency, which results in delaying the formation of metastasis [339]. Interestingly, cells may initiate proliferation, ultimately contributing to the onset

of bone metastatic disease after years or even decades following surgical removal and chemical treatment of the primary tumour [57]. By creating a consensus dormancy-interaction network, Dilara et al. found that ENO2 was enriched which is likely related to the molecular mechanism of dormancy activation [340]. ENO2 played a role in adaptation to serum starvation, hypoxia and chemotherapy, potentially enabling tumour cells to enter a dormant state in reaction to adverse microenvironmental conditions [340]. Currently, an increasing number of treatments are under development to target dormant cells, as some researchers believe that maintaining DTCs in a dormant state could present a more viable therapeutic approach compared to targeting the more aggressive tumour cells [341, 342]. For instance, the CDK4/6 inhibitors have been demonstrated the ability to induce tumour cells into a quiescent state across various cancer models [343, 344]. Hence, if the mechanism by which ENO2 contributes to the regulation of cancer dormancy is demonstrated, it would be expected to emerge as a novel target for dormant cells in PCa bone metastases. In addition, ENO2 has been identified as a gene related to amino acid biosynthesis, was observed to be upregulated during osteogenic differentiation as a DEGs [249]. Moreover, ENO2 also has been found not only responsive to mechanical stimuli but also its knockdown induces alterations in the expression of crucial DEGs governing osteoclast and osteoblast function [242]. Thus, ENO2 have believed to become the potential target for the treatment of PCa bone metastasis.

Subsequently, further RNA-Seq analysis have confirmed the outcomes mentioned above that ENO2 plays a crucial role in regulating hormone levels, metabolic processes, EMT and cell cycle (**Chapter 7**). Specifically, ENO2 might regulate those biological processes via mediating E2F pathway. For instance, among the six co-dysregulated genes directly related to PCa progression identified via retrospective analysis, *CAT* and *CDH7* were discovered to have direct or indirect associations with the E2F pathway [282, 283]. Initiation of the cell cycle is triggered by appropriate stimuli

and promoted by the transcriptional activity of E2F family members, which regulate the transcription of S-phase cell cyclins and genes essential for DNA replication, DNA repair, apoptosis [345]. Indeed, E2F is not only known to be involved in cell cycle regulation, but also in regulating tumour dormancy [346]. Dormant cancer cells, which were found to be regulated by retinoblastoma (Rb)-E2F and E2F, commonly undergo cell cycle arrest during the G0/G1 phase [346]. Rb proteins inhibit the transcription of genes regulating the cell cycle machinery by directly binding to the transactivation domain of canonical E2F transcription factors [347]. Besides Rb proteins, non-canonical E2F proteins such as E2F6, E2F7, and E2F8, could independently inhibit the transcription of cell cycle regulators [347]. In addition, the upregulation of G2M checkpoint after ENO2 loss also indicates the disruption of cell cycle, leading to abnormal regulation and imbalance of the cell cycle.

Finally, the potential side-effect of targeting ENO2 are issues that cannot be ignored before ENO2 becomes a clinically available therapeutic target. Given that ENO2 is mainly expressed in the nervous system and plays a key role in glycolytic metabolism, its absence is concerned to cause severe neurological dysfunction and metabolic disorders [108]. Since glioma cells covering the passenger deletion of ENO1 were found to be highly dependent on ENO2, a specific inhibitor of ENO2, POMHEX, have been developed to treat ENO1-deficient cancers [239]. Lin et al. established a safety and toxicity testing for POMHEX in nude mice and primates [239]. It was discovered that mice administered POMHEX intravenously at doses of up to 10 mg/kg per day exhibited a consistent tolerance without hemolytic anemia. Interestingly, the maximum single tolerated dose was determined to be 30 mg/kg. Although reductions in body weight and subcutaneous fat were observed at such high elevated doses, these effects were reversible upon drug discontinuation [239]. Following long-term injection of >2 weeks, ENO1-deficient glioblastoma was completely eradicated and cured in three-fifths of POMHEX-treated mice and did not relapse after treatment was discontinued

[239]. In addition, high exposure to ENO2 in primates has been observed to exhibit a favorable safety profile. Despite inducing hypoglycemia in cynomolgus monkeys, intravenous administration of 35 mg/kg of POMHEX did not result in significant hemolysis or anemia and was well tolerated even at this high dose. Hypoglycemia can be effectively addressed with a simple glucose infusion in such cases [239]. In cell culture medium, POMHEX was observed to undergo rapidly a hydrolyzation to its half-ester, HemiPOMHEX, within 24 hours, primarily due to the presence of ubiquitous carboxylesterase enzymes in biological fluids. The half-life of HemiPOMHEX in primates is ten times longer than in mice with approximately 5 minutes, leading to increased drug exposure [239]. Besides, *Eno2* knockout mice exhibit viability and fertility, confirming that pharmacological inhibition of ENO2 is well tolerated at the organismal level [109].

8.2 Future Plan

8.2.1 Short term technical plan

The influences of paralogous genes ENO1 and ENO3 in jointly regulating the malignant progression of PCa cells subsequent to ENO2 dysfunction has not been confirmed by stable ENO2 knockout clones. Therefore, to elucidate their potential roles, future investigations will need to validate the expression patterns of ENO1 and ENO3 in the context of stable ENO2 knockout clones. Specifically, the assessment will be conducted through qRT-PCR to verify the transcriptional changes and western blotting for comprehensive translational analysis. By studying the interactions among these paralogous genes in the absence of ENO2 function, we aim to reveal the complex molecular mechanisms underlying PCa progression, thereby defining the development of targeted therapeutic interventions.

Moving forward, our future research efforts will focus on further elucidating the mechanisms of cellular dormancy upon ENO2 knockdown in PCa cells. Building upon

my initial findings, I plan to conduct comprehensive investigations aimed at confirming the dormant state of ENO2-knockout cells through DiD staining, which is a widely used technique for detecting quiescent or dormant cell populations [348]. Subsequently, the fluorescence-activated cell sorting (FACS) will be employed to quantify the frequency of DiD-positive cells in comparison to WT cells allowing for the reliable assessments of dormancy induction, while multi-photon microscopy will be adopted to understand their colonization in bone of both WT and KO *in vivo*. Additionally, we also aim to combine my previous RNA-Seq results including the discovery that ENO2 is associated with cell cycle regulation, to more deeply study the molecular pathways involved in regulating dormancy. Specifically, the G2M checkpoint-related genes will be established through qRT-PCR to verify the transcriptional changes and western blotting for comprehensive translational analysis. In terms of enhancing techniques for studying cellular behavior, time-lapse video could be used as a dependable method for evaluating cell migration with extending the exposure timepoints until wound closure becomes more apparent. Moreover, although preliminary research on the impact of ENO2 deficiency on glycolysis metabolism has shown promising results, the current understanding remains incomplete. Therefore, I intend to conduct additional Seahorse glycolysis level analyses to provide a more comprehensive examination of this aspect in future studies.

Expanding upon my current research, our future plans involve the application of advanced co-culture or conditioned medium systems to deeper explore into the influence of ENO2 on the complex interactions between PCa cells and bone microenvironment components. Specifically, I plan to employ co-culture models consisting of osteoblasts and osteoclasts in conjunction with PCa ENO2-KO cells to elucidate the impact of ENO2 on osteoblast proliferation and differentiation using the CyQUANT assay and Alizarin Red staining, respectively. Subsequently, I will investigate the effects of ENO2 on osteoclast differentiation through tartrate-resistant

acid phosphatase (TRAP) staining. By comprehensively analyzing the responses of bone microenvironment components to ENO2 manipulation, the goal is to reveal the underlying mechanisms of PCa skeletal metastasis and identify potential therapeutic targets.

Moreover, determining which cells within prostate tumours express ENO2 will be essential for elucidating the function of this protein in PCa progression. It will require detailed cellular profiling of ENO2 expression in various tumour cell populations, including both cancer cells and cells within the tumour microenvironment. For instance, if ENO2-positive fibroblasts are implicated in the metastasis, they may play a critical role in facilitating the spread of PCa cells, particularly to bone and possibly to other non-skeletal sites. The investigations could help to reveal specific ENO2-expressing cell types that are involved in promoting aggressive tumour phenotypes or resistance to therapy.

Furthermore, RNA-Seq analysis has revealed that ENO2 plays a crucial role in regulating PCa bone metastasis by modulating the E2F pathway. Hence, it is necessary to conduct verification experiments *in vitro* to clarify whether ENO2 deletion affects E2F pathway-related genes, such as *CAT* and *CDH17*, which have been reported to be related to E2F. This study will also be carried out on genes, including *DAZAP2*, *ACSS1* and *TMLHE*, that have not yet been reported to be related to E2F but have been found enriched in the E2F pathway in Chip-seq based datasets. Specifically, the E2F-related genes will be established through qRT-PCR to verify the transcriptional changes, Western blotting for comprehensive translational analysis.

A further area of interest is the potential link between ENO2 and the transition to NEPC, a highly aggressive subtype associated with treatment resistance and poor prognosis [33]. Loss of ENO2 expression and its effect on NE markers should be evaluated to

determine whether ENO2 influences the NEPC transition. It could clarify whether ENO2 plays an active role in this phenotypic shift or serves as an early marker for NED. Understanding ENO2's role in this process may provide insights into therapeutic strategies targeting NEPC, offering new approaches to manage this challenging form of PCa.

Finally, if time permitting, we aim to explore the therapeutic potential of the ENO2-specific inhibitor POMHEX in *in vitro* functional assays and *in vivo* validation experiments. By targeting ENO2 with specific inhibitors, insights into the feasibility and effectiveness of pharmacological intervention in reducing PCa progression and metastasis can be gained. These comprehensive experiments represent a critical step in understanding of the role of ENO2 in PCa biology and in identifying new therapeutic strategies to against malignancy.

8.2.2 Long term research plan

Considering the potential side-effects and drug toxicity associated with delivering ENO2-targeting drugs systemically in patients, achieving tissue-specific nanoparticle drug delivery becomes crucial for targeting PCa tumour cells within specific bone metastases [349]. One promising approach involves conjugating nanoparticles with bisphosphonates to facilitate bone-specific drug delivery [350]. By adjusting parameters such as size, surface functionalization and selection of targeting ligands, nanoparticles can be designed to selectively bind to specific receptors or molecules on target cells, thereby achieving targeted delivery [351]. It has broad application prospects in the field of drug delivery which could increase the local concentration of drugs and reduce damage to healthy tissues [352]. In PCa bone metastasis, this strategy can be applied by using the affinity of bisphosphonates for bone tissue, thereby enabling enhanced accumulation of nanoparticles and related drugs at this specific metastatic sites [353]. Therefore, incorporating this approach into future

research and clinical trials could significantly advance the management of PCa and other metastatic diseases.

8.3 General conclusion

Collectively, the outcomes of my study support the original hypothesis and demonstrate that enolase 2 is a key player in PCa bone metastasis. ENO2 functionally contributes to PCa bone metastasis possibly via regulating E2F pathway and provided insights in further developing ENO2 oriented treatment in fighting this deadly disease. Genetic and pharmaceutical manipulation of ENO2 will be adopted to further explore its functional involvements in PCa progression and the potential as a pharmaceutical target.

Appendix Tables

Appendix Table 1. List of search strategies of Web of Science, Ovid MEDLINE® and PubMed.

Web of Science	Ovid MEDLINE®	PubMed
TS= ('cancer' OR '*carcinoma' OR 'neoplasm\$')	(cancer or carcinoma or tumo\$r neoplasm\$).mp.	((("prostate cancer"[All Fields]) OR ("prostate carcinoma"[All Fields]) OR ("prostate neoplasms"[All Fields]) OR ("prostate tumour"[All Fields]))
TS= ('ENO2 protein\$' OR 'ENO2 Gene' OR 'ENO2)	(ENO2 protein\$ or ENO2 Gene or ENO2).mp.	((("cancer"[All Fields]) OR ("tumor"[All Fields]) OR ("tumour"[All Fields]) OR ("carcinoma"[All Fields]) OR ("neoplasma"[All Fields]))
TS= ('Enolase 2')	Enolase 2.mp.	((("eno2"[All Fields]) OR ("eno2 protein"[All Fields]) OR ("eno2 gene"[All Fields]))
TS= ('Gamma Enolase' OR Gamma-Enolase')	(Gamma Enolase or Gamma- Enolase).mp.	("enolase 2"[All Fields]) OR ("gamma enolase"[All Fields])
TS= ('Neuronal Enriched Enolase' OR 'Neural Enriched Enolase')	(Neuronal Enriched Enolase or Neural Enriched Enolase).mp.	Neuronal Enolase
TS= ('Neuron-Specific Enolase' OR 'Neuron Specific Gamma Enolase')	(Neuron-Specific Enolase or Neuron Specific Gamma Enolase or	((("neuron specific gamma enolase"[All Fields]) OR

OR 'Neuron-Specific Gamma Enolase' OR 'NSE')	Neuron- Specific Gamma Enolase or NSE).mp.	("neuron specific enolase"[All Fields])) OR ("nse"[All Fields])
TS= ('2-Phospho-D-Glycerate Hydro\$Lyase' OR '2 Phospho D Glycerate Hydro\$Lyase')	2-Phospho-D-Glycerate Hydro\$Lyase or 2 Phospho D Glycerate Hydro\$Lyase).mp.	"2 phospho d glycerate hydro lyase"[All Fields]
TS= ('2-Phosphoglycerate Dehydratase' OR '2 Phosphoglycerate Dehydratase')	(2-Phosphoglycerate Dehydratase or 2 Phosphoglycerate Dehydratase).mp.	"2 phosphoglycerate dehydratase"[All Fields]
TS= ('Nervous System-Specific Enolase' OR 'Nervous System Specific Enolase')	(Nervous System-Specific Enolase or Nervous System Specific Enolase).mp.	"nervous system specific enolase"[All Fields]
TS= ('prostat* Carcinoma\$' OR 'carcinom\$, prostate')	(prostat* Carcinoma\$ or carcinom\$, prostate).mp.	((("metastasis"[All Fields]) OR ("metastatic"[All Fields])) OR ("metastases"[All Fields])) OR ("metastases"[All Fields]))
TS= ('prostat* Cancer' OR 'cancer, prostate')	(prostat* Cancer or cancer, prostate).mp.	#3 OR #4 OR #5 OR #6 OR #7 OR #8 OR #9
TS= ('prostat* tumo\$r' OR 'tumo\$r, prostate')	prostat* tumo\$r or tumo\$r, prostate).mp	#1 AND #2 AND #10 AND #11
TS= ('prostat* neoplasm\$' OR 'neoplasm\$, prostate')	(prostat* neoplasm\$ or neoplasm\$, prostate).mp.	#1 AND #2 AND #10 AND #11 Filters: Review
TS= ('metastas*s')	metastas*s.mp.	#12 NOT #13
#2 OR #3 OR #4 OR #5 OR #6 OR #7 OR #8 OR #9	2 or 3 or 4 or 5 or 6 or 7 or 8 or 9	
#10 OR #11 OR #12 OR #13	10 or 11 or 12 or 13	

#1 AND #14 AND #15 AND #16	1 and 14 and 15 and 16
#1 AND #14 AND #15 AND #16 and Preprint Citation Index (Exclude Database) and Review Article (Exclude Document Types)	limit 17 to "review articles" – 17 not 18 –

Appendix Table 2. List of exclusive studies

Number	Studies	Reason of excluded
1	Terminal neuroendocrine differentiation of human prostate carcinoma cells in response to increased intracellular cyclic AMP	non-available data
2	Immunohistochemical staining and serotest markers during development of a sarcomatoid and small cell prostate tumor	non-available data
3	BCL-2 proto-oncogene expression in prostate cancer and its relationship to the prostatic neuroendocrine cell	no full text
4	A more objective staging of advanced prostate cancer--routine recognition of malignant endocrine structures: the assessment of serum TPS, PSA, and NSE values	non-available data
5	[Neuroendocrine primary cutaneous carcinoma. Therapeutic aspects in 13 patients]	non-available data
6	Androgen-repressed phenotype in human prostate cancer	non-available data
7	Neuroendocrine stains and proliferative indices of prostatic adenocarcinomas in transurethral resection samples	non-available data
8	Serum chromogranin A: Early detection of hormonal resistance in prostate cancer patients	non-available data
9	Cushing's syndrome in prostate cancer. An aggressive course of prostatic malignancy	non-available data
10	EGR1 target genes in prostate carcinoma cells identified by microarray analysis	non-available data
11	Serum chromogranin-A in advanced prostate cancer	non-available data
12	M1 prostate cancer with a serum level of prostate-specific antigen less than 10 ng/mL	non-available data
13	[Study of the hormone-refractory prostate cancer clinical practice in an anti-cancer center]	non-available data

14	Expression of matrix metalloproteinase-9 and bombesin/gastrin-releasing peptide in human prostate cancers and their lymph node metastases	non-available data
15	Cytotoxic treatment of aggressive prostate tumors with or without neuroendocrine elements	non-available data
16	Elevated serum progastrin-releasing peptide (31-98) in metastatic and androgen-independent prostate cancer patients	no full text
17	Neuroendocrine serum tumour markers in hormone-resistant prostate cancer	no full text
18	Pretreatment serum level of neuron specific enolase (NSE) as a prognostic factor in metastatic prostate cancer patients treated with endocrine therapy	non-available data
19	Metastatic prostate cancer with normal level of serum prostate-specific antigen	non-available data
20	Expression matrix metalloproteinase-9 and bombesin/gastrin-releasing peptide in human prostate cancers and their lymph node metastases	non-available data
21	Hypercalcemia in prostate cancer with positive neuron-specific enolase stain	non-available data
22	Prostate cancer with small-cell morphology: an immunophenotypic subdivision	non-available data
23	Changes in chromogranin A serum levels during endocrine therapy in metastatic prostate cancer patients	non-available data
24	The chromogranin-A (CgA) in prostate cancer	non-available data
25	Docetaxel and cisplatin in patients with metastatic androgen independent prostate cancer and circulating neuroendocrine markers	non-available data
26	Liver metastases in prostate carcinoma: clinical characteristics and outcome	no full text
27	Correlation of three immunohistochemically detected markers of neuroendocrine differentiation with clinical predictors of disease progression in prostate cancer	non-available data
28	Monitoring of total and free prostate-specific antigen, neuroendocrine markers and testosterone in patients with localised-prostate cancer treated by brachytherapy or conformal radiotherapy	no full text

29	The impact of diet and micronutrient supplements on the expression of neuroendocrine markers in murine lady transgenic prostate	non-available data
30	Neuroendocrine differentiation of prostate cancer cells: A survival mechanism during early stages of metastatic colonization of bone	no full text
31	Combining carboplatin and etoposide in docetaxel-pretreated patients with castration-resistant prostate cancer: a prospective study evaluating also neuroendocrine features	non-available data
32	Neuroendocrine differentiation in prostate carcinoma: focusing on its pathophysiologic mechanisms and pathological features	no full text
33	LNCaP Atlas: gene expression associated with in vivo progression to castration-recurrent prostate cancer	non-available data
34	Wnt-11 promotes neuroendocrine-like differentiation, survival and migration of prostate cancer cells	non-available data
35	Phase II study of carboplatin and etoposide in patients with anaplastic progressive metastatic castration-resistant prostate cancer (mCRPC) with or without neuroendocrine differentiation: results of the French Genito-Urinary Tumor Group (GETUG) P01 trial	non-available data
36	Gastrin-releasing peptide: predictor of castration-resistant prostate cancer?	non-available data
37	Diverse roles for Snail transcription factor in epithelial-mesenchymal transition (EMT) and neuroendocrine differentiation (NED) in human prostate cancer	no full text
38	The effects of short-term genistein intervention on prostate biomarker expression in patients with localised prostate cancer before radical prostatectomy	non-available data
39	ERK1 Mediated Epithelial-Mesenchymal Transition and Neuroendocrine Development in Prostate Cancer Cells That Survive High-dose Ionizing Radiation	non-available data
40	Estrogen Promotes Prostate Cancer Cell Migration via Paracrine Release of ENO1 from Stromal Cells	non-available data

41	Anterior gradient 2 (AGR2): blood-based biomarker elevated in metastatic prostate cancer associated with the neuroendocrine phenotype	non-available data
42	SNAI2/Slug gene is silenced in prostate cancer and regulates neuroendocrine differentiation, metastasis-suppressor and pluripotency gene expression	non-available data
43	Chemotherapy with Gemcitabine and Cisplatin for Advanced Ductal Adenocarcinoma of the Prostate: Clinical Courses of Two Patients	no full text
44	Chromogranin A and Enolase levels in serum as prognostic factors in castration prostate cancer resistant	no full text
45	Whole-genome sequencing of circulating tumor DNA reveals relevance of focal amplifications for the management of metastatic prostate cancer	non-available data
46	The New Combination Docetaxel, Prednisone and Curcumin in Patients with Castration-Resistant Prostate Cancer: A Pilot Phase II Study	non-available data
47	The proliferation marker Ki67, but not neuroendocrine expression, is an independent factor in the prediction of prognosis of primary prostate cancer patients	non-available data
48	Potential of sulfasalazine as a therapeutic sensitizer for CD44 splice variant 9-positive urogenital cancer	non-available data
49	Whole-genome plasma sequencing reveals focal amplifications as a driving force in metastatic prostate cancer	non-available data
50	Influence of abiraterone acetate on circulating neuromediators in chemotherapy-naïve castration-resistant prostate cancer	non-available data
51	[Etoposide and Carboplatin Effective for Treatment of Small Cell Carcinoma of Prostate: A Report of Two Cases]	Japanese
52	Antitumor activity of interferon- β 1a in hormone refractory prostate cancer with neuroendocrine differentiation	non-available data

53	Influence of abiraterone acetate on neuroendocrine differentiation in chemotherapy-naive metastatic castration-resistant prostate cancer	non-available data
54	Chromogranin A and neurone-specific enolase variations during the first 3 months of abiraterone therapy predict outcomes in patients with metastatic castration-resistant prostate cancer	non-available data
55	Successful Radiotherapy for Advanced Small Cell Carcinoma of the Prostate with Syndrome of Inappropriate Secretion of Antidiuretic Hormone	non-available data
56	Chromogranin A and neurone-specific enolase serum levels as predictors of treatment outcome in patients with metastatic castration-resistant prostate cancer undergoing abiraterone therapy	non-available data
57	Prospective Evaluation of Neuromediator Dynamics in Castration-Resistant Prostate Cancer Patients During Docetaxel	non-available data
58	Loss of PSMA Expression in Non-neuroendocrine Dedifferentiated Acinar Prostate Cancer	no full text
59	Anaplastic Lymphoma Kinase Mutation (ALK F1174C) in Small Cell Carcinoma of the Prostate and Molecular Response to Alectinib	non-available data
60	Reduction of two histone marks, H3k9me3 and H3k27me3 by epidrug induces neuroendocrine differentiation in prostate cancer	non-available data
61	Imaging Somatostatin Receptor Activity in Neuroendocrine-differentiated Prostate Cancer	non-available data
62	MicroRNA-652 induces NED in LNCaP and EMT in PC3 prostate cancer cells	non-available data
63	Expression of neuroendocrine differentiation markers in lethal metastatic castration-resistant prostate cancer	no full text
64	Phase I Trial of the Combination of Docetaxel, Prednisone, and Pasireotide in Metastatic Castrate-Resistant Prostate Cancer	non-available data

65	Cell-Free DNA and Neuromediators in Detecting Aggressive Variant Prostate Cancer	non-available data
66	Blocking the Feedback Loop between Neuroendocrine Differentiation and Macrophages Improves the Therapeutic Effects of Enzalutamide (MDV3100) on Prostate Cancer	non-available data
67	Neuroendocrine differentiation markers guide treatment sequence selection in metastatic castration-resistant prostate cancer	no full text
68	An Experimental Platform for Characterizing Cancer Biomarkers with Capabilities in Noninvasive and Continuous Screening	non-available data
69	Serum Neuroendocrine Markers Predict Therapy Outcome of Patients with Metastatic Castration-Resistant Prostate Cancer: A Meta-Analysis	Meta-analysis
70	Effect of abiraterone combined with prednisone on serum CgA and NSE in metastatic castration-resistant prostate cancer without previous chemotherapy	non-available data
71	Pancreatic metastasis from locally recurrent neuroendocrine differentiated prostate cancer after radical prostatectomy	non-available data
72	Neuroendocrine Differentiation and Response to PSMA-Targeted Radioligand Therapy in Advanced Metastatic Castration-Resistant Prostate Cancer: A Single-Center Retrospective Study	Retrospective study
73	Effective treatment of relapsed prostate small cell carcinoma with amrubicin: report of a case	Case report
74	The Correlation between PSCA Expression and Neuroendocrine Differentiation in Prostate Cancer	non-available data
75	Enzalutamide-Induced Upregulation of PCAT6 Promotes Prostate Cancer Neuroendocrine Differentiation by Regulating miR-326/HNRNPA2B1 Axis	non-available data
76	Dermatomyositis associated with prostate adenocarcinoma with neuroendocrine differentiation	non-available data

77	A Novel Enolase-1 Antibody Targets Multiple Interacting Players in the Tumor Microenvironment of Advanced Prostate Cancer	non-available data
78	A case of metastatic treatment-emergent small cell/neuroendocrine prostate cancer with BRCA2 mutation diagnosed by liver biopsy	Case report

Appendix Table 3. List of 7 databases of PCa patient samples in NCBI GEO for retrospective study.

GEO accession number
GDS1439
GDS4824
GDS5072
GDS4109
GDS3289
GDS1746
GDS1309

Appendix Table 4. Quality assessment for clinical studies using a modified Newcastle-Ottawa scale (NOS).

Study ID	Selection				Comparability	Outcomes			Total (out of 10)
	Representativeness of the exposed cohort (☆☆)	Selection of the non-exposed cohort (☆)	Ascertainment of exposure (☆☆)	Demonstration that outcome of interest was not present at start of study (☆)	Comparability of cohorts on the basis of the design or analysis (☆☆)	Assessment of outcome (☆☆)	Was follow-up long enough for outcomes to occur (☆)	Adequacy of follow up of cohorts (☆☆)	
Kim et al. 2017	☆	☆	☆	☆	☆	☆	☆	☆	☆☆☆☆☆☆ (6)
Kessel et al. 2020	☆	/	☆	☆	☆	☆	☆	☆	☆☆☆☆☆☆☆ (7)
Szarvas et al. 2021	☆	☆	☆	☆	☆	☆	☆	☆	☆☆☆☆☆☆☆☆ (8)

Good quality: 3 or 4 ☆ in selection domain and 1 or 2 ☆ in comparability domain and 2 or 3 ☆ in outcome/exposure domain.

Fair quality: 2 ☆ in selection domain and 1 or 2 ☆ in comparability domain and 2 or 3 ☆ in outcome/exposure domain.

Poor quality: 0 or 1 ☆ in selection domain or 0 ☆ in comparability domain or 0 or 1 ☆ in outcome/exposure domain.

Appendix Table 5. Quality assessment for *in vitro* studies using the OHAT RoB tool.

Bias domain	Questions	Study ID	
		Bock et al. 2019	Bery et al. 2020
Selection	<i>randomization</i>	++	++
	<i>allocation concealment</i>	++	++
Performance	<i>identical experimental conditions</i>	++	++
	<i>blinding of researchers</i>	--	--
Exclusion	<i>complete outcome data</i>	+	+
Detection	<i>exposure characterization</i>	++	-
	<i>outcome assessment</i>	++	-
Selective Reporting	<i>outcome reporting</i>	++	++
Other potential threats	<i>statistical methods</i>	++	--

‘++’ designate definitely low risk of bias, ‘+’ designate probably low risk of bias, ‘-’ designate probably high risk of bias, and ‘--’ designate definitely high risk of bias.

Appendix Table 6. Certainty of evidence for meta-analysis outcomes using Cochrane guidelines.

GRADE criteria	Rating (circle one)	Footnotes (explain reasons for down- or upgrading)	Quality of the evidence (Circle one)
Outcome: 1. RNA-seq data			
Study design	RCT (starts as high quality) Non-RCT (starts as low quality)	From <i>in vitro</i> studies. But the <i>in vitro</i> results were validated by examining ENO2 expression levels using cBioportal's clinical PCa gene expression profiling dataset.	⊕⊕⊕⊕ High ⊕⊕⊕○ Moderate ⊕⊕○○ Low ⊕○○○ Very Low
Risk of Bias (use the Cochrane Risk of Bias tables and figures)	No serious (-1) very serious (-2)	Plausible bias unlikely to seriously alter the results.	
Inconsistency	No serious (-1) very serious (-2)	Highly heterogeneous from independent experiments in the individual article. Same methodology.	
Indirectness	No serious (-1) very serious (-2)	Indirectness does not appear to be an issue.	
Imprecision	No serious (-1) very serious (-2)	Dichotomous outcomes, n number of events is less than 300.	
Publication Bias	Undetected Strongly suspected (-1)	No funnel plot asymmetry tests were possible.	
Other (upgrading factors, circle all that apply)	Large effect (+1 or +2) Dose response (+1 or +2) No Plausible confounding (+1 or +2)	NA	

GRADE criteria	Rating (circle one)	Footnotes (explain reasons for down- or upgrading)	Quality of the evidence (Circle one)
Outcome: 2. mRNA copy number (q RT-PCR)			
Study design	RCT (starts as high quality) Non-RCT (starts as low quality)	From clinical study. CTCs were enriched from patients and healthy individuals for qRT-PCR analysis, rather than clinical trials.	⊕⊕⊕⊕ High ⊕⊕⊕○ Moderate ⊕⊕○○ Low ⊕○○○ Very Low
Risk of Bias (use the Cochrane Risk of Bias tables and figures)	No serious (-1) very serious (-2)	Plausible bias unlikely to seriously alter the results.	
Inconsistency	No serious (-1) very serious (-2)	Highly heterogeneous from independent experiments in the individual article. Same methodology.	
Indirectness	No serious (-1) very serious (-2)	Indirectness does not appear to be an issue.	
Imprecision	No serious (-1) very serious (-2)	Dichotomous outcomes, n number of events is less than 300.	
Publication Bias	Undetected Strongly suspected (-1)	No funnel plot asymmetry tests were possible.	
Other (upgrading factors, circle all that apply)	Large effect (+1 or +2) Dose response (+1 or +2) No Plausible confounding (+1 or +2)	NA	

GRADE criteria	Rating (circle one)	Footnotes (explain reasons for down- or upgrading)	Quality of the evidence (Circle one)
Outcome: 3. Serum ENO2 protein level (Serum biomarker analysis)			
Study design	RCT (starts as high quality) Non-RCT (starts as low quality)	From clinical study. The effects of serum ENO2 protein level in patients, rather than clinical trials.	
Risk of Bias (use the Cochrane Risk of Bias tables and figures)	No serious (-1) very serious (-2)	Plausible bias unlikely to seriously alter the results.	⊕⊕⊕⊕ High
Inconsistency	No serious (-1) very serious (-2)	Highly heterogeneous from independent experiments in the individual article. Same methodology.	⊕⊕⊕○ Moderate
Indirectness	No serious (-1) very serious (-2)	Indirectness does not appear to be an issue.	⊕⊕○○ Low
Imprecision	No serious (-1) very serious (-2)	Dichotomous outcomes, n number of events is less than 300.	⊕○○○ Very Low
Publication Bias	Undetected Strongly suspected (-1)	No funnel plot asymmetry tests were possible.	
Other (upgrading factors, circle all that apply)	Large effect (+1 or +2) Dose response (+1 or +2) No Plausible confounding (+1 or +2)	NA	
GRADE criteria	Rating (circle one)	Footnotes (explain reasons for down- or upgrading)	Quality of the evidence (Circle one)
Outcome: 4. Relative mRNA expression (q RT-PCR)			
Study design	RCT (starts as high quality) Non-RCT (starts as low quality)	From <i>in vitro</i> studies. The impact of ENO2 expression in vitro in PCa cell lines with or without androgen supplement.	
Risk of Bias (use the Cochrane Risk of Bias tables and figures)	No serious (-1) very serious (-2)	Plausible bias unlikely to seriously alter the results.	⊕⊕⊕⊕ High
Inconsistency	No serious (-1) very serious (-2)	Highly heterogeneous from independent experiments in the individual article. Same methodology.	⊕⊕⊕○ Moderate
Indirectness	No serious (-1) very serious (-2)	Indirectness does not appear to be an issue.	⊕⊕○○ Low
Imprecision	No serious (-1) very serious (-2)	Dichotomous outcomes, n number of events is less than 300.	⊕○○○ Very Low
Publication Bias	Undetected Strongly suspected (-1)	No funnel plot asymmetry tests were possible.	
Other (upgrading factors, circle all that apply)	Large effect (+1 or +2) Dose response (+1 or +2) No Plausible confounding (+1 or +2)	NA	

GRADE criteria	Rating (circle one)	Footnotes (explain reasons for down- or upgrading)	Quality of the evidence (Circle one)
Outcome: 5. Relative mRNA expression (q RT-PCR)			
Study design	RCT (starts as high quality) Non-RCT (starts as low quality)	From <i>in vitro</i> studies. The impact of ENO2 expression in vitro in PCa cell lines co-culture or mono-culture.	
Risk of Bias (use the Cochrane Risk of Bias tables and figures)	No serious (-1) very serious (-2)	Plausible bias unlikely to seriously alter the results.	⊕⊕⊕⊕ High
Inconsistency	No serious (-1) very serious (-2)	Low heterogeneous from independent experiments in the individual article. Same methodology. Thus inconsistency does not seem to be an issue.	⊕⊕⊕○ Moderate
Indirectness	No serious (-1) very serious (-2)	Indirectness does not appear to be an issue.	⊕⊕○○ Low
Imprecision	No serious (-1) very serious (-2)	Dichotomous outcomes, n number of events is less than 300.	⊕○○○ Very Low
Publication Bias	Undetected Strongly suspected (-1)	No funnel plot asymmetry tests were possible.	
Other (upgrading factors, circle all that apply)	Large effect (+1 or +2) Dose response (+1 or +2) No Plausible confounding (+1 or +2)	NA	

Appendix Table 7. List of differentially expressed genes in PC3 cells with ENO2 knockout.

ENTREZID	SYMBOL	logFC	AveExpr	t	P.Value	adj.P.Val	B
23462	HEY1	-2.7149123	6.05901619	-22.60476	7.55E-12	1.04E-07	17.7056841
54658	UGT1A1	-3.0847778	5.38008432	-19.579456	4.68E-11	3.24E-07	15.8885211
55636	CHD7	-6.7680005	3.08262955	-18.13247	1.23E-10	4.97E-07	13.6917535
4628	MYH10	-2.1954359	5.62893917	-17.91376	1.44E-10	4.97E-07	14.7437177
80059	LRRTM4	-8.1523882	-0.6539521	-16.043199	5.71E-10	1.58E-06	11.2837279
139065	SLITRK4	-7.8610357	-0.8225181	-15.378158	9.66E-10	2.11E-06	10.9440518
2192	FBLN1	-7.8225331	1.36590297	-15.253278	1.07E-09	2.11E-06	10.9499423
3898	LAD1	1.86341496	4.50503478	15.0039738	1.31E-09	2.27E-06	12.4690741
10076	PTPRU	2.11184916	4.48651491	14.3599552	2.25E-09	3.47E-06	11.9110151
2013	EMP2	-2.0844103	4.46081279	-13.553337	4.59E-09	6.35E-06	11.2822783
4163	MCC	-1.7128003	4.7085362	-12.741851	9.74E-09	1.22E-05	10.4692917
6920	TCEA3	-6.2588635	1.04530365	-12.425114	1.32E-08	1.43E-05	9.2518703
286411	LINC00632	-7.1817445	-1.2428711	-12.410772	1.34E-08	1.43E-05	9.13313594
2624	GATA2	-4.5571249	2.24779439	-12.173016	1.69E-08	1.57E-05	9.84437169
5754	PTK7	-6.7355577	1.04400969	-12.108575	1.80E-08	1.57E-05	8.98593137
643988	FNDC10	2.66456426	1.63649237	12.1050609	1.81E-08	1.57E-05	9.9788963
1038	CDR1	-6.8193678	-0.6635401	-11.72671	2.65E-08	2.16E-05	8.65344846
1832	DSP	-3.6737941	2.30759395	-11.636394	2.91E-08	2.24E-05	9.44182455
5618	PRLR	-6.2348156	0.13709543	-11.581856	3.08E-08	2.24E-05	8.56108846
2817	GPC1	-1.5982162	5.51912912	-11.378584	3.80E-08	2.63E-05	8.95139036
79864	JHY	-5.8370925	-0.4275457	-11.203286	4.57E-08	3.01E-05	8.23623432
6549	SLC9A2	-3.2995015	2.41730698	-11.055909	5.35E-08	3.37E-05	8.88941781
27253	PCDH17	-7.2176368	-1.2508582	-10.934639	8.82E-08	5.30E-05	7.67285611
85301	COL27A1	-3.361989	2.97899564	-10.724409	1.05E-07	6.04E-05	8.27362828
6262	RYR2	-5.6185279	-2.1810677	-10.383613	1.12E-07	6.22E-05	7.43626338
164832	LONRF2	-1.0835746	6.29701761	-10.263759	1.29E-07	6.67E-05	7.57113942
2195	FAT1	-1.0080911	6.86225645	-10.253995	1.30E-07	6.67E-05	7.52064707
8440	NCK2	-5.3082796	0.57714625	-10.113856	1.53E-07	7.55E-05	7.36555059
3398	ID2	-2.0930839	2.97209915	-9.9454377	1.86E-07	8.87E-05	7.64238557
3485	IGFBP2	-5.4690963	-0.3237979	-9.8854695	1.99E-07	8.95E-05	7.07670744
101927167	GATA2-AS1	-5.4356727	-2.2465594	-9.8808003	2.00E-07	8.95E-05	6.9754193
57631	LRCH2	-1.9866551	3.31016517	-9.7451157	2.35E-07	0.00010173	7.36212448
23127	COLGALT2	2.5873817	1.14083331	9.64438253	2.65E-07	0.00011124	7.33068217
51477	ISYNA1	1.75755213	3.66465515	9.79947223	2.90E-07	0.00011745	6.99389281
7570	ZNF22	-6.8924925	0.00191605	-10.246245	2.97E-07	0.00011745	6.7078252
22875	ENPP4	-5.2977001	-2.3915598	-9.4652522	3.29E-07	0.00012655	6.56297424
6424	SFRP4	-4.9746742	-2.5337245	-9.3691543	3.70E-07	0.00013844	6.45117608
126353	MISP	1.04470559	5.08348273	9.29538193	4.05E-07	0.00014758	6.42103239
4100	MAGEA1	-3.2826544	2.06207752	-9.2519456	4.28E-07	0.00015157	6.86877624

8495	PPFIBP2	-4.2529073	0.47422858	-9.1938594	4.59E-07	0.00015157	6.56306299
58528	RRAGD	-2.9822941	1.62009324	-9.1837043	4.65E-07	0.00015157	6.77929426
55190	NUDT11	-3.6016568	1.28478053	-9.1739648	4.71E-07	0.00015157	6.72289377
4897	NRCAM	-4.2335173	0.94103793	-9.1129925	5.08E-07	0.00015982	6.56633261
91179	SCARF2	-1.6344779	3.59242769	-8.9190534	6.49E-07	0.00019953	6.26407351
9695	EDEM1	-0.9245288	6.99767292	-8.848064	7.10E-07	0.00021367	5.72238899
6364	CCL20	-5.1859353	-1.6420315	-8.8190972	7.37E-07	0.00021391	5.948158
10231	RCAN2	-5.1925759	-2.4531481	-8.8139124	7.42E-07	0.00021391	5.89695181
3598	IL13RA2	1.5989852	3.32297565	8.68887068	8.72E-07	0.00024025	5.86324189
793	CALB1	2.47823134	1.43959886	8.68668516	8.74E-07	0.00024025	6.11601098
51438	MAGEC2	-4.5714084	0.20823425	-8.6637088	9.00E-07	0.00024025	5.88641015
23250	ATP11A	-0.9678726	5.89651812	-8.6617826	9.03E-07	0.00024025	5.54961225
26022	TMEM98	-1.5893532	3.7446722	-8.6436039	9.24E-07	0.00024135	5.87113873
171019	ADAMTS19	-5.1798768	-1.6278626	-8.5428503	1.05E-06	0.00027017	5.64986131
1911	PHC1	-2.3785535	1.9791796	-8.3012766	1.45E-06	0.00035726	5.6569506
2034	EPAS1	0.80775617	6.25904024	8.29965778	1.45E-06	0.00035726	4.98154573
2879	GPX4	0.82168166	7.20481228	8.28952012	1.47E-06	0.00035726	4.92606416
5727	PTCH1	4.64582299	-3.0700606	8.27816275	1.50E-06	0.00035726	5.40570138
140862	ISM1	-5.0140071	0.00401243	-8.2391841	1.58E-06	0.00037007	5.3508975
5793	PTPRG	-4.9772196	-1.3645506	-8.2008719	1.66E-06	0.00038318	5.27182082
5010	CLDN11	-4.9280945	-2.5225837	-8.1823248	1.70E-06	0.00038645	5.19898979
4162	MCAM	-2.7239001	2.16358685	-8.1433427	1.80E-06	0.00040082	5.44512296
5139	PDE3A	-1.9135465	3.04989223	-8.1039583	1.89E-06	0.00041614	5.25508346
8437	RASAL1	2.96788816	-0.1135315	8.05060491	2.04E-06	0.00044055	5.34662609
6317	SERPINB3	-5.2508349	-1.2769938	-8.0559599	2.15E-06	0.00045813	5.0537713
1122	CHML	-0.8452707	8.28153205	-7.9849529	2.23E-06	0.00046742	4.47312692
7552	ZNF711	-1.517807	3.61419395	-7.9660125	2.29E-06	0.00046778	4.94482479
822	CAPG	0.86500386	5.42139605	7.96269326	2.30E-06	0.00046778	4.56153156
92840	REEP6	1.1203296	4.0068943	7.93236191	2.40E-06	0.00047536	4.70220165
50810	HDGFL3	-1.1443843	4.49850119	-7.9228892	2.43E-06	0.00047536	4.71372638
146429	SLC22A31	-4.5718399	-1.962378	-7.9197537	2.44E-06	0.00047536	4.91445566
1284	COL4A2	-0.8857525	6.06475505	-7.807563	2.85E-06	0.0005478	4.32017594
10570	DPYSL4	-1.4430323	3.45171952	-7.794141	2.90E-06	0.00055052	4.72182964
1282	COL4A1	-1.0466541	4.78679799	-7.7739216	2.99E-06	0.00055329	4.4451548
64699	TMPRSS3	-2.124115	2.06634618	-7.7712266	3.00E-06	0.00055329	4.91588266
27148	STK36	-1.0297571	4.96425147	-7.69855	3.32E-06	0.00060468	4.30615645
55841	WWC3	-4.682107	-1.8891822	-7.6731698	3.44E-06	0.00061858	4.62322907
83604	TMEM47	-4.1942272	-1.472307	-7.6588466	3.51E-06	0.00062313	4.61170113
3959	LGALS3BP	-1.42546	3.55328661	-7.6379156	3.62E-06	0.00063374	4.47341292
23657	SLC7A11	-0.9236797	6.74907087	-7.5704621	4.01E-06	0.00069371	3.91169779
3397	ID1	-0.9459927	5.91402797	-7.4882505	4.48E-06	0.00076508	3.86197435
285671	RNF180	-5.480275	-0.8683537	-7.9178442	4.72E-06	0.00078779	4.38425735
5156	PDGFRA	-2.0348841	3.14870069	-7.7603281	4.79E-06	0.00078779	4.36464548

57713	SFMBT2	2.19426665	0.75921649	7.4409357	4.79E-06	0.00078779	4.46448998
55217	TMLHE	-4.6681347	-2.7897043	-7.4343989	4.84E-06	0.00078779	4.28775615
10157	AASS	-0.8837858	5.01355984	-7.3557795	5.42E-06	0.0008724	3.77474549
23420	NOMO1	1.42235796	2.49219947	7.31166654	5.78E-06	0.00091951	4.04036548
5090	PBX3	1.24684079	3.10375609	7.27525793	6.10E-06	0.00095765	3.88106226
90161	HS6ST2	-1.6470924	2.80695101	-7.268256	6.16E-06	0.00095765	4.06184961
93145	OLFM2	-2.9415428	1.05622241	-7.2189441	6.62E-06	0.001018	4.20417134
255738	PCSK9	-1.360172	4.06822531	-7.1950552	7.15E-06	0.00108093	3.68281004
1009	CDH11	-2.5792241	0.74999968	-7.1632776	7.19E-06	0.00108093	4.12604552
23363	OBSL1	-0.7636021	5.8202662	-7.1350306	7.49E-06	0.00110832	3.32273085
357	SHROOM2	-4.2767321	-2.1797781	-7.1318032	7.53E-06	0.00110832	3.92478358
84622	ZNF594	-1.570276	2.43870059	-7.0309524	8.75E-06	0.00127404	3.75630706
55619	DOCK10	-0.9065147	5.85176058	-6.9450377	9.95E-06	0.00141995	3.02798467
2778	GNAS	-0.6614403	8.07020883	-6.9447115	9.95E-06	0.00141995	2.90000622
2043	EPHA4	-1.7343029	2.57895345	-6.9357087	1.01E-05	0.00142464	3.60032971
558	AXL	1.55904686	2.35892349	6.91922581	1.03E-05	0.00144571	3.45992857
4194	MDM4	-0.8029655	6.32890389	-6.883861	1.09E-05	0.00150062	2.88358591
57689	LRRC4C	-4.1244733	-2.248691	-6.8813053	1.10E-05	0.00150062	3.59166058
152485	ZNF827	-0.7725368	5.6701519	-6.8540937	1.14E-05	0.00154843	2.89769463
7675	ZNF121	-0.8493888	5.40367047	-6.8387254	1.17E-05	0.00156958	2.91143515
3417	IDH1	-0.8005268	6.39549398	-6.8313764	1.18E-05	0.00157172	2.79442216
51255	RNF181	0.81742793	5.19981815	6.82424245	1.19E-05	0.00157172	2.85434715
122622	ADSS1	1.17939677	3.01696959	6.81415082	1.21E-05	0.00157172	3.18351364
6281	S100A10	1.16020345	7.93183583	8.10532306	1.22E-05	0.00157172	3.024114
57594	HOMEZ	1.18270113	2.89513078	6.79665454	1.25E-05	0.00159585	3.17807934
91754	NEK9	0.81172454	4.67518805	6.78151653	1.27E-05	0.00161815	2.8538522
4325	MMP16	-0.8374165	5.35739749	-6.7680013	1.30E-05	0.00163687	2.80320256
56154	TEX15	-0.7682234	5.5187604	-6.7489214	1.34E-05	0.00165802	2.7478295
114805	GALNT13	-0.8620143	5.05090723	-6.7478249	1.34E-05	0.00165802	2.81689852
4249	MGAT5	-0.9075271	7.33532047	-7.0445721	1.47E-05	0.00179782	2.62351077
1005	CDH7	-2.320542	1.18262715	-6.6495965	1.56E-05	0.00189445	3.34801884
8514	KCNAB2	0.85037483	4.92937136	6.6420033	1.58E-05	0.00190013	2.59382625
6487	ST3GAL3	0.98523078	3.57506409	6.63623376	1.59E-05	0.00190062	2.80110975
84059	ADGRV1	-0.8037026	5.54552533	-6.6216763	1.63E-05	0.00192251	2.54104215
139221	PWWP3B	-3.5907469	-1.0271666	-6.6177784	1.64E-05	0.00192251	3.25749943
203522	INTS6L	-2.1910044	1.12773865	-6.5958547	1.70E-05	0.00197224	3.26454741
51776	MAP3K20	-0.6685893	6.960194	-6.5862884	1.72E-05	0.00198505	2.36336883
54884	RETSAT	0.75763813	5.94683987	6.57179362	1.76E-05	0.0020096	2.37849287
10882	C1QL1	1.16435577	2.80921346	6.56773823	1.77E-05	0.0020096	2.82938969
121551	ABTB3	3.90718904	-0.806465	7.11304941	1.80E-05	0.00202405	3.32781299
8050	PDHX	-0.7275832	5.41408433	-6.5463998	1.83E-05	0.00203179	2.43154913
54558	SPATA6	2.09518577	0.77528747	6.54507651	1.84E-05	0.00203179	3.11179969
10715	CERS1	-3.1225078	-0.0927367	-6.51116	1.93E-05	0.00210529	3.16359426

5256	PHKA2	-0.7735532	6.04959437	-6.5108712	1.94E-05	0.00210529	2.30422118
151354	LRATD1	-1.703839	3.79121996	-7.1712492	1.95E-05	0.00210529	2.88853787
26232	FBXO2	1.21244929	2.67374161	6.5017233	1.96E-05	0.00210663	2.74521255
64359	NXN	-4.2417365	-0.7524872	-6.5223958	1.99E-05	0.00211749	3.09353205
56171	DNAH7	-1.5084998	3.0855687	-6.4775613	2.04E-05	0.00215337	2.77281148
54039	PCBP3	2.43975361	-0.6027584	6.46984	2.06E-05	0.00215337	3.10454015
23252	OTUD3	-0.9413778	6.20083139	-6.7956233	2.07E-05	0.00215337	2.32791458
54891	INO80D	-0.8866527	4.32467797	-6.4592017	2.10E-05	0.00216774	2.47278341
4166	CHST6	-1.2789289	2.81563145	-6.4532881	2.12E-05	0.00217176	2.76452134
84885	ZDHHC12	0.71166293	4.99720654	6.44568175	2.14E-05	0.0021817	2.26728212
1728	NQO1	-0.7040825	7.40059825	-6.4278219	2.21E-05	0.00222748	2.08520986
100506465	LINC01234	-2.2566923	0.83360696	-6.4043399	2.29E-05	0.00227575	2.98879115
90120	TMEM250	0.68042975	6.82256814	6.40047145	2.30E-05	0.00227575	2.0483065
7407	VAR51	2.51943731	0.57163108	6.63310322	2.40E-05	0.00235385	2.92901915
144501	KRT80	2.77495399	0.76469762	7.02727663	2.43E-05	0.00237123	2.98387536
57480	PLEKHG1	-4.014892	-2.3267427	-6.3296261	2.58E-05	0.00249235	2.82834523
54207	KCNK10	-1.7678423	4.3897061	-7.5834606	2.64E-05	0.00251037	2.63621736
7477	WNT7B	0.71468904	5.51262083	6.3127375	2.65E-05	0.00251037	1.98838995
1903	S1PR3	-4.431029	-1.7731495	-6.4230716	2.66E-05	0.00251037	2.8236073
54552	GNL3L	-0.664951	7.30326028	-6.3070208	2.67E-05	0.00251037	1.88809226
23641	LDOC1	-2.0376198	5.72959183	-9.1405506	2.69E-05	0.00251037	2.75361894
6096	RORB	-1.3877166	3.42901577	-6.3262628	2.70E-05	0.00251037	2.41811636
51315	KRCC1	1.16584011	3.0683705	6.2901944	2.74E-05	0.00251942	2.32545125
7041	TGFB111	-1.9273874	1.52009616	-6.2886026	2.75E-05	0.00251942	2.73597802
768	CA9	2.10408437	5.45446837	9.78991379	2.77E-05	0.00251957	2.75706715
283352	TMEM132D-AS1	3.73452862	-2.7781032	6.26464869	2.86E-05	0.00256694	2.76576529
8660	IRS2	-1.3678229	2.55737138	-6.2586403	2.88E-05	0.00256694	2.49910169
10331	B3GNT3	0.72026083	5.94564124	6.25731781	2.89E-05	0.00256694	1.85921448
123920	CMTM3	-1.109547	3.24925197	-6.25455	2.90E-05	0.00256694	2.34661345
401074	LINC00960	2.87856976	-0.9665183	6.25247208	2.91E-05	0.00256694	2.78080515
84875	PARP10	1.22601598	3.26780144	6.29256244	2.97E-05	0.00260344	2.22098387
8862	APLN	0.67959684	5.07828818	6.19975404	3.17E-05	0.00275298	1.84886964
79983	POF1B	-4.2928953	1.73253558	-7.5419703	3.18E-05	0.00275298	2.89935487
285679	C5orf60	-4.0530502	-1.8869284	-6.1913931	3.21E-05	0.00275298	2.63976188
1107	CHD3	-0.6710484	7.98290791	-6.1887983	3.22E-05	0.00275298	1.66741529
3855	KRT7	1.36106255	2.12459026	6.1854155	3.24E-05	0.00275298	2.32523467
3329	HSPD1	-0.5892688	10.9396025	-6.1812538	3.26E-05	0.00275456	1.63101422
3336	HSPE1	-0.7023007	6.40237211	-6.156408	3.40E-05	0.00284958	1.68296885
79366	HMG5	-0.8297715	5.49825368	-6.1487722	3.44E-05	0.0028568	1.76651565
84443	FRMPD3	-2.0998915	1.31273778	-6.1473638	3.45E-05	0.0028568	2.53913555
90423	ATP6V1E2	0.78282847	4.60876869	6.12636608	3.57E-05	0.00293769	1.78829079
85315	PAQR8	1.45758155	1.57500285	6.10523532	3.69E-05	0.00300411	2.28731666

1948	EFNB2	-0.7649756	5.71473211	-6.1052216	3.69E-05	0.00300411	1.66231142
5874	RAB27B	-0.780127	6.2967083	-6.1079093	3.83E-05	0.00309652	1.57746391
84634	KISS1R	2.85760634	-0.09638	6.36706791	3.95E-05	0.00316955	2.50807685
23551	RASD2	1.89364331	0.27242253	6.05925523	3.98E-05	0.00316955	2.3957566
55327	LIN7C	-0.722563	5.48381143	-6.0578255	3.99E-05	0.00316955	1.60784495
57060	PCBP4	-0.7592006	5.31890802	-6.0214438	4.23E-05	0.00334369	1.57179587
84926	SPRYD3	0.63738008	5.9114228	6.01313471	4.29E-05	0.00337005	1.44950552
8406	SRPX	-0.8606752	4.56094875	-5.9847458	4.49E-05	0.00351004	1.63519416
847	CAT	-0.6484199	6.33633725	-5.9765387	4.55E-05	0.00352476	1.38047547
139818	DOCK11	-0.7718944	7.46465781	-6.1605013	4.56E-05	0.00352476	1.38686516
3081	HGD	-2.6390237	1.45946258	-6.2478393	4.61E-05	0.00354363	2.32916678
65124	SOWAHC	-0.6088107	6.62160321	-5.9562273	4.70E-05	0.00358147	1.32577524
83696	TRAPPC9	0.66367119	5.24877883	5.9554273	4.71E-05	0.00358147	1.41403266
3909	LAMA3	-0.6688389	6.80415247	-5.9515927	4.74E-05	0.00358436	1.30909591
284656	EPHA10	1.09863313	2.41502542	5.94573568	4.79E-05	0.0035993	1.87599399
1503	CTPS1	0.62713426	7.66626872	5.93767712	4.85E-05	0.0036275	1.23965619
3653	IPW	-0.8455187	4.18300232	-5.8995271	5.16E-05	0.0038416	1.55639338
116412	ZNF837	1.86285677	1.0436407	5.89605467	5.19E-05	0.00384298	2.02283387
9563	H6PD	0.7371757	5.52194552	5.87481882	5.38E-05	0.00392591	1.24490834
2049	EPHB3	-1.6389236	2.54199887	-5.9009994	5.39E-05	0.00392591	1.88750746
84649	DGAT2	0.85354619	4.4984411	5.85187412	5.59E-05	0.00403185	1.33501426
1796	DOK1	1.14459788	2.12127507	5.851006	5.59E-05	0.00403185	1.76915154
79684	MSANTD2	-0.7409626	5.24901903	-5.8333533	5.76E-05	0.00410904	1.25777388
84246	MED10	0.65468346	5.99756361	5.83279867	5.76E-05	0.00410904	1.13301761
9619	ABCG1	3.96616194	-2.1855854	6.13102279	5.84E-05	0.00410904	2.17053439
401024	FSIP2	-2.1557817	2.17241173	-6.1752125	5.85E-05	0.00410904	1.99822224
23505	TMEM131	-0.636908	6.88414376	-5.8222561	5.87E-05	0.00410904	1.08148296
5236	PGM1	0.62615596	6.9260741	5.82097279	5.88E-05	0.00410904	1.06225477
54020	SLC37A1	2.47800931	-1.2480083	5.81729614	5.91E-05	0.0041134	2.10568823
6468	FBXW4	0.79088786	3.83967008	5.79946657	6.09E-05	0.00421576	1.36102496
2886	GRB7	0.97651543	3.81139818	5.77593449	6.34E-05	0.00434164	1.3203364
2919	CXCL1	-1.872012	1.12805167	-5.7757878	6.34E-05	0.00434164	1.93946967
170958	ZNF525	-4.4896728	0.98150117	-6.7903153	6.55E-05	0.00446484	2.1858604
6457	SH3GL3	-2.0988302	0.66015474	-5.7495405	6.62E-05	0.00447921	1.94943806
64114	TMBIM1	-0.7053376	5.19648529	-5.7480212	6.64E-05	0.00447921	1.11455774
57414	RHBDD2	0.66618201	5.25728681	5.74530388	6.67E-05	0.00447921	1.05019028
8818	DPM2	0.5854015	6.0474812	5.72792202	6.86E-05	0.00458062	0.94782051
654463	FER1L6	-1.084686	4.37019894	-5.9105267	6.88E-05	0.00458062	1.30742943
157695	TDRP	-1.1719713	2.75767646	-5.7203804	6.95E-05	0.00460124	1.54160823
23768	FLRT2	-1.0080503	3.92068074	-5.717703	6.98E-05	0.00460124	1.30331167
9404	LPXN	0.76724024	4.55987574	5.70290798	7.16E-05	0.00464462	1.0685638
6925	TCF4	-0.8690235	4.50155108	-5.6955441	7.25E-05	0.00466408	1.14847126
654	BMP6	0.79209746	4.50063334	5.68563104	7.37E-05	0.00472027	1.04772063

10052	GJC1	-0.6152166	6.35949548	-5.680978	7.43E-05	0.0047214	0.86606193
29984	RHOD	0.77887611	4.98976631	5.67999394	7.44E-05	0.0047214	0.96723245
4105	MAGEA6	0.59887326	6.16266067	5.66922063	7.57E-05	0.00477942	0.83741111
2892	GRIA3	-3.2459945	-1.6077075	-5.6672779	7.60E-05	0.00477942	1.85547115
124936	CYB5D2	0.90752374	3.24964682	5.66268214	7.66E-05	0.00479467	1.23307329
83473	KATNAL2	1.24326642	1.92150375	5.65981744	7.69E-05	0.0047961	1.47699257
55698	RADIL	-2.7711819	0.16042982	-5.641083	7.94E-05	0.00488364	1.81983135
1949	EFNB3	-3.790273	-0.2679815	-5.7801632	8.11E-05	0.00496527	1.83618842
90956	ADCK2	0.62168863	5.32857622	5.62124384	8.21E-05	0.00499781	0.82553539
4664	NAB1	-0.6344041	5.65442078	-5.6139648	8.31E-05	0.00499781	0.81518973
8744	TNFSF9	0.75217803	4.1231523	5.61135719	8.35E-05	0.00499781	0.98352992
115704	EVI5L	0.71894042	4.79932974	5.61074668	8.36E-05	0.00499781	0.87279357
27075	TSPAN13	0.75540298	5.61466637	5.66582063	8.38E-05	0.00499781	0.79368492
56655	POLE4	0.62483323	5.63154723	5.60843464	8.39E-05	0.00499781	0.77174779
875	CBS	-1.0367174	4.02841547	-5.6134764	8.46E-05	0.00500066	1.09271295
2921	CXCL3	-2.5810291	0.81007298	-5.632853	8.77E-05	0.00513219	1.69050982
7421	VDR	0.62707373	5.74603803	5.58087062	8.79E-05	0.00513219	0.71265191
58499	ZNF462	-0.7115751	5.51204618	-5.5765868	8.85E-05	0.0051478	0.77082523
3575	IL7R	-1.2566585	4.36705848	-6.1095901	8.91E-05	0.00516152	1.17328571
4940	OAS3	0.71260142	5.37581989	5.56918983	8.96E-05	0.00516923	0.72700466
7133	TNFRSF1B	1.5156193	1.41574467	5.56641486	9.01E-05	0.00517202	1.40301009
168544	ZNF467	-0.9353546	4.36542361	-5.5637769	9.05E-05	0.00517372	0.94817693
51330	TNFRSF12A	0.68311249	6.84113025	5.60057894	9.14E-05	0.00520393	0.6212508
3631	INPP4A	-0.6439494	5.15737528	-5.541646	9.39E-05	0.00530577	0.75528169
92370	PXYLP1	-1.4395979	2.15290554	-5.5370975	9.47E-05	0.00532516	1.35925093
1622	DBI	-0.6267422	6.50900419	-5.5321661	9.55E-05	0.00534819	0.59385988
51455	REV1	-0.6165192	5.26872236	-5.5229665	9.70E-05	0.00541054	0.70449782
27112	NALF2	-4.3615619	-1.1983137	-5.9029965	9.74E-05	0.00541385	1.69335396
9056	SLC7A7	-2.2388706	1.26244859	-5.556837	9.96E-05	0.00551487	1.50442462
165679	SPTSSB	1.03106562	4.6333551	6.00749363	0.00010035	0.00551518	0.88287306
10178	TENM1	-0.7048153	6.25413584	-5.5222531	0.00010043	0.00551518	0.56986949
6567	SLC16A2	-3.1569979	-1.7041978	-5.4927744	0.00010207	0.00558323	1.58344174
53820	RIPPLY3	-2.8147492	-0.0619098	-5.485625	0.00010332	0.00562943	1.57534924
3576	CXCL8	-1.8503364	2.39086779	-5.7786984	0.00010538	0.00569681	1.33812731
53373	TPCN1	0.81623511	6.098213	5.8218607	0.000107	0.00573937	0.61452504
9582	APOBEC3B	1.07965867	3.40250461	5.5575908	0.00010806	0.00577365	0.8772962
51334	PRR16	-1.7670885	1.80092623	-5.4451538	0.00011072	0.00589141	1.28479382
347735	SERINC2	0.69662578	5.43640603	5.44307071	0.00011111	0.00589141	0.49703964
2556	GABRA3	0.87445356	3.45251852	5.43742687	0.00011219	0.00592588	0.79766074
8325	FZD8	0.62237422	5.94363516	5.42578072	0.00011445	0.00601956	0.4215521
10322	SMYD5	0.59293626	6.31001667	5.4215892	0.00011527	0.00601988	0.39034334
8347	H2BC4	1.38257528	2.00536776	5.42687508	0.00011601	0.00603543	1.0399178
254359	ZDHHC24	0.83134728	3.42208872	5.40999047	0.00011759	0.00609479	0.75811545

79581	SLC52A2	0.71302288	9.3617136	5.69602622	0.00011946	0.00616406	0.38743348
84448	ABLM2	1.55290458	1.13986708	5.39905699	0.00011982	0.00616406	1.16162327
51074	APIP	-0.640862	5.47459493	-5.394439	0.00012077	0.00619012	0.44858888
80144	FRAS1	-0.59182	5.69115142	-5.3898418	0.00012173	0.00621617	0.41197074
10810	WASF3	-2.8024734	-0.7216532	-5.3865585	0.00012242	0.00622836	1.42394903
9378	NRXN1	-3.3993401	2.64167301	-7.0571241	0.00012449	0.00631085	1.60107056
9480	ONECUT2	-0.9122991	4.34718248	-5.3730557	0.0001258	0.00633094	0.60858272
593	BCKDHA	0.72604206	4.50871094	5.367629	0.00012647	0.00634121	0.4861573
659	BMPR2	-0.6542943	5.49997398	-5.3601255	0.00012811	0.00638694	0.38421692
4862	NPAS2	-0.7590001	7.21713264	-5.6782595	0.0001283	0.00638694	0.37595273
6755	SSTR5	0.65809422	5.94456834	5.34835469	0.00013074	0.00643863	0.28265743
5434	POLR2E	0.73497453	7.15126412	5.61736723	0.0001358	0.00661238	0.29418373
905	CCNT2	-0.6416781	5.29418564	-5.3255137	0.00013599	0.00661238	0.34958725
23526	ARHGAP45	0.62920163	4.65900733	5.32473105	0.00013618	0.00661238	0.38838253
10409	BASP1	-4.1194938	-1.4789514	-5.6083579	0.00014042	0.00679454	1.34801892
9265	CYTH3	0.60144358	5.1652349	5.29640699	0.00014301	0.00686968	0.26706131
3702	ITK	-1.3138856	2.30252544	-5.289407	0.00014475	0.00688655	0.88988979
389677	RBM12B	-0.6149754	5.73777857	-5.2876505	0.00014519	0.00688655	0.22396413
6004	RGS16	-0.682977	5.02388649	-5.2872139	0.0001453	0.00688655	0.32512761
120	ADD3	-0.6044477	5.84833143	-5.282824	0.00014641	0.00690163	0.20278483
2954	GSTZ1	0.78978324	3.76939152	5.28201236	0.00014662	0.00690163	0.46230927
84929	FIBCD1	2.38912316	0.1348284	5.54063212	0.00014809	0.00693054	1.17876085
388963	C2orf81	1.43646086	0.99179949	5.27568918	0.00014824	0.00693054	0.97265539
7031	TFF1	1.01430424	3.84663014	5.49791139	0.00015153	0.00703168	0.49910806
22989	MYH15	-0.7910268	5.23229162	-5.3209015	0.00015221	0.00703168	0.27499893
4151	MB	1.13690366	1.88098733	5.2596017	0.00015243	0.00703168	0.78554934
6382	SDC1	0.77848595	8.14811679	5.7381725	0.00015373	0.00705667	0.21270287
8708	B3GALT1	-0.9617611	3.27274625	-5.2530413	0.00015418	0.00705667	0.60436943
10962	MLLT11	-1.1664709	2.77719075	-5.2478653	0.00015557	0.00708205	0.71474506
101927501	PINCR	-1.8247982	0.51565477	-5.2427844	0.00015695	0.007111684	1.10003658
4674	NAP1L2	-1.4822678	1.43269481	-5.2412731	0.00015736	0.007111684	0.9637544
57679	ALS2	-0.6371526	4.73030766	-5.2302765	0.0001604	0.00719844	0.26707142
414	ARSD	1.50104354	1.30252719	5.22635749	0.0001615	0.00719844	0.82709566
65065	NBEAL1	-0.5953205	5.1118881	-5.2079069	0.00016677	0.00735029	0.16252981
2026	ENO2	-1.1796696	4.99289326	-6.0025498	0.00016847	0.00740151	0.50595339
79625	NDNF	-0.7803624	4.1830732	-5.1962286	0.00017021	0.00745404	0.31267182
55970	GNG12	0.5861029	7.00664482	5.19403396	0.00017086	0.0074542	-0.0536267
390	RND3	-0.6406566	5.63045414	-5.1926004	0.00017129	0.0074542	0.06510143
80820	EEPD1	0.58154013	5.16231476	5.18910708	0.00017233	0.00747628	0.07424448
2272	FHIT	-2.9606006	-1.7808255	-5.1734152	0.00017712	0.00763616	1.07545886
84674	CARD6	1.45834852	1.50367923	5.17085846	0.00017792	0.00764573	0.69279482
285313	IGSF10	-3.279809	-1.0047206	-5.1691453	0.00017845	0.00764573	1.07070686
143686	SESN3	-0.7011953	4.89204101	-5.1653707	0.00017963	0.007649	0.125578

10319	LAMC3	-0.646352	5.41843572	-5.1543799	0.00018312	0.00774982	0.02448667
6608	SMO	-1.6602956	2.15692603	-5.2311983	0.00018588	0.00783363	0.72367961
388403	YPEL2	-1.800244	0.92842648	-5.1447543	0.00018623	0.00783363	0.88158622
23255	MTCL1	-0.6277924	6.66532999	-5.1306539	0.00019265	0.00797096	-0.1446678
57590	WDFY1	-0.6659123	5.44401568	-5.1229172	0.0001935	0.00797096	-0.0367805
7189	TRAF6	-0.7565682	4.33559078	-5.12153	0.00019397	0.00797096	0.14939341
7855	FZD5	-0.813762	4.47235887	-5.1211385	0.0001941	0.00797096	0.12720059
253559	CADM2	1.01314082	2.91528979	5.11914879	0.00019478	0.00797518	0.32959575
3241	HPCAL1	0.75466041	7.88917594	5.55218956	0.00019751	0.00800586	-0.0527893
26999	CYFIP2	-1.3565461	2.27232051	-5.1109347	0.00019761	0.00800586	0.58074879
3399	ID3	-1.7659996	4.65137887	-6.7387209	0.00019785	0.00800586	0.69837777
6508	SLC4A3	-1.3268564	3.56786644	-5.4876573	0.00019851	0.00800941	0.46615199
6303	SAT1	0.63067321	5.66791994	5.10414661	0.00019998	0.00804526	-0.1363512
64857	PLEKHG2	-0.9104645	3.94828708	-5.1003021	0.00020134	0.00805621	0.19547371
84440	RAB11FIP4	-2.623559	-0.8454539	-5.1000744	0.00020142	0.00805621	0.95606959
2014	EMP3	0.60026942	5.39578414	5.09566469	0.00020299	0.00808967	-0.1235437
7033	TFF3	1.85836871	0.10420444	5.09280675	0.00020401	0.00808967	0.78181157
5742	PTGS1	2.22906179	2.57869167	6.69311927	0.00020682	0.00817775	0.84664125
54149	C21orf91	-0.8327664	3.9347479	-5.0794795	0.00020885	0.00823442	0.15111048
322	APBB1	-1.0042383	2.72271428	-5.0753742	0.00021037	0.0082706	0.39961563
5027	P2RX7	1.75691391	-0.1438504	5.07137409	0.00021185	0.00827313	0.77771638
55556	ENOSF1	-0.6195089	6.04977325	-5.070382	0.00021222	0.00827313	-0.2017344
970	CD70	0.81012964	4.87217933	5.26283454	0.00021375	0.00828318	-0.0329716
113278	SLC52A3	1.34174808	0.98363974	5.06526682	0.00021414	0.00828318	0.60326406
4709	NDUFB3	-0.5895098	5.29547517	-5.0649169	0.00021428	0.00828318	-0.1252868
7130	TNFAIP6	-1.1427002	2.80289665	-5.044569	0.00022211	0.00851845	0.33983213
163933	FAM43B	0.83902304	3.28079901	5.0429773	0.00022273	0.00851845	0.12460177
5764	PTN	-3.2750123	-0.6559814	-5.0771436	0.000223	0.00851845	0.8705239
79929	MAP6D1	-1.1177487	3.41737829	-5.0938207	0.00022348	0.00851845	0.23129286
160851	DGKH	-0.6112639	5.70392388	-5.0396189	0.00022406	0.00851845	-0.2233894
53342	IL17D	1.02910344	2.0529475	5.03582624	0.00022556	0.0085522	0.35420974
730091	LINC00886	1.106846	2.29512453	5.03275989	0.00022679	0.00857516	0.29516598
9241	NOG	0.91323215	3.43201263	5.01491415	0.00023406	0.00876963	0.03958981
5649	RELN	1.05267558	2.77432751	5.01381895	0.00023451	0.00876963	0.16713765
284361	EMC10	0.61011955	6.34299798	5.00944447	0.00023718	0.00879981	-0.3614203
84058	WDR54	0.73434112	3.96204796	4.9879199	0.00024552	0.00903178	-0.1068388
57188	ADAMTSL3	0.93710819	2.71664934	4.98682538	0.00024599	0.00903178	0.13366548
10911	UTS2	-1.7086763	2.52323254	-5.334513	0.00024604	0.00903178	0.47301939
25946	ZNF385A	1.07048493	4.00224653	5.45324732	0.00025137	0.00917932	0.0471478
2004	ELK3	0.96150919	4.01255834	5.24236276	0.00025139	0.00917932	-0.0354712
9802	DAZAP2	0.5902359	5.43669964	4.97199921	0.00025255	0.00919742	-0.3546409
288	ANK3	-0.5894813	7.24281471	-4.9641572	0.00025803	0.00934774	-0.4768011
64077	LHPP	0.82444161	3.05125294	4.9541062	0.0002607	0.00939548	0.00803877

55422	ZNF331	-0.6700003	4.67977627	-4.9509331	0.00026218	0.00942407	-0.2300267
22873	DZIP1	5.09609183	-1.2744119	6.41996001	0.00027108	0.00965035	0.96128377
55959	SULF2	0.71314194	7.50778362	5.2844249	0.00027117	0.00965035	-0.4002757
92305	TMEM129	0.66341856	5.41941616	4.94379786	0.00027408	0.00970066	-0.4305456
23542	MAPK8IP2	1.76433489	0.5838057	4.9166867	0.00028339	0.01000466	0.38556876
116931	MED12L	-0.7539305	3.79549707	-4.8998266	0.00028716	0.01007669	-0.1547489
54626	HES2	1.34247652	2.48923073	5.19272012	0.00028755	0.01007669	0.13062895
23424	TDRD7	0.69997343	3.78480436	4.89893859	0.00028761	0.01007669	-0.2352223
57482	CRACD	-0.7000591	5.27298533	-4.9041943	0.00028975	0.0101258	-0.4244117
4121	MAN1A1	0.63077653	6.61651378	4.97346174	0.00029513	0.01023389	-0.5641583
1277	COL1A1	-1.3204647	4.63262688	-5.8236811	0.00029562	0.01023389	0.06849051
5129	CDK18	0.641658	5.27302545	4.8832233	0.0002958	0.01023389	-0.5007484
8228	PNPLA4	0.65928013	3.94515818	4.88112151	0.00029691	0.01023822	-0.2959297
137970	UNC5D	-0.7933623	3.85030537	-4.8751835	0.00030008	0.01030469	-0.2078212
339975	LOC339975	-2.225033	0.18813452	-4.8550728	0.00031107	0.01062938	0.47470912
10161	LPAR6	-0.8897874	3.55648697	-4.848401	0.00031481	0.01070426	-0.1919575
1687	GSDME	0.88910382	3.66088954	4.88523903	0.00031695	0.0107508	-0.2996669
342979	PALM3	-1.4927006	1.06481352	-4.8397714	0.00031971	0.01081787	0.30978402
63924	CIDEC	-1.092996	2.37104396	-4.8275817	0.00032678	0.0109498	0.02687301
1462	VCAN	-0.5868638	6.97650177	-4.8370558	0.00032981	0.01098339	-0.7146293
22795	NID2	-1.0816066	2.62475724	-4.8190617	0.00033181	0.01098339	-0.0385686
101928176	LINC01411	1.59237665	0.18968621	4.81541914	0.00033399	0.01098339	0.28190397
26504	CNNM4	-0.5898322	5.31881839	-4.8127959	0.00033556	0.01098339	-0.5930542
894	CCND2	-2.8481083	-1.3145991	-4.8127868	0.00033557	0.01098339	0.48326249
151473	SLC16A14	-1.2306132	2.3453872	-4.8088839	0.00033793	0.01098339	0.00872184
92017	SNX29	0.70440899	3.50510129	4.80571983	0.00033986	0.01101466	-0.3520656
54848	ARHGEF38	-1.900991	0.77404494	-4.8039727	0.00034092	0.01102347	0.3035211
55652	SLC48A1	0.58978019	4.34815756	4.79819226	0.00034448	0.01108117	-0.5208877
7135	TNNI1	1.87578836	-0.8756222	4.79624393	0.00034569	0.01108117	0.37354931
23467	NPTXR	0.84947955	4.12824718	4.93120762	0.00034614	0.01108117	-0.4346523
10202	DHRS2	1.71450052	1.15016768	5.00752927	0.00034671	0.01108117	0.1639041
4070	TACSTD2	-2.1744284	0.86303421	-4.8627847	0.00035051	0.01115106	0.31143897
23671	TMEFF2	-2.7599557	-0.595682	-4.7852686	0.00035258	0.01119128	0.42075726
2869	GRK5	0.62811513	4.22224944	4.77900987	0.00035658	0.01126636	-0.5349132
80312	TET1	-1.4047752	3.33841263	-5.2264706	0.00036774	0.01154484	-0.0713389
1956	EGFR	0.62645629	5.60433959	4.7759468	0.00036789	0.01154484	-0.7552817
5575	PRKAR1B	0.59313447	5.09631775	4.75777576	0.00037048	0.01159967	-0.7110255
91133	L3MBTL4	-0.8951262	3.17009269	-4.7507782	0.00037518	0.01169403	-0.2913941
253868	CRMA	-3.019481	-1.7239742	-4.7485507	0.00037669	0.01171472	0.37638569
23209	MLC1	2.53925425	-1.769307	4.74343566	0.00038018	0.01179681	0.34347171
80055	PGAP1	-0.6173615	4.91608863	-4.7390839	0.00038318	0.01186322	-0.6680241
22982	DIP2C	-0.8294322	3.25382663	-4.7344649	0.00038639	0.01192144	-0.347051
151507	MSL3P1	-0.750768	3.85391111	-4.7338992	0.00038679	0.01192144	-0.4734235

376267	RAB15	-0.8590224	3.14459187	-4.7309921	0.00038882	0.01193104	-0.3272275
100506473	C2orf49-DT	-1.2422205	1.79103977	-4.7270816	0.00039158	0.01197904	-0.0293913
407975	MIR17HG	-1.0846378	3.82703643	-4.9843094	0.00039283	0.01197904	-0.3440547
9201	DCLK1	-1.0178749	3.79378304	-4.8846786	0.00039302	0.01197904	-0.3867355
387895	LINC00944	1.87533731	-0.4531665	4.72158931	0.00039548	0.01200238	0.19512101
64798	DEPTOR	0.62318641	4.09508798	4.71844193	0.00039774	0.01204443	-0.6253266
151556	GPR155	-0.901659	2.8488609	-4.713952	0.00040098	0.01208968	-0.2948318
10325	RRAGB	-0.7279172	3.92043173	-4.7026631	0.00040925	0.01228555	-0.5449268
577	ADGRB3	-0.9492405	2.97999761	-4.7014418	0.00041016	0.01228608	-0.3421173
2920	CXCL2	-1.6989333	0.77352568	-4.6959939	0.00041422	0.01235556	0.10071564
5364	PLXNB1	-1.0741816	5.83641901	-5.6832081	0.00041657	0.01235556	-0.4533756
2264	FGFR4	-0.6093209	4.71279121	-4.690931	0.00041804	0.01235556	-0.7223234
6318	SERPINB4	-3.0869616	-1.3240334	-4.6891327	0.0004194	0.01235556	0.27508863
27247	NFU1	0.62915342	4.19423037	4.68858139	0.00041982	0.01235556	-0.6995438
646278	PDCD6IPP2	-2.1559604	0.16336016	-4.6883379	0.00042	0.01235556	0.17802834
84532	ACSS1	-0.8445572	4.13011897	-4.6990756	0.00042231	0.01235556	-0.6013304
653820	FAM72B	0.58514306	4.34036595	4.68518592	0.00042241	0.01235556	-0.7298297
79070	POGLUT2	-0.7833739	4.8943022	-4.8090101	0.00042486	0.01235556	-0.700269
51112	TRAPPC12	0.6067506	4.42096219	4.67898376	0.00042718	0.01235556	-0.7555051
9424	KCNK6	-1.2515214	1.77898515	-4.6770577	0.00042868	0.01235556	-0.1208187
9976	CLEC2B	-0.8572828	4.8334238	-4.9215184	0.00043039	0.01235556	-0.6456151
84959	UBASH3B	0.91513983	5.13855034	5.27854561	0.00043049	0.01235556	-0.6159754
55825	PECR	-0.989431	2.87782652	-4.6725989	0.00043216	0.01235556	-0.3706285
3914	LAMB3	0.79519239	4.35217419	4.80014317	0.00043359	0.01235556	-0.7055611
399665	EEIG1	0.8138338	5.89164007	5.19212034	0.00043502	0.01235556	-0.7309625
10324	KLHL41	-1.7289137	0.65833544	-4.6670875	0.0004365	0.01235556	0.06559761
643911	CRNDE	-1.1948111	2.16437212	-4.6644585	0.00043858	0.01238689	-0.223509
58504	ARHGAP22	0.69513245	3.75194295	4.65953951	0.00044252	0.01241503	-0.6712651
3207	HOXA11	0.83297544	3.49696036	4.65872761	0.00044317	0.01241503	-0.6280648
7975	MAFK	0.61261793	5.24866746	4.64634799	0.00045324	0.01264606	-0.938697
1292	COL6A2	-0.7921247	3.34366897	-4.637516	0.00046058	0.01269705	-0.5485493
729852	UMAD1	0.70168995	3.75549367	4.63627047	0.00046162	0.01270053	-0.7179577
27035	NOX1	-1.6947807	0.86879668	-4.624145	0.00047191	0.01291328	-0.0455619
374946	DRAXIN	-2.4573568	-0.7859511	-4.623383	0.00047257	0.01291328	0.14416335
4502	MT2A	0.67668306	6.40478532	4.86584269	0.00048391	0.01304083	-0.985157
51761	ATP8A2	1.91617444	-0.1899932	4.60984628	0.00048436	0.01304083	-0.0403603
27128	CYTH4	1.42591058	0.91440641	4.60067903	0.00049251	0.01320903	-0.228355
222663	SCUBE3	-1.1700573	1.80198823	-4.5924442	0.00049996	0.01335835	-0.2855668
10687	PNMA2	-1.773862	0.1007648	-4.5923888	0.00050001	0.01335835	0.00129822
285755	PPIL6	0.87272506	2.28390591	4.58603624	0.00050583	0.01344763	-0.515117
221184	CPNE2	-1.2314618	1.72775754	-4.5849428	0.00050684	0.01344763	-0.2794753
8900	CCNA1	1.23299352	1.07427008	4.58443659	0.00050731	0.01344763	-0.2842362
1611	DAP	0.86372516	7.51452847	5.42100916	0.00050846	0.01344763	-0.8417533

8536	CAMK1	-0.8514953	3.2692499	-4.5824214	0.00050918	0.01344763	-0.6288812
5608	MAP2K6	-1.3558911	2.33512027	-4.6352198	0.00051081	0.01346484	-0.3714079
33	ACADL	-1.2798843	1.7291555	-4.5773454	0.00051392	0.01346994	-0.2947522
339983	NAT8L	-0.6161078	4.77869283	-4.5747489	0.00051636	0.01350834	-0.9508562
60437	CDH26	-2.6113514	2.91833448	-5.9218957	0.00052013	0.01358119	0.07544307
83690	CRISPLD1	-1.2109656	2.11157186	-4.5694059	0.00052142	0.01358936	-0.391333
150946	GAREM2	1.14612239	2.8871693	4.81842633	0.00052351	0.01359865	-0.5669576
606495	CYB5RL	0.7283689	3.1316147	4.56629197	0.00052439	0.01359865	-0.7222438
9256	TSPOAP1	-4.2303294	-1.2559719	-5.1207488	0.00052473	0.01359865	0.20630634
158219	TTC39B	-1.8267595	0.10787628	-4.5480337	0.00054219	0.0139208	-0.0804698
3006	H1-2	0.7661394	4.05445737	4.56815389	0.00054932	0.01407785	-0.9421517
200765	TIGD1	-1.0324113	2.50099908	-4.5385195	0.0005517	0.01411273	-0.5372719
81562	LMAN2L	-0.5956625	4.46483802	-4.537513	0.00055272	0.01411273	-0.9679182
115749	C12orf56	-2.9134496	-1.4194418	-4.5338277	0.00055646	0.01413481	0.01178334
140680	C20orf96	-0.7433864	4.13278993	-4.5321405	0.00055818	0.01413481	-0.9020314
100289341	MAN1B1-DT	1.13525608	1.55289066	4.52912985	0.00056127	0.01413481	-0.4768212
358	AQP1	4.64424431	0.25011798	6.49736267	0.00056146	0.01413481	0.33917889
130916	MTERF4	-0.6075761	4.38045875	-4.5286532	0.00056176	0.01413481	-0.9678906
100506714	NUP50-DT	0.84921454	2.99681916	4.52690748	0.00056355	0.01415433	-0.7733254
100287482	SMKR1	0.73922674	3.27561569	4.52423656	0.00056632	0.01419795	-0.8306047
113655	MFSD3	0.6317556	5.75373537	4.61965164	0.00058524	0.01454067	-1.1995218
6272	SORT1	0.75820707	4.12133939	4.54187668	0.00059107	0.01465915	-1.022851
4669	NAGLU	0.68289167	3.67030019	4.49515263	0.00059733	0.01476147	-0.9637967
727897	MUC5B	2.12538051	8.38416358	7.94258601	0.0005996	0.01477814	-0.2888336
135398	C6orf141	-0.5949525	5.40693996	-4.4918106	0.000601	0.01477814	-1.2066261
22901	ARSG	0.82260046	2.54342901	4.48761309	0.00060565	0.01480847	-0.7520126
147804	TPM3P9	-0.8199541	3.62291853	-4.479333	0.00061493	0.01494622	-0.8973544
1464	CSPG4	-1.5840071	1.19506665	-4.4787352	0.0006156	0.01494622	-0.3641389
400931	MIRLET7BHG	-1.221161	2.92292558	-4.6267273	0.00062997	0.01511947	-0.6628895
3008	H1-4	1.75277276	-0.5754939	4.46581985	0.00063039	0.01511947	-0.2471938
55313	CPPED1	0.78254618	3.22502463	4.46438494	0.00063205	0.01513318	-0.9371208
201294	UNC13D	1.95553775	-0.1582069	4.48730615	0.00064425	0.0153934	-0.3115533
118788	PIK3AP1	-0.9063451	2.54726871	-4.4532355	0.00064515	0.0153934	-0.7184171
7784	ZP3	0.60804579	3.95375247	4.45065307	0.00064822	0.01542607	-1.1001469
375248	ANKRD36	-0.9991402	2.85399025	-4.4502123	0.00064874	0.01542607	-0.7761172
84699	CREB3L3	-2.6922451	-1.3605812	-4.4450877	0.00065489	0.01549237	-0.1404312
124976	SPNS2	0.87316776	2.40002301	4.44403091	0.00065617	0.01549605	-0.8037152
257313	UTS2B	-1.1533687	5.45835379	-5.4881568	0.00067034	0.01566216	-0.8423759
3491	CCN1	0.93853301	4.32081674	4.88904427	0.00067417	0.01566216	-1.0044385
8876	VNN1	-1.7566708	2.63365272	-5.0219361	0.00067452	0.01566216	-0.4586169
441518	RTL8B	0.64430586	4.26117478	4.42006986	0.00068578	0.01582517	-1.2159304
254065	BRWD3	-0.62121	5.36193898	-4.4261522	0.00068743	0.01582517	-1.3335337
4311	MME	-2.7232406	-0.6161756	-4.4435479	0.0006884	0.01582517	-0.2067937

9047	SH2D2A	0.80688838	2.7363756	4.40325214	0.00070738	0.01602203	-0.9512326
10449	ACAA2	-1.1859705	1.73190671	-4.4001456	0.00071145	0.01602876	-0.6252446
5782	PTPN12	0.63680403	5.8220089	4.5661678	0.00071191	0.01602876	-1.3799818
3800	KIF5C	-1.2453438	5.54147613	-5.6229321	0.00071231	0.01602876	-0.847891
100500850	MIR3682	-2.6701668	-1.3786207	-4.394614	0.00071875	0.01612124	-0.2272219
113263	GLCCI1	0.65091317	4.33431437	4.38932547	0.00072581	0.01620566	-1.2892391
284992	CCDC150	-1.0545431	2.35570973	-4.38764	0.00072807	0.01620566	-0.7845392
4337	MOCS1	0.63156665	3.92339136	4.38678258	0.00072922	0.01620566	-1.2160216
84552	PARD6G	-0.954655	2.80131112	-4.3845119	0.00073229	0.01624059	-0.8927208
503639	DUXAP10	0.79434764	2.88879049	4.38161849	0.00073621	0.01624953	-1.0205699
83943	IMMP2L	0.6424881	3.52432374	4.37977373	0.00073873	0.01625317	-1.1514842
80164	PRR36	-1.2419398	1.92694124	-4.3783774	0.00074064	0.0162616	-0.7028296
55728	N4BP2	-0.6878267	3.69390747	-4.37408	0.00074654	0.01632133	-1.1217612
2925	GRPR	-0.6047752	4.67617303	-4.3485755	0.00078261	0.01687964	-1.3631557
100506990	FAM86B2-DT	-2.8959872	-1.3254574	-4.3501349	0.00078428	0.01687964	-0.3083813
3434	IFIT1	-0.9486708	2.59853285	-4.3388489	0.00079684	0.01709208	-0.9427348
57234	LINC00869	-1.7920311	0.30134169	-4.3371341	0.00079937	0.01709208	-0.4837537
11148	HHLA2	-1.9194033	1.12855373	-4.4865994	0.00079956	0.01709208	-0.5247307
283212	KLHL35	0.99246087	1.52727245	4.33649393	0.00080032	0.01709208	-0.8285851
26270	FBXO6	-0.8362529	3.62535017	-4.3290087	0.0008115	0.01725098	-1.1805057
119391	GSTO2	-1.2832908	1.26089809	-4.3257641	0.0008164	0.0173019	-0.6770706
123099	DEGS2	1.48273424	-0.2616488	4.32064172	0.00082419	0.01742957	-0.5495372
153579	BTNL9	-2.026165	0.56309973	-4.3621027	0.00082665	0.01743227	-0.5165253
23120	ATP10B	-2.0554707	-0.854192	-4.318423	0.00082759	0.01743227	-0.3938812
126298	IRGQ	-0.7317693	4.09285419	-4.3115675	0.00083818	0.01757514	-1.3128287
8864	PER2	-0.6007892	4.34771018	-4.3081054	0.00084358	0.01763498	-1.3783869
5881	RAC3	-0.6676249	4.55564408	-4.2953948	0.00086373	0.01784051	-1.4362028
2290	FOXG1	-2.5856522	-1.154363	-4.2889995	0.00087405	0.01794844	-0.4138982
100131551	LINC00887	2.10531713	-1.431927	4.28894379	0.00087414	0.01794844	-0.4784617
9537	TP53I11	-0.8048963	2.98467247	-4.2853932	0.00087993	0.01804048	-1.1329337
56912	IFT46	-0.6535035	4.18491988	-4.2834713	0.00088308	0.01805155	-1.3916898
80169	CTC1	-0.697523	4.30534977	-4.2749152	0.00089724	0.01831394	-1.4256951
23178	PASK	-0.6030697	4.17364876	-4.2711181	0.00090359	0.01836247	-1.4155547
4811	NID1	-0.6401601	6.25710083	-4.4670887	0.00092156	0.01865917	-1.6297864
5099	PCDH7	-1.0758384	1.73969928	-4.2598465	0.00092274	0.01865917	-0.8997204
80323	CCDC68	-0.8978583	2.82192424	-4.2572248	0.00092726	0.01870601	-1.1486578
30846	EHD2	0.73476547	3.51495109	4.25291891	0.00093472	0.01877446	-1.394974
1380	CR2	-1.8892865	0.46406893	-4.2498442	0.00094009	0.01881674	-0.6603608
54510	PCDH18	-0.8141471	2.94899374	-4.2486286	0.00094222	0.01881674	-1.197816
10814	CPLX2	-2.5002079	-1.4057703	-4.2486021	0.00094226	0.01881674	-0.4799022
83861	RSPH3	0.70840217	3.00688621	4.23723085	0.00096244	0.01913677	-1.3180375
89796	NAV1	-0.656134	3.89439768	-4.2349086	0.00096661	0.0191647	-1.4259893
51303	FKBP11	-0.7157944	4.23163409	-4.2328189	0.00097039	0.01921196	-1.4899844

2257	FGF12	-2.4803828	-1.4280352	-4.2307787	0.00097408	0.01925762	-0.5106304
57134	MAN1C1	-4.8943582	-1.2021231	-5.145853	0.00097848	0.01931692	-0.2720011
283229	CRACR2B	1.00223782	2.05813706	4.22716183	0.00098067	0.0193221	-1.1444563
7099	TLR4	1.23967743	0.82847122	4.22648864	0.00098191	0.0193221	-0.9046743
148932	MOB3C	0.78910861	3.88014372	4.333108	0.00098293	0.0193221	-1.4631419
9926	LPGAT1	-0.6018223	5.59754414	-4.2644745	0.00100503	0.01953454	-1.733141
146691	TOM1L2	0.63919367	4.99735682	4.29532917	0.00102044	0.01976474	-1.6949324
98	ACYP2	0.90476897	2.04769088	4.20548058	0.00102116	0.01976474	-1.1842726
153	ADRB1	-1.9014238	-0.3479853	-4.1944445	0.00104242	0.02009199	-0.664319
10420	TESK2	0.91342746	1.76131523	4.18432711	0.00106231	0.02030575	-1.1621654
4986	OPRK1	-2.4657115	-0.5237162	-4.2008379	0.00106495	0.02032799	-0.6407762
375057	STUM	-0.9299184	7.35891445	-5.150854	0.00107332	0.02043147	-1.4992572
2766	GMPR	0.60804266	3.54177952	4.16811544	0.00109501	0.02076211	-1.5552953
8420	SNHG3	-0.7041751	5.82967424	-4.4699886	0.00109519	0.02076211	-1.7133543
374393	FAM111B	1.35693665	4.65733212	5.50402964	0.00110709	0.0209304	-1.204612
8553	BHLHE40	0.75378017	6.37929154	4.69191906	0.00111907	0.02109915	-1.6991744
23491	CES3	-1.4919084	0.76769965	-4.1533725	0.00112564	0.02119423	-0.8975161
6496	SIX3	-1.3336078	0.88320345	-4.1436932	0.00114623	0.02139122	-0.9483841
79815	NIPAL2	0.63969199	3.71689236	4.14337031	0.00114692	0.02139122	-1.6404802
65249	ZSWIM4	0.84167694	3.00823999	4.1392569	0.00115859	0.02147704	-1.5117509
59	ACTA2	1.87555612	-1.3966956	4.13764848	0.00115929	0.02147704	-0.7518901
200407	CREG2	-0.7538682	3.2936415	-4.1357283	0.00116346	0.02152563	-1.4903674
79890	RIN3	0.87617417	3.48425347	4.29519577	0.00116575	0.02153907	-1.5346516
202151	RANBP3L	-2.4689234	-1.6691274	-4.1326229	0.00117025	0.02158648	-0.6793703
2647	BLOC1S1	0.71221317	2.81543036	4.13149374	0.00117273	0.02158648	-1.4781458
90592	ZNF700	-0.8528797	2.74387344	-4.1313764	0.00117299	0.02158648	-1.3689662
7222	TRPC3	-2.519106	-1.4981066	-4.1298895	0.00117627	0.02161798	-0.6861799
7226	TRPM2	-0.6782245	4.23045813	-4.1249845	0.00118713	0.02178875	-1.7004146
84945	ABHD13	-0.5839429	4.24763973	-4.1220662	0.00119365	0.0218604	-1.718228
8123	PWAR5	-0.9187861	2.51340605	-4.1218211	0.00119419	0.0218604	-1.3324526
94031	HTRA3	1.77334421	-0.9526301	4.11937231	0.00119969	0.02193201	-0.8323114
147991	DPY19L3	-0.6170575	4.08002464	-4.1164401	0.00120631	0.02199486	-1.6940999
2852	GPER1	0.92961618	4.05980475	4.52760847	0.00122697	0.02223643	-1.5706839
503637	DUXAP8	0.62003423	3.83317557	4.10435461	0.00123398	0.02223643	-1.7358164
55175	KLHL11	-0.5945862	4.23453528	-4.0994927	0.00124529	0.02237254	-1.7576645
606	NBEAP1	-0.8439117	3.29085544	-4.0981277	0.00124849	0.02238057	-1.5561043
148534	TLCD4	0.78633029	4.63645665	4.41504383	0.00125665	0.02244175	-1.7391697
284293	HMSD	-1.2543504	0.90071103	-4.0946084	0.00125676	0.02244175	-1.0464044
727936	GXYLT2	-1.4489346	0.79735432	-4.0853671	0.00127877	0.02269707	-1.0345236
23308	ICOSLG	1.07003515	1.44781584	4.08197108	0.00128696	0.02280379	-1.293197
100270680	CASC11	-1.5455874	1.39005489	-4.1307697	0.00128857	0.02280379	-1.1121241
57730	ANKRD36B	-0.9164764	2.19084416	-4.0761795	0.00130104	0.02293644	-1.3521559
79094	CHAC1	-0.9710526	2.84607123	-4.0771884	0.00130603	0.02299514	-1.4919481

89801	PPP1R3F	0.73512301	2.59335839	4.07141714	0.00131274	0.02305075	-1.5472504
79646	PANK3	-0.6399277	5.80067895	-4.2596022	0.00131442	0.02305075	-1.9544621
55137	FIGN	-0.7123646	3.05363783	-4.0670048	0.00132368	0.0231001	-1.5721653
2686	GGT7	-1.02322	2.15851705	-4.063507	0.00133241	0.02319407	-1.3557893
59335	PRDM12	1.35944635	0.13401014	4.06282198	0.00133413	0.0231948	-1.0847404
192683	SCAMP5	-0.7153809	3.00704427	-4.0576097	0.00134728	0.02323541	-1.5794638
51378	ANGPT4	-2.4358898	-1.1301318	-4.0570335	0.00134874	0.02323541	-0.8260281
8969	H2AC11	1.42230679	-0.1781859	4.05176683	0.00136217	0.0233595	-1.0564826
79090	TRAPPC6A	0.98090808	2.03260084	4.04675336	0.00137509	0.02355179	-1.4818775
83715	ESPN	0.95038496	1.89974703	4.04163807	0.0013884	0.02372099	-1.4641911
26002	MOXD1	2.14361379	0.66033835	4.59402937	0.00139391	0.0237625	-0.9807154
64129	TINAGL1	1.31003174	2.60046382	4.52161473	0.00139426	0.0237625	-1.3841987
4550	RNR2	-0.9312124	12.9214839	-5.0621947	0.00143249	0.02420129	-1.7864104
9911	TMCC2	0.77591639	2.94304909	4.02448317	0.00143399	0.02420129	-1.7133627
84952	CGNL1	-1.1161165	1.98777444	-4.0150024	0.00145985	0.02450322	-1.4128179
286002	SLC26A4-AS1	-1.8224053	-0.2079858	-4.0146805	0.00146074	0.02450322	-1.0127595
84141	EVA1A	1.17929006	2.92487182	4.44828852	0.00148056	0.02474573	-1.5273285
26873	OPLAH	-0.6679741	5.65553427	-4.2349504	0.00149578	0.0249399	-2.0425573
8970	H2BC11	1.03211069	1.9546121	4.00000807	0.00150173	0.02498139	-1.5574506
286	ANK1	0.9003014	3.05573671	4.10946573	0.00150623	0.02498139	-1.7290086
857	CAV1	0.5810745	6.83239806	4.20711686	0.00150892	0.02498139	-2.1788058
100505994	LUCAT1	1.69645766	-0.6022657	3.98749049	0.00153763	0.02527223	-1.1193183
2863	GPR39	1.47266864	0.31584007	3.97854355	0.00156382	0.02561059	-1.2770731
126820	DNAI3	1.53780944	-0.521873	3.97660831	0.00156955	0.02563206	-1.1478054
54910	SEMA4C	-0.6865001	4.22256824	-3.9802403	0.00157578	0.02563206	-1.9842388
65268	WNK2	-2.234059	3.66289439	-5.4310282	0.00157619	0.02563206	-1.1125761
2330	FMO5	1.05750555	1.05341402	3.96793249	0.00159549	0.02582453	-1.4299698
1015	CDH17	-3.1424442	-1.5634041	-4.1391544	0.00160037	0.02587328	-0.9093167
54328	GPR173	-0.6933517	3.61534288	-3.9648253	0.00160488	0.02587664	-1.8827776
57711	ZNF529	-0.7832972	2.91975764	-3.9626588	0.00161147	0.02590143	-1.733478
83716	CRISPLD2	1.1290033	0.7763309	3.95802517	0.00162565	0.02606873	-1.3935208
80176	SPSB1	0.60712941	4.45534695	3.96248963	0.00162935	0.02609786	-2.1322639
407006	MIR221	-2.1260341	-0.5914872	-3.9558874	0.00163223	0.02611379	-1.0632326
57669	EPB41L5	-0.7118938	3.54042372	-3.9535299	0.00163952	0.02620016	-1.8913417
22835	ZFP30	-1.0091074	1.77137603	-3.9518056	0.00164488	0.02622516	-1.4941183
122970	ACOT4	2.40034047	-1.5226489	4.02801139	0.00165976	0.02640167	-1.0523617
5325	PLAGL1	0.61632213	4.16988134	3.94330897	0.00167152	0.02652776	-2.1108015
64881	PCDH20	-0.9020748	2.59227322	-3.9361053	0.00169446	0.02673849	-1.7071163
4301	AFDN	-1.0209351	5.26083778	-4.7275907	0.00169733	0.0267533	-1.8267231
9148	NEURL1	1.16047667	1.49872567	3.94350551	0.0016998	0.02676176	-1.5790569
641364	SLC7A11-AS1	-2.283411	-1.6011028	-3.9327205	0.00170535	0.02681857	-1.031077
643641	ZNF862	0.81247622	2.79461937	3.93196959	0.00170778	0.02682623	-1.8580532
22900	CARD8	-0.7254892	3.09316507	-3.925878	0.00172758	0.02707589	-1.8479029

54718	BTN2A3P	-1.1001581	1.87013258	-3.9212843	0.00174267	0.02721994	-1.5583589
285148	IAH1	0.62352364	3.31500846	3.91677792	0.00175761	0.02728191	-1.9915765
101927798	LOC101927798	-4.034409	0.56286232	-4.793916	0.0017739	0.02742901	-0.8407496
4571	TRNP	-0.7738925	7.0190747	-4.5413143	0.0017905	0.02765489	-2.1283486
376940	ZC3H6	0.74921957	2.48122628	3.90296504	0.00180421	0.02771198	-1.8481333
5991	RFX3	-0.6901848	3.04198268	-3.8965566	0.00182626	0.02791921	-1.8984856
114625	ERMAP	0.73101867	3.21625568	3.89611476	0.00182779	0.02791921	-2.0162291
11037	STON1	-1.5899295	0.01514324	-3.8949155	0.00183195	0.0279519	-1.2692385
6909	TBX2	-0.6113803	4.9236157	-3.9306675	0.00183602	0.02796588	-2.2530017
100499467	LINC00673	0.76697893	2.72808584	3.89341539	0.00183717	0.02796588	-1.920372
4501	MT1X	-0.6714052	3.80364237	-3.8929099	0.00183893	0.02796588	-2.0627664
1747	DLX3	-1.5382253	0.16339882	-3.8916838	0.00184321	0.02797697	-1.3002802
6913	TBX15	1.52724506	-0.7687742	3.89154293	0.0018437	0.02797697	-1.2710809
7637	ZNF84	0.91036863	2.19527861	3.88185694	0.00187788	0.02836844	-1.8329772
2104	ESRRG	-1.7902159	-0.3048049	-3.8813329	0.00187975	0.02836844	-1.2445159
1788	DNMT3A	-0.6265454	4.06368085	-3.8804662	0.00188284	0.02838417	-2.1403211
10205	MPZL2	0.65753799	3.25005175	3.87870899	0.00188913	0.02839419	-2.0550274
100507588	TGFBR3L	0.77679963	2.19239092	3.87422526	0.00190527	0.02859764	-1.8389409
284434	NWD1	1.2123253	0.87920689	3.87138969	0.00191555	0.028712	-1.5833234
128209	KLF17	1.02339976	1.06134273	3.87098007	0.00191704	0.028712	-1.6137666
3059	HCLS1	-1.7222546	-0.2533997	-3.8647544	0.00193982	0.02899053	-1.2815303
4688	NCF2	2.27095944	0.41042642	4.4319092	0.00195638	0.02918544	-1.2546418
1491	CTH	0.60593135	4.04247937	3.85644274	0.00197068	0.02932461	-2.25542
257407	C2orf72	-2.3147088	1.94640595	-4.5969547	0.00199904	0.02965134	-1.2651491
285966	TCAF2	0.87217949	2.11739816	3.84731592	0.00200514	0.02968338	-1.8783476
22921	MSRB2	0.82025767	2.21693692	3.84445803	0.00201605	0.02977602	-1.9034223
220972	MARCHF8	0.85724628	2.12346034	3.83611194	0.00204828	0.03009142	-1.9035816
348487	FAM131C	0.60105353	3.59194757	3.8341662	0.00205587	0.03017088	-2.205373
55818	KDM3A	0.58974207	5.66037213	3.99551179	0.0020767	0.03031568	-2.4470792
11033	ADAP1	-1.7203348	-0.7121267	-3.826926	0.00208436	0.03036359	-1.3019314
6622	SNCA	-0.7253478	3.63463218	-3.8250091	0.00209197	0.03044215	-2.1545872
130617	ZFAND2B	-0.6168021	3.65701028	-3.8188907	0.00211645	0.03060556	-2.1786254
2707	GJB3	1.28727788	4.89520045	5.0651513	0.00214321	0.03089568	-1.8942624
100134444	KCNJ18	3.58120585	-1.3486951	4.50965091	0.00219278	0.03131666	-1.087885
283358	B4GALNT3	-0.6101448	4.41422565	-3.7930631	0.00222305	0.03153098	-2.3778919
1755	DMBT1	-2.3927283	-1.924211	-3.7929185	0.00222367	0.03153098	-1.2745792
80320	SP6	1.43637985	-0.1155458	3.79290279	0.00222373	0.03153098	-1.5520734
6273	S100A2	1.12407315	5.76316493	4.96075934	0.00223953	0.03165768	-2.0584562
2353	FOS	1.22526445	1.20101082	3.81689231	0.00224555	0.03171037	-1.7918525
10815	CPLX1	0.91289098	3.43386023	4.05087791	0.00225234	0.03177377	-2.1270659
154860	FEZF1-AS1	0.87894837	1.66913198	3.78561247	0.00225481	0.03177636	-1.8992593
6583	SLC22A4	0.84826978	1.62288852	3.78291815	0.00226641	0.03190733	-1.8940138
57458	TMCC3	0.70430701	3.25932082	3.78131409	0.00227335	0.03192839	-2.2453301

4773	NFATC2	1.37174151	2.95687295	4.50559322	0.00227714	0.03192839	-1.8254311
1298	COL9A2	-1.5898938	0.0373757	-3.7785354	0.00228541	0.03201195	-1.4832201
79873	NUDT18	0.85595637	1.56330822	3.77736487	0.00229051	0.03205097	-1.8918483
151525	WDSUB1	-0.6828669	3.13609364	-3.7740712	0.00230493	0.03215515	-2.1519687
29070	CCDC113	0.62255774	3.13828205	3.76862623	0.00232897	0.03233048	-2.23899
11069	RAPGEF4	-0.9743065	3.28998257	-3.9392999	0.00232944	0.03233048	-2.0737818
5950	RBP4	-1.0456307	4.91500229	-4.500547	0.00233132	0.03233048	-2.0999743
57325	KAT14	0.5964266	3.17605653	3.76299377	0.0023541	0.03240243	-2.2586339
401321	LINC00997	0.61401449	3.50008215	3.76298967	0.00235412	0.03240243	-2.3269363
283422	LINC01559	2.07327752	0.5674225	4.26325128	0.00237177	0.03243471	-1.4935067
80063	ATF7IP2	-0.7234468	2.79018153	-3.7586185	0.00237381	0.03243471	-2.1034477
4846	NOS3	3.47846969	-1.5002325	4.38102619	0.00238512	0.0325199	-1.1826905
84941	HSH2D	0.83383149	2.20572541	3.75323423	0.0023983	0.03260418	-2.0756297
65217	PCDH15	-1.3881105	0.27891255	-3.7532193	0.00239837	0.03260418	-1.5767327
79400	NOX5	-1.4038164	0.66974144	-3.7516362	0.00240562	0.03263861	-1.6447178
80212	CCDC92	1.28921239	0.92568862	3.77095056	0.00241795	0.03274164	-1.8131969
22983	MAST1	-0.5826856	3.9798381	-3.7483808	0.0024206	0.03274362	-2.3822567
55061	SUSD4	-0.8686938	2.91242004	-3.7371199	0.00248202	0.03335947	-2.162921
4922	NTS	-1.953455	-0.0962368	-3.7440458	0.00248536	0.03335947	-1.5217819
64651	CSRNP1	0.62478464	3.02547999	3.73232094	0.0024959	0.03337267	-2.2871306
151126	ZNF385B	-0.9826629	2.44337341	-3.7302089	0.00251493	0.03349769	-2.0628153
2561	GABRB2	-1.5743363	0.07903785	-3.7274103	0.00251939	0.0335249	-1.5935278
100128191	TMPO-AS1	0.81258531	2.05357675	3.72489012	0.00253154	0.03362186	-2.0980117
100506054	RNASEH1-DT	0.59904513	4.09835746	3.71438628	0.00258281	0.03407388	-2.5375153
2901	GRIK5	1.84299618	-1.3764889	3.71333335	0.00258801	0.03410993	-1.5255932
92737	DNER	1.3300903	1.97016596	4.05388816	0.00261786	0.03433985	-1.9349439
27433	TOR2A	0.65832116	3.38396187	3.70508379	0.0026291	0.03436949	-2.4135906
165055	CCDC138	-0.6285373	3.64372324	-3.7030518	0.00263932	0.03445807	-2.4019102
23015	GOLGA8A	-0.6231977	6.82172257	-4.0308842	0.00268747	0.03482384	-2.6688346
2709	GJB5	2.41943488	-1.1154059	3.92267611	0.00269383	0.03487363	-1.4893243
10675	CSPG5	0.83714116	1.92383825	3.68713446	0.00272081	0.03519001	-2.1422892
166336	PRICKLE2	-1.6063773	0.02782459	-3.6853713	0.00272999	0.03527139	-1.6609061
23314	SATB2	-0.6243811	4.19702143	-3.6848059	0.00273295	0.03527139	-2.5468451
100616408	MIR5047	-0.695947	3.57856412	-3.6810306	0.00275274	0.03547032	-2.4232698
9185	REPS2	0.67577954	3.21392242	3.67575209	0.00278065	0.03566398	-2.4387812
101927922	LINC01479	-1.4072217	-0.0162529	-3.6744456	0.00278761	0.03570463	-1.6827834
55799	CACNA2D3	1.41364977	-0.680218	3.67385525	0.00279075	0.03570463	-1.6850977
50636	ANO7	-0.7927532	2.66173291	-3.6706167	0.00280809	0.03575078	-2.2385094
5865	RAB3B	1.67949915	0.85515085	3.98646208	0.00281279	0.03577028	-1.7965587
26499	PLEK2	0.92354098	5.3686534	4.43305096	0.00281711	0.03577028	-2.4139492
5800	PTPRO	-2.4218917	-1.5625359	-3.6639045	0.00284436	0.03607854	-1.510153
347746	PWARSN	-0.9396148	1.66216952	-3.6544289	0.00289638	0.03647225	-2.0410941
2888	GRB14	-0.6313477	3.66825967	-3.6528944	0.00290489	0.03651302	-2.5011275

342909	ZNF284	-1.0304862	1.41374843	-3.6516659	0.00291173	0.03655729	-1.9923126
138428	PTRH1	0.65617975	3.42986125	3.64772507	0.00293377	0.03660991	-2.534079
100287171	WASHC1	-0.5854148	4.49044424	-3.6420919	0.00296556	0.03686915	-2.6861466
100125556	FAM86JP	0.59656175	3.0691555	3.64176868	0.0029674	0.03686915	-2.46824
55450	CAMK2N1	-2.9913535	-0.8182468	-3.8899079	0.00299489	0.0370772	-1.4763276
23048	FNBP1	0.66916766	6.19604475	4.04975401	0.00299794	0.0370772	-2.7172072
55300	PI4K2B	0.63919703	4.31644499	3.73598402	0.00301594	0.03721334	-2.6752496
51191	HERC5	-0.6999741	3.7226183	-3.6397272	0.00301743	0.03721334	-2.5424795
5292	PIM1	0.65818135	4.52563353	3.79385739	0.00303155	0.03732534	-2.6795953
8448	DOC2A	-0.6152968	4.15211201	-3.6294043	0.00303846	0.03737712	-2.6424332
29958	DMGDH	1.52493441	-0.7181772	3.62822414	0.00304533	0.03742839	-1.767553
4053	LTBP2	0.79235276	2.36297402	3.62760948	0.00304892	0.03743921	-2.3521476
167359	NIM1K	0.61101635	3.05702113	3.6243859	0.00306779	0.0374715	-2.4991232
10794	ZNF460	-0.7282759	2.66300392	-3.6180183	0.00310543	0.03776921	-2.3456577
10795	ZNF268	0.96841639	1.65890161	3.61710369	0.00311087	0.03779753	-2.2270674
8997	KALRN	-0.5994267	3.34955593	-3.6153923	0.00312109	0.03788836	-2.5112576
101927027	CHROMR	-0.8072363	2.10114934	-3.6117515	0.00314293	0.0381039	-2.227313
54507	ADAMTSL4	-1.0313256	1.80322984	-3.6115154	0.00314435	0.0381039	-2.1404604
8858	PROZ	-2.211082	-1.0971925	-3.5951126	0.00324473	0.03897903	-1.6603167
3767	KCNJ11	-0.8451608	2.10499961	-3.593669	0.00325372	0.0390363	-2.2571086
389549	FEZF1	1.30350004	0.49665619	3.5934413	0.00325514	0.0390363	-2.034317
3176	HNMT	-0.6996238	3.01450764	-3.5925685	0.00326059	0.0390678	-2.476829
404281	YY2	-0.7455683	2.44255735	-3.585242	0.0033067	0.03951763	-2.3585697
5737	PTGFR	-0.7565114	4.7875982	-3.8689721	0.00339945	0.04041893	-2.6879287
219865	OR8G5	-1.5337275	-0.5399747	-3.5703363	0.00340256	0.04041893	-1.8004752
100630918	PARTICL	0.95685843	1.30420374	3.56713121	0.00342354	0.04059741	-2.2385935
7621	ZNF70	-0.8728007	1.79487649	-3.5647644	0.00343911	0.04064382	-2.2453953
100506142	RHOQ-AS1	-1.6873754	-0.5486308	-3.563084	0.00345022	0.040656	-1.8000891
8303	SNN	-1.0636886	1.49144577	-3.5570646	0.00349028	0.04079565	-2.1821968
79858	NEK11	0.90465863	1.38719295	3.55554441	0.00350048	0.04085097	-2.2777444
2256	FGF11	0.97091576	0.82806406	3.55547838	0.00350092	0.04085097	-2.1634737
9590	AKAP12	0.77843779	8.71805887	4.29227992	0.00353927	0.04110658	-2.7917131
55715	DOK4	-1.0305387	1.06233209	-3.5447603	0.00357366	0.04142034	-2.1269835
79924	ADM2	-1.4103931	0.91327916	-3.5480093	0.00360874	0.04173465	-2.0827162
286207	CFAP157	0.61477714	2.91250536	3.53812374	0.00361947	0.04178871	-2.6352611
1286	COL4A4	-1.3108565	0.23711866	-3.5379689	0.00362054	0.04178871	-1.9776672
5731	PTGER1	0.9053576	1.34838876	3.53203017	0.00366205	0.04212723	-2.3149851
78987	CRELD1	-0.6001144	3.953137	-3.5306432	0.00367181	0.04216944	-2.7950639
100129434	LOC100129434	-0.8309556	4.07098115	-3.7691014	0.00369503	0.04233227	-2.6604968
1891	ECH1	-0.6458344	5.90546185	-3.8455691	0.00370117	0.04233227	-2.9232495
11062	DUS4L	0.58617119	3.60368367	3.52503411	0.00371156	0.04237977	-2.8066281
10512	SEMA3C	0.68066761	3.44238781	3.54310797	0.00371749	0.04241247	-2.7677404
255394	TCP11L2	0.9298828	2.67203953	3.67083119	0.00374064	0.04255839	-2.5363224

1368	CPM	0.69647921	3.33449744	3.54121713	0.00374172	0.04255839	-2.7520847
54514	DDX4	1.4073557	-0.8489532	3.51899005	0.00375488	0.0426305	-1.949533
54751	FBLIM1	-0.929996	4.2278417	-3.9274258	0.00376641	0.04272406	-2.6090373
85363	TRIM5	0.81491267	2.30008421	3.51372941	0.003793	0.04299049	-2.5575473
648791	PPP1R3G	1.20832289	0.45725998	3.51143687	0.00380974	0.04310688	-2.1791587
3693	ITGB5	0.63248258	5.89273988	3.84113614	0.00382263	0.04314956	-2.9788799
53340	SPA17	0.67738635	2.35286326	3.4997156	0.00389648	0.04376901	-2.5907215
7942	TFEB	0.79248338	1.98077128	3.49416174	0.00393828	0.0440241	-2.5246259
126129	CPT1C	1.01713718	1.45912127	3.4884107	0.00398204	0.04429856	-2.4277461
284802	FRG1BP	1.5078605	-0.7650263	3.48687981	0.00399377	0.04439337	-2.0253008
4319	MMP10	1.55671506	-0.667437	3.48381386	0.00401737	0.04461984	-2.0457919
19	ABCA1	1.02924256	2.52770834	3.71000694	0.00405653	0.04487471	-2.5406019
80774	LIMD2	-1.3462297	0.22076752	-3.4603746	0.0042025	0.04604304	-2.1180152
253650	ANKRD18A	-0.6416898	3.73607365	-3.4571016	0.00422903	0.04622869	-2.8889551
25961	NUDT13	-0.6745621	3.58711574	-3.4539899	0.00425441	0.04635964	-2.8618032
79088	ZNF426	0.8311222	1.51223872	3.45165925	0.00427352	0.04649464	-2.5045694
3981	LIG4	-0.580575	3.80206911	-3.4495415	0.00429095	0.04656555	-2.9278659
161779	PGBD4	-0.8514206	2.05571608	-3.4492489	0.00429337	0.04656555	-2.5253283
8623	ASMTL	-0.866308	2.6511898	-3.4551536	0.00429887	0.04656555	-2.6548765
4214	MAP3K1	-0.829385	1.99523977	-3.4461395	0.00431912	0.04666691	-2.5200061
221662	RBM24	-1.4647608	0.11624583	-3.4460697	0.0043197	0.04666691	-2.1281584
163732	CITED4	1.07157535	1.09234498	3.44466531	0.00433138	0.04675662	-2.4323121
3897	L1CAM	1.51273662	-0.6675589	3.44376538	0.00433888	0.04680111	-2.1168736
55653	BCAS4	-0.7469577	2.94095984	-3.4346787	0.00441538	0.04723518	-2.7578996
100505839	SH3PXD2A-AS1	1.32028152	-0.1552385	3.43452682	0.00441667	0.04723518	-2.2160397
4599	MX1	1.41836066	-0.9661988	3.43129884	0.00444418	0.04741946	-2.0958088
7047	TGM4	1.47549246	-0.6042687	3.42728218	0.00447866	0.04771371	-2.1583102
26267	FBXO10	0.58160009	3.32547674	3.42644107	0.00448591	0.04775422	-2.9382309
8544	PIR	-0.7287291	2.53329529	-3.4205261	0.00453725	0.04804207	-2.6964094
27004	TCL6	0.83872055	1.70532096	3.41797842	0.00455954	0.04814547	-2.6108799
6819	SULT1C2	-1.5911021	-0.4814883	-3.4178191	0.00456094	0.04814547	-2.0866484
197	AHSG	-1.7902629	-1.3142229	-3.4157094	0.0045795	0.0481944	-1.9841999
26153	KIF26A	-3.4461172	-1.7143141	-3.790401	0.00463725	0.04851043	-1.7949806
55504	TNFRSF19	-1.6827845	0.49474384	-3.4953613	0.00465018	0.04851043	-2.192905
1326	MAP3K8	-0.757453	2.32646742	-3.4076761	0.00465084	0.04851043	-2.673844
645369	TMEM200C	-0.8739597	4.45635628	-3.80827	0.00467669	0.04858916	-2.8699988
169611	OLFML2A	0.58147667	2.97155857	3.40195685	0.00470231	0.04869673	-2.9114818
439990	LINC00857	0.65879751	4.79224361	3.65249771	0.00470438	0.04869673	-3.1037379
401541	CENPP	0.58389876	3.51266277	3.40165931	0.00470501	0.04869673	-3.0259776
63827	BCAN	2.35072727	3.25136851	5.0714834	0.00471168	0.04869673	-2.1874141
10344	CCL26	1.02075957	2.00313875	3.51700312	0.00472394	0.04878697	-2.6441861
119395	CALHM3	1.49072479	-1.281232	3.3983291	0.00473526	0.04886746	-2.1151482

3554	IL1R1	-2.0635155	-1.0615547	-3.397405	0.00474369	0.04888155	-2.0370644
729262	NUTM2B	1.80641144	-1.4773737	3.39688422	0.00474845	0.04889417	-2.0980349
10461	MERTK	-0.9308421	2.90993036	-3.5140665	0.00475307	0.04890542	-2.7364611
951	CD37	-0.9829717	1.5080521	-3.3868061	0.00484147	0.0494108	-2.5125045
2019	EN1	-1.080191	1.57091051	-3.3824529	0.00488221	0.04966412	-2.5326481
9481	SLC25A27	-0.6603671	2.7195165	-3.3818909	0.0048875	0.04966412	-2.8171073
692058	SNORD11	-2.208081	-1.7657003	-3.3818565	0.00488782	0.04966412	-2.0111473
649946	RPL23AP64	-1.4413271	-0.5850669	-3.3793009	0.00491193	0.04987247	-2.1504632

Appendix Table 8. List of differentially expressed genes in 22Rv1 cells with ENO2 knockout.

ENTREZID	SYMBOL	logFC	AveExpr	t	P.Value	adj.P.Val	B
5604	MAP2K1	-0.646158	6.2762902	-6.684093	0.001145	0.0498174	-1.004474
6476	SI	-2.868025	-0.54674	-6.681088	0.001147	0.0498174	-0.181728
4166	CHST6	-2.071325	0.2345728	-6.672911	0.001153	0.0498174	-0.172209
56477	CCL28	-2.736604	-0.89815	-6.671697	0.001154	0.0498174	-0.200483
9060	PAPSS2	1.545902	2.820892	6.667272	0.001159	0.0498174	-0.516661
55568	GALNT10	-1.449923	6.746105	-6.782553	0.00116	0.0498174	-1.00234
816	CAMK2B	-1.181153	3.892402	-6.703074	0.00113	0.0496026	-0.604545
3399	ID3	-0.597234	8.0006071	-6.715482	0.00112	0.0494843	-1.051215
285513	GPRIN3	-2.619156	1.610551	-6.725025	0.001122	0.0494843	-0.199567
2668	GDNF	0.823914	4.4337399	6.723231	0.001115	0.04944	-0.751826
201232	SLC16A13	-1.902178	0.383428	-6.748001	0.001096	0.0490042	-0.127319
10788	IQGAP2	-2.202936	-0.077131	-6.746985	0.001097	0.0490042	-0.120866
342977	NANOS3	-3.82838	-2.316183	-6.746955	0.001097	0.0490042	-0.215197
64084	CLSTN2	-4.228813	0.5357288	-6.788367	0.0011	0.0490042	-0.12359
23034	SAMD4A	-1.513484	3.6677536	-6.750266	0.001101	0.0490042	-0.511112
26499	PLEK2	-1.23913	2.086469	-6.792376	0.001064	0.0480649	-0.252847
57493	HEG1	2.055205	2.8396672	6.876831	0.001064	0.0480649	-0.403383
122402	TDRD9	0.68555	5.2760236	6.80565	0.001054	0.0479872	-0.816306
157285	PRAG1	-3.498616	3.0304347	-6.925593	0.001056	0.0479872	-0.248278
9061	PAPSS1	-1.514141	7.7153857	-6.943832	0.001044	0.0477135	-0.925306
103724390	LINC01287	-1.999183	0.8996547	-6.841509	0.001029	0.0471999	-0.082054
23531	MMD	-1.908859	5.0401333	-6.999938	0.001007	0.0471281	-0.592552
4828	NMB	-3.998159	3.3819053	-6.989176	0.001014	0.0471281	-0.182766
9802	DAZAP2	0.639627	8.5717089	6.862203	0.001015	0.0471281	-0.935469
55504	TNFRSF19	1.832648	2.7599032	6.897145	0.001021	0.0471281	-0.354884
11099	PTPN21	-1.124363	3.051809	-6.849482	0.001024	0.0471281	-0.351078
474	ATOH1	5.071875	-2.396638	6.934913	0.001025	0.0471281	-0.067832
79098	C1orf116	-2.085215	7.9239404	-7.025081	0.00099	0.0469182	-0.859478
5051	PAFAH2	-1.142878	5.1065285	-6.913266	0.000997	0.0469182	-0.67015
3798	KIF5A	-1.06489	3.2963131	-6.888223	0.000998	0.0469182	-0.36821
9086	EIF1AY	1.545175	4.1225791	6.963411	0.000998	0.0469182	-0.550683
348801	LNP1	1.262674	1.8440026	6.910248	0.000983	0.0468171	-0.186704
5277	PIGA	-0.919051	4.9864579	-6.922124	0.000976	0.046599	-0.648525
1811	SLC26A3	-2.69243	0.3695476	-6.943253	0.000962	0.0461003	0.005924
10227	MFSD10	-0.582708	6.0218409	-6.956777	0.000953	0.0458382	-0.769747
100287477	LOC100287477	-4.582467	-1.337821	-6.996394	0.000931	0.0458274	-0.047228
101927843	LINC01687	-5.503185	0.2758597	-7.074943	0.000936	0.0458274	0.004106
202151	RANBP3L	-2.220349	0.566325	-6.980152	0.000939	0.0458274	0.02569

9644	SH3PXD2A	-1.707175	4.6401961	-7.099079	0.00094	0.0458274	-0.478149
83482	SCRT1	-3.349125	1.1995417	-7.02218	0.000941	0.0458274	0.025537
140612	ZFP28	1.16158	2.0343664	6.969103	0.000946	0.0458274	-0.169341
284680	SPATA46	-3.248469	-0.746613	-6.963431	0.000949	0.0458274	-0.027528
1140	CHRNA1	-1.113213	3.6671764	-6.962966	0.00095	0.0458274	-0.369597
8411	EEA1	0.597965	6.1737102	6.962036	0.00095	0.0458274	-0.792017
9886	RHOBTB1	-1.434903	2.6016708	-7.040574	0.000902	0.0448328	-0.134683
2222	FDFT1	-0.585317	8.3724122	-7.0736	0.000883	0.0443819	-0.775557
102723631	CT45A10	2.6461	0.9608242	7.084303	0.000888	0.0443819	0.025902
23031	MAST3	-0.882963	4.5461044	-7.062873	0.000889	0.0443819	-0.46882
283316	CD163L1	2.31332	0.0531389	7.061204	0.00089	0.0443819	0.071482
23114	NFASC	-1.403663	4.9975306	-7.180112	0.000867	0.0437877	-0.473099
283358	B4GALNT3	-1.768147	2.9542047	-7.102699	0.000867	0.0437877	-0.127923
6721	SREBF2	-0.640063	8.6041634	-7.119352	0.000857	0.043614	-0.740703
84293	PRXL2A	-0.677612	5.7486637	-7.133437	0.00085	0.0435497	-0.604058
960	CD44	-0.694967	5.7713808	-7.129732	0.000852	0.0435497	-0.608819
7106	TSPAN4	-1.013264	4.5952749	-7.126925	0.000853	0.0435497	-0.419752
2739	GLO1	-1.084069	8.8629626	-7.242103	0.000835	0.0431192	-0.688657
79038	ZFYVE21	-0.726199	5.316192	-7.159423	0.000836	0.0431192	-0.527088
9609	RAB36	0.753953	4.3717964	7.15913	0.000836	0.0431192	-0.409136
124739	USP43	-0.841087	3.944863	-7.158351	0.000836	0.0431192	-0.291115
51090	PLLP	-2.479237	0.5453657	-7.189114	0.00082	0.0429303	0.159813
58483	LINC00474	-6.072353	-1.604865	-7.308602	0.000807	0.0425545	0.078856
8324	FZD7	1.32619	1.680358	7.211646	0.000808	0.0425545	0.046863
11313	LYPLA2	-0.63264	6.0023695	-7.211605	0.000808	0.0425545	-0.573427
9531	BAG3	0.587389	5.3784291	7.230064	0.000799	0.0425062	-0.507232
1992	SERPINB1	-0.790762	6.0280902	-7.240767	0.000793	0.0423684	-0.550149
90627	STARD13	1.232458	2.8588331	7.250599	0.000788	0.0423462	-0.088963
342892	ZNF850	0.882673	3.4658873	7.247225	0.00079	0.0423462	-0.188992
1717	DHCR7	-0.600934	7.4544435	-7.315142	0.000757	0.0410835	-0.584062
57221	ARFGEF3	-0.799962	8.6163683	-7.308199	0.00076	0.0410835	-0.599487
79411	GLB1L	-1.069234	3.5319267	-7.306305	0.000761	0.0410835	-0.103203
89790	SIGLEC10	2.043234	1.0968431	7.330911	0.000749	0.0408945	0.18708
4036	LRP2	-4.785114	1.2036433	-7.436253	0.000746	0.0408662	0.252036
1015	CDH17	-7.709803	0.0109052	-7.503976	0.000735	0.0405868	0.18791
5563	PRKAA2	-1.392327	4.9839278	-7.413538	0.000736	0.0405868	-0.277774
1429	CRYZ	-0.770362	4.9978873	-7.354582	0.000738	0.0405868	-0.332652
84532	ACSS1	-2.326368	1.1416044	-7.390792	0.000721	0.0404722	0.27328
390010	NKX1-2	-2.620478	0.606529	-7.385897	0.000724	0.0404722	0.281327
63917	GALNT11	-0.63806	6.7139729	-7.381808	0.000725	0.0404722	-0.505259
219654	ZCCHC24	-0.852534	3.9419774	-7.376808	0.000728	0.0404722	-0.132214
1769	DNAH8	-3.626132	-0.877616	-7.431196	0.000703	0.0397117	0.212171

9445	ITM2B	0.774526	6.3406382	7.460077	0.000691	0.0392657	-0.43245
55312	RFK	0.648329	5.9688056	7.455438	0.000693	0.0392657	-0.406719
64641	EBF2	-2.636721	-0.270555	-7.47569	0.000684	0.0392284	0.302095
414	ARSD	-0.65518	5.1203464	-7.471602	0.000686	0.0392284	-0.271016
2641	GCG	-4.645292	-2.496552	-7.469262	0.000687	0.0392284	0.163846
4880	NPPC	-2.341798	0.9609628	-7.491257	0.000678	0.0391472	0.340533
6029	RN7SL1	-2.313965	4.3377572	-7.660204	0.000669	0.0387796	0.015594
9663	LPIN2	0.798995	4.5933874	7.533914	0.00066	0.0385998	-0.173909
60529	ALX4	-1.332905	2.2215198	-7.527365	0.000663	0.0385998	0.248901
3775	KCNK1	0.851726	3.8853809	7.526649	0.000663	0.0385998	-0.060294
26032	SUSD5	1.889194	0.8926325	7.553435	0.000652	0.0385094	0.347023
147111	NOTUM	-2.614422	0.6482957	-7.549603	0.000654	0.0385094	0.379806
9788	MTSS1	-0.925883	4.1241993	-7.575118	0.000644	0.0382129	-0.019265
25976	TIPARP	0.897616	4.3147686	7.610048	0.00063	0.0375545	-0.075063
22829	NLGN4Y	1.422276	2.4650539	7.633075	0.000621	0.0371795	0.233939
642515	PRRT1B	-4.082577	3.7797146	-7.827527	0.000606	0.0364889	0.301568
345630	FBLL1	-1.254339	2.988514	-7.670546	0.000607	0.0364889	0.243927
112495	GTF3C6	-0.712885	6.7550273	-7.717894	0.00059	0.0363578	-0.265407
57689	LRRC4C	2.323736	-0.516132	7.717832	0.00059	0.0363578	0.471862
216	ALDH1A1	-6.219217	-1.158416	-7.800587	0.000594	0.0363578	0.337405
4161	MC5R	-4.28067	-2.593125	-7.707006	0.000594	0.0363578	0.269133
25888	ZNF473	-1.093118	5.7814862	-7.708617	0.000596	0.0363578	-0.18177
140462	ASB9	-3.43409	3.7592752	-7.8502	0.000598	0.0363578	0.312937
28958	COA3	-1.078049	6.1673415	-7.712525	0.0006	0.0363578	-0.225737
10397	NDRG1	-2.985711	4.7117397	-7.901521	0.00058	0.036185	0.147392
3082	HGF	-5.822765	3.4843756	-7.977418	0.000555	0.0348953	0.50908
9600	PITPNM1	-0.724424	6.5599802	-7.813179	0.000557	0.0348953	-0.186338
2128	EVX1	-2.622078	-0.103419	-7.857677	0.000543	0.0344077	0.525035
9832	JAKMIP2	-5.037458	0.5754832	-7.911253	0.000544	0.0344077	0.489738
4615	MYD88	-0.764594	4.6539962	-7.850977	0.000545	0.0344077	0.073692
576	ADGRB2	-1.349604	5.4590189	-7.973195	0.000524	0.0336613	0.036063
3171	FOXA3	-3.783178	-0.657408	-7.913428	0.000525	0.0336613	0.470144
55160	ARHGEF10L	-1.973321	3.7663877	-7.966985	0.000526	0.0336613	0.328271
29775	CARD10	-0.76614	5.397146	-7.978174	0.000505	0.032752	0.045716
4883	NPR3	-0.61776	6.4633449	-7.992528	0.000501	0.0326196	-0.058429
596	BCL2	0.811976	4.1653465	8.027864	0.000491	0.0321836	0.235969
63027	SLC22A23	-1.343759	5.8367242	-8.102968	0.000492	0.0321836	0.062435
961	CD47	0.886871	5.5603805	8.043379	0.000487	0.0320863	0.046282
2185	PTK2B	-0.625213	7.2319252	-8.065824	0.00048	0.0320046	-0.047468
658	BMPR1B	1.341211	4.0182542	8.057934	0.000482	0.0320046	0.280155
55258	THNSL2	1.096345	3.1910212	8.055393	0.000483	0.0320046	0.409052
91074	ANKRD30A	-5.551574	0.1331388	-8.162566	0.00047	0.0317213	0.573301

29974	A1CF	-6.987222	2.4972901	-8.26921	0.000471	0.0317213	0.701024
8287	USP9Y	1.693012	4.53319	8.196989	0.000472	0.0317213	0.246415
340706	VWA2	-2.21982	2.3521481	-8.119039	0.000466	0.0316915	0.64143
9751	SNPH	-3.679837	0.4750368	-8.138257	0.000461	0.0314861	0.674599
5187	PER1	-0.632208	6.1236434	-8.161275	0.000454	0.0312152	0.083589
11309	SLCO2B1	-5.17368	-0.958314	-8.185109	0.000449	0.0309599	0.554236
3554	IL1R1	-2.758063	4.7712777	-8.399461	0.000438	0.0304908	0.47064
55612	FERMT1	-0.811588	5.0887061	-8.218438	0.00044	0.0304908	0.254175
338758	ATP2B1-AS1	1.655078	1.44108	8.271697	0.000427	0.0298579	0.750797
284233	CYP4F35P	-4.094696	2.4709372	-8.414537	0.000424	0.0297752	0.806648
2152	F3	3.85321	4.1990889	8.469957	0.000421	0.0297724	0.509061
64215	DNAJC1	0.761798	5.0029786	8.315208	0.000416	0.0295473	0.297394
6778	STAT6	-5.568555	4.6755356	-8.502924	0.000414	0.0295226	0.74906
126567	C2CD4C	-5.539812	-0.973458	-8.373527	0.000407	0.0291449	0.632457
2650	GCNT1	0.999212	6.1386273	8.374349	0.000403	0.0289933	0.212304
1831	TSC22D3	-1.668003	5.1058054	-8.493765	0.000399	0.0289475	0.429835
5208	PFKFB2	-0.733478	6.6925806	-8.385797	0.0004	0.0289475	0.190873
55332	DRAM1	-1.465861	3.1278454	-8.413436	0.000394	0.0289174	0.711398
51477	ISYNA1	-0.93897	7.0149833	-8.405064	0.000396	0.0289174	0.19027
56128	PCDHB8	1.258478	3.4657309	8.436769	0.000389	0.0286909	0.610883
1793	DOCK1	-0.858749	6.4558006	-8.503184	0.000375	0.0277885	0.285565
11012	KLK11	-6.377092	1.7266391	-8.696156	0.000371	0.0277239	0.845484
6296	ACSM3	-3.130521	2.5832675	-8.605566	0.000372	0.0277239	0.895707
1646	AKR1C2	-6.97993	0.3585161	-8.645521	0.000372	0.0277239	0.732624
5033	P4HA1	0.663009	5.7032023	8.5678	0.000362	0.0273603	0.374536
83857	TMTC1	1.402124	5.6237505	8.657675	0.000362	0.0273603	0.405198
165679	SPTSSB	-1.517144	2.6805519	-8.595195	0.000356	0.0272268	0.87699
9048	ARTN	-1.507949	2.3917184	-8.64196	0.000347	0.0267844	0.931165
201895	SMIM14	-0.879964	7.1524212	-8.6345	0.000349	0.0267844	0.331372
64595	TTYT15	1.532165	4.1311588	8.682395	0.00034	0.0267686	0.66117
221935	SDK1	-5.176232	-2.049292	-8.666258	0.000343	0.0267686	0.719781
8325	FZD8	-1.866778	4.7742946	-8.775893	0.000343	0.0267686	0.667009
85414	SLC45A3	-1.807211	6.1791515	-8.849083	0.000344	0.0267686	0.472072
80115	BAIAP2L2	-1.494829	5.0811401	-8.700643	0.000345	0.0267686	0.57972
5142	PDE4B	1.747589	3.2503601	8.724935	0.000332	0.026738	0.820795
100129046	BCAR3-AS1	-3.612334	-1.307005	-8.707457	0.000335	0.026738	0.750052
2043	EPHA4	2.442728	3.1406428	8.821348	0.000335	0.026738	0.851903
23169	SLC35D1	-0.823222	4.8405483	-8.70518	0.000335	0.026738	0.602538
27151	CPAMD8	-3.416647	0.9456071	-8.75986	0.000326	0.0265261	1.027842
55809	TRERF1	0.860257	4.4304722	8.806642	0.000318	0.0264362	0.691397
10221	TRIB1	-1.26966	6.3846984	-8.850151	0.000322	0.0264362	0.49019
171425	CLYBL	-1.651079	2.2808193	-8.778916	0.000322	0.0264362	1.022942

146336	SSTR5-AS1	-6.764886	-1.978591	-8.867213	0.000323	0.0264362	0.785453
51527	GSKIP	-0.8606	5.0712007	-8.8208	0.000315	0.0264087	0.642127
152789	JAKMIP1	-4.200462	-2.325629	-8.819621	0.000315	0.0264087	0.741729
354	KLK3	-1.706606	3.4449986	-8.842417	0.000312	0.0263847	0.935718
5412	UBL3	-0.961144	5.8629039	-8.898253	0.000302	0.0257568	0.590069
91523	PCED1B	-1.779306	1.886613	-8.935067	0.000297	0.0255228	1.134871
1363	CPE	0.7757	6.5647427	8.92622	0.000298	0.0255228	0.532107
55313	CPPED1	-1.128	4.4134752	-8.964816	0.000292	0.0252974	0.842924
58480	RHO	0.875697	7.2619685	8.980657	0.00029	0.0252334	0.538993
80022	MYO15B	-1.513426	3.9450866	-9.048419	0.000279	0.0252082	0.984292
51313	GASK1B	-2.185374	2.872923	-9.04803	0.000279	0.0252082	1.143014
311	ANXA11	-0.952328	6.6527334	-9.028299	0.000282	0.0252082	0.603023
4324	MMP15	-1.490795	5.8119949	-9.102618	0.000283	0.0252082	0.710216
27239	GPR162	-1.12016	4.1311152	-9.013232	0.000285	0.0252082	0.912627
84708	LNK1	-2.700489	0.3113894	-8.994897	0.000287	0.0252082	1.115457
2740	GLP1R	-5.000654	0.2448529	-8.993681	0.000288	0.0252082	0.98558
5627	PROS1	-1.280631	4.6744658	-9.106795	0.000271	0.0247781	0.890049
10437	IFI30	-1.736185	4.9356365	-9.246724	0.000262	0.0241022	0.924052
56261	GPCPD1	0.956013	4.5593767	9.186409	0.00026	0.0240707	0.900747
55902	ACSS2	-0.888612	5.0157876	-9.212924	0.000256	0.0238919	0.88611
10581	IFITM2	-9.170593	0.6644341	-9.450444	0.000253	0.023867	1.029622
84440	RAB11FIP4	-0.859195	5.987925	-9.227116	0.000255	0.023867	0.773711
51816	ADA2	-4.936187	4.1465592	-9.569979	0.000239	0.0228278	1.342375
3625	INHBB	-2.013203	5.0721436	-9.474235	0.00024	0.0228278	1.037924
5295	PIK3R1	0.897189	5.4283304	9.39735	0.000233	0.022445	0.911217
63934	ZNF667	2.246247	3.0653822	9.482364	0.000228	0.0220946	1.269888
288	ANK3	-1.841188	5.0797788	-9.566162	0.000226	0.0220418	1.079852
143686	SESN3	0.838885	5.3443377	9.500557	0.000222	0.0217284	0.980472
7328	UBE2H	-0.876132	7.9744433	-9.555742	0.000216	0.0216683	0.872027
51109	RDH11	-1.255498	7.6413877	-9.615767	0.000216	0.0216683	0.886821
7366	UGT2B15	-4.679516	-0.892313	-9.539034	0.000217	0.0216683	1.0812
5358	PLS3	-0.674189	7.4648967	-9.526265	0.000219	0.0216683	0.861934
5095	PCCA	-1.343642	3.8265081	-9.519257	0.00022	0.0216683	1.257426
400710	ZNF473CR	-4.241105	0.3371117	-9.618209	0.000209	0.0214535	1.304862
2705	GJB1	-7.567252	-0.683503	-9.750525	0.000209	0.0214535	1.141796
2261	FGFR3	-0.91867	6.4097081	-9.60683	0.00021	0.0214535	0.961772
64849	SLC13A3	-1.097941	4.5319028	-9.713973	0.000199	0.0207749	1.255129
10110	SGK2	-5.457848	1.7496426	-9.908996	0.000193	0.0203637	1.495608
55529	PIP4P2	1.487995	4.4173252	9.784193	0.000193	0.0203637	1.265971
7404	UTY	1.738379	3.0398381	9.783035	0.000193	0.0203637	1.448273
57573	ZNF471	1.872056	3.1256142	9.769096	0.000194	0.0203637	1.43163
5362	PLXNA2	-3.005634	4.3033182	-10.05962	0.000188	0.020279	1.490042

3732	CD82	-2.557978	1.3549804	-9.878991	0.000184	0.020153	1.601457
105369209	LOC105369209	-5.095091	-1.371074	-9.864154	0.000185	0.020153	1.176682
7222	TRPC3	-2.04892	3.0066164	-9.925031	0.00018	0.0199336	1.594068
9245	GCNT3	-4.471948	-2.508064	-9.917241	0.000181	0.0199336	1.10894
285419	LINC01091	-4.61311	-2.44137	-10.12093	0.000164	0.0194676	1.178564
26137	ZBTB20	-1.817989	4.658374	-10.07656	0.000168	0.0194676	1.465656
7850	IL1R2	-5.523365	0.111108	-10.03605	0.000171	0.0194676	1.336475
65266	WNK4	-2.07151	1.954566	-10.033	0.000171	0.0194676	1.69155
847	CAT	-1.270664	6.127232	-10.02531	0.000171	0.0194676	1.228919
165545	DQX1	-1.631042	2.5432385	-10.02362	0.000172	0.0194676	1.663706
130589	GALM	-1.925369	2.8657621	-10.01858	0.000172	0.0194676	1.644745
57633	LRRN1	-4.022902	0.604607	-10.01569	0.000172	0.0194676	1.499703
6652	SORD	0.728007	6.3013072	10.00131	0.000173	0.0194676	1.17578
257106	ARHGAP30	2.22301	1.3699412	9.997581	0.000174	0.0194676	1.674082
90246	LOC90246	1.075016	4.7931692	10.17417	0.00016	0.019358	1.425075
223082	ZNRF2	1.245877	3.4804983	10.24946	0.000154	0.0188392	1.639896
146760	RTN4RL1	-2.46843	2.67912	-10.33806	0.000148	0.018227	1.821701
79071	ELOVL6	-1.015649	6.5607259	-10.39748	0.000144	0.0178805	1.390568
56649	TMPRSS4	-4.975791	-1.883151	-10.42917	0.000142	0.0177693	1.316992
1369	CPN1	-4.712553	-2.420085	-10.4544	0.00014	0.0177494	1.277024
57715	SEMA4G	-3.316945	4.1183099	-10.69793	0.000141	0.0177494	1.824467
1271	CNTFR	-1.252412	4.427191	-10.53514	0.000135	0.0176313	1.711221
57732	ZFYVE28	-2.36247	2.9156148	-10.52079	0.000136	0.0176313	1.89906
9619	ABCG1	-3.525233	1.1735382	-10.61285	0.00013	0.0173488	1.847449
100128252	ZNF667-AS1	1.547305	3.1819415	10.59485	0.000132	0.0173488	1.84832
84677	DSCR8	-6.734752	-0.592636	-10.6753	0.000127	0.0170951	1.477806
2786	GNG4	-1.322591	5.0974454	-10.70181	0.000125	0.0169819	1.71231
3977	LIFR	1.336837	4.190091	10.72718	0.000124	0.0169437	1.79248
266727	MDGA1	-3.884864	2.3601033	-10.79523	0.000121	0.016779	2.014989
694	BTG1	1.247085	7.1853264	10.78446	0.000121	0.016779	1.557362
1645	AKR1C1	-4.56529	-0.011772	-10.76961	0.000122	0.016779	1.61662
350	APOH	-6.148494	-2.34649	-10.884	0.000116	0.0164107	1.442878
148932	MOB3C	-3.114082	1.6856183	-10.88292	0.000116	0.0164107	2.035821
57630	SH3RF1	-1.3735	4.7609574	-11.00838	0.000109	0.0164024	1.908397
10544	PROCR	-2.101776	2.2201487	-10.98597	0.00011	0.0164024	2.120363
283460	HNF1A-AS1	-6.060499	-1.188515	-10.96024	0.000112	0.0164024	1.529725
1298	COL9A2	-2.720964	1.610324	-10.95099	0.000112	0.0164024	2.070216
22809	ATF5	-2.000843	5.7979219	-11.10089	0.000113	0.0164024	1.791662
9722	NOS1AP	-4.204313	0.9545482	-10.92762	0.000113	0.0164024	1.870584
56937	PMEPA1	0.905905	9.0059836	11.14083	0.000103	0.0158685	1.728465
140456	ASB11	-5.721481	-2.589091	-11.19211	0.000101	0.0158354	1.491073
4233	MET	-2.981352	2.9448576	-11.16964	0.000102	0.0158354	2.196756

7277	TUBA4A	-2.821521	5.0477588	-11.53842	9.82E-05	0.0155765	2.093348
256949	KANK3	-1.792193	4.1912225	-11.40791	9.21E-05	0.0147632	2.191106
440482	ANKRD20A5P	-2.55008	3.4127331	-11.52657	8.76E-05	0.0144697	2.332853
56667	MUC13	-1.23428	5.5958248	-11.50361	8.85E-05	0.0144697	2.041124
10370	CITED2	-0.920991	7.9931738	-11.50314	8.85E-05	0.0144697	1.903111
6451	SH3BGRL	1.709675	5.0414168	11.48376	8.93E-05	0.0144697	2.062966
2625	GATA3	-5.087214	2.6393079	-11.74133	8.40E-05	0.0142211	2.309065
359845	RFLNB	1.610973	3.2271145	11.72593	8.07E-05	0.0138176	2.371298
101978785	PCAT14	-3.322996	1.9245132	-11.81018	7.79E-05	0.0137801	2.396597
79068	FTO	-1.367564	6.7440575	-11.77225	7.91E-05	0.0137801	2.077156
58526	MID1IP1	-1.301234	5.7754168	-11.76059	7.95E-05	0.0137801	2.146604
4613	MYCN	-6.616007	-2.056861	-12.07639	6.99E-05	0.0137452	1.766319
727	C5	-1.894291	5.6843106	-12.06819	7.18E-05	0.0137452	2.306561
57495	NWD2	-2.103848	3.4644323	-11.97604	7.28E-05	0.0137452	2.511695
9971	NR1H4	-6.633913	-2.001487	-11.9745	7.29E-05	0.0137452	1.749741
6690	SPINK1	-9.407253	1.5800759	-12.1253	7.53E-05	0.0137452	1.844619
5783	PTPN13	1.036063	5.4551505	11.8809	7.57E-05	0.0137452	2.198702
64087	MCCC2	-1.231765	8.755324	-11.86864	7.61E-05	0.0137452	2.075738
55614	KIF16B	-1.707229	5.379383	-11.86518	7.62E-05	0.0137452	2.258505
10057	ABCC5	1.205976	6.0448729	11.85341	7.65E-05	0.0137452	2.13753
7429	VIL1	-5.946198	5.3552311	-12.52294	6.71E-05	0.0137007	2.613682
94241	TP53INP1	-2.729863	6.4128137	-12.48809	6.80E-05	0.0137007	2.356523
7276	TTR	-5.679175	-1.775945	-12.23611	6.56E-05	0.0135844	1.796984
116844	LRG1	-4.998644	-2.221047	-12.31769	6.35E-05	0.0133389	1.753041
11189	CELF3	-3.517764	2.9511726	-12.36035	6.25E-05	0.0133044	2.675909
150771	ITPRIPL1	-5.30183	-0.076282	-12.42011	6.10E-05	0.013185	1.976879
7544	ZFY	1.631093	3.7104841	12.49902	5.92E-05	0.0129739	2.661068
340267	COL28A1	-4.030335	0.4382799	-12.55773	5.79E-05	0.0128713	2.254533
197	AHSG	-5.882169	-1.687017	-12.80016	5.27E-05	0.0124326	1.924191
55603	TENT5A	1.16908	5.8466641	12.76192	5.35E-05	0.0124326	2.559231
85416	ZIC5	-2.674005	3.3650381	-12.72447	5.43E-05	0.0124326	2.821647
2875	GPT	-2.509593	4.6379486	-12.73572	5.50E-05	0.0124326	2.733886
79962	DNAJC22	-0.933514	6.540612	-12.68693	5.51E-05	0.0124326	2.493613
4072	EPCAM	-1.77649	5.7850923	-13.5128	4.05E-05	0.0121223	2.921945
93145	OLFM2	-3.311913	2.0329079	-13.50464	4.06E-05	0.0121223	2.979762
3039	HBA1	-4.742325	-0.148322	-13.44999	4.14E-05	0.0121223	2.226033
1636	ACE	-2.289858	5.1572962	-13.42119	4.21E-05	0.0121223	2.97081
127707	KLHDC7A	-6.579774	-2.058807	-13.24175	4.47E-05	0.0121223	2.00157
3026	HABP2	-7.061228	-1.806143	-13.14757	4.63E-05	0.0121223	2.014177
7036	TFR2	-1.553776	4.4001716	-13.13118	4.66E-05	0.0121223	2.900623
8284	KDM5D	1.328874	5.2129303	13.12247	4.67E-05	0.0121223	2.769478
6568	SLC17A1	-5.634427	-1.818009	-13.09845	4.71E-05	0.0121223	1.964886

8644	AKR1C3	-7.414313	2.6075668	-13.23129	4.72E-05	0.0121223	2.462473
100533178	PRORY	1.756547	2.8245307	13.00051	4.89E-05	0.0121223	2.918936
8490	RGS5	-2.093218	2.8712081	-12.97963	4.93E-05	0.0121223	2.916588
4646	MYO6	-1.464401	7.9668101	-12.97362	4.94E-05	0.0121223	2.5769
340024	SLC6A19	-6.490237	-2.10566	-12.96438	4.96E-05	0.0121223	1.943401
6542	SLC7A2	-1.581838	4.7558276	-12.96146	4.96E-05	0.0121223	2.796558
1152	CKB	-1.143934	9.4449904	-13.74934	3.72E-05	0.0120598	2.898111
10050	SLC17A4	-6.603871	-0.888525	-14.37159	3.00E-05	0.0114224	2.273641
100133941	CD24	-2.728386	3.6635894	-14.36073	3.01E-05	0.0114224	3.405959
54996	MTARC2	-4.704841	0.1563996	-14.18698	3.19E-05	0.0114224	2.448052
1907	EDN2	-2.409319	2.8538451	-14.12949	3.26E-05	0.0114224	3.305251
90102	PHLDB2	-9.799564	1.8212377	-14.24533	3.30E-05	0.0114224	2.310757
726	CAPN5	-3.74969	2.538766	-14.05161	3.35E-05	0.0114224	3.190408
146456	TMED6	-3.931835	1.7220265	-14.03034	3.37E-05	0.0114224	2.997187
8653	DDX3Y	1.751855	5.5653113	13.96601	3.45E-05	0.0114224	3.083411
1644	DDC	-7.570163	1.4632074	-14.65762	2.72E-05	0.0110249	2.532206
81033	KCNH6	-5.792414	3.511405	-14.80702	2.74E-05	0.0110249	3.313791
6755	SSTR5	-7.51251	-1.524499	-14.84776	2.56E-05	0.0108889	2.330489
51231	VRK3	-1.420624	5.7356799	-14.95373	2.47E-05	0.0108258	3.465897
79817	MOB3B	-3.624225	2.5508288	-15.88234	1.84E-05	0.0107617	3.68497
316	AOX1	-5.572379	1.1375126	-15.51453	2.06E-05	0.0107617	2.866541
6192	RPS4Y1	1.477164	6.7622113	15.41926	2.13E-05	0.0107617	3.555085
2564	GABRE	-3.965319	1.2637106	-15.36765	2.16E-05	0.0107617	3.168828
57758	SCUBE2	-4.691111	0.7788929	-15.33042	2.19E-05	0.0107617	2.857
26762	HAVCR1	-8.065227	-1.161644	-15.26877	2.23E-05	0.0107617	2.426224
1759	DNM1	-2.906692	3.6016899	-15.21451	2.27E-05	0.0107617	3.67685
169200	TMEM64	1.443785	6.3347986	15.15786	2.31E-05	0.0107617	3.478555
1482	NKX2-5	2.202259	3.0012407	15.06349	2.38E-05	0.0107617	3.638295
84649	DGAT2	-2.514472	4.3767802	-16.2861	1.63E-05	0.0101809	4.017974
2638	GC	-7.959146	-1.233514	-16.25767	1.64E-05	0.0101809	2.550947
2893	GRIA4	-4.496633	3.0165667	-16.75861	1.41E-05	0.0095689	3.892528
10085	EDIL3	-5.192836	1.8896911	-17.56311	1.12E-05	0.0090109	3.56169
55217	TMLHE	-8.702031	-0.803055	-17.32603	1.20E-05	0.0090109	2.711084
6197	RPS6KA3	-1.521506	6.6297098	-17.26164	1.22E-05	0.0090109	4.189113
3040	HBA2	-6.278131	1.1455168	-17.12616	1.27E-05	0.0090109	2.98612
3817	KLK2	-2.03223	5.5365535	-17.90718	1.02E-05	0.0089389	4.451762
338761	C1QL4	-3.694145	3.0306627	-18.28919	9.19E-06	0.0085603	4.338743
85462	FHDC1	-2.900337	7.1888323	-20.63078	5.37E-06	0.0084571	5.091348
92292	GLYATL1	-2.058432	5.6031536	-19.63189	6.48E-06	0.0084571	4.922518
115265	DDIT4L	-2.471672	5.3327479	-19.23991	7.16E-06	0.0084571	4.831312
1803	DPP4	-6.671243	1.6069537	-18.97752	7.66E-06	0.0084571	3.268559
8864	PER2	-1.709323	6.504502	-18.71953	8.20E-06	0.0084571	4.632333

2267	FGL1	-7.275582	0.3154678	-18.65778	8.33E-06	0.0084571	2.867954
10924	SMPDL3A	-2.041848	6.0862506	-18.60016	8.46E-06	0.0084571	4.623573
89822	KCNK17	-6.338163	1.1285163	-18.57611	8.51E-06	0.0084571	3.134618
57035	RSRP1	-2.318669	6.5671245	-27.52782	1.22E-06	0.0079651	6.590413
374393	FAM111B	-2.033609	8.9326563	-24.93786	1.99E-06	0.0079651	6.102354
650	BMP2	-2.308941	5.3662253	-24.71538	2.08E-06	0.0079651	6.038629
57224	NHSL1	-1.940023	5.9822267	-23.15459	2.87E-06	0.0079651	5.744936
64081	PBLD	-3.062923	5.2104054	-21.99941	3.69E-06	0.0079651	5.46972
147991	DPY19L3	-1.691309	6.9565957	-21.97431	3.71E-06	0.0079651	5.461792
51129	ANGPTL4	-3.419021	6.4027534	-22.05107	3.74E-06	0.0079651	5.482332

Supplementary Figures

Supplementary Figure 1. Cell line authentication report for PC3.



Over forty years of experience



Laboratory Report

Test Requested Cell Line Authentication
Case Number C-23751b
Date Sample Received 01/10/2021
Date Sample Tested 01/10/2021
Date Sample Reported 12/10/2021

Sample Name	Sample/Comparison Profile Source	Sample Number	DNA Number
PC3	University of Sheffield	S-1053546	D-1053546
CRL-1435 PC3	DSMZ Database	N/A	N/A

Table of Allelic Data

STR Locus	Genotypes		Match vs. Mis-Match
	PC3 (Test Sample)	CRL-1435 PC3 (Comparison Sample)	
D5	13 13	13 13	Match
D13	11 11	11 11	Match
D7	8 11	8 11	Match
D16	11 11	11 11	Match
vWA	17 17	17 17	Match
AmeI	X X	X X	Match
TPOX	8 9	8 9	Match
CSF1PO	11 11	11 11	Match
TH01	6 7	6 7	Match

Matching Percentage: 100%
Outcome: Related

The outcome percentage is calculated using a formulae which compares the number of alleles present against the number of alleles shared between the two DNA profiles. The outcome is designated one of the following statements based upon the outcome percentage:

Related (>80%) The Cell Lines are considered to be related.
Inconclusive (56-79%) Further profiling is required to determine whether the profiles are related.
No Match (55%>) It is considered that the two cell lines are unrelated.
Misidentified Cell Lines have been found to match a different donor within the database

Reported By: Ms. Eleanor Ralston (Senior Scientist)

Authorised By: Ms. Cara Shrimplin (Scientist - Genomics)

Date: 13/10/2021

These test results should only be used in conjunction with a client's information. The results relate only to the items sampled, as received and tested at this time.

2
2

Supplementary Table 2. Cell line authentication report for 22RV1.



Over forty years of experience



Laboratory Report

Test Requested Cell Line Authentication
Case Number C-23751a
Date Sample Received 01/10/2021
Date Sample Tested 01/10/2021
Date Sample Reported 12/10/2021

Sample Name	Sample/Comparison Profile Source	Sample Number	DNA Number
22RV1	University of Sheffield	S-1053545	D-1053545
CRL-2505 22RV1	DSMZ Database	N/A	N/A



Table of Allelic Data

STR Locus	Genotypes		Match vs. Mis-Match
	22RV1 (Test Sample)	CRL-2505 22RV1 (Comparison Sample)	
D5	11 13	11 12 13	Mis-Match
D13	9 12	9 12	Match
D7	9 10 11	9 10 11	Match
D16	12 12	12 12	Match
vWA	15 21	15 21	Match
Amel	X Y	X Y	Match
TPOX	8 8	8 8	Match
CSF1PO	10 11	10 11	Match
TH01	6 9.3	6 9.3	Match

Matching Percentage: 97%
Outcome: Related

The outcome percentage is calculated using a formulae which compares the number of alleles present against the number of alleles shared between the two DNA profiles. The outcome is designated one of the following statements based upon the outcome percentage:

Related (>80%) The Cell Lines are considered to be related.
Inconclusive (56-79%) Further profiling is required to determine whether the profiles are related.
No Match (55%>) It is considered that the two cell lines are unrelated.
Misidentified Cell Lines have been found to match a different donor within the database

Reported By: Ms. Eleanor Ralston (Senior Scientist) 
Authorised By: Ms. Cara Shrimplin (Scientist - Genomics) 
Date: 13/10/2021

These test results should only be used in conjunction with a client's information. The results relate only to the items sampled, as received and tested at this time.

2
2

Supplementary Figure 3. Cell line authentication report for WPMY-1.



Laboratory Report

Test Requested: Cell Line Authentication
 Case Number: C25727b
 Date Sample Received: 28/04/2022
 Date Sample Tested: 28/04/2022
 Date Sample Reported: 16/05/2022

Sample Name	Sample/Comparison Profile Source	Sample Number	DNA Number
WPMY-1 Human Prostate Myofibroblast	University of Sheffield	S-1058083	D-1058083
WPMY-1	Cellosaurus Database	N/A	N/A

Table of Allelic Data

STR Locus	Genotypes		Match vs. Mis-Match
	WPMY-1 Human Prostate Myofibroblast (Test Sample)	WPMY-1 (Comparison Sample)	
D5	12 15	12 15	Match
D13	8 14	8 14	Match
D7	10 11	10 11	Match
D16	9 9	9 9	Match
vWA	14 18	14 18	Match
Amel	X X	X Y	Mis-Match
TPOX	8 11	8 11	Match
CSF1PO	13 13	13 13	Match
TH01	8 9.3	8 9.3	Match

Matching Percentage: **97%**
 Outcome: **Related**

The outcome percentage is calculated using a formulae which compares the number of alleles present against the number of alleles shared between the two DNA profiles. The outcome is designated one of the following statements based upon the outcome percentage:

Related (>80%) The Cell Lines are considered to be related.
 Inconclusive (56-79%) Further profiling is required to determine whether the profiles are related.
 No Match (55%>) It is considered that the two cell lines are unrelated.
 Misidentified Cell Lines have been found to match a different donor within the database

Reported By: Mr. Benjamin Hickey (Laboratory Scientist)

Authorised By: Ms. Eleanor Ralston (Senior Scientist)

Date: 18/05/2022

These test results should only be used in conjunction with a client's information. The results relate only to the items sampled, as received and tested at this time.

Supplementary Figure 4. Cell line authentication report for DU145 and LNCaP-LN3.

Eurofins Genomics Europe Applied Genomics GmbH, Anzinger Str. 7 a, D-85560 Ebersberg

Ning WANG
University of Sheffield, Medical School
Beech Hill Road
s10 2rx sheffield
Great Britain



SOP_APG_Zelllinienauthentizität_A04_1.0

Certificate Cell Line Authentication Test Order ID: 11108118925

Report date: 04.10.2022

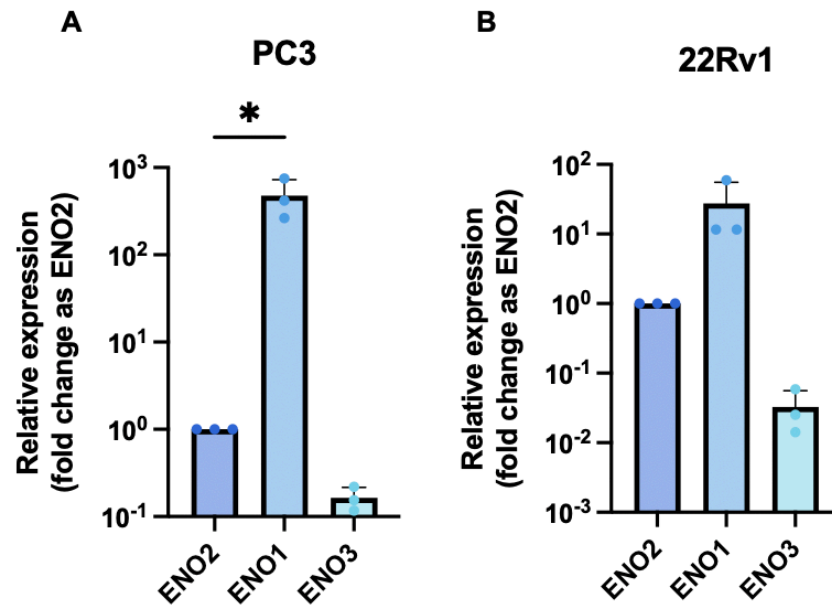
Method:

Genetic characteristics were determined by PCR-single-locus-technology.
16 independent PCR-systems D8S1179, D21S11, D7S820, CSF1PO, D3S1358, TH01, D13S317, D16S539, D2S1338, AMEL, D5S818, FGA, D19S433, vWA, TPOX and D18S51 were investigated.
(ASN-0002 core markers are colored grey, Thermo Fisher, AmpFISTR® Identifier® Plus PCR Amplification Kit)
In parallel, positive and negative controls were carried out yielding correct results.

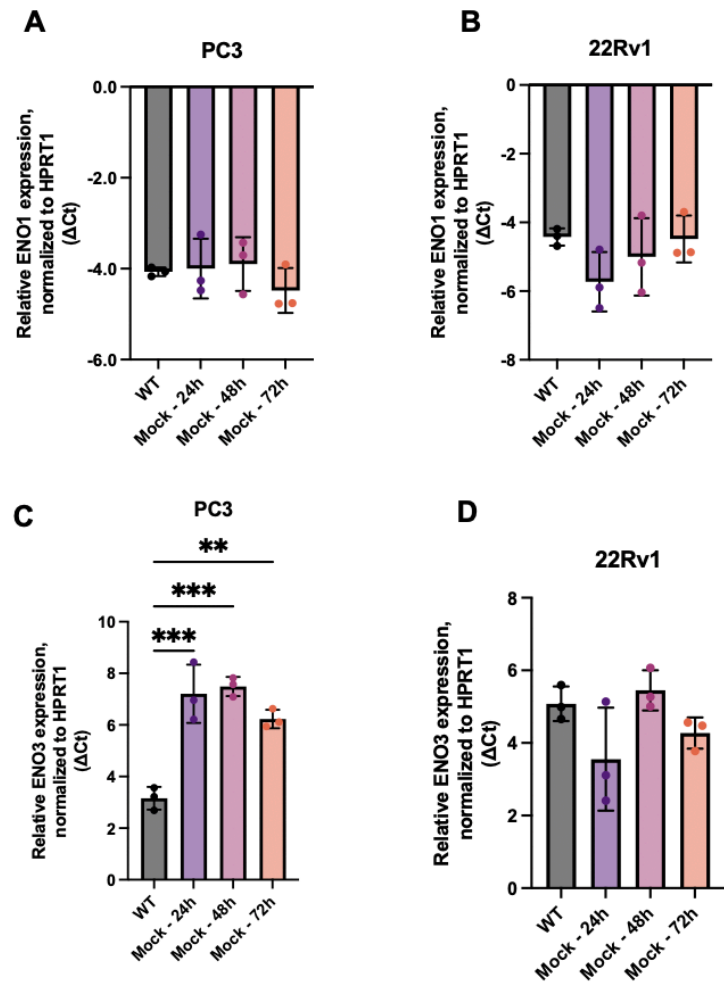
Result:

Client Sample Name	DU145 test	LNCaP LN3
Sample Code	CL00008831	CL00008832
D8S1179	13,13	11,12,13,14,15,16,17
D21S11	29,31.2	28,29,30,31.2,32.2,33.2
D7S820	8,11	9,1,10,3,11,3
CSF1PO	11,11	10,11,12
D3S1358	16,16	15,16,17
TH01	6,7	9,9
D13S317	11,11	9,10,12,13,14
D16S539	11,11	11,12,13
D2S1338	18,20	17,18
D19S433	14,14	12,2,13,2,14,15
vWA	17,17	16,18,19,20
TPOX	8,9	8,9
D18S51	14,15	10,11,12,13
AMEL	X,X	X,Y
D5S818	13,13	11,12,13
FGA	24,24	18,19,20

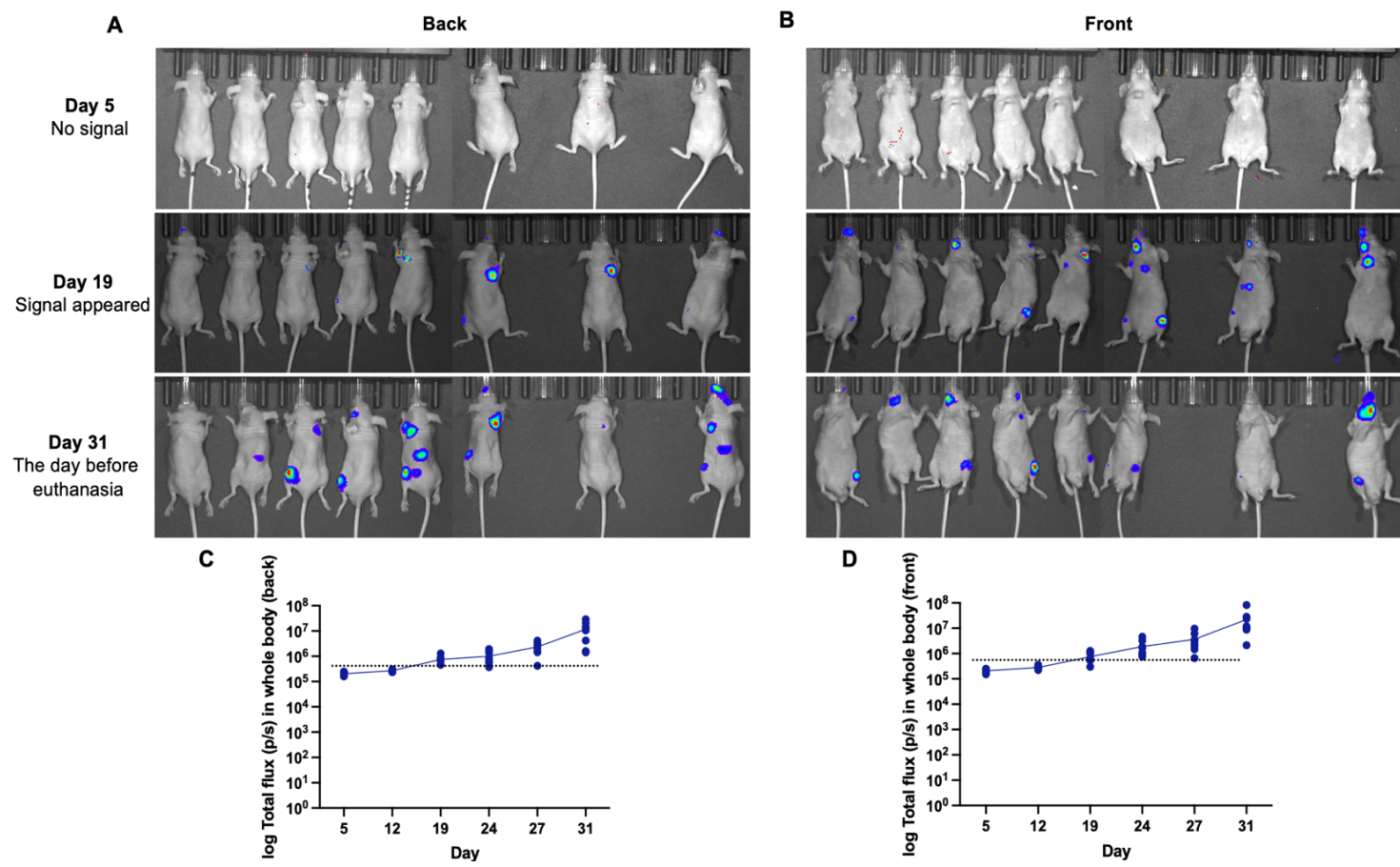
Supplementary Figure 5. (A and B) The relative expression of ENO1 and ENO3 were normalized to ENO2 with a $2^{-\Delta\Delta C_t}$ fold change in PC3 and 22Rv1 WT cells. The data are mean \pm standard deviation (n=3). One- way ANOVA with Dunnett multiple comparisons. *p<0.05.



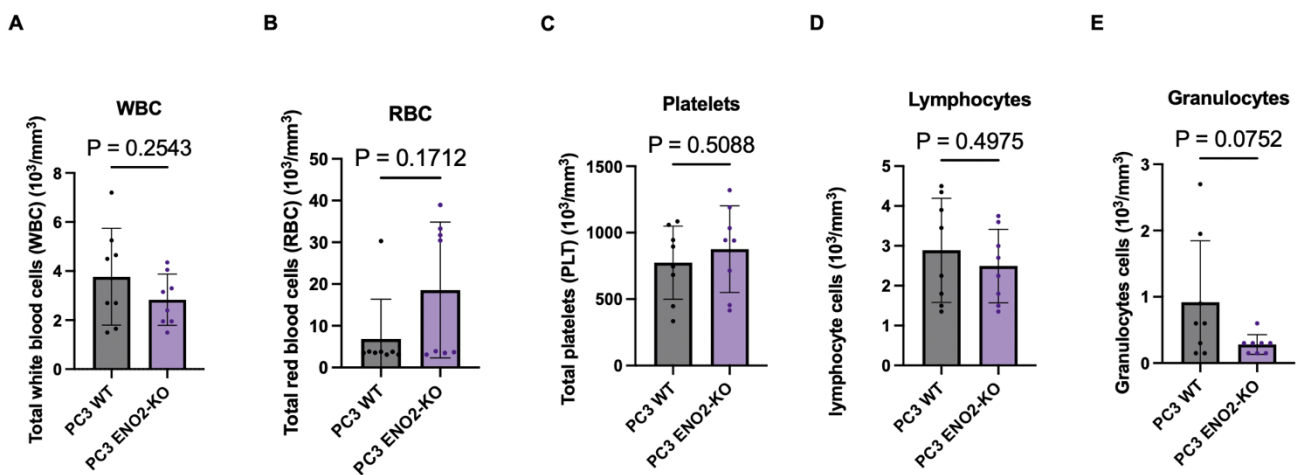
Supplementary Figure 6. (A and B) Expression of ENO1 of mock controls at 24, 48 and 72-hour time points were normalized to HPRT1 compared to PC3 and 22Rv1 WT, shown as ΔCt . (C and D) Expression of ENO3 of mock controls at 24, 48 and 72-hour time points were normalized to HPRT1 compared to PC3 and 22Rv1 WT, shown as ΔCt . The data are mean \pm standard deviation (n=3). One- way ANOVA with Dunnett multiple comparisons. **p<0.01 and ***p<0.001.



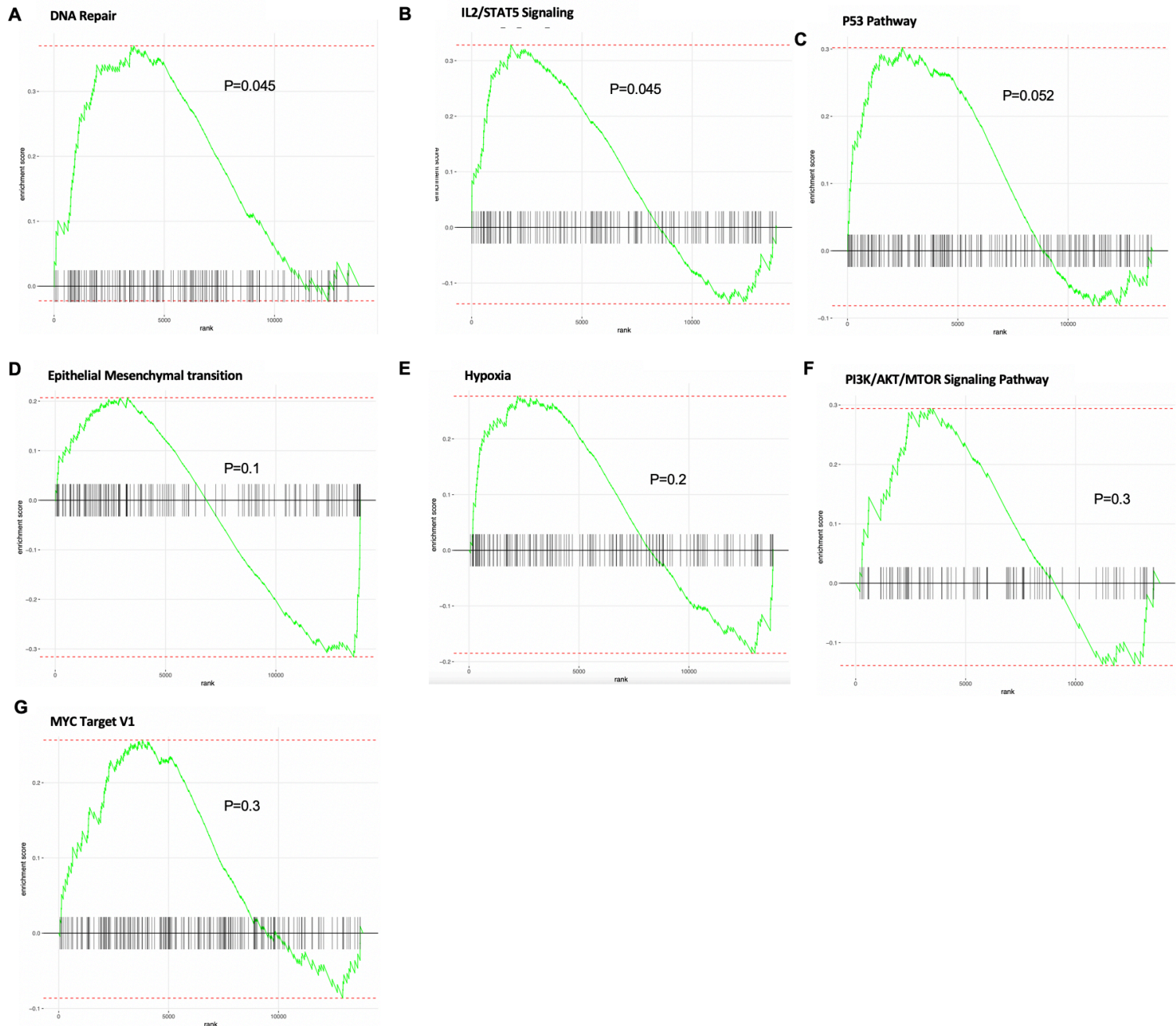
Supplementary Figure 7. The effect for the development of PCa bone metastasis in an intracardiacaly injected PC3 xenograft model. (A and B) The skeletal tumour growth in the control cohort was only examined by IVIS measurement on the back and front sides of the mice on Days 5, 19, and 31 after injection, respectively. **(C and D)** Tumor burden in control mice decreased within 31 days, measured as log total flux (photons/second). The data are mean \pm standard deviation (n=8).



Supplementary Figure 8. The effect of genetically inhibition of ENO2 in immune cells in whole blood. (A) The number total white blood cells from Balb/c mice of two different groups (B) The number total red blood cells from Balb/c mice of two different groups (C) The number platelets from Balb/c mice of two different groups (D) The number lymphocytes from Balb/c mice of two different groups (E) The number granulocytes from Balb/c mice of two different groups. The data are mean \pm standard deviation (n=8). Unpaired t-test.

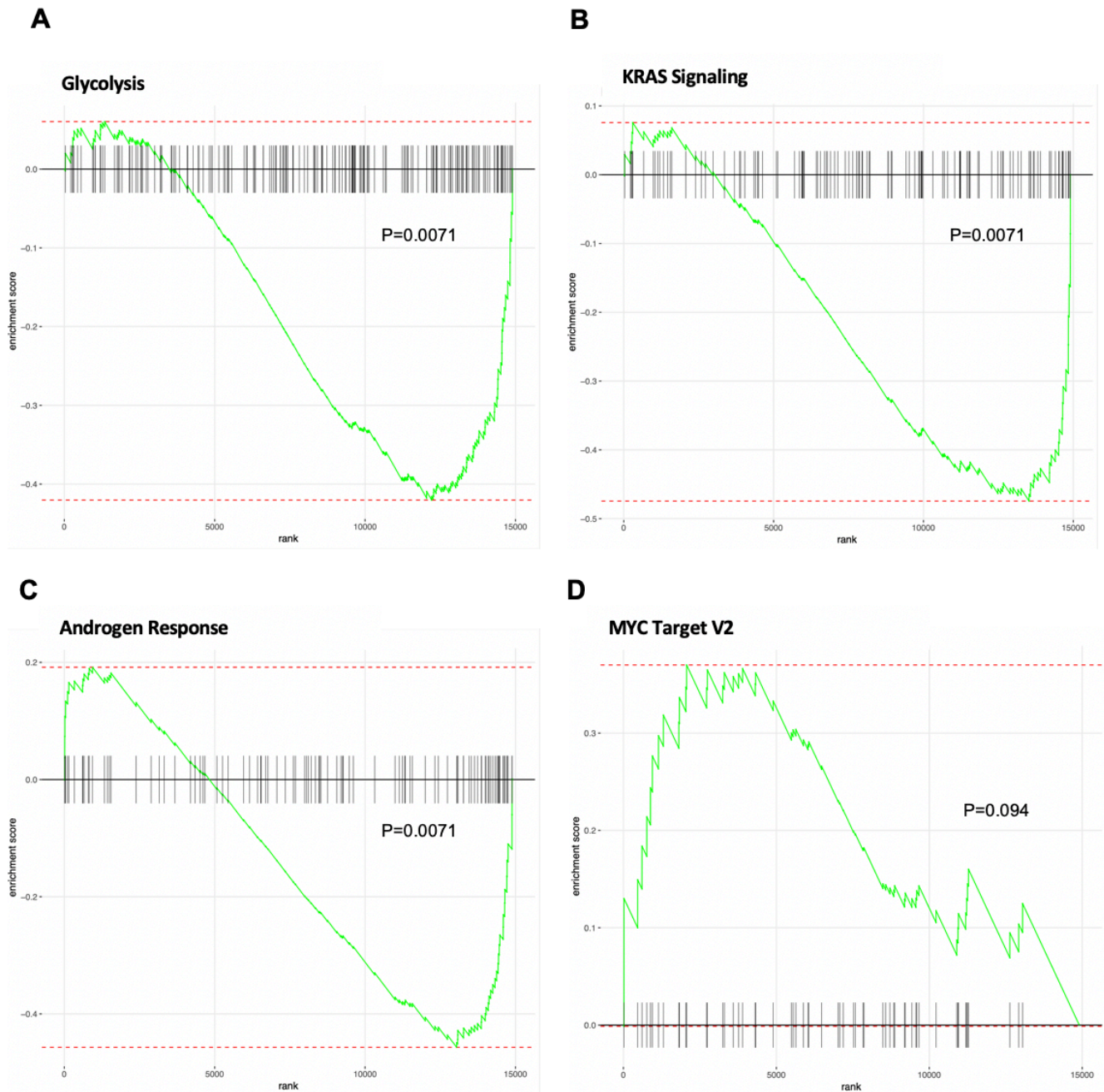


Supplementary Figure 9. GSEA results showed the tumour related enriched hallmarks and pathways in PC3 cells after ENO2 knockout. The p values are represented on the figure.



Supplementary Figure 10. GSEA results showed the tumour and metabolic related enriched hallmarks and pathways in 22Rv1 cells after ENO2 knockout.

The p values are represented on the figure.



Scientific Appendix

Buffer	
Loading buffer	<p>5.2 ml Trizma HCl (Sigma-Aldrich, No. T3253;1 M) pH 6.8 (use Trizma Base (Sigma-Aldrich, No. T6066) 1M to adjust pH)</p> <p>1g DL-Dithiothreitol (DTT; Sigma-Aldrich, No. 43819)</p> <p>1.3 g SDS (Melford, No. B2008) in 37°C to dissolve.</p> <p>6.5 ml glycerol (Sigma-Aldrich, No. G9012)</p> <p>130 µl 10% Bromophenol Blue (Sigma-Aldrich, No. B6896)</p> <p>Stir for 30 min.</p> <p>Store in -20 °C.</p>
RIPA lysis buffer	<p>1 ml 1% Triton X-100</p> <p>0.5 g 0.5% (w/v) sodium deoxycholate (Sigma-Aldrich, No. D6750) 0.1 g 0.1% (w/v) SDS</p> <p>Trizma HCl (50 mM using 0.788g in 100 ml) pH 7.4</p> <p>0.877 g NaCl (Thermo Fisher Scientific, No. S/3100/65;150mM)</p> <p>Store in -4°C.</p>
Tris buffer saline solution (TBS)	<p>For 1 L:</p> <p>60.57 g Trizma Base (500 mM) 78.8 g Trizma HCl (500 mM) 175.32 g NaCl (3 M)</p> <p>Store in room temperature</p>
10X Tris-acetate-EDTA (TAE) buffer	<p>For 1L:</p> <p>48.5 g Trizma Base in 800 ml deionized water</p> <p>11.4 ml Glacial acetic acid (Alfa Aesar, 64-19-7)</p> <p>20 ml 0.5M EDTA (BDH, 104245S) pH 8.0</p> <p>Add deionized water to 1L</p> <p>Store in room temperature</p>

References

1. Bhavsar, A. and S. Verma, *Anatomic imaging of the prostate*. Biomed Res Int, 2014. **2014**: p. 728539.
2. Verze, P., T. Cai, and S. Lorenzetti, *The role of the prostate in male fertility, health and disease*. Nat Rev Urol, 2016. **13**(7): p. 379-86.
3. Henry, G.H., et al., *A Cellular Anatomy of the Normal Adult Human Prostate and Prostatic Urethra*. Cell Rep, 2018. **25**(12): p. 3530-3542 e5.
4. Rawla, P., *Epidemiology of Prostate Cancer*. World J Oncol, 2019. **10**(2): p. 63-89.
5. Bray, F., et al., *Global cancer statistics 2022: GLOBOCAN estimates of incidence and mortality worldwide for 36 cancers in 185 countries*. CA Cancer J Clin, 2024.
6. Tang, D.G., *Understanding and targeting prostate cancer cell heterogeneity and plasticity*. Semin Cancer Biol, 2022. **82**: p. 68-93.
7. Bostwick, D.G., *The pathology of early prostate cancer*. CA Cancer J Clin, 1989. **39**(6): p. 376-93.
8. Albertsen, P.C., J.A. Hanley, and J. Fine, *20-year outcomes following conservative management of clinically localized prostate cancer*. JAMA, 2005. **293**(17): p. 2095-101.
9. Kang, J., et al., *Tumor microenvironment mechanisms and bone metastatic disease progression of prostate cancer*. Cancer Lett, 2022. **530**: p. 156-169.
10. Gupta, S., et al., *Prostate Cancer: How Young is too Young?* Curr Urol, 2017. **9**(4): p. 212-215.
11. Institute, N.C., *Cancer Stat Facts: Prostate Cancer [Internet]*. 2020, National Cancer Institute Bethesda, MD, USA.
12. Powell, I.J., et al., *Evidence supports a faster growth rate and/or earlier transformation to clinically significant prostate cancer in black than in white American men, and influences racial progression and mortality disparity*. J Urol,

2010. **183**(5): p. 1792-6.
13. Eeles, R., et al., *The genetic epidemiology of prostate cancer and its clinical implications*. Nat Rev Urol, 2014. **11**(1): p. 18-31.
 14. Cramer, S.D., et al., *Association Between Genetic Polymorphisms in the Prostate-Specific Antigen Gene Promoter and Serum Prostate-Specific Antigen Levels*. JNCI: Journal of the National Cancer Institute, 2003. **95**(14): p. 1044-1053.
 15. Noda, D., et al., *ELAC2, a putative prostate cancer susceptibility gene product, potentiates TGF-beta/Smad-induced growth arrest of prostate cells*. Oncogene, 2006. **25**(41): p. 5591-600.
 16. Xu, J., et al., *Germline mutations and sequence variants of the macrophage scavenger receptor 1 gene are associated with prostate cancer risk*. Nat Genet, 2002. **32**(2): p. 321-5.
 17. Erkkö, H., et al., *A recurrent mutation in PALB2 in Finnish cancer families*. Nature, 2007. **446**(7133): p. 316-9.
 18. Xu, J., et al., *Evidence for a prostate cancer susceptibility locus on the X chromosome*. Nat Genet, 1998. **20**(2): p. 175-9.
 19. Bostwick, D.G., et al., *Human prostate cancer risk factors*. Cancer, 2004. **101**(10 Suppl): p. 2371-490.
 20. Pienta, K.J. and P.S. Esper, *Risk factors for prostate cancer*. Ann Intern Med, 1993. **118**(10): p. 793-803.
 21. Descotes, J.-L., *Diagnosis of prostate cancer*. Asian Journal of Urology, 2019. **6**(2): p. 129-136.
 22. Sekhoacha, M., et al., *Prostate Cancer Review: Genetics, Diagnosis, Treatment Options, and Alternative Approaches*. Molecules, 2022. **27**(17).
 23. Prensner, J.R., et al., *Beyond PSA: the next generation of prostate cancer biomarkers*. Sci Transl Med, 2012. **4**(127): p. 127rv3.
 24. Lilja, H., D. Ulmert, and A.J. Vickers, *Prostate-specific antigen and prostate*

- cancer: prediction, detection and monitoring*. Nat Rev Cancer, 2008. **8**(4): p. 268-78.
25. Lintula, S., et al., *Relative concentrations of hK2/PSA mRNA in benign and malignant prostatic tissue*. Prostate, 2005. **63**(4): p. 324-9.
 26. Epstein, J.I., et al., *The 2005 International Society of Urological Pathology (ISUP) Consensus Conference on Gleason Grading of Prostatic Carcinoma*. Am J Surg Pathol, 2005. **29**(9): p. 1228-42.
 27. Humphrey, P.A., *Gleason grading and prognostic factors in carcinoma of the prostate*. Mod Pathol, 2004. **17**(3): p. 292-306.
 28. Pierorazio, P.M., et al., *Prognostic Gleason grade grouping: data based on the modified Gleason scoring system*. BJU Int, 2013. **111**(5): p. 753-60.
 29. Brawley, S., R. Mohan, and C.D. Nein, *Localized Prostate Cancer: Treatment Options*. Am Fam Physician, 2018. **97**(12): p. 798-805.
 30. Falzarano, S.M. and C. Magi-Galluzzi, *Staging prostate cancer and its relationship to prognosis*. Diagnostic Histopathology, 2010. **16**(9): p. 432-438.
 31. Li, J. and Z. Wang, *The pathology of unusual subtypes of prostate cancer*. Chin J Cancer Res, 2016. **28**(1): p. 130-43.
 32. Ranasinha, N., et al., *Ductal adenocarcinoma of the prostate: A systematic review and meta-analysis of incidence, presentation, prognosis, and management*. BJUI Compass, 2021. **2**(1): p. 13-23.
 33. Bhagirath, D., et al., *Novel, non-invasive markers for detecting therapy induced neuroendocrine differentiation in castration-resistant prostate cancer patients*. Sci Rep, 2021. **11**(1): p. 8279.
 34. Arora, K. and C.E. Barbieri, *Molecular Subtypes of Prostate Cancer*. Curr Oncol Rep, 2018. **20**(8): p. 58.
 35. Dragan, J., J. Kania, and M. Salagierski, *Active surveillance in prostate cancer management: where do we stand now?* Arch Med Sci, 2021. **17**(3): p. 805-811.
 36. Patel, M.I. and D.M. Poon, *Fast Facts: Prostate Cancer*. 2023: Karger Medical

and Scientific Publishers.

37. Wilt, T.J., et al., *Radical prostatectomy versus observation for localized prostate cancer*. New England Journal of Medicine, 2012. **367**(3): p. 203-213.
38. Knudsen, K.E. and H.I. Scher, *Starving the addiction: new opportunities for durable suppression of AR signaling in prostate cancer*. Clin Cancer Res, 2009. **15**(15): p. 4792-8.
39. Harris, W.P., et al., *Androgen deprivation therapy: progress in understanding mechanisms of resistance and optimizing androgen depletion*. Nat Clin Pract Urol, 2009. **6**(2): p. 76-85.
40. Cornford, P., et al., *EAU-ESTRO-SIOG Guidelines on Prostate Cancer. Part II: Treatment of Relapsing, Metastatic, and Castration-Resistant Prostate Cancer*. Eur Urol, 2017. **71**(4): p. 630-642.
41. Perera, M., et al., *Intermittent versus continuous androgen deprivation therapy for advanced prostate cancer*. Nat Rev Urol, 2020. **17**(8): p. 469-481.
42. Russell, N. and M. Grossmann, *Management of bone and metabolic effects of androgen deprivation therapy*. Urologic Oncology: Seminars and Original Investigations, 2021. **39**(10): p. 704-712.
43. Huang, Y., et al., *Molecular and cellular mechanisms of castration resistant prostate cancer*. Oncol Lett, 2018. **15**(5): p. 6063-6076.
44. Watson, P.A., V.K. Arora, and C.L. Sawyers, *Emerging mechanisms of resistance to androgen receptor inhibitors in prostate cancer*. Nat Rev Cancer, 2015. **15**(12): p. 701-11.
45. Aggarwal, R.R., et al., *Androgen receptor (AR) amplification in patients (pts) with metastatic castration resistant prostate cancer (mCRPC) resistant to abiraterone (Abi) and enzalutamide (Enz): Preliminary results from the SU2C/PCF/AACR West Coast Prostate Cancer Dream Team (WCDT)*. 2015, American Society of Clinical Oncology.
46. Lavaud, P., et al., *Next-generation androgen receptor inhibitors in non-*

- metastatic castration-resistant prostate cancer*. Ther Adv Med Oncol, 2020. **12**: p. 1758835920978134.
47. Saad, F., *Evidence for the efficacy of enzalutamide in postchemotherapy metastatic castrate-resistant prostate cancer*. Ther Adv Urol, 2013. **5**(4): p. 201-10.
 48. Taylor, A.K., et al., *PARP inhibitors in metastatic prostate cancer*. Frontiers in Oncology, 2023. **13**.
 49. Ragupathi, A., et al., *Targeting the BRCA1/2 deficient cancer with PARP inhibitors: Clinical outcomes and mechanistic insights*. Front Cell Dev Biol, 2023. **11**: p. 1133472.
 50. Saleem, S., et al., *Contemporaneous and upcoming trends in immunotherapy for prostate cancer: review*. Ann Med Surg (Lond), 2023. **85**(8): p. 4005-4014.
 51. Kim, J., et al., *FOXA1 inhibits prostate cancer neuroendocrine differentiation*. Oncogene, 2017. **36**(28): p. 4072-4080.
 52. Spetsieris, N., et al., *Neuroendocrine and Aggressive-Variant Prostate Cancer*. Cancers (Basel), 2020. **12**(12).
 53. Perlmutter, M.A. and H. Lepor, *Androgen deprivation therapy in the treatment of advanced prostate cancer*. Rev Urol, 2007. **9 Suppl 1**(Suppl 1): p. S3-8.
 54. Puente, J., et al., *Docetaxel in prostate cancer: a familiar face as the new standard in a hormone-sensitive setting*. Ther Adv Med Oncol, 2017. **9**(5): p. 307-318.
 55. Abidi, A., *Cabazitaxel: A novel taxane for metastatic castration-resistant prostate cancer-current implications and future prospects*. J Pharmacol Pharmacother, 2013. **4**(4): p. 230-7.
 56. Rowe, P., A. Koller, and S. Sharma, *Physiology, Bone Remodeling*, in *StatPearls*. 2024: Treasure Island (FL).
 57. Shupp, A.B., et al., *Cancer Metastases to Bone: Concepts, Mechanisms, and Interactions with Bone Osteoblasts*. Cancers (Basel), 2018. **10**(6).

58. Augat, P. and S. Schorlemmer, *The role of cortical bone and its microstructure in bone strength*. Age Ageing, 2006. **35 Suppl 2**: p. ii27-ii31.
59. Keaveny, T.M., et al., *Biomechanics of trabecular bone*. Annu Rev Biomed Eng, 2001. **3**: p. 307-33.
60. Capulli, M., R. Paone, and N. Rucci, *Osteoblast and osteocyte: games without frontiers*. Arch Biochem Biophys, 2014. **561**: p. 3-12.
61. Bonewald, L.F., *The amazing osteocyte*. J Bone Miner Res, 2011. **26**(2): p. 229-38.
62. Takahashi, N., et al., *Cells of bone: osteoclast generation*, in *Principles of bone biology*. 2002, Elsevier. p. 109-126.
63. Stenbeck, G., *Formation and function of the ruffled border in osteoclasts*. Semin Cell Dev Biol, 2002. **13**(4): p. 285-92.
64. Hauschka, P., et al., *Growth factors in bone matrix. Isolation of multiple types by affinity chromatography on heparin-Sepharose*. Journal of Biological Chemistry, 1986. **261**(27): p. 12665-12674.
65. Norgaard, M., et al., *Skeletal related events, bone metastasis and survival of prostate cancer: a population based cohort study in Denmark (1999 to 2007)*. J Urol, 2010. **184**(1): p. 162-7.
66. Yang, W., et al., *Research progress of bone metastases: From disease recognition to clinical practice*. Front Oncol, 2022. **12**: p. 1105745.
67. Wong, S.K., et al., *Prostate Cancer and Bone Metastases: The Underlying Mechanisms*. Int J Mol Sci, 2019. **20**(10).
68. Lamouille, S., J. Xu, and R. Derynck, *Molecular mechanisms of epithelial–mesenchymal transition*. Nature Reviews Molecular Cell Biology, 2014. **15**(3): p. 178-196.
69. Berish, R.B., et al., *Translational models of prostate cancer bone metastasis*. Nat Rev Urol, 2018. **15**(7): p. 403-421.
70. Clarke, N.W., C.A. Hart, and M.D. Brown, *Molecular mechanisms of metastasis*

- in prostate cancer*. Asian J Androl, 2009. **11**(1): p. 57-67.
71. Fisher, M.L., et al., *Type II transglutaminase stimulates epidermal cancer stem cell epithelial-mesenchymal transition*. Oncotarget, 2015. **6**(24): p. 20525-39.
 72. Esposito, M., T. Guise, and Y. Kang, *The Biology of Bone Metastasis*. Cold Spring Harb Perspect Med, 2018. **8**(6).
 73. Wang, N., et al., *Mitotic quiescence, but not unique "stemness," marks the phenotype of bone metastasis-initiating cells in prostate cancer*. Faseb j, 2015. **29**(8): p. 3141-50.
 74. van der Toom, E.E., J.E. Verdone, and K.J. Pienta, *Disseminated tumor cells and dormancy in prostate cancer metastasis*. Curr Opin Biotechnol, 2016. **40**: p. 9-15.
 75. Giacchetti, F.G., *Mechanisms governing metastatic dormancy and reactivation*. Cell, 2013. **155**(4): p. 750-64.
 76. Park, S.Y. and J.S. Nam, *The force awakens: metastatic dormant cancer cells*. Exp Mol Med, 2020. **52**(4): p. 569-581.
 77. Paget, S., *The distribution of secondary growths in cancer of the breast*. 1889. Cancer Metastasis Rev, 1989. **8**(2): p. 98-101.
 78. Croucher, P.I., M.M. McDonald, and T.J. Martin, *Bone metastasis: the importance of the neighbourhood*. Nature Reviews Cancer, 2016. **16**(6): p. 373-386.
 79. Nandana, S. and L.W. Chung, *Prostate cancer progression and metastasis: potential regulatory pathways for therapeutic targeting*. Am J Clin Exp Urol, 2014. **2**(2): p. 92-101.
 80. Roudier, M.P., et al., *Histopathological assessment of prostate cancer bone osteoblastic metastases*. J Urol, 2008. **180**(3): p. 1154-60.
 81. Logothetis, C.J. and S.H. Lin, *Osteoblasts in prostate cancer metastasis to bone*. Nat Rev Cancer, 2005. **5**(1): p. 21-8.
 82. Ye, L., H.G. Kynaston, and W.G. Jiang, *Bone metastasis in prostate cancer:*

- molecular and cellular mechanisms (Review)*. Int J Mol Med, 2007. **20**(1): p. 103-11.
83. Karst, M., et al., *Roles of stromal cell RANKL, OPG, and M-CSF expression in biphasic TGF-beta regulation of osteoclast differentiation*. J Cell Physiol, 2004. **200**(1): p. 99-106.
 84. Baron, R., S. Ferrari, and R.G. Russell, *Denosumab and bisphosphonates: different mechanisms of action and effects*. Bone, 2011. **48**(4): p. 677-92.
 85. Macherey, S., et al., *Bisphosphonates for advanced prostate cancer*. Cochrane Database Syst Rev, 2017. **12**(12): p. CD006250.
 86. Gupta, N., et al., *Usefulness of radium-223 in patients with bone metastases*. Proc (Bayl Univ Med Cent), 2017. **30**(4): p. 424-426.
 87. Reinstein, Z.Z., et al., *Overcoming immunosuppression in bone metastases*. Crit Rev Oncol Hematol, 2017. **117**: p. 114-127.
 88. Cutruzzola, F., et al., *Glucose Metabolism in the Progression of Prostate Cancer*. Front Physiol, 2017. **8**: p. 97.
 89. Ahmad, F., M.K. Cherukuri, and P.L. Choyke, *Metabolic reprogramming in prostate cancer*. British Journal of Cancer, 2021. **125**(9): p. 1185-1196.
 90. Barron, E.S. and C. Huggins, *The metabolism of the prostate; transamination and citric acid*. J Urol, 1946. **55**: p. 385-90.
 91. Flavin, R., G. Zadra, and M. Loda, *Metabolic alterations and targeted therapies in prostate cancer*. J Pathol, 2011. **223**(2): p. 283-94.
 92. Costello, L.C. and R.B. Franklin, *The clinical relevance of the metabolism of prostate cancer; zinc and tumor suppression: connecting the dots*. Mol Cancer, 2006. **5**: p. 17.
 93. Zheng, J., *Energy metabolism of cancer: Glycolysis versus oxidative phosphorylation (Review)*. Oncol Lett, 2012. **4**(6): p. 1151-1157.
 94. Liu, I.J., et al., *Fluorodeoxyglucose positron emission tomography studies in diagnosis and staging of clinically organ-confined prostate cancer*. Urology,

2001. **57**(1): p. 108-11.
95. Liberti, M.V. and J.W. Locasale, *The Warburg Effect: How Does it Benefit Cancer Cells?* Trends Biochem Sci, 2016. **41**(3): p. 211-218.
 96. Warburg, O., *On respiratory impairment in cancer cells.* Science, 1956. **124**(3215): p. 269-70.
 97. Chen, Z., et al., *Hypoxic microenvironment in cancer: molecular mechanisms and therapeutic interventions.* Signal Transduct Target Ther, 2023. **8**(1): p. 70.
 98. Pfeiffer, T., S. Schuster, and S. Bonhoeffer, *Cooperation and competition in the evolution of ATP-producing pathways.* Science, 2001. **292**(5516): p. 504-7.
 99. Lunt, S.Y. and M.G. Vander Heiden, *Aerobic glycolysis: meeting the metabolic requirements of cell proliferation.* Annu Rev Cell Dev Biol, 2011. **27**: p. 441-64.
 100. Vaupel, P., *Metabolic microenvironment of tumor cells: a key factor in malignant progression.* Exp Oncol, 2010. **32**(3): p. 125-7.
 101. Wang, W., et al., *The phosphatidylinositol 3-kinase/akt cassette regulates purine nucleotide synthesis.* J Biol Chem, 2009. **284**(6): p. 3521-8.
 102. Lim, S.O., et al., *EGFR Signaling Enhances Aerobic Glycolysis in Triple-Negative Breast Cancer Cells to Promote Tumor Growth and Immune Escape.* Cancer Res, 2016. **76**(5): p. 1284-96.
 103. Guo, D., et al., *EGFR signaling through an Akt-SREBP-1-dependent, rapamycin-resistant pathway sensitizes glioblastomas to antiproliferative therapy.* Sci Signal, 2009. **2**(101): p. ra82.
 104. Guo, D., et al., *An LXR agonist promotes glioblastoma cell death through inhibition of an EGFR/AKT/SREBP-1/LDLR-dependent pathway.* Cancer Discov, 2011. **1**(5): p. 442-56.
 105. Villa, G.R., et al., *An LXR-Cholesterol Axis Creates a Metabolic Co-Dependency for Brain Cancers.* Cancer Cell, 2016. **30**(5): p. 683-693.
 106. Chen, S. and N. Sang, *Hypoxia-Inducible Factor-1: A Critical Player in the Survival Strategy of Stressed Cells.* J Cell Biochem, 2016. **117**(2): p. 267-78.

107. Corcoran, S.E. and L.A. O'Neill, *HIF1alpha and metabolic reprogramming in inflammation*. J Clin Invest, 2016. **126**(10): p. 3699-3707.
108. Ni, J., et al., *Beyond ENO1, emerging roles and targeting strategies of other enolases in cancers*. Molecular Therapy - Oncolytics, 2023. **31**: p. 100750.
109. Muller, F.L., et al., *Passenger deletions generate therapeutic vulnerabilities in cancer*. Nature, 2012. **488**(7411): p. 337-342.
110. Zhang, C., et al., *ENO1 promotes antitumor immunity by destabilizing PD-L1 in NSCLC*. Cell Mol Immunol, 2021. **18**(8): p. 2045-2047.
111. Royds, J., et al., *Comparison of beta enolase and myoglobin as histological markers of rhabdomyosarcoma*. Journal of clinical pathology, 1985. **38**(11): p. 1258-1260.
112. Vizin, T. and J. Kos, *Gamma-enolase: a well-known tumour marker, with a less-known role in cancer*. Radiol Oncol, 2015. **49**(3): p. 217-26.
113. Isgrò, M.A., P. Bottoni, and R. Scatena, *Neuron-Specific Enolase as a Biomarker: Biochemical and Clinical Aspects*. Adv Exp Med Biol, 2015. **867**: p. 125-43.
114. Cata, J.P., B. Abdelmalak, and E. Farag, *Neurological biomarkers in the perioperative period*. Br J Anaesth, 2011. **107**(6): p. 844-58.
115. Soh, M.A., et al., *Arsenic, cadmium and neuron specific enolase (ENO2, γ -enolase) expression in breast cancer*. Cancer Cell Int, 2011. **11**(1): p. 41.
116. Ponting, C.P., et al., *PDZ domains: targeting signalling molecules to sub-membranous sites*. Bioessays, 1997. **19**(6): p. 469-79.
117. Hafner, A., N. Obermajer, and J. Kos, *gamma-1-syntrophin mediates trafficking of gamma-enolase towards the plasma membrane and enhances its neurotrophic activity*. Neurosignals, 2010. **18**(4): p. 246-58.
118. Viores, S.A., M.M. Herman, and L.J. Rubinstein, *Electron-immunocytochemical localization of neuron-specific enolase in cytoplasm and on membranes of primary and metastatic cerebral tumours and on glial*

- filaments of glioma cells*. Histopathology, 1986. **10**(9): p. 891-908.
119. Hanahan, D., *Hallmarks of Cancer: New Dimensions*. Cancer Discovery, 2022. **12**(1): p. 31-46.
 120. Hanahan, D. and R.A. Weinberg, *Hallmarks of cancer: the next generation*. Cell, 2011. **144**(5): p. 646-74.
 121. Vesselle, H., et al., *Lung cancer proliferation correlates with [F-18]fluorodeoxyglucose uptake by positron emission tomography*. Clin Cancer Res, 2000. **6**(10): p. 3837-44.
 122. Vander Heiden, M.G., L.C. Cantley, and C.B. Thompson, *Understanding the Warburg Effect: The Metabolic Requirements of Cell Proliferation*. Science, 2009. **324**(5930): p. 1029-1033.
 123. Denko, N.C., *Hypoxia, HIF1 and glucose metabolism in the solid tumour*. Nat Rev Cancer, 2008. **8**(9): p. 705-13.
 124. Amann, T., et al., *GLUT1 expression is increased in hepatocellular carcinoma and promotes tumorigenesis*. Am J Pathol, 2009. **174**(4): p. 1544-52.
 125. Hu, Z.Y., et al., *Glycolytic genes in cancer cells are more than glucose metabolic regulators*. J Mol Med (Berl), 2014. **92**(8): p. 837-45.
 126. Tapia, F.J., et al., *Neuron-specific enolase is produced by neuroendocrine tumours*. Lancet, 1981. **1**(8224): p. 808-11.
 127. Gao, C., et al., *Diagnostic role and prognostic value of tumor markers in high-grade gastro-enteropancreatic neuroendocrine neoplasms*. Pancreatology, 2023. **23**(2): p. 204-212.
 128. Zhang, J., et al., *Serum Biomarker Status with a Distinctive Pattern in Prognosis of Gastroenteropancreatic Neuroendocrine Carcinoma*. Neuroendocrinology, 2022. **112**(8): p. 733-743.
 129. Yan, T., et al., *Neuronal markers are expressed in human gliomas and NSE knockdown sensitizes glioblastoma cells to radiotherapy and temozolomide*. BMC Cancer, 2011. **11**(1): p. 524.

130. Sanzey, M., et al., *Comprehensive analysis of glycolytic enzymes as therapeutic targets in the treatment of glioblastoma*. PloS one, 2015. **10**(5): p. e0123544.
131. Lu, L., et al., *Neuron-specific enolase promotes stem cell-like characteristics of small-cell lung cancer by downregulating NBL1 and activating the BMP2/Smad/ID1 pathway*. Oncogenesis, 2022. **11**(1): p. 21.
132. Lv, C., et al., *ENO2 Promotes Colorectal Cancer Metastasis by Interacting with the LncRNA CYTOR and Activating YAP1-Induced EMT*. Cells, 2022. **11**(15): p. 2363.
133. Yukimoto, R., et al., *Specific activation of glycolytic enzyme enolase 2 in BRAF V600E-mutated colorectal cancer*. Cancer Sci, 2021. **112**(7): p. 2884-2894.
134. Chen, W.-J., et al., *ENO2 affects the EMT process of renal cell carcinoma and participates in the regulation of the immune microenvironment*. Oncol Rep, 2023. **49**(2): p. 33.
135. Gao, L., et al., *Mediation of PKM2-dependent glycolytic and non-glycolytic pathways by ENO2 in head and neck cancer development*. J Exp Clin Cancer Res, 2023. **42**(1): p. 1.
136. Liu, C.-c., et al., *ENO2 Promotes Cell Proliferation, Glycolysis, and Glucocorticoid-Resistance in Acute Lymphoblastic Leukemia*. Cellular Physiology and Biochemistry, 2018. **46**(4): p. 1525-1535.
137. Chen, W.J., et al., *ENO2 affects the EMT process of renal cell carcinoma and participates in the regulation of the immune microenvironment*. Oncol Rep, 2023. **49**(2).
138. Macedo, F., et al., *Bone Metastases: An Overview*. Oncol Rev, 2017. **11**(1): p. 321.
139. Ren, Y., et al., *Predicting survival of patients with bone metastasis of unknown origin*. Front Endocrinol (Lausanne), 2023. **14**: p. 1193318.
140. Kaighn, M.E., et al., *Establishment and characterization of a human prostatic*

- carcinoma cell line (PC-3)*. Invest Urol, 1979. **17**(1): p. 16-23.
141. Stone, K.R., et al., *Isolation of a human prostate carcinoma cell line (DU 145)*. Int J Cancer, 1978. **21**(3): p. 274-81.
 142. Sramkoski, R.M., et al., *A new human prostate carcinoma cell line, 22Rv1*. In Vitro Cell Dev Biol Anim, 1999. **35**(7): p. 403-9.
 143. Horoszewicz, J.S., et al., *LNCaP model of human prostatic carcinoma*. Cancer Res, 1983. **43**(4): p. 1809-18.
 144. Balbay, M.D., et al., *Highly metastatic human prostate cancer growing within the prostate of athymic mice overexpresses vascular endothelial growth factor*. Clin Cancer Res, 1999. **5**(4): p. 783-9.
 145. Wu, T.T., et al., *Establishing human prostate cancer cell xenografts in bone: induction of osteoblastic reaction by prostate-specific antigen-producing tumors in athymic and SCID/bg mice using LNCaP and lineage-derived metastatic sublines*. Int J Cancer, 1998. **77**(6): p. 887-94.
 146. Baley, P.A., et al., *Progression to androgen insensitivity in a novel in vitro mouse model for prostate cancer*. J Steroid Biochem Mol Biol, 1995. **52**(5): p. 403-13.
 147. Foster, B.A., et al., *Characterization of prostatic epithelial cell lines derived from transgenic adenocarcinoma of the mouse prostate (TRAMP) model*. Cancer Res, 1997. **57**(16): p. 3325-30.
 148. Webber, M.M., et al., *Human cell lines as an in vitro/in vivo model for prostate carcinogenesis and progression*. Prostate, 2001. **47**(1): p. 1-13.
 149. Zamore, P.D., et al., *RNAi: double-stranded RNA directs the ATP-dependent cleavage of mRNA at 21 to 23 nucleotide intervals*. Cell, 2000. **101**(1): p. 25-33.
 150. Gavrillov, K. and W.M. Saltzman, *Therapeutic siRNA: principles, challenges, and strategies*. Yale J Biol Med, 2012. **85**(2): p. 187-200.
 151. Jinek, M. and J.A. Doudna, *A three-dimensional view of the molecular*

- machinery of RNA interference*. Nature, 2009. **457**(7228): p. 405-12.
152. Ran, F.A., et al., *Genome engineering using the CRISPR-Cas9 system*. Nature Protocols, 2013. **8**(11): p. 2281-2308.
 153. Doudna, J.A. and E. Charpentier, *The new frontier of genome engineering with CRISPR-Cas9*. Science, 2014. **346**(6213): p. 1258096.
 154. Perez-Pinera, P., et al., *RNA-guided gene activation by CRISPR-Cas9–based transcription factors*. Nature Methods, 2013. **10**(10): p. 973-976.
 155. Csepregi, R., et al., *Complex Formation of Resorufin and Resazurin with B-Cyclodextrins: Can Cyclodextrins Interfere with a Resazurin Cell Viability Assay?* Molecules, 2018. **23**(2): p. 382.
 156. Rampersad, S.N., *Multiple Applications of Alamar Blue as an Indicator of Metabolic Function and Cellular Health in Cell Viability Bioassays*. Sensors, 2012. **12**(9): p. 12347-12360.
 157. Jones, L.J., et al., *Sensitive determination of cell number using the CyQUANT® cell proliferation assay*. Journal of Immunological Methods, 2001. **254**(1): p. 85-98.
 158. Zhang, J., et al., *Visualization of caspase-3-like activity in cells using a genetically encoded fluorescent biosensor activated by protein cleavage*. Nature Communications, 2013. **4**(1): p. 2157.
 159. McStay, G.P., G.S. Salvesen, and D.R. Green, *Overlapping cleavage motif selectivity of caspases: implications for analysis of apoptotic pathways*. Cell Death Differ, 2008. **15**(2): p. 322-31.
 160. Jonkman, J.E., et al., *An introduction to the wound healing assay using live-cell microscopy*. Cell Adh Migr, 2014. **8**(5): p. 440-51.
 161. Grada, A., et al., *Research Techniques Made Simple: Analysis of Collective Cell Migration Using the Wound Healing Assay*. Journal of Investigative Dermatology, 2017. **137**(2): p. e11-e16.
 162. Bouxsein, M.L., et al., *Guidelines for assessment of bone microstructure in*

- rodents using micro-computed tomography. *Journal of Bone and Mineral Research*, 2010. **25**(7): p. 1468-1486.
163. Pijuan, J., et al., *In vitro Cell Migration, Invasion, and Adhesion Assays: From Cell Imaging to Data Analysis*. *Frontiers in Cell and Developmental Biology*, 2019. **7**.
 164. Martin, M., *Cutadapt removes adapter sequences from high-throughput sequencing reads*. 2011, 2011. **17**(1): p. 3.
 165. Kim, D., B. Langmead, and S.L. Salzberg, *HISAT: a fast spliced aligner with low memory requirements*. *Nature Methods*, 2015. **12**(4): p. 357-360.
 166. Liao, Y., G.K. Smyth, and W. Shi, *featureCounts: an efficient general purpose program for assigning sequence reads to genomic features*. *Bioinformatics*, 2013. **30**(7): p. 923-930.
 167. Law, C.W., et al., *voom: precision weights unlock linear model analysis tools for RNA-seq read counts*. *Genome Biology*, 2014. **15**(2): p. R29.
 168. Wickham, H. and H. Wickham, *Ggplot2: Elegant graphics for data analysis*. . 2016: Springer.
 169. Young, M.D., et al., *Gene ontology analysis for RNA-seq: accounting for selection bias*. *Genome Biology*, 2010. **11**(2): p. R14.
 170. Korotkevich, G., et al., *Fast gene set enrichment analysis*. *bioRxiv*, 2021: p. 060012.
 171. Szklarczyk, D., et al., *STRING v11: protein-protein association networks with increased coverage, supporting functional discovery in genome-wide experimental datasets*. *Nucleic Acids Res*, 2019. **47**(D1): p. D607-d613.
 172. Mi, H., et al., *Protocol Update for large-scale genome and gene function analysis with the PANTHER classification system (v.14.0)*. *Nature Protocols*, 2019. **14**(3): p. 703-721.
 173. David, M., et al., *Preferred reporting items for systematic reviews and meta-analyses: the PRISMA statement*. *BMJ*, 2009. **339**: p. b2535.

174. Boerckel, J.D., et al., *Microcomputed tomography: approaches and applications in bioengineering*. Stem Cell Res Ther, 2014. **5**(6): p. 144.
175. Fischer, A.H., et al., *Hematoxylin and eosin staining of tissue and cell sections*. CSH Protoc, 2008. **2008**: p. pdb.prot4986.
176. Zlowodzki, M., et al., *How to interpret a meta-analysis and judge its value as a guide for clinical practice*. Acta Orthop, 2007. **78**(5): p. 598-609.
177. Higgins, J.P.T. and S.G. Thompson, *Quantifying heterogeneity in a meta-analysis*. Statistics in Medicine, 2002. **21**(11): p. 1539-1558.
178. Stang, A., *Critical evaluation of the Newcastle-Ottawa scale for the assessment of the quality of nonrandomized studies in meta-analyses*. Eur J Epidemiol, 2010. **25**(9): p. 603-5.
179. *OHAT Risk of Bias Rating Tool for Human and Animal Studies*. 2015.
180. Ryan R, H.S., *How to GRADE the quality of the evidence*. Cochrane Consumers and Communication Group,, 2016. **Version 3.0**.
181. Tang, Z., et al., *GEPIA: a web server for cancer and normal gene expression profiling and interactive analyses*. Nucleic Acids Res, 2017. **45**(W1): p. W98-W102.
182. Li, C., et al., *GEPIA2021: integrating multiple deconvolution-based analysis into GEPIA*. Nucleic Acids Res, 2021. **49**(W1): p. W242-w246.
183. Cerami, E., et al., *The cBio cancer genomics portal: an open platform for exploring multidimensional cancer genomics data*. Cancer Discov, 2012. **2**(5): p. 401-4.
184. Gao, J., et al., *Integrative analysis of complex cancer genomics and clinical profiles using the cBioPortal*. Sci Signal, 2013. **6**(269): p. pl1.
185. de Bruijn, I., et al., *Analysis and Visualization of Longitudinal Genomic and Clinical Data from the AACR Project GENIE Biopharma Collaborative in cBioPortal*. Cancer Res, 2023. **83**(23): p. 3861-3867.
186. Mishra, P., et al., *Descriptive statistics and normality tests for statistical data*.

- Ann Card Anaesth, 2019. **22**(1): p. 67-72.
187. Rebello, R.J., et al., *Prostate cancer*. Nature Reviews Disease Primers, 2021. **7**(1): p. 9.
 188. Csizmarik, A., et al., *Mechanisms and markers of resistance to androgen signaling inhibitors in patients with metastatic castration-resistant prostate cancer*. Urologic Oncology: Seminars and Original Investigations, 2021. **39**(10): p. 728.e13-728.e24.
 189. Huang, J., et al., *Immunohistochemical characterization of neuroendocrine cells in prostate cancer*. Prostate, 2006. **66**(13): p. 1399-406.
 190. Zheng, Y., et al., *Insulin-like growth factor 1-induced enolase 2 deacetylation by HDAC3 promotes metastasis of pancreatic cancer*. Signal Transduction and Targeted Therapy, 2020. **5**(1): p. 53.
 191. Zeng, F., et al., *TRAF6 as a potential target in advanced breast cancer: a systematic review, meta-analysis, and bioinformatics validation*. Scientific Reports, 2023. **13**(1): p. 4646.
 192. Bery, F., et al., *The Calcium-Sensing Receptor is A Marker and Potential Driver of Neuroendocrine Differentiation in Prostate Cancer*. Cancers, 2020. **12**(4).
 193. Kessel, K., et al., *Molecular analysis of circulating tumor cells of metastatic castration-resistant Prostate Cancer Patients receiving ¹⁷⁷Lu-PSMA-617 Radioligand Therapy*. Theranostics, 2020. **10**(17): p. 7645-7655.
 194. Szarvas, T., et al., *Comprehensive analysis of serum chromogranin A and neuron-specific enolase levels in localized and castration-resistant prostate cancer*. Bju International, 2021. **127**(1): p. 44-55.
 195. Bock, N., et al., *Engineering osteoblastic metastases to delineate the adaptive response of androgen-deprived prostate cancer in the bone metastatic microenvironment*. Bone research, 2019. **7**: p. 13.
 196. Beltran, H., et al., *Molecular Characterization of Neuroendocrine Prostate Cancer and Identification of New Drug Targets*. Cancer Discovery, 2011. **1**(6):

- p. 487-495.
197. Beltran, H., et al., *Divergent clonal evolution of castration-resistant neuroendocrine prostate cancer*. Nat Med, 2016. **22**(3): p. 298-305.
 198. Cunningham, D. and Z. You, *In vitro and in vivo model systems used in prostate cancer research*. J Biol Methods, 2015. **2**(1).
 199. Johnson, B.E., et al., *Retention of Chromosome 3 in Extrapulmonary Small Cell Cancer Shown by Molecular and Cytogenetic Studies*. JNCI: Journal of the National Cancer Institute, 1989. **81**(16): p. 1223-1228.
 200. Mertz, K.D., et al., *Molecular characterization of TMPRSS2-ERG gene fusion in the NCI-H660 prostate cancer cell line: a new perspective for an old model*. Neoplasia, 2007. **9**(3): p. 200-6.
 201. Tomlins, S.A., et al., *Integrative molecular concept modeling of prostate cancer progression*. Nature Genetics, 2007. **39**(1): p. 41-51.
 202. Varambally, S., et al., *Integrative genomic and proteomic analysis of prostate cancer reveals signatures of metastatic progression*. Cancer Cell, 2005. **8**(5): p. 393-406.
 203. Zhu, Y., et al., *Role of androgen receptor splice variant-7 (AR-V7) in prostate cancer resistance to 2nd-generation androgen receptor signaling inhibitors*. Oncogene, 2020. **39**(45): p. 6935-6949.
 204. Rice, M.A., S.V. Malhotra, and T. Stoyanova, *Second-Generation Antiandrogens: From Discovery to Standard of Care in Castration Resistant Prostate Cancer*. Front Oncol, 2019. **9**: p. 801.
 205. Di Lauro, L., et al., *Docetaxel, oxaliplatin, and capecitabine combination chemotherapy for metastatic gastric cancer*. Gastric Cancer, 2014. **17**(4): p. 718-724.
 206. Zhao, J., et al., *Cross-Resistance Among Next-Generation Antiandrogen Drugs Through the AKR1C3/AR-V7 Axis in Advanced Prostate Cancer*. Mol Cancer Ther, 2020. **19**(8): p. 1708-1718.

207. Sekino, Y. and J. Teishima, *Molecular mechanisms of docetaxel resistance in prostate cancer*. *Cancer Drug Resist*, 2020. **3**(4): p. 676-685.
208. Tu, C., et al., *Proteomic Analysis of Charcoal-Stripped Fetal Bovine Serum Reveals Changes in the Insulin-like Growth Factor Signaling Pathway*. *J Proteome Res*, 2018. **17**(9): p. 2963-2977.
209. Lin, D.L., et al., *Bone metastatic LNCaP-derivative C4-2B prostate cancer cell line mineralizes in vitro*. *Prostate*, 2001. **47**(3): p. 212-21.
210. Schmidt-Rohr, K., *Oxygen Is the High-Energy Molecule Powering Complex Multicellular Life: Fundamental Corrections to Traditional Bioenergetics*. *ACS Omega*, 2020. **5**(5): p. 2221-2233.
211. Bader, D.A., et al., *Mitochondrial pyruvate import is a metabolic vulnerability in androgen receptor-driven prostate cancer*. *Nature Metabolism*, 2019. **1**(1): p. 70-85.
212. Plymate, S.R., C. Sprenger, and M.C. Haffner, *Starving lethal prostate cancer by targeting heat shock proteins and glycolytic enzymes*. *Cell Rep Med*, 2022. **3**(2): p. 100493.
213. Eidelman, E., et al., *The Metabolic Phenotype of Prostate Cancer*. *Frontiers in Oncology*, 2017. **7**.
214. Zwahlen, M., A. Renehan, and M. Egger, *Meta-analysis in medical research: Potentials and limitations*. *Urologic Oncology: Seminars and Original Investigations*, 2008. **26**(3): p. 320-329.
215. Walker, E., A.V. Hernandez, and M.W. Kattan, *Meta-analysis: Its strengths and limitations*. *Cleve Clin J Med*, 2008. **75**(6): p. 431-9.
216. Lin, L. and H. Chu, *Quantifying publication bias in meta-analysis*. *Biometrics*, 2018. **74**(3): p. 785-794.
217. Levin, V.A., et al., *Different changes in protein and phosphoprotein levels result from serum starvation of high-grade glioma and adenocarcinoma cell lines*. *J Proteome Res*, 2010. **9**(1): p. 179-91.

218. Ciarlo, M., et al., *Regulation of neuroendocrine differentiation by AKT/hnRNPK/AR/ β -catenin signaling in prostate cancer cells*. Int J Cancer, 2012. **131**(3): p. 582-90.
219. Cipriani, C., et al., *The Interplay Between Bone and Glucose Metabolism*. Frontiers in Endocrinology, 2020. **11**.
220. Dagvadorj, A., et al., *Androgen-regulated and highly tumorigenic human prostate cancer cell line established from a transplantable primary CWR22 tumor*. Clin Cancer Res, 2008. **14**(19): p. 6062-72.
221. Henry, M.D., et al., *Spiculated periosteal response induced by intraosseous injection of 22Rv1 prostate cancer cells resembles subset of bone metastases in prostate cancer patients*. The Prostate, 2005. **65**(4): p. 347-354.
222. Pulukuri, S.M., et al., *RNA interference-directed knockdown of urokinase plasminogen activator and urokinase plasminogen activator receptor inhibits prostate cancer cell invasion, survival, and tumorigenicity in vivo*. J Biol Chem, 2005. **280**(43): p. 36529-40.
223. Tai, S., et al., *PC3 is a cell line characteristic of prostatic small cell carcinoma*. Prostate, 2011. **71**(15): p. 1668-79.
224. Nelson, S.J., et al., *Metabolic imaging of patients with prostate cancer using hyperpolarized [$1\text{-}^{13}\text{C}$]pyruvate*. Sci Transl Med, 2013. **5**(198): p. 198ra108.
225. Zha, Z., et al., *Neuron specific enolase promotes tumor metastasis by activating the Wnt/ β -catenin pathway in small cell lung cancer*. Transl Oncol, 2021. **14**(4): p. 101039.
226. Kaur, G. and J.M. Dufour, *Cell lines: Valuable tools or useless artifacts*. Spermatogenesis, 2012. **2**(1): p. 1-5.
227. Bezek, S., et al., *Chapter 11 - Pathophysiology and clinical implementation of traumatic brain injury biomarkers: neuron-specific enolase*, in *Biomarkers for Traumatic Brain Injury*, A.H.B. Wu and W.F. Peacock, Editors. 2020, Academic Press. p. 169-182.

228. Ediriweera, M.K. and S. Jayasena, *The Role of Reprogrammed Glucose Metabolism in Cancer*. Metabolites, 2023. **13**(3).
229. Chen, M.-L., et al., *A Novel Enolase-1 Antibody Targets Multiple Interacting Players in the Tumor Microenvironment of Advanced Prostate Cancer*. Molecular Cancer Therapeutics, 2022. **21**(8): p. 1337-1347.
230. Chen, J., et al., *ENO3 promotes colorectal cancer progression by enhancing cell glycolysis*. Medical Oncology, 2022. **39**(6): p. 80.
231. Deep, G., et al., *Role of E-cadherin in antimigratory and antiinvasive efficacy of silibinin in prostate cancer cells*. Cancer Prev Res (Phila), 2011. **4**(8): p. 1222-32.
232. Hsiao, K.-C., et al., *Surface α -enolase promotes extracellular matrix degradation and tumor metastasis and represents a new therapeutic target*. PloS one, 2013. **8**(7): p. e69354.
233. Principe, M., et al., *Targeting of surface alpha-enolase inhibits the invasiveness of pancreatic cancer cells*. Oncotarget, 2015. **6**(13): p. 11098.
234. Tian, X., et al., *Development and validation of a hypoxia-stemness-based prognostic signature in pancreatic adenocarcinoma*. Frontiers in Pharmacology, 2022. **13**: p. 939542.
235. Li, Z., et al., *Novel hypoxia-related gene signature for predicting prognoses that correlate with the tumor immune microenvironment in NSCLC*. Frontiers in Genetics, 2023. **14**: p. 1115308.
236. Cui, H., et al., *ENO3 Inhibits Growth and Metastasis of Hepatocellular Carcinoma via Wnt/ β -Catenin Signaling Pathway*. Front Cell Dev Biol, 2021. **9**: p. 797102.
237. Mittal, V., *Epithelial Mesenchymal Transition in Tumor Metastasis*. Annu Rev Pathol, 2018. **13**: p. 395-412.
238. Leonard, P.G., et al., *SF2312 is a natural phosphonate inhibitor of enolase*. Nature Chemical Biology, 2016. **12**(12): p. 1053-1058.

239. Lin, Y.-H., et al., *An enolase inhibitor for the targeted treatment of ENO1-deleted cancers*. Nature Metabolism, 2020. **2**(12): p. 1413-1426.
240. Namiki, M., S. Ueno, and Y. Kitagawa, *Role of hormonal therapy for prostate cancer: perspective from Japanese experiences*. Transl Androl Urol, 2012. **1**(3): p. 160-72.
241. Hensel, J. and G.N. Thalmann, *Biology of Bone Metastases in Prostate Cancer*. Urology, 2016. **92**: p. 6-13.
242. Wang, Z., et al., *Screening of key candidate genes and pathways for osteocytes involved in the differential response to different types of mechanical stimulation using a bioinformatics analysis*. Journal of Bone and Mineral Metabolism, 2019. **37**(4): p. 614-626.
243. Dai, J., et al., *Mouse models for studying prostate cancer bone metastasis*. Bonekey Rep, 2016. **5**: p. 777.
244. Simmons, J.K., et al., *Review of Animal Models of Prostate Cancer Bone Metastasis*. Veterinary Sciences, 2014. **1**(1): p. 16-39.
245. Tae, J.H. and I.H. Chang, *Animal models of bone metastatic prostate cancer*. Investig Clin Urol, 2023. **64**(3): p. 219-228.
246. Xu, W., et al., *Age-related trabecular bone loss is associated with a decline in serum Galectin-1 level*. BMC Musculoskelet Disord, 2021. **22**(1): p. 394.
247. Hahn, M., et al., *Trabecular bone pattern factor—a new parameter for simple quantification of bone microarchitecture*. Bone, 1992. **13**(4): p. 327-330.
248. Guise, T.A., *The vicious cycle of bone metastases*. J Musculoskelet Neuronal Interact, 2002. **2**(6): p. 570-2.
249. Qiu, W., et al., *Kaempferol prevents aseptic loosening via enhance the Wnt/ β -catenin signaling pathway in vitro and in vivo*. Eur J Med Res, 2023. **28**(1): p. 505.
250. Hoffman, R.M., *Application of GFP imaging in cancer*. Lab Invest, 2015. **95**(4): p. 432-52.

251. Motamed, S., et al., *Migration and Differentiation of Neural Stem Cells Diverted From the Subventricular Zone by an Injectable Self-Assembling beta-Peptide Hydrogel*. Front Bioeng Biotechnol, 2019. **7**: p. 315.
252. Todd, V.M. and R.W. Johnson, *Hypoxia in bone metastasis and osteolysis*. Cancer Lett, 2020. **489**: p. 144-154.
253. Ottewill, P.D., et al., *Castration-induced bone loss triggers growth of disseminated prostate cancer cells in bone*. Endocrine-Related Cancer, 2014. **21**(5): p. 769-781.
254. Morrissey, C., et al., *Effects of androgen deprivation therapy and bisphosphonate treatment on bone in patients with metastatic castration-resistant prostate cancer: results from the University of Washington Rapid Autopsy Series*. Journal of Bone and Mineral Research, 2013. **28**: p. 333-340.
255. Böckelmann, L.C., et al., *Efficacy of zoledronic acid for the elimination of disseminated tumor cells in a clinically relevant, spontaneously metastatic prostate cancer xenograft model*. Bone, 2023. **171**: p. 116741.
256. Park, S.H., M.R. Eber, and Y. Shiozawa, *Models of Prostate Cancer Bone Metastasis*, in *Bone Research Protocols*, A.I. Idris, Editor. 2019, Springer New York: New York, NY. p. 295-308.
257. Clegg, N., et al., *Molecular characterization of prostatic small-cell neuroendocrine carcinoma*. Prostate, 2003. **55**(1): p. 55-64.
258. Xu, H., et al., *Aberrant expression of multiple glycolytic enzyme genes is significantly associated with disease progression and survival outcomes in prostate cancers*. Am J Clin Exp Urol, 2023. **11**(6): p. 530-541.
259. Korotkevich, G., V. Sukhov, and A. Sergushichev, *Fast gene set enrichment analysis*. bioRxiv, 2019: p. 060012.
260. Sherman, B.T., et al., *DAVID: a web server for functional enrichment analysis and functional annotation of gene lists (2021 update)*. Nucleic Acids Res, 2022. **50**(W1): p. W216-w221.

261. Formaggio, N., M.A. Rubin, and J.P. Theurillat, *Loss and revival of androgen receptor signaling in advanced prostate cancer*. *Oncogene*, 2021. **40**(7): p. 1205-1216.
262. Sampson, N., et al., *In vitro model systems to study androgen receptor signaling in prostate cancer*. *Endocr Relat Cancer*, 2013. **20**(2): p. R49-64.
263. Han, Z., et al., *Differential Expression of E2F Transcription Factors and Their Functional and Prognostic Roles in Human Prostate Cancer*. *Frontiers in Cell and Developmental Biology*, 2022. **10**.
264. Kent, L.N. and G. Leone, *The broken cycle: E2F dysfunction in cancer*. *Nature Reviews Cancer*, 2019. **19**(6): p. 326-338.
265. Wang, Y., et al., *Centrosome-associated regulators of the G(2)/M checkpoint as targets for cancer therapy*. *Mol Cancer*, 2009. **8**: p. 8.
266. Oshi, M., et al., *The E2F Pathway Score as a Predictive Biomarker of Response to Neoadjuvant Therapy in ER+/HER2- Breast Cancer*. *Cells*, 2020. **9**(7).
267. Formaggio, N., M.A. Rubin, and J.-P. Theurillat, *Loss and revival of androgen receptor signaling in advanced prostate cancer*. *Oncogene*, 2021. **40**(7): p. 1205-1216.
268. Hodgson, K., et al., *The role of GCNT1 mediated O-glycosylation in aggressive prostate cancer*. *Scientific Reports*, 2023. **13**(1): p. 17031.
269. Liebl, M.C., et al., *DAZAP2 acts as specifier of the p53 response to DNA damage*. *Nucleic Acids Research*, 2021. **49**(5): p. 2759-2776.
270. Nagasaka, M., et al., *ID3 is a novel target gene of p53 and modulates lung cancer cell metastasis*. *Biochemical and Biophysical Research Communications*, 2024. **708**: p. 149789.
271. Pathria, G., et al., *RanBP3 Regulates Melanoma Cell Proliferation via Selective Control of Nuclear Export*. *Journal of Investigative Dermatology*, 2016. **136**(1): p. 264-274.

272. Li, J., et al., *The clinical significance of collagen family gene expression in esophageal squamous cell carcinoma*. PeerJ, 2019. **7**: p. e7705.
273. Qiu, H.-b., et al., *Targeting CDH17 suppresses tumor progression in gastric cancer by downregulating Wnt/ β -catenin signaling*. PloS one, 2013. **8**(3): p. e56959.
274. Hussain, S.P., et al., *p53-Induced Up-Regulation of MnSOD and GPx but not Catalase Increases Oxidative Stress and Apoptosis*. Cancer Research, 2004. **64**(7): p. 2350-2356.
275. Li, X. and C. Ma, *Alpha-2-Heremans-Schmid-glycoprotein (AHSG) a potential biomarker associated with prognosis of chromophobe renal cell carcinoma: The PROPOLIS study*. Health Sci Rep, 2022. **5**(6): p. e878.
276. von Grabowiecki, Y., et al., *Rab11-FIP1/RCP Functions as a Major Signalling Hub in the Oncogenic Roles of Mutant p53 in Cancer*. Front Oncol, 2021. **11**: p. 804107.
277. Yeon, S.Y., et al., *Frameshift Mutations in Repeat Sequences of ANK3, HACD4, TCP10L, TP53BP1, MFN1, LCMT2, RNMT, TRMT6, METTL8 and METTL16 Genes in Colon Cancers*. Pathol Oncol Res, 2018. **24**(3): p. 617-622.
278. Chwee, J.Y., et al., *Apoptotic Cells Release IL1 Receptor Antagonist in Response to Genotoxic Stress*. Cancer Immunology Research, 2016. **4**(4): p. 294-302.
279. Woo, J.S., et al., *TRPC3 cation channel plays an important role in proliferation and differentiation of skeletal muscle myoblasts*. Experimental & Molecular Medicine, 2010. **42**(9): p. 614-627.
280. Wang, Q., et al., *Circadian clock gene Per2 plays an important role in cell proliferation, apoptosis and cell cycle progression in human oral squamous cell carcinoma*. Oncol Rep, 2016. **35**(6): p. 3387-3394.
281. Rouillard, A.D., et al., *The harmonizome: a collection of processed datasets gathered to serve and mine knowledge about genes and proteins*. Database,

2016. **2016**: p. baw100.
282. Tournier, B., et al., *Integrative Clinical and DNA Methylation Analyses in a Population-Based Cohort Identifies CDH17 and LRP2 as Risk Recurrence Factors in Stage II Colon Cancer*. *Cancers (Basel)*, 2022. **15**(1).
 283. Xie, Q., et al., *E2F transcription factor 1 regulates cellular and organismal senescence by inhibiting Forkhead box O transcription factors*. *Journal of Biological Chemistry*, 2014. **289**(49): p. 34205-34213.
 284. Gentile, G., et al., *Functional Genomics Identifies Tis21-Dependent Mechanisms and Putative Cancer Drug Targets Underlying Medulloblastoma Shh-Type Development*. *Front Pharmacol*, 2016. **7**: p. 449.
 285. Guo, L., et al., *PER2 integrates circadian disruption and pituitary tumorigenesis*. *Theranostics*, 2023. **13**(8): p. 2657-2672.
 286. Chaussepied, M. and D. Ginsberg, *E2F and signal transduction pathways*. *Cell Cycle*, 2005. **4**(3): p. 392-6.
 287. Ather, S.H., et al., *SeqAcademy: an educational pipeline for RNA-Seq and ChIP-Seq analysis*. *F1000Res*, 2018. **7**.
 288. Deng, Q., et al., *E2F8 contributes to human hepatocellular carcinoma via regulating cell proliferation*. *Cancer Res*, 2010. **70**(2): p. 782-91.
 289. Kent, L.N., et al., *E2f8 mediates tumor suppression in postnatal liver development*. *The Journal of clinical investigation*, 2016. **126**(8): p. 2955-2969.
 290. Dasari, V.K., et al., *DNA METHYLATION REGULATES THE EXPRESSION OF Y CHROMOSOME SPECIFIC GENES IN PROSTATE CANCER*. *The Journal of Urology*, 2002. **167**(1): p. 335-338.
 291. Luo, S.Q., et al., *The effects of promoter methylation on downregulation of DAZAP2 in multiple myeloma cell lines*. *PLoS One*, 2012. **7**(7): p. e40475.
 292. Udagawa, N., et al., *Origin of osteoclasts: mature monocytes and macrophages are capable of differentiating into osteoclasts under a suitable microenvironment prepared by bone marrow-derived stromal cells*.

- Proceedings of the national academy of sciences, 1990. **87**(18): p. 7260-7264.
293. Schug, Z.T., et al., *Acetyl-CoA synthetase 2 promotes acetate utilization and maintains cancer cell growth under metabolic stress*. Cancer Cell, 2015. **27**(1): p. 57-71.
 294. Filippi, A., J. Aurelian, and M.M. Mocanu, *Analysis of the Gene Networks and Pathways Correlated with Tissue Differentiation in Prostate Cancer*. Int J Mol Sci, 2024. **25**(7).
 295. Battisti, V., et al., *Oxidative stress and antioxidant status in prostate cancer patients: relation to Gleason score, treatment and bone metastasis*. Biomed Pharmacother, 2011. **65**(7): p. 516-24.
 296. Jacobsen, F., et al., *Cadherin-17 (CDH17) expression in human cancer: A tissue microarray study on 18,131 tumors*. Pathology - Research and Practice, 2024. **256**: p. 155175.
 297. Okada, T., et al., *Expression of Cadherin-17 Promotes Metastasis in a Highly Bone Marrow Metastatic Murine Breast Cancer Model*. Biomed Res Int, 2017. **2017**: p. 8494286.
 298. Güzel, Ö., et al., *The Role of Pentraxin-3, Fetuin-A and Sirtuin-7 in the Diagnosis of Prostate Cancer*. Urol J, 2021. **19**(3): p. 196-201.
 299. Ochieng, J., et al., *Impact of Fetuin-A (AHSG) on Tumor Progression and Type 2 Diabetes*. International Journal of Molecular Sciences, 2018. **19**(8): p. 2211.
 300. Xie, J., M.J. Baumann, and L.R. McCabe, *Adsorption of serum fetuin to hydroxylapatite does not contribute to osteoblast phenotype modifications*. Journal of Biomedical Materials Research Part A: An Official Journal of The Society for Biomaterials, The Japanese Society for Biomaterials, and The Australian Society for Biomaterials and the Korean Society for Biomaterials, 2005. **73**(1): p. 39-47.
 301. Mintz, P.J., et al., *Discovery and horizontal follow-up of an autoantibody signature in human prostate cancer*. Proceedings of the National Academy of

- Sciences, 2015. **112**(8): p. 2515-2520.
302. Schäfer, C., et al., *The serum protein α 2-Heremans-Schmid glycoprotein/fetuin-A is a systemically acting inhibitor of ectopic calcification.* The Journal of clinical investigation, 2003. **112**(3): p. 357-366.
 303. Liu, X., X. Wang, and Q. Zheng, *The Role of Ladinin-1 in Cancer.* Highlights in Science, Engineering and Technology, 2023. **54**: p. 31-36.
 304. Liu, Y., et al., *Knockdown of protein tyrosine phosphatase receptor U inhibits growth and motility of gastric cancer cells.* Int J Clin Exp Pathol, 2014. **7**(9): p. 5750-61.
 305. Gu, J., et al., *PTPRU, As A Tumor Suppressor, Inhibits Cancer Stemness By Attenuating Hippo/YAP Signaling Pathway.* Onco Targets Ther, 2019. **12**: p. 8095-8104.
 306. Rumman, M. and J. Dhawan, *PTPRU, a quiescence-induced receptor tyrosine phosphatase negatively regulates osteogenic differentiation of human mesenchymal stem cells.* Biochemical and Biophysical Research Communications, 2022. **636**: p. 41-49.
 307. Barbarino, J.M., et al., *PharmGKB summary: very important pharmacogene information for UGT1A1.* Pharmacogenet Genomics, 2014. **24**(3): p. 177-83.
 308. Koliwad, S.K., N.E. Gray, and J.C. Wang, *Angiopoietin-like 4 (Angptl4): A glucocorticoid-dependent gatekeeper of fatty acid flux during fasting.* Adipocyte, 2012. **1**(3): p. 182-187.
 309. Eich, M.-L., et al., *Characterization of glycine-N-acyltransferase like 1 (GLYATL1) in prostate cancer.* The Prostate, 2019. **79**(14): p. 1629-1639.
 310. Sinha, R., et al., *LRRTM4: A Novel Regulator of Presynaptic Inhibition and Ribbon Synapse Arrangements of Retinal Bipolar Cells.* Neuron, 2020. **105**(6): p. 1007-1017.e5.
 311. Yim, Y.S., et al., *Slitrks control excitatory and inhibitory synapse formation with LAR receptor protein tyrosine phosphatases.* Proc Natl Acad Sci U S A, 2013.

- 110**(10): p. 4057-62.
312. Gong, J., et al., *Increased Expression of Fibulin-1 Is Associated With Hepatocellular Carcinoma Progression by Regulating the Notch Signaling Pathway*. Front Cell Dev Biol, 2020. **8**: p. 478.
 313. Lim, M.M.K., et al., *Targeting metabolic flexibility via angiopoietin-like 4 protein sensitizes metastatic cancer cells to chemotherapy drugs*. Mol Cancer, 2018. **17**(1): p. 152.
 314. Belandia, B., et al., *Hey1, a mediator of notch signaling, is an androgen receptor corepressor*. Mol Cell Biol, 2005. **25**(4): p. 1425-36.
 315. Ahmat Amin, M.K.B., A. Shimizu, and H. Ogita, *The Pivotal Roles of the Epithelial Membrane Protein Family in Cancer Invasiveness and Metastasis*. Cancers (Basel), 2019. **11**(11).
 316. Panjawatnan, P., et al., *MON-512 A De Novo Frameshift Mutation of FAM111B Gene Resulting in Progressive Osseous Heteroplasia in an African American Boy: First Case Report*. Journal of the Endocrine Society, 2019. **3**(Supplement_1).
 317. Wang, W., et al., *Silencing of FAM111B inhibits tumor growth and promotes apoptosis by decreasing AKT activity in ovarian cancer*. Exp Biol Med (Maywood), 2023. **248**(12): p. 1043-1055.
 318. Sun, H., et al., *FAM111B, a direct target of p53, promotes the malignant process of lung adenocarcinoma*. Onco Targets Ther, 2019. **12**: p. 2829-2842.
 319. Chen, G., C. Deng, and Y.P. Li, *TGF- β and BMP signaling in osteoblast differentiation and bone formation*. Int J Biol Sci, 2012. **8**(2): p. 272-88.
 320. Feeley, B.T., et al., *Influence of BMPs on the Formation of Osteoblastic Lesions in Metastatic Prostate Cancer**. Journal of Bone and Mineral Research, 2009. **20**(12): p. 2189-2199.
 321. Kwon, H., et al., *Development of an in vitro model to study the impact of BMP-2 on metastasis to bone*. Journal of Tissue Engineering and Regenerative

- Medicine, 2010. **4**(8): p. 590-599.
322. Msaouel, P., et al., *Bone microenvironment-targeted manipulations for the treatment of osteoblastic metastasis in castration-resistant prostate cancer*. Expert Opin Investig Drugs, 2013. **22**(11): p. 1385-400.
 323. Katzenwadel, A. and P. Wolf, *Androgen deprivation of prostate cancer: Leading to a therapeutic dead end*. Cancer Lett, 2015. **367**(1): p. 12-7.
 324. Body, J.J., S. Casimiro, and L. Costa, *Targeting bone metastases in prostate cancer: improving clinical outcome*. Nat Rev Urol, 2015. **12**(6): p. 340-56.
 325. Franz, M.-C., et al., *Zinc transporters in prostate cancer*. Molecular aspects of medicine, 2013. **34**(2-3): p. 735-741.
 326. Wright, K., et al., *Cancer-Associated Fibroblasts: Master Tumor Microenvironment Modifiers*. Cancers (Basel), 2023. **15**(6).
 327. Kharroubi, A.T. and H.M. Darwish, *Diabetes mellitus: The epidemic of the century*. World J Diabetes, 2015. **6**(6): p. 850-67.
 328. Lee, J., E. Giovannucci, and J.Y. Jeon, *Diabetes and mortality in patients with prostate cancer: a meta-analysis*. Springerplus, 2016. **5**(1): p. 1548.
 329. de Beer, J.C. and L. Liebenberg, *Does cancer risk increase with HbA1c, independent of diabetes?* Br J Cancer, 2014. **110**(9): p. 2361-8.
 330. Chan, J.M., et al., *History of diabetes, clinical features of prostate cancer, and prostate cancer recurrence-data from CaPSURE (United States)*. Cancer Causes Control, 2005. **16**(7): p. 789-97.
 331. Feng, X., et al., *The association of diabetes with risk of prostate cancer defined by clinical and molecular features*. Br J Cancer, 2020. **123**(4): p. 657-665.
 332. Travis, R.C., et al., *A Meta-analysis of Individual Participant Data Reveals an Association between Circulating Levels of IGF-I and Prostate Cancer Risk*. Cancer Res, 2016. **76**(8): p. 2288-2300.
 333. Kasper, J.S., et al., *Hormonal profile of diabetic men and the potential link to prostate cancer*. Cancer Causes Control, 2008. **19**(7): p. 703-10.

334. Grossmann, M., et al., *Low Testosterone Levels Are Common and Associated with Insulin Resistance in Men with Diabetes*. The Journal of Clinical Endocrinology & Metabolism, 2008. **93**(5): p. 1834-1840.
335. Basaria, S., et al., *Hyperglycemia and insulin resistance in men with prostate carcinoma who receive androgen-deprivation therapy*. Cancer, 2006. **106**(3): p. 581-8.
336. Smith, M.R., H. Lee, and D.M. Nathan, *Insulin sensitivity during combined androgen blockade for prostate cancer*. J Clin Endocrinol Metab, 2006. **91**(4): p. 1305-8.
337. Lv, C., et al., *ENO2 Promotes Colorectal Cancer Metastasis by Interacting with the LncRNA CYTOR and Activating YAP1-Induced EMT*. Cells, 2022. **11**(15).
338. Neophytou, C.M., T.C. Kyriakou, and P. Papageorgis, *Mechanisms of Metastatic Tumor Dormancy and Implications for Cancer Therapy*. Int J Mol Sci, 2019. **20**(24).
339. Pantel, K. and R.H. Brakenhoff, *Dissecting the metastatic cascade*. Nat Rev Cancer, 2004. **4**(6): p. 448-56.
340. Uzuner, D., et al., *Transcriptional landscape of cellular networks reveal interactions driving the dormancy mechanisms in cancer*. Sci Rep, 2021. **11**(1): p. 15806.
341. Recasens, A. and L. Munoz, *Targeting Cancer Cell Dormancy*. Trends Pharmacol Sci, 2019. **40**(2): p. 128-141.
342. Phan, T.G. and P.I. Croucher, *The dormant cancer cell life cycle*. Nature Reviews Cancer, 2020. **20**(7): p. 398-411.
343. Piezzo, M., et al., *Targeting Cell Cycle in Breast Cancer: CDK4/6 Inhibitors*. Int J Mol Sci, 2020. **21**(18).
344. Crozier, L., et al., *CDK4/6 inhibitors induce replication stress to cause long-term cell cycle withdrawal*. The EMBO journal, 2022. **41**(6): p. e108599.
345. Fouad, S., D. Hauton, and V. D'Angiolella, *E2F1: Cause and Consequence of*

- DNA Replication Stress*. Front Mol Biosci, 2020. **7**: p. 599332.
346. Min, H.Y. and H.Y. Lee, *Cellular Dormancy in Cancer: Mechanisms and Potential Targeting Strategies*. Cancer Res Treat, 2023. **55**(3): p. 720-736.
 347. Fischer, M., et al., *Coordinating gene expression during the cell cycle*. Trends Biochem Sci, 2022. **47**(12): p. 1009-1022.
 348. Jubelin, C., et al., *Identification of MCM4 and PRKDC as new regulators of osteosarcoma cell dormancy based on 3D cell cultures*. Biochimica et Biophysica Acta (BBA) - Molecular Cell Research, 2024. **1871**(3): p. 119660.
 349. Wilczewska, A.Z., et al., *Nanoparticles as drug delivery systems*. Pharmacological Reports, 2012. **64**(5): p. 1020-1037.
 350. Lin, Y., et al., *Calcium-bisphosphonate Nanoparticle Platform as a Prolonged Nanodrug and Bone-Targeted Delivery System for Bone Diseases and Cancers*. ACS Appl Bio Mater, 2021. **4**(3): p. 2490-2501.
 351. Yetisgin, A.A., et al., *Therapeutic Nanoparticles and Their Targeted Delivery Applications*. Molecules, 2020. **25**(9).
 352. Chehelgerdi, M., et al., *Progressing nanotechnology to improve targeted cancer treatment: overcoming hurdles in its clinical implementation*. Molecular Cancer, 2023. **22**(1): p. 169.
 353. Zhong, Y. and S. Li, *New Progress in Improving the Delivery Methods of Bisphosphonates in the Treatment of Bone Tumors*. Drug Des Devel Ther, 2021. **15**: p. 4939-4959.